



TECHNISCHE UNIVERSITÄT MÜNCHEN

TUM School of Life Sciences Weihenstephan
Lehrstuhl für Molekulare Ernährungsmedizin

The relationship between lipid metabolites and the recruitment of uncoupling protein 1

Sebastian Dieckmann

Vollständiger Abdruck der von der TUM School of Life Sciences Weihenstephan der Technischen Universität München zur Erlangung des akademischen Grades eines

Doktors der Naturwissenschaften

(Dr. rer. nat.)

genehmigten Dissertation.

Vorsitzender: Prof. Dr. Dirk Haller

Prüfende der Dissertation:

1. Prof. Dr. Martin Klingenspor
2. Prof. Dr. Nina Henriette Uhlenhaut

Die Dissertation wurde am 26.04.2021 bei der Technischen Universität München eingereicht und durch die TUM School of Life Sciences Weihenstephan der Technischen Universität München am 26.08.2021 angenommen.

CONTENT

ABBREVIATIONS	V
ABSTRACT	VI
ZUSAMMENFASSUNG	VII
1 INTRODUCTION	1
1.1 OVERWEIGHT AND OBESITY	1
1.2 ADIPOSE TISSUE - WHITE, BRITE AND BROWN	2
1.3 UCP1-MEDIATED NON-SHIVERING THERMOGENESIS	3
1.4 RELEVANCE OF LIPIDS IN HUMAN NUTRITION AND AS FUNCTIONAL MOLECULES IN ADIPOSE TISSUE METABOLISM	6
1.5 AIMS	7
2 GENERAL MATERIAL AND METHODS	9
2.1 ANIMALS	9
2.1.1 STUDYING UCP1-DEPENDENT THERMOGENESIS – A MATTER OF TEMPERATURE	9
2.1.2 TEMPERATURE DEPENDENT CHANGES IN OXYLIPIN AND LIPID METABOLISM	9
2.1.3 STUDYING THE EFFECT OF DIETARY FATTY ACIDS ON RECRUITMENT OF BROWN AND BRITE ADIPOCYTES	11
2.1.4 STUDYING THE CONTRIBUTION OF UCP1 TO THE DEVELOPMENT OF DIO	12
2.2 INDIRECT CALORIMETRY	15
2.3 TISSUE DISSECTION	16
2.4 MATRIX-ASSISTED LASER DESORPTION IONIZATION MASS SPECTROMETRY IMAGING	16
2.5 IMMUNOHISTOCHEMISTRY	17
2.6 STATISTICAL ANALYSIS	19
3 FATTY ACID METABOLITE PROFILING REVEALS OXYLIPINS AS MARKERS OF BROWN BUT NOT BRITE ADIPOSE TISSUE	20
3.1 ABSTRACT	20
3.2 AUTHOR CONTRIBUTIONS	20
3.3 INTRODUCTION	21
3.4 MATERIAL AND METHODS	22
3.4.1 ANIMAL EXPERIMENTS	22
3.4.2 HUMAN SUBJECTS	22
3.4.3 OXYLIPIN AND ENDOCANNABINOID PROFILING	23

3.4.4	RNA ISOLATION AND QUANTITATIVE REAL-TIME PCR (QRT-PCR)	23
3.4.5	STATISTICAL ANALYSIS	23
3.5	RESULTS	23
3.5.1	THE ABUNDANCE OF ADIPOSE TISSUE OXYLIPINS DIFFERS BETWEEN MICE AND HUMANS	24
3.5.2	THE GLOBAL OXYLIPIN PROFILE IS A SURROGATE MARKER FOR THE ABUNDANCE OF BROWN BUT NOT BRITE ADIPOCYTES	26
3.5.3	THE OXYLIPINS 5-HETE AND 5,6-EET ARE POTENTIAL MARKERS OF BROWN ADIPOCYTE ABUNDANCE IN BAT IN MICE AND HUMANS	28
3.6	DISCUSSION	30
4	<u>NO EFFECT OF DIETARY FISH OIL SUPPLEMENTATION ON THE RECRUITMENT OF BROWN AND BRITE ADIPOCYTES IN MICE OR HUMANS UNDER THERMONEUTRAL CONDITIONS</u>	34
4.1	ABSTRACT	34
4.2	AUTHOR CONTRIBUTIONS	34
4.3	INTRODUCTION	35
4.4	MATERIAL AND METHODS	40
4.4.1	ANIMALS AND HOUSING	40
4.4.2	DIETARY PUFA SUPPLEMENTATION OF MICE	40
4.4.3	CL-316,243 TREATMENT	41
4.4.4	ORAL GLUCOSE TOLERANCE TESTS	41
4.4.5	OXYLIPIN ANALYSIS	41
4.4.6	HISTOLOGY	41
4.4.7	SDS-PAGE AND WESTERN BLOT	41
4.4.8	RNA ISOLATION AND QUANTITATIVE REAL-TIME PCR OF MURINE SAMPLES	42
4.4.9	HUMAN DIETARY INTERVENTION STUDY	42
4.4.10	GENE EXPRESSION ANALYSES IN HUMAN ABDOMINAL SUBCUTANEOUS ADIPOSE TISSUE	43
4.4.11	LIPIDOMIC ANALYSIS OF HUMAN PLASMA	44
4.4.12	DOSAGE INFORMATION	44
4.4.13	STATISTICS	44
4.5	RESULTS	45
4.5.1	FISH OIL AND BORAGE OIL SUPPLEMENTATIONS CAUSE DIVERGENT CHANGES IN PUFA METABOLISM	45
4.5.2	DIETARY N3-PUFA SUPPLEMENTATION DOES NOT INFLUENCE THE RECRUITMENT OF THERMOGENIC ADIPOCYTES IN MURINE ADIPOSE TISSUES	50
4.5.3	DIETARY N3-PUFA SUPPLEMENTATION DOES NOT INFLUENCE THE DEVELOPMENT OF DIET-INDUCED OBESITY	56

4.5.4	DIETARY N3-PUFA SUPPLEMENTATION DOES NOT PROMOTE BROWNING OF WAT IN HUMAN SUBJECTS	58
4.5.5	DISCUSSION	61

5 SUSCEPTIBILITY TO DIET-INDUCED OBESITY AT THERMONEUTRAL CONDITIONS IS INDEPENDENT OF UCP1 **66**

5.1	ABSTRACT	66
5.2	AUTHORS CONTRIBUTION	66
5.3	INTRODUCTION	67
5.4	MATERIAL AND METHODS	68
5.4.1	ANIMAL MODEL	68
5.4.2	INDIRECT CALORIMETRY, BASAL METABOLIC RATE AND NA TESTS	69
5.4.3	COLLECTION OF FOOD SPILLAGE AND FAECES	69
5.4.4	DETERMINATION OF ENERGY CONTENT OF FOOD AND FAECES BY BOMB CALORIMETRY	70
5.4.5	THERMAL IMAGING	70
5.4.6	GENOTYPING	70
5.4.7	RNA ISOLATION AND CDNA SYNTHESIS AND SEQUENCING	71
5.4.8	PROTEIN EXPRESSION ANALYSIS BY SDS-PAGE AND WESTERN BLOT	71
5.4.9	DNA EXTRACTION AND 16S rRNA SEQUENCING	72
5.4.10	LIPID EXTRACTION AND MASS SPECTROMETRY ANALYSIS	72
5.4.11	DATA ANALYSIS AND STATISTICS	73
5.5	RESULTS	74
5.5.1	DELETION OF UCP1 EXON 2 LEADS TO A LOSS OF PROTEIN EXPRESSION	74
5.5.2	THERMOGENIC DEFICIENCY LEADS TO DECREASED BODY WEIGHT IN YOUNG KO MICE	75
5.5.3	UCP1-KO AND WT MICE HAVE SIMILAR SUSCEPTIBILITY TO DIO AT THERMONEUTRALITY	77
5.5.4	PLASMA LIPID COMPOSITION OF UCP1-KO AND UCP1-WT MICE IS COMPARABLE	79
5.5.5	LACK OF UCP1 IS ASSOCIATED WITH THE ABUNDANCE OF SPECIFIC MICROBIAL GENERA	80
5.5.6	UCP1-KO MICE HAVE SIMILAR ENERGY BALANCE AT THERMONEUTRALITY	82
5.6	DISCUSSION	85

6 SPATIAL RECRUITMENT OF CARDIOLIPINS IN WHITE ADIPOSE TISSUE AFTER COLD STIMULATION IS INDEPENDENT OF UCP1 **88**

6.1	ABSTRACT	88
6.2	AUTHORS CONTRIBUTION	88
6.3	INTRODUCTION	89
6.4	MATERIAL AND METHODS	90
6.4.1	ANIMALS	90

6.4.2	CRYOSECTIONING	90
6.4.3	MATRIX APPLICATION	91
6.4.4	MALDI-MSI	91
6.4.5	IMMUNOHISTOCHEMISTRY	91
6.4.6	LC-MS/MS ANALYSIS	92
6.4.7	DATA ANALYSIS	92
6.5	RESULTS	93
6.5.1	MALDI-MSI YIELDS REPRODUCIBLE RESULTS WITHIN DIFFERENT SECTIONS OF IWAT	93
6.5.2	IDENTIFICATION AND ANNOTATION OF REGION-SPECIFIC <i>M/Z</i> INTERVALS	94
6.5.3	VALIDATION OF ANNOTATED LIPID SPECIES BY HIGH RESOLUTION LC-MS/MS	108
6.5.4	CL 68:3 AND CL 68:4 ARE UPREGULATED BY COLD INDEPENDENT OF UCP1	108
6.6	DISCUSSION	111
7	<u>GENERAL DISCUSSION</u>	<u>113</u>
8	<u>REFERENCES</u>	<u>119</u>
	<u>EIDESSTÄTTLICHE ERKLÄRUNG</u>	<u>146</u>
	<u>PUBLICATION LIST</u>	<u>147</u>
	<u>SUPPLEMENTS</u>	<u>148</u>
	<u>ACKNOWLEDGMENTS</u>	<u>159</u>

ABBREVIATIONS

1

12,13-DiHOME	12,13-dihydroxy-9Z-octadecenoic acid
12-HEPE	12-hydroxyeicosapentaenoic acid
14-HDoHE	14-Hydroxydocosahexaenoic acid
15d-PGJ2	15-Deoxy-Delta-12,14-prostaglandin J2

A

AA	arachidonic acid
AC	adenyl cyclase
ALA	α -linolenic acid
ANOVA	analysis of variance
ATGL	adipose triglyceride lipase
ATP	adenosine triphosphate
AUC	area under the curve
AXOS	arabinoxylan oligosaccharides

B

BAT	brown adipose tissue
iBAT	interscapular brown adipose tissue
BMI	body mass index
BMR	basal metabolic rate

C

cAMP	cyclic adenosine monophosphate
CD	control diet
Cidea	cell death-inducing DNA fragmentation factor, alpha subunit-like effector A
CL	cardiolipins
CMC	carboxymethylcellulose
COX	cyclooxygenase
CREB	cAMP response element binding protein
CYP450	cytochrome P450

D

DG	diacylglycerols
DHA	docosahexaenoic acid
DIABLO	data integration analysis for biomarker discovery using latent variable approaches for 'omics studies
DIO	diet-induced obesity

E

EET	epoxyeicosatrienoic acid
5,6-EET	5,6-epoxyeicosatrienoic acid
5-oxoEET	5-oxo- epoxyeicosatrienoic acid
EPA	eicosapentaenoic acid

G

Gtf2b	general transcription factor IIB
--------------	----------------------------------

H

HET	heterozygous
HETE	hydroxyeicosatetraenoic acid
15-HETE	15-hydroxyeicosatetraenoic acid
5-HETE	5-hydroxyeicosatetraenoic acid
HFD	high-fat diet
HODE	hydroxyoctadecadienoic acid
13-HODE	13-hydroxyoctadecadienoic acid
9-HODE	9-hydroxyoctadecadienoic acid
HSL	hormone sensitive lipase

I

IFD	intermediate-fat diet
IHC	immunohistochemistry
iSST	interscapular skin surface temperature

K

KO	knockout
-----------	----------

L

LA	linoleic acid
LMSD	LIPID MAPS® Structure Database
LOX	lipoygenase

M

m/z	mass over charge ratio
MALDI-MSI	matrix-assisted laser desorption ionization mass spectrometry imaging
MetS	metabolic syndrome
MOFA	multi-omics factor analysis
MTBE	methyl-tert-butyl-ether

N

NA	noradrenaline
NST	non-shivering thermogenesis

P

PCA	principal component analysis
PGE2	prostaglandin E2
PGHS	prostaglandin H synthase
PGI2	prostacyclin
PKA	protein kinase A
PLS-DA	partial least-squares discriminant analysis
PPAR	peroxisome proliferator-activated receptor
PPARα	peroxisome proliferator-activated receptor alpha
PPARγ	peroxisome proliferator-activated receptor gamma
PUFA	polyunsaturated fatty acid
n3-PUFA	omega-3 polyunsaturated fatty acid
n6-PUFA	omega-6 polyunsaturated fatty acid

R

ROC	receiver operating characteristic
RT	room temperature

T

TBS	Tris-buffered saline
TBST	Tris-buffered saline with 0.1% Tween-20
TG	triacylglycerol
TNFα	tumor necrosis factor alpha
TOF	time of flight
TRPV4	transient receptor potential vanilloid 4

U

UCP1	uncoupling protein 1
-------------	----------------------

W

WAT	white adipose tissue
iWAT	inguinal white adipose tissue
WT	wildtype

Z

zOTU	zero-radius operational taxonomic unit
-------------	--

ABSTRACT

Brown adipose tissue (BAT) is specialized on producing heat through the metabolization of glucose and fatty acids. This process termed non-shivering thermogenesis (NST) is mediated by the uncoupling protein 1 (UCP1), expressed in mitochondria of brown adipocytes. Activated UCP1 in BAT can increase energy expenditure and facilitate body and fat mass loss. These properties render BAT a promising target to tackle the obesity epidemic. One major limitation in harvesting the potential of BAT is its limited availability especially in obese persons. Recently the presence of a second type of UCP1 expressing adipocyte, the brite (brown-in-white) adipocytes has been established. These cells can derive from direct conversion of white adipocytes in white adipose tissue (WAT) upon stimulation by cold. Conversion of white into brite adipocytes is a promising way to bypass the issue of limited BAT capacity. However, human environmental thermal conditions render UCP1 and thus brown and brite adipocytes by default inactive. Thus, means to increase the abundance of these adipocytes are as crucial as those stimulating UCP1 activity. Omega-3 polyunsaturated fatty acids (n3-PUFA) and multiple lipid derivatives derived from n6- and n3-PUFA have been shown to stimulate recruitment of brown and brite adipocytes in cell culture models. However, the evidence of studies *in vivo* in humans is still scarce and studies in mice yield controversial results. The latter might be due to improper choice of housing conditions in which UCP1 is chronically active and thus do not reflect the human environment.

Analysis of fatty acid metabolites in adipose tissue samples of human and mice housed at temperatures reflecting the human environment demonstrated that the global fatty acid metabolite profile distinguishes between BAT and WAT in mice but not humans. However, some fatty acid metabolites were associated with the abundance of brown and brite adipocytes in both mice and humans. Further, the potential to modulate the abundance of specific lipid derivatives by supplementation of their n6- and n3-PUFA precursors was investigated in mice. The global fatty acid metabolite profile could be modulated by dietary intervention, but these changes were not associated to changes in the potential to recruit brown or brite adipocytes. Studying a novel UCP1 knockout mouse model demonstrated that the abundance of UCP1 in a human-like thermal environment does not influence the susceptibility of mice to diet-induced obesity. A fundamental issue of studying the brown and brite adipocytes in human and mice respectively might be the relatively low abundance in relation to total cell number in tissue homogenates. To address this issue a lipid imaging method was established, enabling the regional investigation of lipid metabolism in WAT and thus may be a valuable tool to investigate changes in lipid metabolism of less abundant cell types.

In general, the presented data corroborates the importance of the thermal environment in murine studies investigating the potential of lipid derived metabolites to recruit UCP1 derived NST.

ZUSAMMENFASSUNG

Braunes Fettgewebe (BAT) ist auf die Produktion von Wärme durch die Verstoffwechslung von Glukose und Fettsäuren spezialisiert. Dieser als zitterfreie Thermogenese (NST) bezeichnete Prozess wird durch das Entkopplerprotein 1 (UCP1) vermittelt, das in den Mitochondrien brauner Fettzellen exprimiert wird. Aktiviertes UCP1 in BAT kann den Energieverbrauch erhöhen und somit die Reduzierung von Körper- und Fettmasse erleichtern. Diese Eigenschaften machen BAT zu einem vielversprechenden Ziel zur Bekämpfung der Adipositas-Epidemie. Eine Haupt-Einschränkung bei der Nutzung des Therapiepotenzials von BAT ist die begrenzte Verfügbarkeit, insbesondere in adipösen Personen. Kürzlich wurde die Existenz eines zweiten Typs UCP1 exprimierender Fettzellen, den „brite“ (braun in weiß) Adipozyten, bestätigt. Diese Zellen können unter anderem aus der direkten Umwandlung von in weißem Fettgewebe (WAT) lokalisierten weißen Adipozyten, durch die Stimulation mit Kälte, entstehen. Die Umwandlung von weißen in „brite“ Adipozyten ist eine vielversprechende Möglichkeit, das Problem der begrenzten BAT-Kapazität zu umgehen. Allerdings sind sowohl UCP1 wie auch braune und „brite“ Adipozyten in der gewöhnlichen thermischen menschlichen Umwelt inaktiv. Daher sind Möglichkeiten die Anzahl dieser Fettzellen zu erhöhen ebenso wichtig wie solche, die die UCP1-Aktivität stimulieren. Sowohl mehrfachungesättigte omega-3 Fettsäuren (n3-PUFA) und mehrere von n6- und n3-PUFA abgeleitete Metabolite können die Rekrutierung von braunen und „brite“ Adipozyten im Zellkulturmodell stimulieren. Untersuchungen *in vivo* am Menschen sind jedoch bisher selten und Studien an Mäusen liefern widersprüchliche Ergebnisse. Letzteres könnte durch die unsachgemäße Wahl der Haltungsbedingungen bedingt sein, in denen UCP1 chronisch aktiv ist und somit nicht die menschliche Situation darstellen.

Die Analyse von Fettsäuremetaboliten in Fettgewebeproben von Menschen sowie Mäusen, die bei an die menschliche Umgebung angepassten Temperaturen gehalten wurden, zeigte, dass sich das globale Profil der Fettsäuremetabolite von BAT und WAT bei Mäusen, aber nicht aber bei Menschen unterscheidet. Einige Fettsäuremetabolite waren jedoch sowohl bei Mäusen als auch bei Menschen mit der Anzahl von braunen und „brite“ Adipozyten assoziiert. Außerdem wurde das Potenzial zur Beeinflussung der Abundanz spezifischer Lipidderivate durch Zuführung ihrer n6- und n3-PUFA-Vorstufen in Mäusen untersucht. Das globale Profil der Fettsäuremetabolite konnte durch eine Ernährungsintervention beeinflusst werden. Dies war jedoch nicht mit Veränderungen des Potenzials zur Rekrutierung brauner oder „brite“ Adipozyten verbunden. Die Untersuchung eines neuen UCP1 „knockout“ Mausmodells zeigte, dass die UCP1 Menge allein, in einer der menschlichen thermischen Umwelt angepassten Umgebung, keinen Einfluss auf die Entstehung von Diät-induzierter-Adipositas hat. Ein grundsätzliches Problem bei der Untersuchung der braunen und „brite“ Adipozyten bei Menschen und Mäusen ist ihre relativ geringe Anzahl im Verhältnis zur Gesamtzellzahl im homogenisierten Gewebe. Um dieses Problem

zu umgehen, wurde ein bildgebendes Verfahren zur regionalen Untersuchung des Lipidstoffwechsels in WAT etabliert. Diese Methode stellt ein wertvolles Werkzeug zur Untersuchung von Veränderungen im Lipidstoffwechsel von weniger häufig vorkommenden Zelltypen dar.

Zusammengefasst bestätigen die präsentierten Daten die Bedeutung der thermischen Umgebung in murinen Studien, die sich mit dem Potenzial von Lipidmetaboliten zur Rekrutierung von UCP1 abhängiger NST untersuchen.

1 INTRODUCTION

1.1 OVERWEIGHT AND OBESITY

The prevalence of overweight and obesity has risen tremendously during the past decades and continues to grow to epidemic proportions. Overweight and obesity are defined by the body mass index (BMI), ranging from 25 kg/m^2 to $< 30 \text{ kg/m}^2$ for overweight and $> 30 \text{ kg/m}^2$ for obesity. Obesity is associated with several comorbidities, collectively termed *metabolic syndrome* (MetS) including cardiovascular disease and type 2 diabetes mellitus. About a quarter of adults worldwide was obese in 2016, accounting for about 3 million premature deaths (OECD 2019). This leads to a remarkable socioeconomic impact e.g., decreasing income by 2% and increasing healthcare costs by 4% per point BMI $> 30 \text{ kg/m}^2$ (Kjellberg et al. 2017).

Obesity results from a chronic positive energy balance, with energy intake exceeding energy expenditure. Consequently, obesity treatments aim to reduce energy intake and simultaneously increase energy expenditure to generate a negative energy balance, thus induce weight loss. The currently two most efficient treatment options are lifestyle interventions and/or bariatric surgery. Lifestyle interventions aim to increase physical activity in conjunction with dietary adaptation to decrease energy intake. While lifestyle interventions are very effective their success is limited due to poor adherence to the program influenced by multiple parameters (Burgess, Hassmén, and Pumpa 2017). Bariatric surgery is currently mostly used in severe cases of obesity (BMI $> 40 \text{ kg/m}^2$) to facilitate weight loss by decreasing gastric volume and altering gastrointestinal signaling (Pucci and Batterham 2019). Both strategies however face a common issue – the long-term maintenance (> 5 years) of the achieved weight loss (Anderson et al. 2001). Besides potentially low adherence of individuals to recommended lifestyles one of the underlying mechanisms is a substantial reduction of energy expenditure in response to weight loss (Rosenbaum et al. 2008). Pharmacological options supporting weight loss and its maintenance exclusively target energy intake (Ruban et al. 2019).

Consequently, means to increase energy expenditure besides physical activity are essential to complement current treatment options. Here, progress in the understanding in adipose tissue metabolism during the last decade, especially the re-discovery of brown adipose tissue (BAT) in adult humans (Nedergaard, Bengtsson, and Cannon 2007; Cypess et al. 2009; van Marken Lichtenbelt et al. 2009; Virtanen et al. 2009), has opened potential novel therapeutic strategies.

1.2 ADIPOSE TISSUE – WHITE, BRITE AND BROWN

Obesity is characterized by an excessive accumulation of adipose tissue due to a chronic excess of energy intake. Consequently, understanding adipose tissue physiology is a key factor to understand the etiology of obesity.

The characteristic cell type of adipose tissue are adipocytes. So far, three distinct types of adipocytes - white, brite and brown - have been characterized. White adipocytes are responsible for storage of excessive energy in form of triacylglycerol (TG). Their accumulation in the subcutaneous and visceral adipose tissue is colloquially known as “fat”. Morphologically, these adipocytes are characterized by a unilocular lipid droplet framed by a thin round rim of cytoplasm and a squeezed nucleus (Figure 1). In contrast, brown adipocytes, the second type of adipocytes have multiple lipid droplets (multilocular) and a round nucleus (Figure 1). The difference in morphology indicates the different functions these cells have. In contrast to white adipocytes, brown adipocytes do not primarily store energy but are involved in thermoregulation through the dissipation of heat (see chapter 1.3). The third type of adipocyte has been “established” in the last decade. The brite (brown-in-white) or “beige” adipocytes are characterized by an intermediate appearance of brown and white adipocytes (Figure 1). Brite adipocytes emerge within white adipose tissue (WAT) upon sympathetic stimulation via β_3 -adrenergic receptor signaling. Although their primary function is still a matter of debate, brite adipocytes like brown adipocytes, can dissipate heat, thus contribute to energy expenditure.

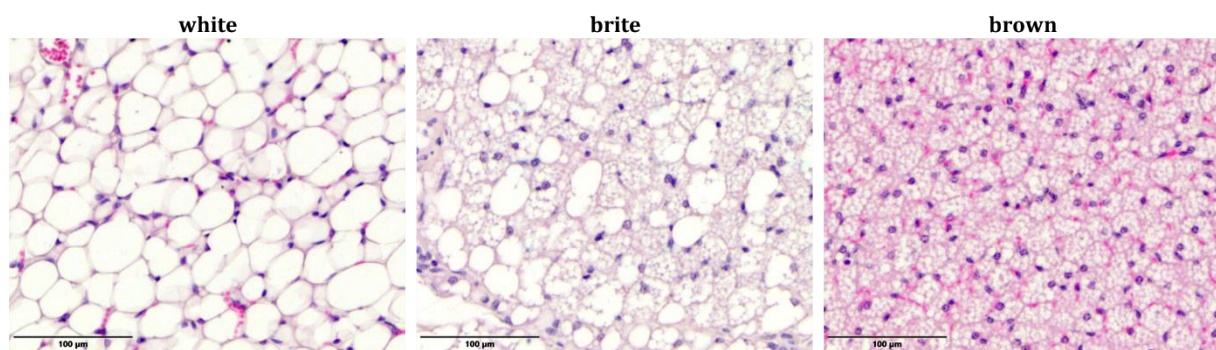


Figure 1: Morphology of white, brite and brown adipocytes.

Images of white and brown adipose tissue sections demonstrating characteristic morphology of white, brite and brown adipocytes. Nuclei stained in blue (hematoxylin) and cytoplasm stained in red (eosin).

Brite adipocytes are of major interest in the field of obesity treatments as there is evidence that these cells partly derive from direct conversion of white adipocytes (Rosenwald et al. 2013; Y. H. Lee et al. 2015). This would have double benefit, since not only these cells are able to increase energy expenditure but also directly decrease the number of white adipocytes thus ameliorating the effects of excessive fat accumulation.

1.3 UCP1-MEDIATED NON-SHIVERING THERMOGENESIS

Adaptive thermogenesis enables endothermic animals to maintain a constant body temperature over a broad range of environmental conditions. Within the thermoneutral zone of animals body core temperature can be maintained without use of active mechanisms (Gordon 2012). Below this temperature zone animals need to recruit heat producing mechanisms to cope with increased heat loss to the environment. This adaptive heat production is mediated by shivering and non-shivering thermogenesis (NST). Shivering is an adenosine triphosphate (ATP) driven process, producing heat by repeated contraction of skeletal muscle without physical work. Shivering is needed once NST, mediated by BAT, is not sufficient (Cannon and Nedergaard 2004).

NST in BAT is activated by the sympathetic nervous system upon cold exposure through the release and binding of the neurotransmitter noradrenaline (NA) to adrenergic receptors expressed by brown adipocytes (Figure 2). Adrenergic receptors constitute a group of G-protein coupled receptors of which the β_3 -adrenergic subtype is predominantly expressed by rodent brown adipocytes. Ligand binding to β_3 -adrenergic receptors activates a signaling cascade ultimately leading to increased lipolysis and activation of UCP1 (Figure 2). Briefly, the activation of adenylyl cyclase (AC) by β_3 -adrenoreceptor signaling, leads to increased levels of the second messenger cyclic adenosine monophosphate (cAMP). Subsequently, activation of protein kinase A (PKA) by cAMP results in the phosphorylation of the enzymes hormone sensitive lipase (HSL)(Shih and Taberner 1995) and perilipin (Chaudhry and Granneman 1999). Phosphorylation of perilipin liberates the coactivator protein, comparative gene identification-58 (CGI-58), in turn activating adipose triglyceride lipase (ATGL) (Zimmermann et al. 2004; Lass et al. 2006). The lipolytic activity of HSL and ATGL releases free fatty acids from TG, diacylglycerols (DG). Free fatty acids are translocated into mitochondria, where they activate uncoupling protein 1 (UCP1) and serve as fuel for mitochondrial β -oxidation.

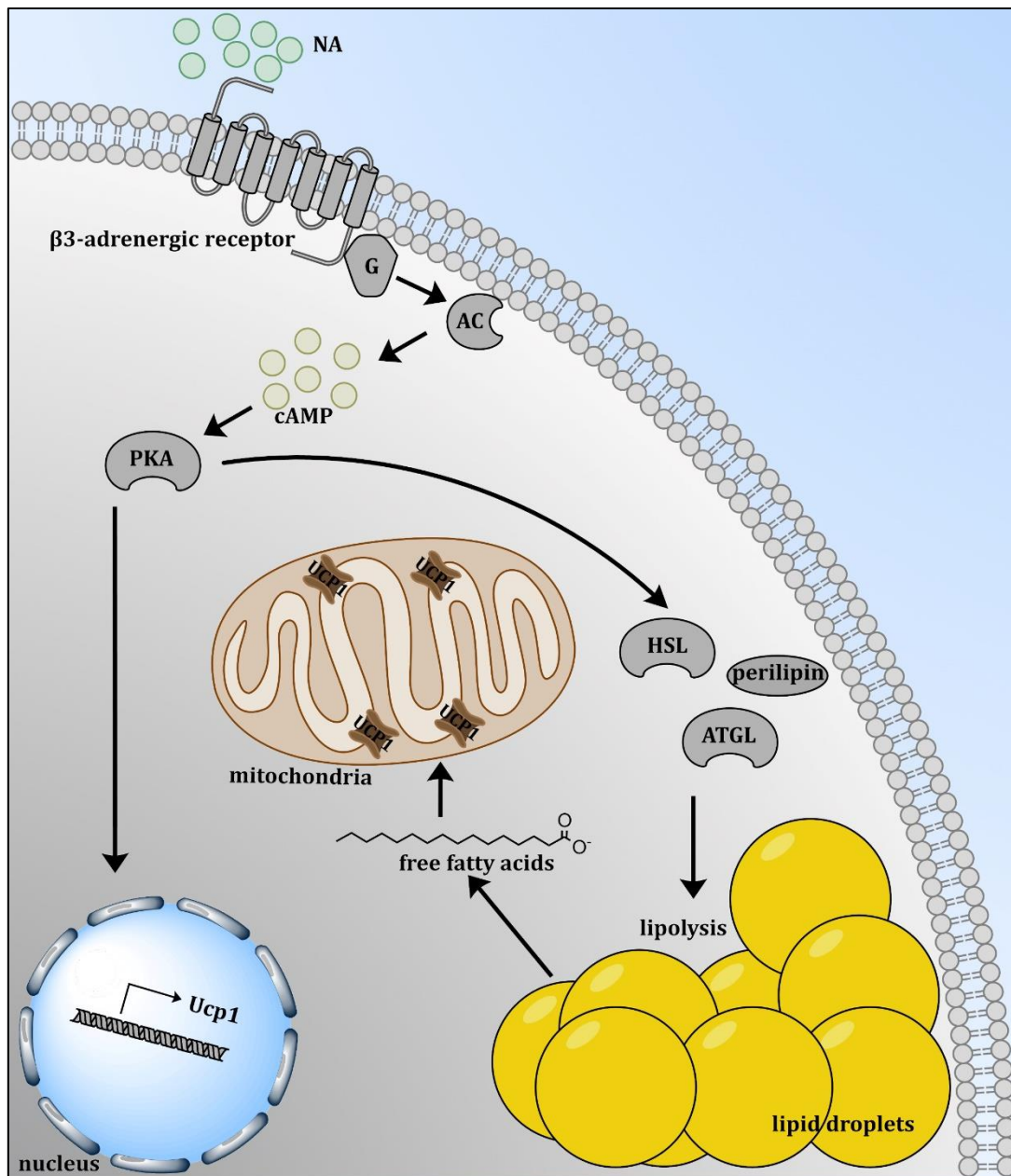


Figure 2: Activation of brown adipocytes by β_3 -adrenergic signaling.

Noradrenaline (NA) is released and binds to the G-protein coupled β_3 -adrenergic receptor. The resulting activation of adenylyl cyclase (AC) leads to increased cyclic adenosine monophosphate (cAMP) levels and the activation of protein kinase A (PKA). PKA induces UCP1 gene transcription in the nucleus and lipolysis by phosphorylating the enzyme hormone sensitive lipase (HSL), perilipin and activation of the enzyme adipose triglyceride lipase (ATGL). Free fatty acids released from lipid droplets by lipolysis are transported to mitochondria and activate UCP1.

UCP1 is exclusively expressed in the inner mitochondrial membrane of brite and brown adipocytes and is the key protein responsible for NST. Briefly, the degradation of free fatty acids derived from lipolysis by β -oxidation and the tricarboxylic acid cycle results in the production of the reduction equivalents NADH and FADH_2 . The electron transport chain uses the energy of these molecules to pump protons from the mitochondrial matrix in the intermembrane space. The resulting concentration gradient between mitochondrial matrix and intermembrane space

generates a proton motive force, that usually is utilized to produce the universal energy currency ATP. In activated brown and brite fat cells however, the proton motive force is uncoupled from ATP production by UCP1 and dissipated in form of heat (Figure 3). The exact mechanism by which UCP1 transports proton is still not fully resolved and several models are discussed (Bertholet and Kirichok 2019). According to the most recent model, UCP1 is activated by free fatty acids, that bind to the substrate binding site of UCP1 by hydrophobic interaction. Subsequently, protons bind to the carboxylic headgroup of the fatty acids in the intermembrane part of UCP1. This leads to a conformational change of UCP1 and the release of the proton in the mitochondrial matrix (Fedorenko, Lishko, and Kirichok 2012).

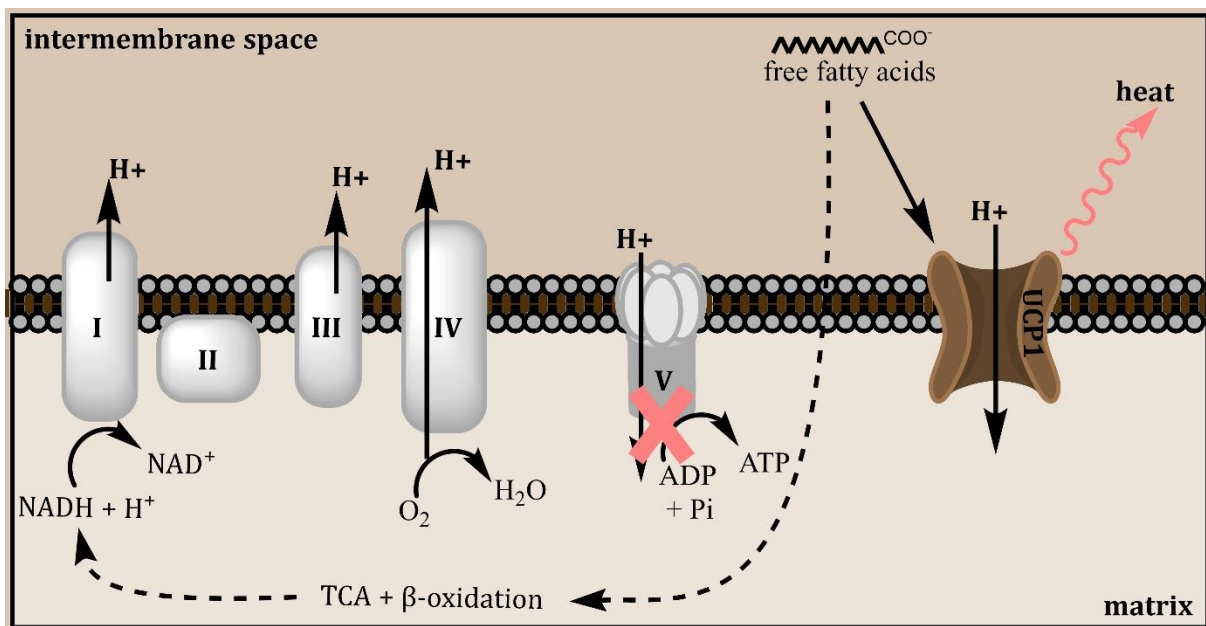


Figure 3: Generation of the proton gradient and utilization by UCP1.

Energy from the reduction equivalent (NADH + H⁺) generated by the tricarboxylic acid cycle (TCA) and β-oxidation of free fatty acids released by lipolysis is used by three complexes (I, II, IV) of the electron transport chain to transport protons (H⁺) over the inner mitochondrial membrane. Free fatty acids activate UCP1 which bypasses adenosine triphosphate (ATP) production (V) and uses the proton gradient to dissipate heat.

In addition to its lipolysis promoting action, PKA rapidly induces transcription of the UCP1 gene via activation of the cAMP response element binding protein (CREB) (Rim and Kozak 2002). Besides CREB, UCP1 gene expression is regulated by transcription factors that bind and regulate nuclear hormone receptors in the promoter region of the UCP1 gene. These include the peroxisome proliferator-activated receptors alpha (PPAR α) and gamma (PPAR γ) (F. Villarroya, Peyrou, and Giralt 2017). Both of these receptors are responsive to several natural compounds like fatty acid derivatives (Ghandour et al. 2016).

1.4 RELEVANCE OF LIPIDS IN HUMAN NUTRITION AND AS FUNCTIONAL MOLECULES IN ADIPOSE TISSUE METABOLISM

Lipids are a heterogeneous group of chemical compounds with a single shared feature, that is being insoluble in water. Consequently, lipids execute a plethora of different functions including energy production (fatty acids) and the storage of energy (e.g. TG) as well as the formation of biological membranes (phospholipids) or transport molecules for other hydrophobic substances (cholesteryl ester). Apart from a few, most lipids either contain or are derived from fatty acids. Fatty acids consist of a hydrocarbon-chain of varying length with a polar carboxylic headgroup ($\text{CH}_3\text{-(CH}_2\text{)}_n\text{-COOH}$) (Figure 4 A). As demonstrated on the example of brown adipocyte activation, fatty acids not only are energy substrates but also functionally implied in biological processes. One important group of fatty acids implied in various biological processes are polyunsaturated fatty acids (PUFA). PUFA are divided into two groups - n6-PUFA and n3-PUFA - depending on the position of first double bond at the third carbon (counted from the end most distant from the carboxylic headgroup) (Figure 4 B). The n3-PUFA, eicosapentaenoic acid (EPA), docosahexaenoic acid (DHA) and α -linolenic acid (ALA) as well as the n6-PUFAs arachidonic acid (AA) and linoleic acid (LA) are an essential element of human nutrition as mammalian cells are not able to (ALA, LA) or have limited capacity to (EPA, DHA, AA) produce these fatty acids (Plourde and Cunnane 2007).

A balanced intake dietary of n6- and n3-PUFA is associated with health benefits while an increase in the n6/n3 ratio is associated with obesity and inflammation (Simopoulos 2016). Increased dietary uptake of n3-PUFA increases the expression of UCP1 in brown and brite adipocytes (M. Kim et al. 2015; J. Kim et al. 2016; Bargut, Silva-e-Silva, et al. 2016; Bargut, Souza-Mello, et al. 2016). Additionally, a group of oxidized n6- and n3-PUFA metabolites, termed oxylipins, is discussed to stimulate brown and brite adipocyte function (Maurer et al. 2019). Oxylipins are generated via one of three enzymatic pathways (by Gabbs et al. 2015)(Figure 4 B). Cyclooxygenase (COX) (also termed prostaglandin H synthase (PGHS)), responsible to produce prostanoids that are important mediators of inflammatory processes. The group of lipoxygenase enzymes (LOX) generate hydroperoxyl-, epoxy- and hydroxy fatty acids by introducing dioxygen into PUFA. Lastly, cytochrome P450 (CYP450) enzymes either generate oxylipins similar to LOX by hydroxylase activity or epoxy fatty acids by epoxygenase activity. Their association to adipose tissue metabolism relies on the affinity of several oxylipins to receptors involved in adipogenesis such as PPAR γ , or G-protein coupled receptors (Barquissau et al. 2017). Elevated UCP1 expression is observed *in vitro* upon treatment with carbaprostacyclin, a stable analogue of the COX derived oxylipin prostacyclin (PGI₂) (Vegiopoulos et al. 2010; Bayindir et al. 2015). Or the LOX derived 9-hydroxyoctadecadienoic acid (9-HODE) and 13-hydroxyoctadecadienoic acid (13-HODE) (Y. H. Lee et al. 2016).

Furthermore, the CYP450 derived 12,13-dihydroxy-9Z-octadecenoic acid (12,13-DiHOME) is a potent activator of fatty acid uptake by BAT and enhances cold tolerance in vivo (Lynes et al. 2017). A second group of PUFA derived molecules implied in energy balance regulation are endocannabinoids (Figure 4 B). The involvement of endocannabinoids in central regulation of energy balance by signaling via the cannabinoid receptor 1 (CB1) is well established (Matias and Di Marzo 2007). CB1 inhibition decreases energy expenditure in mice (Bajzer et al. 2011; Boon et al. 2014) and increased levels of cannabinoids in BAT and WAT after cold exposure or stimulation with the β_3 -adrenergic receptor agonist CL-316,243 suggest a negative feedback mechanism on thermogenic capacity (Krott et al. 2016).

Conclusively, the accumulating evidence suggests that lipid derivatives can promote the recruitment of brown and brite adipocytes or stimulate their function. In addition, with the potential to modulate their abundance via nutrition (Ostermann et al. 2017; Schebb et al. 2014; Balvers et al. 2012) these properties render this class of molecules prospective targets to treat obesity.

1.5 AIMS

Although functional BAT has been confirmed in adult humans, some major challenges persist in order to harness its potential in the fight against obesity. BAT in adult humans is negatively associated with BMI (van Marken Lichtenbelt et al. 2009) and age (Cypess et al. 2009). Thus, the target group for obesity treatment has little BAT to begin with. This is aggravated by the fact that sole recruitment of brown and brite adipocytes is not sufficient as UCP1 is constitutively inactivated. Activation of substantial BAT thermogenesis is possible by acute and chronic mild cold exposure (Yoneshiro et al. 2013; van der Lans et al. 2013; Chondronikola et al. 2014). However, this is not a suitable therapeutic option as freezing is uncomfortable and thus compliance to the treatment would almost certainly be low. Thus, alternative mechanisms to induce UCP1 are necessary.

One possible solution might be dietary interventions increasing the abundance of lipids that induce UCP1. Therefore, the aim of the presented work was to identify and characterize novel lipid metabolites that are associated with the activity of UCP1 to provide a basis for the development of dietary interventions that stimulate UCP1 expression and/or activity.

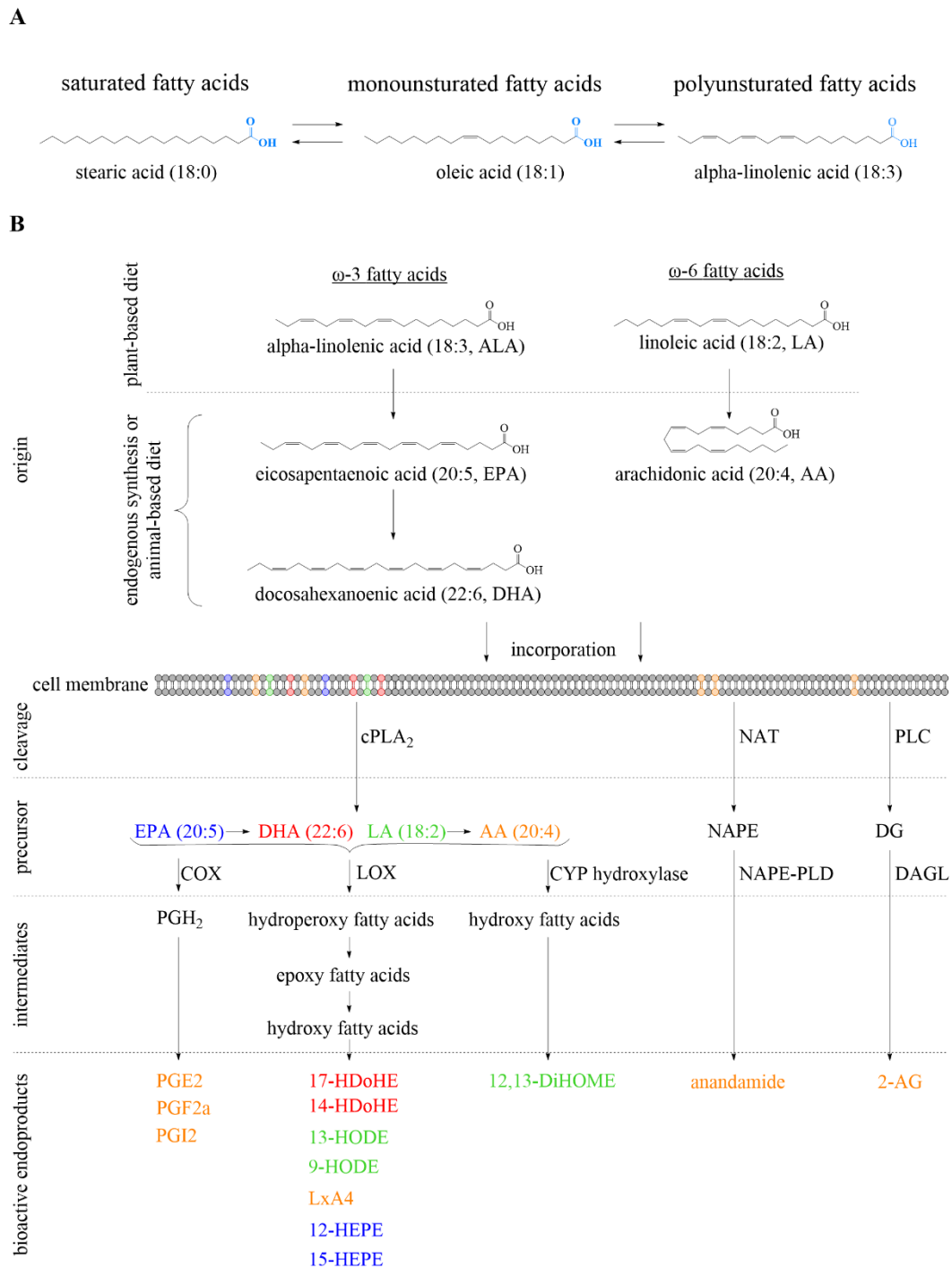


Figure 4: Structure of fatty acids and the synthesis of oxylipins and endocannabinoids.

(A) Fatty acids consist of a hydrocarbon chain (black) and a carboxylic headgroup (blue). Depending on the number of double bonds (DB) in the hydrocarbon chain, fatty acids are grouped in saturated (0 DB), monounsaturated (1 DB) and polyunsaturated (≥ 2 DB) fatty acids, that can be interconverted in each other. (B) Fatty acids derived from plant- or animal-based diets are incorporated into cell membranes as phospholipids. Various cytosolic enzymes can release fatty acids, N-arachidonoyl-phosphatidylethanolamine (NAPE) or diacylglycerols (DG) from membranes. Depending on the enzymatic pathway a variety of different oxylipins and endocannabinoids are produced from the precursor fatty acid. Identical colors indicate the precursor fatty acid. cPLA₂ = cytosolic phospholipase A₂; NAT = N-acyltransferase; PLC = phospholipase C; COX = cyclooxygenase; LOX = lipoxygenase; CYP = cytochrome P450; NAPE-PLD = NAPE phospholipase D; DG = diacylglycerol; DAGL = DAG lipase (adapted and modified from (Maurer et al. 2019)).

2 GENERAL MATERIAL AND METHODS

This chapter provides the rational and additional information for the key materials and methods applied in the chapters 3-6.

2.1 ANIMALS

All animal breeding and experimentations were conducted in the specific-pathogen-free animal husbandry facilities of the Technical University of Munich registered at the local authorities according to §11 of the German Animal Welfare Act (AZ32-568, 01/22/2015). Prior to the start of the experiments mice were housed in groups in individual ventilated cages at an ambient temperature of 23°C ±1°C with *ad libitum* access to chow food (Cat# V1124-300, Ssniff Spezialdiäten GmbH, Soest/Germany) and water. At the beginning of all experiments 8-week-old mice were switched to a chemically defined control diet (CD, Cat# S5745-E720, Ssniff Spezialdiäten GmbH, Soest/Germany), assigned to experimental groups and transferred to climate cabinets (HPP750life, Memmert, Schwabach/Germany). Experiments in climate cabinets were conducted in an open cage system at 55% relative humidity, the respective experimental temperature and a 12/12 hour light/dark cycle (5:00 am/pm CET). An outline of all experimental protocols is given in Figure 5.

2.1.1 Studying UCP1-dependent thermogenesis – a matter of temperature

To interpret the effect of dietary intervention on the recruitment of brown and brite adipocytes, ambient temperature is a crucial factor. The thermoneutral zone of mice is 29-31°C, thus standard housing conditions (23°C ±1°C) of mice are accompanied by a chronic activation of thermoregulatory mechanisms. The major thermogenic mechanism in mice is UCP1-mediated NST in BAT. Studying mice below thermoneutral temperatures aggravates the transfer of results to human context, as humans – due to heating and clothing – live at thermoneutral conditions most of their live. Additionally, UCP1 knockout (UCP1-KO) mice are able to recruit alternative thermogenic mechanisms if housed at temperatures below thermoneutrality. Consequently, all animal experimentation in this work, investigating the effect of dietary fatty acid supplementation on recruitment of thermogenic capacity (Figure 5 C-E) and contribution of UCP1 to the development of diet-induced obesity (DIO) (Figure 5 F), were conducted at 30°C.

2.1.2 Temperature dependent changes in oxylipin and lipid metabolism

Changes in oxylipin metabolism associated to NST (Figure 5 A) investigated in Chapter 3 were studied using C57BL/6J mice acclimatized to 5°C or 30°C for one week.

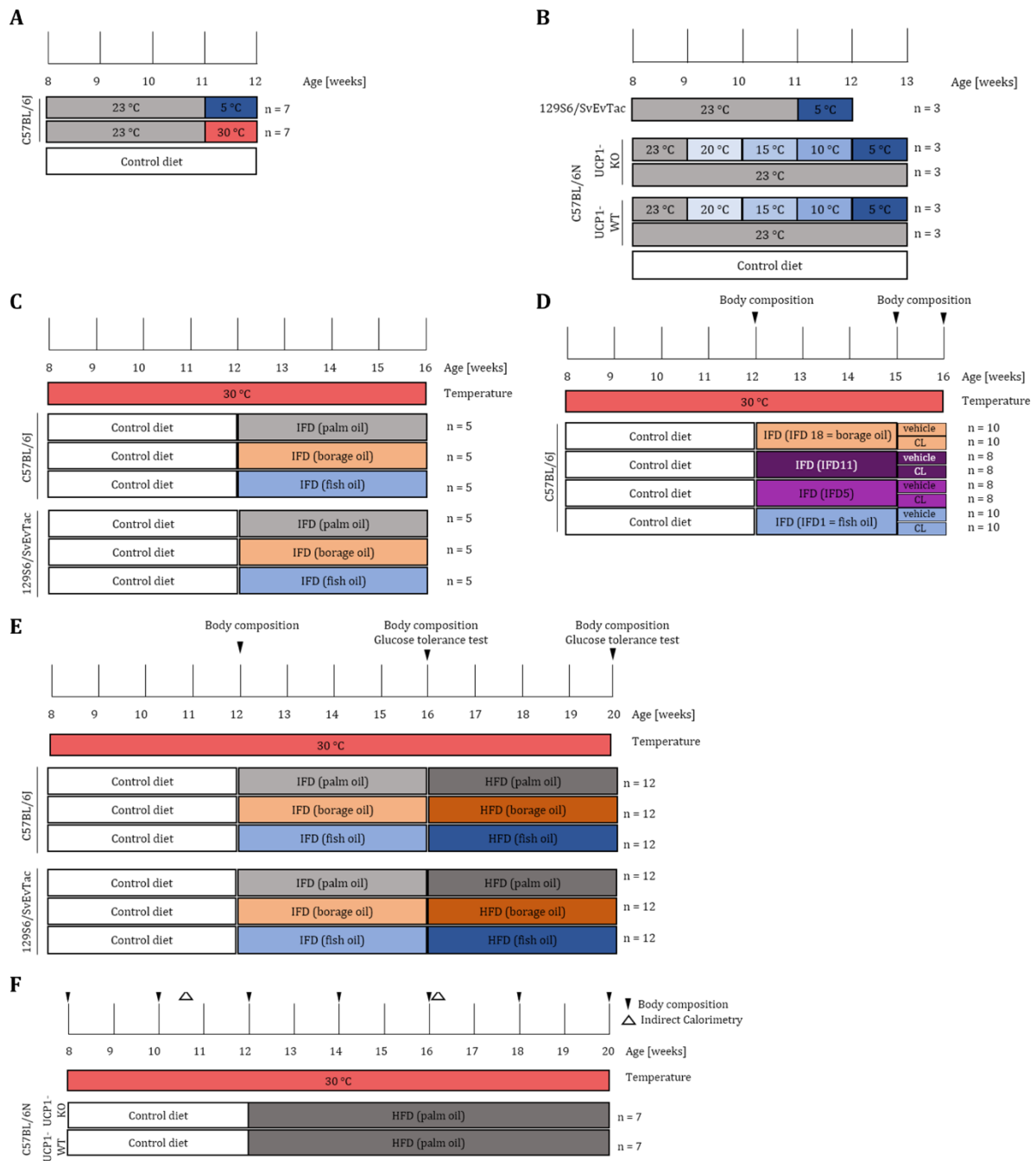


Figure 5: Overview of the animal experimentation protocols.

Experimental protocols corresponding to (A) chapter 3, (B) chapter 6, (C-E) chapter 4, and (F) chapter 5. The respective mouse strains (C57BL/6J, 129S6/SvEvTac or UCP1 wildtype (UCP1-WT) and knockout (UCP1-KO) on a C57BL/6N background), used for the experiments are indicated on the left side of each experimental overview. Group sizes are indicated on the right side of each experimental overview ($n = \#$). Temperature settings of the climate cabinets are provided below the timeline. All mice received control diet at the beginning of the experiment (white bars). In feeding trials (B-E) mice subsequently were switched to experimental diets containing either ~31% (intermediate-fat diet = IFD) or ~48% (high-fat diet = HFD) energy from fat. The main fat source for each diet is indicated in parentheses behind each diet. Numbers behind experimental diets in (C) indicate the ratio of n6/n3 PUFA. To stimulate the recruitment of brown and brite adipocytes at thermoneutrality (C) mice received daily injections of the β_3 -adrenergic receptor agonist CL-316,243 (CL) or saline (vehicle) as control. (B-D modified from (Maurer et al. 2021)).

Changes in lipid metabolism associated to the recruitment of brite adipocytes (Figure 5 B) investigated in Chapter 6 were conducted on 129S6/SvEvTac as well as on UCP1 wildtype (UCP1-WT) and knockout (UCP1-KO) animals on a C57BL/6N background. After 4-weeks acclimatization at 23°C, 129S6/SvEvTac mice were directly transferred to 5°C as they show a high propensity towards browning and thus can cope with this acute temperature drop. The lack of NST capacity due to the absence of UCP1 leads to an inability of UCP1-KO mice to survive acute cold. Yet, UCP1-KO mice can be acclimatized to cold by stepwise reduction of ambient temperature. Consequently, the association of cold induced changes in lipid metabolism with the presence of UCP1 (Figure 5 B), was studied by acclimatizing UCP1-WT and UCP1-KO mice to cold by gradually decreasing ambient temperature each week from 23°C, 20°C, 15°C, 10°C and finally to 5°C for one week.

2.1.3 Studying the effect of dietary fatty acids on recruitment of brown and brite adipocytes

For all feeding trials (Figure 5 C-F) mice were switched to experimental diets after 4 weeks of CD feeding. All diets contained at least 50 g/kg soybean oil (Table 1) and were produced by Ssniff Spezialdiäten GmbH.

Table 1: Nutrient composition of diets. (Adapted from Maurer et al. 2021)

	type of diet		
	CD	IFD	HFD
gross energy [MJ/kg]	17.8	19.7	23.0
metabolizable energy [MJ/kg]	15.3	17.2	19.6
protein [MJ%]	23	20	18
fat [MJ%]	13	31	48
carbohydrate [MJ%]	64	49	34
total protein [g/kg]	240	240	240
casein	240	240	240
total fat [g/kg]	50	140	250
soybean oil	50	50	50
*experimental oil		90	90
palm oil			110
total carbohydrate [g/kg]	633.9	543.9	433.9
corn starch	477.9	387.9	277.9
sucrose	50	50	50
maltodextrin	56	56	56
cellulose	50	50	50
other [g/kg]	76.1	76.1	76.1
butylated hydroxytoluene	0.1	0.1	0.1
l-cystine	2	2	2
choline chloride	2	2	2
vitamins	12	12	12
minerals	60	60	60

*Borage oil, fish oil, a proportionate mixture of both oils, or palm oil were used as experimental fat sources at a total concentration of 90 g/kg. Control diet (CD), intermediate-fat diet (IFD), high-fat diet (HFD).

The effect of dietary fatty acid supplementation on lipid metabolism (Figure 5 C) was studied by feeding mice intermediate-fat diet (IFD) providing ~31% energy from fat, supplemented with 90 g/kg of experimental oils containing different amount of n6- and n3-PUFA (Table 1). Palm oil (Cat# S5745-E141) was used as saturated fatty acid control, while borage (Cat# S5745-E142) and fish oil (Cat# S5745- E143) were supplemented to see the effect of high n6- or n3-PUFA, respectively. Commercial fatty acid analysis was conducted (Research Center Weihenstephan for Brewing and Food Quality) to obtain fatty acid profiles of the diets (Figure 6).

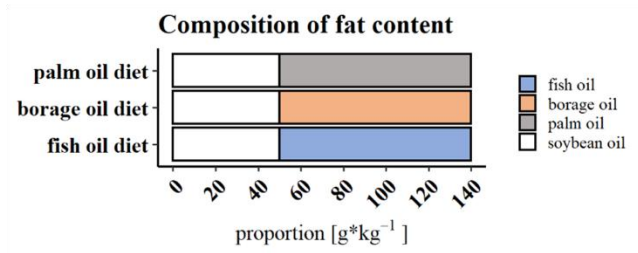
The impact of different n6/n3 ratios in the recruitment of brown and brite adipocytes (Figure 5 D) was investigated with IFDs containing 80 g/kg borage oil + 10 g/kg fish oil (Cat# S5745-E152) or 60 g/kg borage oil + 30 g/kg fish oil (Cat# S5745-E153) in addition to the pure fish oil (Cat# S5745- E143) and borage (Cat# S5745-E142) oil IFDs. Commercial fatty acid analysis was conducted (Bavarian Center for Biomolecular Mass Spectrometry) to obtain fatty acid profiles of the diets (Figure 7). During the last week of the nutritional intervention, mice received daily intraperitoneal injections of either CL-316243 or saline (vehicle) at the same time of day. CL-316,243 is a selective β_3 -adrenergic receptor agonist, thus stimulates the recruitment of brown and brite adipocytes (Cannon and Nedergaard 2004). Stock solutions were prepared diluting CL-316,243 (Cat# ab144605, abcam/UK) in saline (B. Braun Melsungen AG, Melsungen/Germany) at a concentration of 0.04 $\mu\text{g}/\mu\text{l}$. Aliquots of CL-316,243 and saline stored at -20°C and fresh aliquots were thawed every day. Body mass was measured every day prior to the administration of CL-316,243 to calculate the injection volume for a dose of 0.2 mg/kg body mass. Volumes of vehicle treated mice were calculated identically, assuming a CL-316,243 concentration of 0.04 $\mu\text{g}/\mu\text{l}$.

The effect of fish oil on DIO (Figure 5 E) was studied by feeding high-fat diet (HFD) providing ~ 48 % from fat, supplemented with 110 g/kg palm oil in addition to 90 g/kg of either borage oil (Cat# S5745-E146), fish oil (Cat# S5745-E147) or palm oil (Cat# S5745-E722).

2.1.4 Studying the contribution of UCP1 to the development of DIO

The contribution of UCP1 to protect against DIO (Figure 5 F) was performed on a novel UPC1-KO mouse model. Mice were housed at 30°C to avoid the recruitment of alternative thermogenic mechanisms. Obesity was induced by feeding a HFD (Cat# S5745-E722) for 8 weeks. Indirect calorimetry was performed at two time points to assess energy expenditure over several days during CD and HFD feeding.

A



B

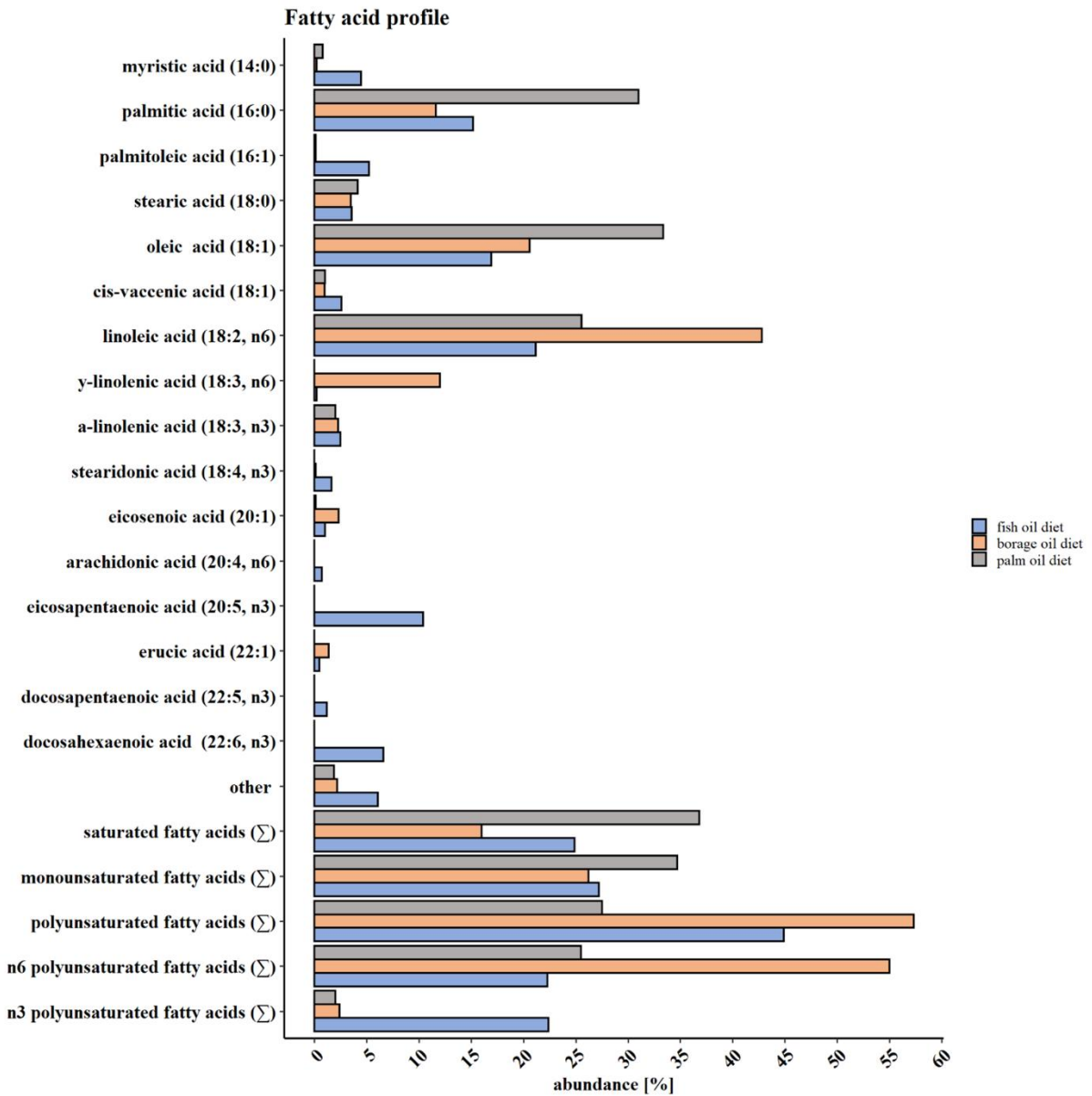
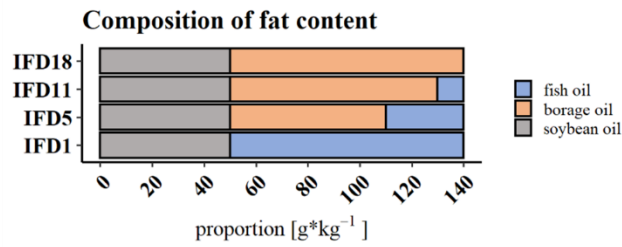


Figure 6: Fat composition and fatty acid profiles of diets based on different fat sources.

(A) Total fat content and (B) fatty acid composition of diets related to experiments Figure 5 B&D. (Modified from (Maurer et al. 2021)).

A



B

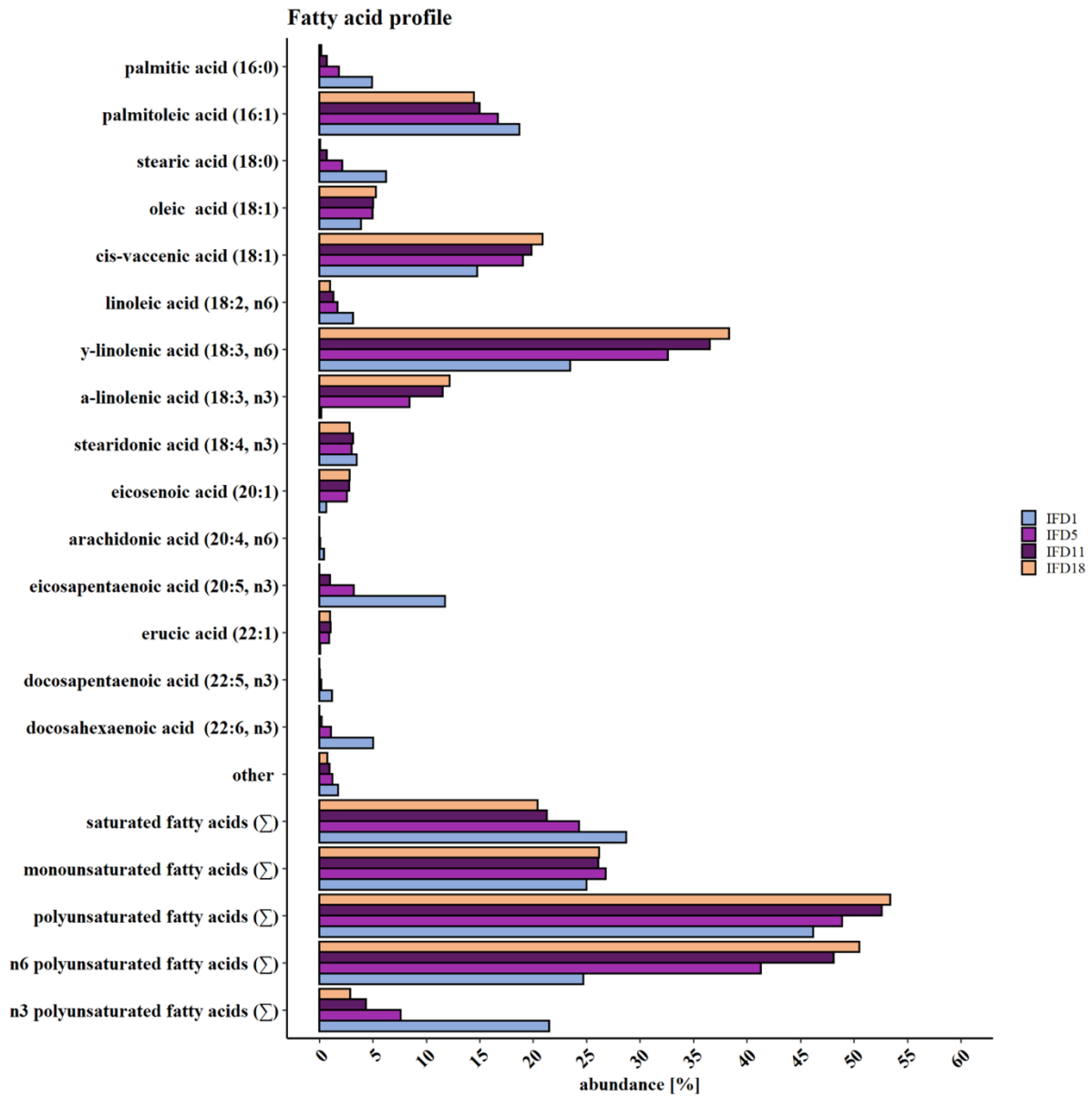


Figure 7: Fat composition and fatty acid profiles of diets with different n6/n3 PUFA ratios. (A) Total fat content and (B) fatty acid composition of diets related to experiment Figure 5 C. (Modified from (Maurer et al. 2021)).

2.2 INDIRECT CALORIMETRY

Indirect calorimetry is a commonly utilized tool to assess energy metabolism and determine thermogenic activity in rodents (Cannon and Nedergaard 2004; Virtue and Vidal-Puig 2013). The maximal capacity of mice for NST can be measured by NA-tests. The injection of a high dose of NA stimulates UCP1-dependent mitochondrial respiration, by activation of β_3 -adrenergic receptors located in BAT. The resulting heat production can be derived by measuring oxygen consumption and carbon dioxide production by the indirect calorimetry.

To assess energy expenditure over several days, mice were transferred in metabolic cages (3-liter volume) in the afternoon, with *ad libitum* access to food and water. Cages were placed in a climate cabinet set to 30°C (TPK 600, Feutron, Greiz/Germany) and connected to the indirect calorimetry system (Lab Master, TSE Systems, Bad Homburg/Germany). Air was continuously extracted from the cages with a flow rate of 33 l/h. A subsample of each cage was analyzed over a period of 1 min every 4-6 minutes, depending on the number of mice in the experiment, dried in a cooling trap and analyzed for oxygen and carbon dioxide content.

Basal metabolic rate (BMR) was measured following the energy expenditure measurement. Therefore, animals were deprived of food in the morning for at least 4 hours. The mean of the four lowest consecutive heat production measurements during the last 90 minutes of fasting was determined as BMR.

NA-tests were performed following determination of BMR. Ambient temperature was reduced to 26°C to avoid hyperthermic reactions in response to NA-injection by facilitating heat loss to the environment. Individual mice were taken out of the climate cabinet, injected intraperitoneally (i.p.) with 1 mg/kg NA (1 mg/kg, Arterenol®, Sanofi, Paris/France) and immediately reconnected to the indirect calorimetry system. Oxygen consumption and carbon dioxide production were continuously measured in 1 min intervals for ~60 min.

Data acquired by indirect calorimetry was processed and analyzed with R (R Core Team 2020). This allows a reproducible, standardized, and transparent analysis without altering the original data as well as the combination of multiple data sets, derived from different cohorts and measurements. Oxygen consumption and carbon dioxide production were calculated based on the comparison between air from cages and an empty reference cage. Heat production was calculated according to the equation (Heldmaier 1975): $heat\ production\ [mW] = (4.44 + 1.43 * respiratory\ exchange\ ratio) * oxygen\ consumption\ [ml/h]$

For graphical representation, oxygen consumption, carbon dioxide production, respiratory exchange ratio and heat production were averaged over a period of 30 minutes. This reduces variability of the data, thus makes it easier to identify trends in the data such as the diurnal pattern

of oxygen consumption (Figure 8 A). The calculations were verified by comparison with the web-based analysis tool CalR (Mina et al. 2018) (Figure 8 B).

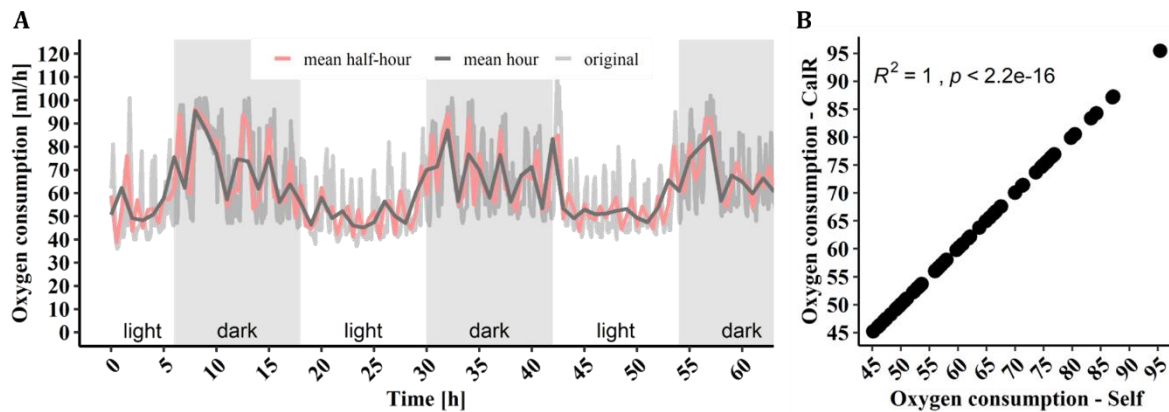


Figure 8: Comparison of different analysis approaches to analyze indirect calorimetry data. (A) Oxygen consumption trajectories of a single mouse. Comparison between raw data (original) and data averaged over a period of 30 min (mean half-hour) or 60 min (mean hour). (B) Comparison of oxygen consumption values averaged over 60 min, obtained from a published analysis tool for indirect calorimetry data (CalR) and the self-calculated (Self). Pearson's correlation coefficient (R^2).

Graphical representation of NA-tests is based on the original data, as averaging leads to a masking of the acute response to NA. The CalR platform by default averages data over a period of 1h. This is an issue for the graphical representation of acute-response measurements such as NA-test with a duration of < 1h. Due to the improved flexibility of the self-written analysis script the web-based tool was dismissed for all indirect calorimetry data analysis.

Maximal NA-induced heat production was calculated as the highest measured value during the 60 min measuring period. Area under the curves (AUC) of heat production served as measure for energy expenditure and were calculated on the original data by the trapezoidal method on the original data.

2.3 TISSUE DISSECTION

At the end of all experiments, mice were killed by carbon dioxide intoxication. Tissues were dissected, weighed and immediately snap-frozen in liquid nitrogen, embedded in carboxymethylcellulose (CMC) on dry ice, or fixed in 10% formalin (Cat# 97.131.000, VWR, Darmstadt/Germany) for histological analysis. Snap-frozen and CMC embedded samples were stored at -80°C until further processing.

2.4 MATRIX-ASSISTED LASER DESORPTION IONIZATION MASS SPECTROMETRY IMAGING

Matrix-assisted laser desorption ionization mass spectrometry imaging (MALDI-MSI) enables the analysis of molecules in their biological environment like sections of tissues. It is frequently used to analyze thermally labile and non-volatile compounds and is therefore suitable for the analysis

of lipids. The basic principle of MALDI-IMS is based on the production of ions, which are desorbed from a matrix-coated sample through bombardment with high-energy laser. The resulting volatile, mostly single charged ions are subsequently separated and detected based on their mass over charge ratio (m/z) in an adjacent time of flight (TOF) mass detector. The movable target plate of the MALDI-MSI device and the focus of the laser beam allow the precise scanning of whole tissue sections in a 100 μm resolution. This results in the acquisition of a two-dimensional map showing the distribution of molecules and their relative intensities.

In this project MALDI-MSI was chosen to study cold-induced changes in tissue lipid metabolism associated to brown and white adipocytes. Therefore, deep-frozen inguinal WAT (iWAT) samples embedded in CMC were sectioned in a cryostat at -35°C . Sections of 16 μm thickness were thaw mounted on conductive ITO-slides (Bruker Daltonik, Bremen/Germany) pre-chilled in the cryostat. Slides were annotated with teaching points using a correction pen (Tipp-Ex, Cat# 8022921, BIC, France) and imaged with a digital single-lens reflex camera (Nikon D5600) mounted on a tripod. Slides were dried at room temperature (RT) in a vacuum desiccator, evacuating for 10 min followed by additional 20 min of drying. Subsequently, matrix application (7 g/l alpha-Cyano-4-hydroxycinnamic acid, 0.2 % trifluoroacetic acid in 60 % acetonitrile) was performed by spraying (ImagePrep, Bruker Daltonik, Bremen) applying the following program:

- (1) Initialization, (2) 0.07 V, 1 cycle, 0.05 V, (3) 0.07 V, 2 cycle, 0.1 V, (4) 0.2 V, 3 cycle, 0.2 V, (5) 0.6/-0.5 V, 4 cycle, 0.3 V.

Coated slides were mounted on a target plate and placed in the MALDI device. The prepared digital image was loaded to the imaging software and aligned with the stage based on the teaching points. Acquisition regions were marked encompassing the visible tissue section based on the digital image. Of note, sections of iWAT are basically transparent and hardly visible on the slide. Editing the digital image by increasing the contrast and pre-marking the circumference of the section in an image manipulation program facilitates the marking of acquisition regions. MALDI-MSI was performed on the MALDI ultrafleXtreme (Bruker Daltonik, Bremen/Germany) with a Smartbeam2-Laser set to "4 large" and a raster size of 100 μm in positive ionization mode.

Data analysis of the MALDI-MSI datasets was performed with the SCiLS software (Version 2016b, Bruker Daltonik Bremen/Germany). Sections of one measurement were loaded as individual regions and combined in one dataset. Baseline correction was performed by convolution with a width of 20.

2.5 IMMUNOHISTOCHEMISTRY

Immunohistochemistry (IHC) was performed on sections of CMC embedded iWAT on polysine-coated slides. Slides were taken from the -20°C and submerged for 5 min in ice-cold tris-buffered

saline (TBS) and subsequently fixed in ice-cold methanol/acetone (1:1) for 10 min. In the following samples were washed twice by submerging slides in TBS for 5 min at RT. Slides were quickly dried to apply liquid barrier marker (Cat# AN92.1, Carl Roth, Karlsruhe/Germany) around the sections. All following steps were performed in a covered staining tray filled with water to limit evaporation of the solutions. Blocking was performed for 2 h at RT in a with TBST (TBS, 0.1% Tween-20) containing 10% normal donkey serum (Cat# S2170-100, VWR, Darmstadt/Germany) and 1% bovine serum albumin (Cat# 8076.3, Carl Roth, Karlsruhe/Germany). Primary antibody against UCP1 (Cat# ab23841, Abcam/UK) was diluted 1:800 in dilution buffer (TBST, 0.25% normal donkey serum, 1% bovine serum albumin) and applied to the samples for 2 h at RT or overnight at 4°C. After primary antibody incubation, samples were washed three times in TBST for 5 min by pipetting. Fluorescence labeling was performed with secondary antibody (Cat# A10040, Thermo Fisher) diluted 1:500 in dilution buffer, in the dark for 2 h at RT or overnight at 4°C. The secondary antibody solution was removed, and samples were stained for 10 min at RT with Hoechst33342 (Cat# 14533, Sigma, Darmstadt/Germany) diluted 1:500 in dilution buffer. Finally, samples were washed three times in TBST for 5 min by pipetting, supplied with mounting medium (Cat# VEC-H-1000-10, Biozol, Eching/Germany), covered by a cover slide and sealed with nail polish.

The validation of the specificity of the signals was performed on control section of BAT of UCP1-WT and UCP1-KO mice. Specificity of the primary antibody was tested by performing the staining on UCP1-KO mice. These mice do not express UCP1 and consequently demonstrate no UCP1 signal (Figure 9). Additionally, specificity of the secondary antibody to UCP1 was confirmed following the staining procedure as described without the addition of the primary antibody against UCP1.

Whole slide scans were generated by acquiring images in x-y-z dimensions, immediately after staining with a fluorescence microscope (Leica DMI6000 B, Filters: Y3 ET, Cat# 11504169 and DAPI ET, Cat# 11504203, Leica Microsystems, Wetzlar/Germany). Movement of the sample in x-y-z images was controlled by the microscopy software (LAS X, Leica Microsystems, Wetzlar/Germany). Images were merged in x-y-dimension to create whole slide images and exported from the microscope software. Subsequently images were identically edited in Fiji (Version 1.53c, (Schindelin et al. 2012)). First images in different z-dimension focus panes were projected on one pane using the extended depth of field (EDOF) algorithm supplied by the EDOF-Easy plugin (Forster et al. 2004). Additionally, brightness and contrast of the resulting image were adjusted identically for all samples.

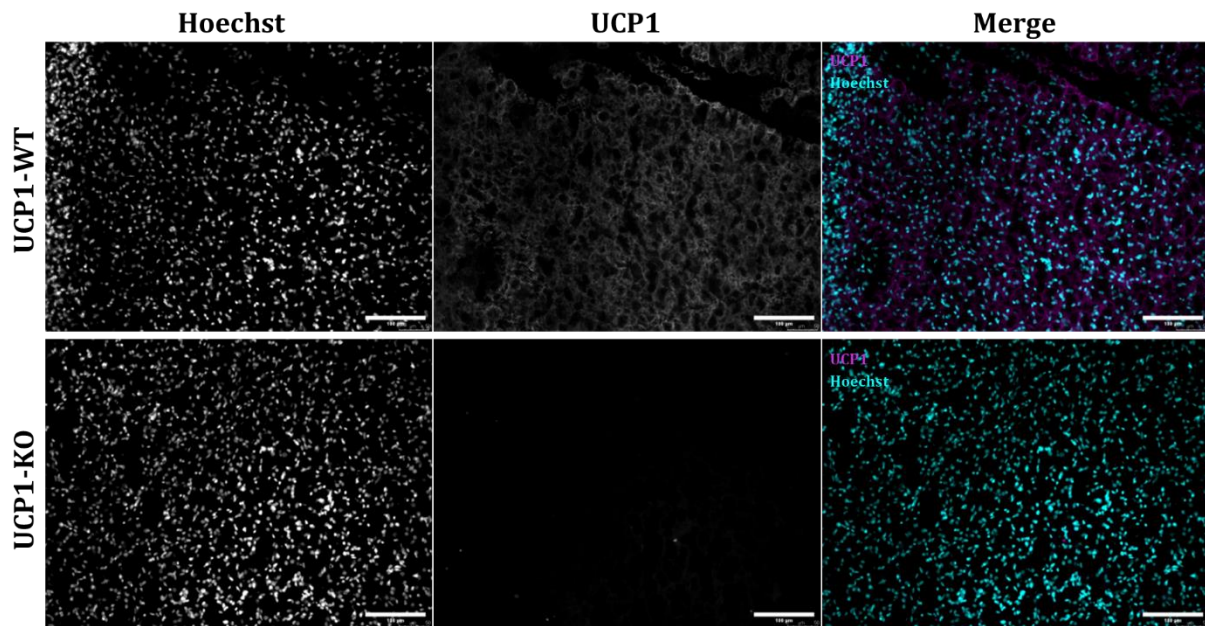


Figure 9: Validation of the UCP1 antibody for immunohistochemistry.

Images of BAT sections from UCP1 knockout (UCP1-KO, lower panel) and UCP1 wildtype (UCP1-WT, upper panel) mice stained with a nuclear stain (Hoechst, left) and an antibody against UCP1 (UCP1, center). The right images represent a composite image of Hoechst (cyan) and UCP1 (magenta). Scale bars indicate 100 μ m.

2.6 STATISTICAL ANALYSIS

Unless otherwise stated statistical analyses were performed with R (R Core Team 2020) and visualized with ggplot2 (Wickham 2016). Principal component analysis (PCA) was performed with the R packages “factoextra” and “FactoMineR”. Significant differences for single comparisons were calculated with the R package “ggpubr”. Two-tailed Student’s t test was applied on data following the assumption of normal distribution. Wilcoxon test was performed for non-normally distributed data. Analysis of variance (ANOVA) and linear model analysis were performed with the R package “stats” and AUC calculation was performed with the R package “DescTools”.

3 FATTY ACID METABOLITE PROFILING REVEALS OXYLIPINS AS MARKERS OF BROWN BUT NOT BRITE ADIPOSE TISSUE

A similar version of this chapter was published: Dieckmann S., Maurer S., Fromme T., Colson C., Virtanen KA., Amri E-Z. and Klingenspor M. (2020) Fatty Acid Metabolite Profiling Reveals Oxylipins as Markers of Brown but Not Brite Adipose Tissue. *Front. Endocrinol.* 11:73. doi: 10.3389/fendo.2020.00073

3.1 ABSTRACT

Metabolites of n6- and n3-PUFA are important signaling molecules implicated in the control of adipogenesis and energy balance regulation. Some of these metabolites belonging to the group of oxylipins have been associated with NST in mice mediated by brown or brite adipose tissue. We aimed to identify novel molecules with thermogenic potential and to clarify the relevance of these findings in a translational context. Therefore, we characterized and compared the oxylipin profiles of murine and human adipose tissues with different abundance of brown or brite adipocytes. A broad panel of 36 fatty acid metabolites was quantified in brown and white adipose tissues of C57BL/6J mice acclimatized to different ambient temperatures and in biopsies of human supraclavicular brown and white adipose tissue. The oxylipin profile of murine brite adipose tissue was not distinguishable from WAT, suggesting that adipose tissue browning *in vivo* is not associated with major changes in the oxylipin metabolism. Human brown and white adipose tissue also exhibited similar metabolite profiles. This is in line with previous studies proposing human BAT to resemble the nature of murine brite adipose tissue representing a heterogeneous mixture of brite and white adipocytes. Although the global oxylipin profile served as a marker for the abundance of thermogenic adipocytes in bona fide brown but not white adipose tissue, we identified 5-Hydroxyeicosatetraenoic acid (5-HETE) and 5,6-Epoxyeicosatrienoic acid (5,6-EET) as individual compounds consistently associated with the abundance of brown or brite adipocytes in human BAT and murine brite fat. Further studies need to establish whether these candidates are mere markers or functional effectors of thermogenic capacity.

3.2 AUTHOR CONTRIBUTIONS

Sebastian Dieckmann performed the molecular analysis, data analysis, data interpretation, and drafted the manuscript.

3.3 INTRODUCTION

Obesity is one of today's major health burdens with a steadily increasing prevalence. It is characterized by excessive fat accumulation and unhealthy expansion of WAT associated with severe comorbidities such as type 2 diabetes and cardiovascular diseases. Obesity is the consequence of a chronic positive energy balance, a state where energy intake exceeds energy expenditure. A major obstacle of obesity management is the maintenance of a given body weight loss, since weight loss is accompanied by a notable and persistent decrease in energy expenditure (Hall and Kahan 2018; Rosenbaum et al. 2008). This decrease in energy expenditure is hardly compensated by physical activity, the only available strategy to increase energy expenditure so far. Consequently, other means to increase energy expenditure are in demand. Thermogenic tissues such as BAT and brite adipose tissue are promising targets. Brite adipose tissue, in contrast to BAT, is an inducible type of fat originating from the recruitment of brown-like, so called brite (or beige) cells with thermogenic properties in WAT. Both tissues dissipate chemical energy from fatty acids and glucose to generate heat, thus increasing energy expenditure. This NST is mediated by UCP1. It is naturally activated upon cold exposure to defend body temperature and during eating to promote meal termination (Y. Li et al. 2018). Although the presence of functional BAT has been confirmed in adult humans (Cypess et al. 2009; Virtanen et al. 2009; Nedergaard, Bengtsson, and Cannon 2007), humans mostly live under thermoneutral conditions (de Jong et al. 2019). Therefore, BAT activation in humans is mostly associated with food intake, whereas cold-induced activation is less prevalent. BAT volume and activity negatively correlate with BMI (van Marken Lichtenbelt et al. 2009), suggesting a lower abundance of active BAT in overweight and obese compared to lean subjects. Consequently, the therapy of obesity by means of BAT and brite fat not only requires strategies to activate it but also to increase its abundance. Several natural compounds and drugs are associated with the activation and recruitment of BAT in mice and humans (Mukherjee, Baranwal, and N. Schade 2016; Yoneshiro, Matsushita, and Saito 2019). Among these are metabolites of n6- and n3-PUFA. Oxygenated PUFA metabolites, belonging to the group of oxylipins, are important signaling molecules implicated in the control of adipogenesis and energy balance regulation (Maurer et al. 2019). These potent and short-lived metabolites are generated by a series of enzymatic steps involving one of three enzyme classes - COX, LOX or CYP (Gabbs et al. 2015). Some oxylipins have been associated with the browning of adipose tissues. The COX derived ARA metabolites prostaglandin E2 (PGE2) and PGI2 facilitate the formation of brite adipocytes in vitro (García-Alonso et al. 2016; Vegiopoulos et al. 2010; Bayindir et al. 2015; Ghandour et al. 2016). The oxylipin 12-hydroxyeicosapentaenoic acid (12-HEPE), identified in a PUFA metabolite screen in murine serum samples, facilitates glucose uptake into brown adipocytes (Leiria et al. 2019). In a similar approach, increased levels of 12,13-DiHOME were identified in oxylipin profiles of human serum after cold acclimatization (Lynes et al. 2017). This

oxylin increases fatty acid uptake into brown adipocytes and presumably UCP1 expression (Lynes et al. 2017). Furthermore, a second class of PUFA derived metabolites, the endocannabinoids, are suggested to be involved in the negative regulation of BAT activity in mice (Krott et al. 2016). Thus, several lines of evidence suggest PUFA-derived metabolites to be involved in the recruitment and activity of thermogenic cells in mice and humans. The aim of the current study was to characterize the oxylin profiles of murine and human adipose tissues with different abundance of brown and brite adipocytes to identify novel molecules with thermogenic potential in a translational context.

We quantified a panel of 36 fatty acid metabolites in brown and white adipose tissues of C57BL/6J mice acclimatized to different ambient temperatures and in biopsies of human supraclavicular brown and white adipose tissue. Our results reveal the global oxylin profile of bona fide brown but not brite adipose tissue as a marker for the abundance of brown adipocytes. Moreover, we identified 5-HETE and 5,6-EET as individual compounds associated with the abundance of brown or brite adipocytes in both human BAT and murine brite fat.

3.4 MATERIAL AND METHODS

3.4.1 Animal Experiments

Eight-week-old male C57BL/6J mice were housed in climate cabinets (HPP750 life, Memmert) at 23 °C and 55 % humidity with a 12/12 hour light/dark cycle. Mice were provided *ad libitum* access to water and a CD (Cat# S5745-E720, Ssniff Spezialdiäten GmbH, Soest/Germany). After an adaptation phase of 3 weeks, mice were assigned to one of two groups and transferred to preconditioned cabinets at 5 °C or 30 °C. After one week, mice were killed by CO₂ exposure and tissues were immediately dissected, snap frozen in liquid nitrogen, and stored at -80 °C until further processing. The experiment was performed according to the German animal welfare law with permission from the district government of Upper Bavaria (Regierung von Oberbayern, reference number ROB-55.2-2532.Vet_02-16-166).

3.4.2 Human subjects

Paired biopsies of BAT and WAT were obtained from the supraclavicular region of 14 healthy male and female subjects. A detailed description of the biopsy procedure and of anthropometric characteristics of this study cohort has been published previously (U Din et al. 2018). Depending on the size of the specimens obtained, BAT and WAT were either entirely subjected to RNA isolation or grinded in liquid nitrogen to obtain aliquots used for both metabolite analysis and RNA isolation.

3.4.3 Oxylin and endocannabinoid profiling

Murine interscapular BAT (iBAT), iWAT and human supraclavicular fat biopsies were grinded in liquid nitrogen. Aliquots of 23-140 mg were subjected to oxylin and endocannabinoid analysis, which was conducted at the Metatoul lipidomic platform (INSERM UMR1048, Toulouse/France), certified to ISO 9001:2015 standards. Metabolite abundance was normalized to tissue mass.

3.4.4 RNA isolation and quantitative real-time PCR (qRT-PCR)

RNA isolation from murine iWAT and supraclavicular BAT as well as human adipose tissues was performed with TRIsure™ (Cat# BIO-38032, Bioline, London/UK) according to the manufacturer's instructions. Precipitated RNA was transferred to spin columns (SV Total RNA Isolation System, Cat# Z3105, Promega, Walldorf/Germany), centrifuged for 1 min with 12,000 x g and further processed according to the supplier's instructions. RNA concentration was determined spectrophotometrically (Infinite 200 PRO NanoQuant, Tecan, Männedorf, CH). Generation of cDNA was performed with 1 µg RNA (SensiFAST™ cDNA Synthesis Kit, Cat# BIO-65053, Bioline, London/UK). qRT-PCR was performed in a 384 well plate format with the LightCycler 480 system (Roche Diagnostics) in a total reaction volume of 12.5 µl containing 6.25 µl 2x SensiMix SYBR no-ROX (Cat# QT650-05, Bioline, London/UK), 250 nM forward and reverse primers and 1 µl template cDNA. Murine primers (UCP1 5'-TCTCTGCCAGGACAGTACCC-3' and 5'-AGAAGCCCAATGATGTTTCAG-3', Tf2b 5'-TGGAGATTTGTCCACCATGA-3' and 5'-GAATTGCCAAACTCATCAAACT-3') and human primers (UCP1 5'-GGAGGCCTTTGTGAAAAACA-3' and 5'-CTTGAAGAAAGCCGTTGGTC-3', TF2B 5'-GCTGTGGAAGTGGACTTGGT-3' and 5'-AGTTTGTCCACTGGGGTGTGTC-3') were produced by Eurofins MWG Operon. Expression of UCP1 was normalized to transcription factor 2b (Tf2b) expression.

3.4.5 Statistical analysis

All statistical analyses were performed using R-Studio (version 1.2.5019) with R version 3.6.1. PCA was performed with the R packages factextra (version 1.0.5) and FactoMineR (version 1.42). Other statistical tests were calculated with the R package ggpubr (version 0.2.3). Wilcoxon test was performed for all group comparisons, after checking the assumption of normal distribution with Shapiro–Wilk test. P-values < 0.05 were deemed statistically significant. The appropriate statistical test, paired or unpaired is mentioned for each figure.

3.5 RESULTS

Adaptive, NST is the key functional difference that discriminates mammalian BAT and WAT. Since almost a decade, the rediscovery of functional BAT in adult humans has intensified efforts to characterize the molecular properties of human adipose tissues and to identify novel thermogenic effectors intended for therapeutic use. Within this scope, oxylin appear to be a promising class

of endogenous compounds affecting the function and recruitment of thermogenic adipocytes in cultured cells of human and murine origin (Maurer et al. 2019). In the course of this study, we further elucidated the association of these metabolites with the recruitment of thermogenic brown and brite adipocytes in a translational context. To this end, we subjected BAT and WAT of murine and human origin to metabolite profiling and analyzed the data in consideration of the tissues' thermogenic properties. Human BAT and WAT biopsies were obtained from the supraclavicular region subsequent to PET imaging under cold-exposed conditions (U Din et al. 2018). Humans live within thermoneutral conditions most of their life (de Jong et al. 2019). Thus, for a more appropriate comparison between mice and humans we acclimatized C57BL/6J mice to 30 °C for one week to mimic the thermal environment of humans. In order to confirm the thermogenic potential of BAT versus WAT in both humans and mice, UCP1 mRNA expression was quantified as a surrogate marker for the abundance of thermogenic competent adipocytes. As expected, all BAT specimens were characterized by considerably higher UCP1 mRNA levels compared to WAT with a wide range of inter-individual variation (Figure 10 A & B). However, mean UCP1 mRNA expression in human and murine BAT was 544-fold and 255-fold higher compared to WAT, respectively. Consequently, human and murine BAT harbor more brown adipocytes than WAT.

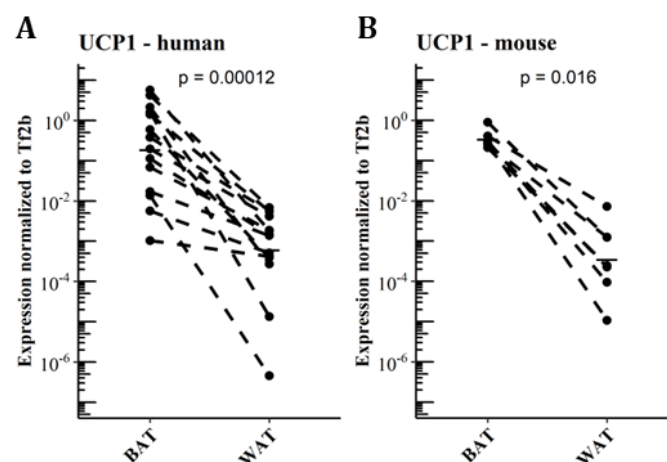


Figure 10: UCP1 gene expression in BAT and WAT of the murine and human study cohorts. (A) *Uncoupling protein 1 (UCP1) mRNA expression in supraclavicular brown adipose tissue (BAT) and white adipose tissue (WAT) of human subjects (n = 14).* (B) *UCP1 mRNA expression in inguinal WAT and supraclavicular BAT of mice housed at 30°C for 1 week (n = 7). P-values are derived from paired Wilcoxon test.*

3.5.1 The abundance of adipose tissue oxylipins differs between mice and humans

To elucidate the regulation of oxylipin production in BAT and WAT, we quantified a broad panel of 33 metabolites representing major oxylipin classes produced by mammalian tissues. Additionally, we quantified the levels of 3 AA-derived endocannabinoids. The oxylipin panel encompasses COX, LOX and CYP-derived metabolites generated by the conversion of AA, its n-6

precursor LA, and the n-3 fatty acids EPA and DHA. Within this setting, LA-derived metabolites were most abundant, while n-3 derived metabolites had a relatively low abundance in iWAT and iBAT of mice (Figure 11 A). This high abundance of LA-derived metabolites was reflected in a high percentage of LOX-derived metabolites (Figure 11 A). In human adipose tissues, the relative abundance followed a slightly different pattern. In both human BAT and WAT, AA-derived metabolites produced via the COX-pathway accounted for a higher percentage of total oxylipin abundance compared to murine fat, which proportionally reduced the relative levels of LA and DHA-derived metabolites (Figure 11 A and B). The contribution of EPA-derived oxylipins to the oxylipins pool was negligible in adipose tissues of both species. Of note, the contribution of CYP derived oxylipins in mice was higher in iBAT compared to iWAT while in humans no notable difference was observed. Despite this similar composition of the oxylipin pools in WAT and BAT, the total abundance of all oxylipins in BAT versus WAT in mice was significantly lower while it was significantly higher in human BAT versus WAT (Figure 11 C & D). These differences are primarily attributed to changes in the abundance of the LA-derived oxylipins 9- and 13-HODE. These two oxylipins are the predominant species in WAT and BAT, accounting for at least 60% of the total oxylipin pool in adipose tissues of both species (Figure 11 A & B). Endocannabinoids represent another class of fatty acid metabolites with potential effects on UCP1-dependent thermogenesis (Krott et al. 2016). Interestingly, the total abundance of the three endocannabinoids was lower in murine WAT versus BAT but higher in human WAT versus BAT, while we observed the exact opposite for total oxylipin abundance (Figure 11 C & D). Ultimately, considering the combined pool of oxylipins and endocannabinoids there was no difference in total metabolite abundance between murine and human WAT or BAT (Figure 11 E). Conclusively, mice and humans are similar in terms of the total production of PUFA metabolites. However, these tissues seem to differ in the partitioning of PUFA metabolism.

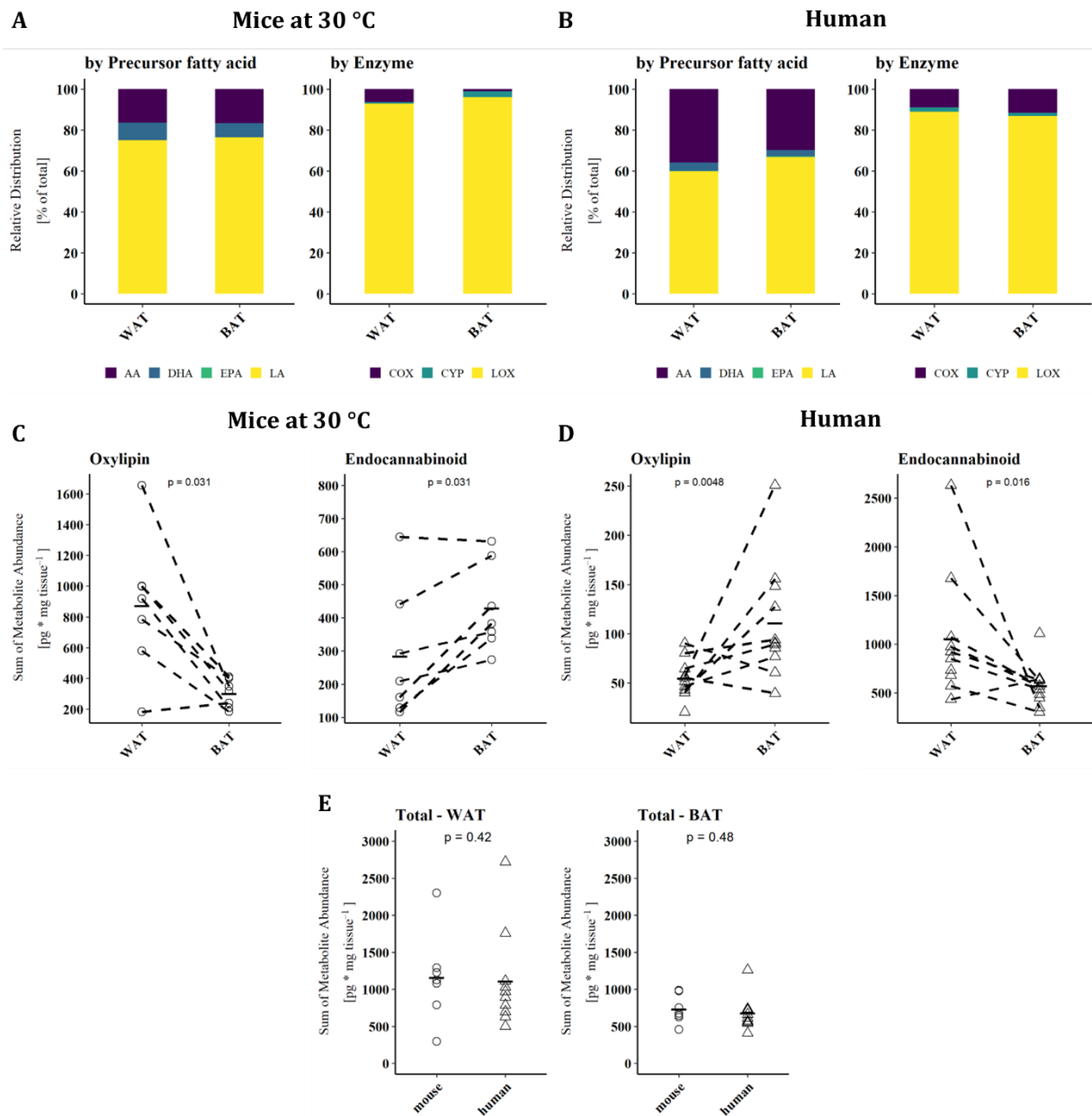


Figure 11: Adipose tissues of mice and men are comparable in terms of oxylipin composition but not abundance.

Relative distribution of oxylipins categorized by their common fatty acid progenitor (left) or enzymatic synthesis pathway (right) for (A) mice at 30°C and (B) humans. Total sum of oxylipins (left) or endocannabinoids (right) for each individual (C) mouse ($n = 7$) or (D) human subject ($n = 10$ for WAT and $n = 11$ for BAT). (E) Total sum of combined oxylipins and endocannabinoids in murine and human WAT and BAT. Statistical analysis paired Wilcoxon test (C) and unpaired Wilcoxon test (D,E).

3.5.2 The global oxylipin profile is a surrogate marker for the abundance of brown but not brite adipocytes

As oxylipin abundance differs between WAT and BAT in both mice and humans, we investigated, whether oxylipins may serve as discriminative markers for the two tissues. Therefore, we applied PCA on the metabolite data of BAT and WAT. In mice, principal components 1 and 2 together explained 82.8 % of the variability between WAT and BAT. In a continuum of these principal

components, murine WAT and BAT formed distinct and separate clusters (Figure 12 A). Thus, murine BAT and WAT can be distinguished by their characteristic oxylipin patterns. In humans, principal components 1 and 2 explained considerably less of the variation between BAT and WAT (54.5%). A distinction of human BAT and WAT according to their specific oxylipin patterns was not possible (Figure 12 B). This was reflected in the analysis of the combined human and murine data set. In this analysis the two species formed distinct clusters separating the murine tissues while human BAT and WAT could not be distinguished (Supplementary Figure 1 A). In contrast to murine BAT, human BAT constitutes a complex, interwoven mixture of both brown and white adipocytes. Consequently, oxylipin patterns established from human tissues may not represent differences on the cellular level of individual brown and white adipocytes and lack discriminative power (Figure 12 B). To overcome this limitation, we transferred oxylipin patterns established from murine BAT and WAT and plotted human oxylipin levels according to these murine principal components. However, human BAT and WAT remained indistinguishable (Supplementary Figure 1B). Surprisingly, the reverse strategy, i.e. plotting murine oxylipin levels according to principal components of human oxylipin variation, murine BAT and WAT could be well separated (Supplementary Figure 1 C). This indicates that oxylipins in humans do not per se lack the variability observed in murine tissues but fail to sharply distribute into the categories BAT and WAT. The lack of discrimination of human supraclavicular BAT and WAT oxylipin patterns are in line with the observation that human supraclavicular BAT does not resemble the characteristics of classical BAT in conventional laboratory mice but rather displays a brite phenotype (de Jong et al. 2019; Chechi, Van Marken Lichtenbelt, and Richard 2018). Indeed, brite adipose tissue obtained from mice housed at 5 °C for 1 week and human supraclavicular BAT were both characterized by increased UCP1 gene expression compared to WAT (Supplementary Figure 2 and Figure 10 A). Murine brite adipose tissue contained a mixed population of unilocular white and multilocular brown/brite cells (Supplementary Figure 3), similarly to the phenotype reported from human supraclavicular BAT (de Jong et al. 2019). We investigated this by comparing oxylipin profiles of iWAT of mice acclimatized to either 30 °C (white adipose tissue) or 5 °C (brite adipose tissue). In this comparison, the principal components 1 and 2 explained a large proportion (81.3 %) of the variation between brite and white adipose tissue (Figure 12 C). However, murine brite and white adipose tissue could not be separated from one another by oxylipin patterns (Figure 12 C), although both formed distinct populations separate from BAT (Supplementary Figure 1 D). Interestingly, BAT of mice acclimatized to 5 °C or 30 °C also formed distinguishable populations (Supplementary Figure 1 D). This suggests the global BAT oxylipin profile as surrogate marker of the abundance of brown adipocytes, since BAT of 5 °C acclimatized mice contained more multilocular brown adipocytes than BAT of mice housed at 30 °C. Conclusively, the oxylipin profiles of adipose tissues allow the discrimination of bona fide BAT and WAT composed of homogenous populations of brown and white adipocytes, respectively. However, it

is either unsuitable to distinguish tissues harboring both types of cells or unable to distinguish brite from white adipocytes. Thus, the oxylipin profile can serve as a surrogate marker for brown adipocyte abundance in murine BAT but not murine brite fat or human BAT.

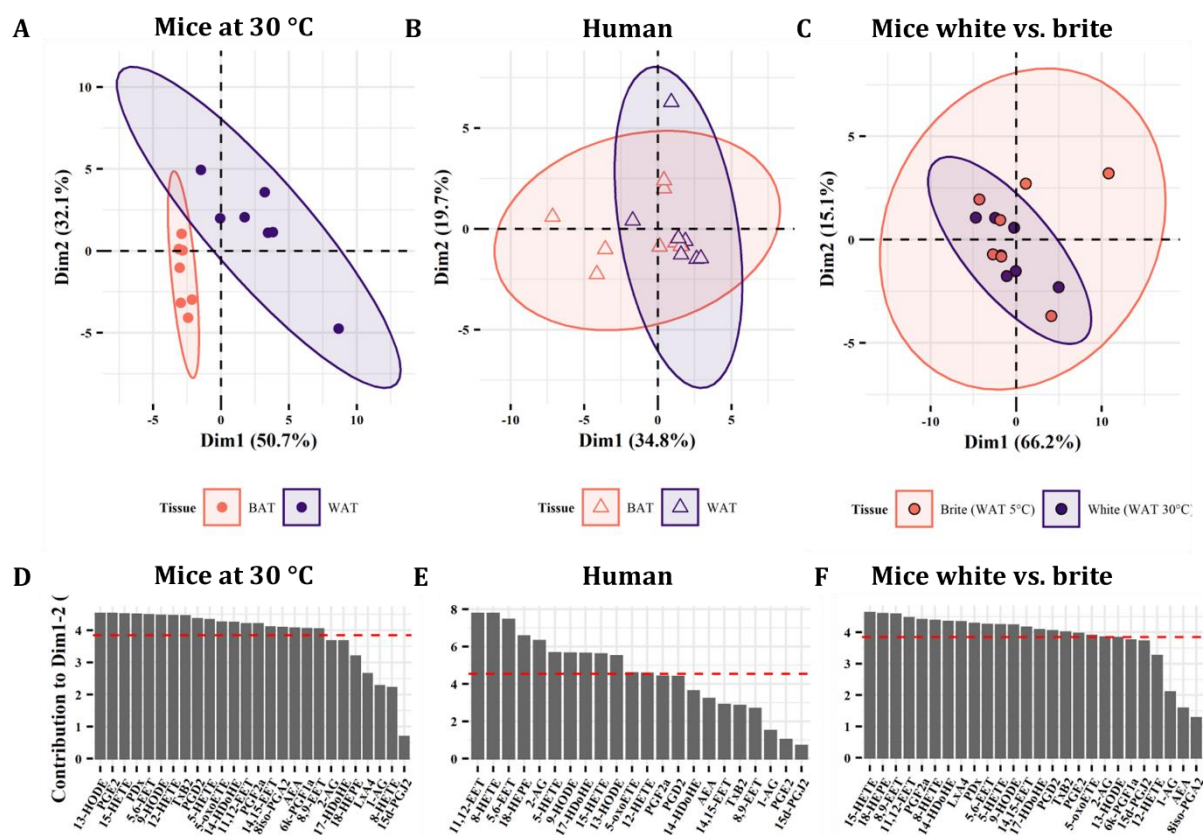


Figure 12: Oxylipin profiles distinguish BAT but not brite adipose tissue from WAT.

Principal component analysis of the oxylipins in BAT and WAT showing the two first principal components (Dim1 and Dim2) in (A) mice at 30°C ($n = 7$) and (B) human ($n = 8$). (C) Principal component analysis of oxylipins in murine WAT acclimatized to 5 or 30°C ($n = 7$). Contribution of the single variables to Dim1 and Dim2 for (D) mice at mice at 30°C, (E) human, and (F) murine WAT acclimatized to 5 or 30°C for 1 week. Red dashed line indicates the average contribution of all variables.

3.5.3 The oxylipins 5-HETE and 5,6-EET are potential markers of brown adipocyte abundance in BAT in mice and humans

The oxylipin profile serves as a potential surrogate measure for the abundance of brown but not brite adipocytes. We asked which metabolites contributed the most to this phenomenon and whether we could identify novel oxylipins associated with the recruitment of brown and brite adipocytes. Therefore, we investigated the contribution of individual oxylipins to the principal components 1 and 2. In the murine adipose tissues, more than two-thirds of the measured fatty acid metabolites contribute higher-than-average to the first two principal components (Figure 12 D & F). In contrast, less than half of the compounds did so in the human tissues (Figure 12 E). Interestingly, several compounds previously associated with the recruitment of brown and brite adipocytes, namely 9- and 13-HODE (Y. H. Lee et al. 2016), the PGI2 degradation product 6k-

PGF1 α (Vegiopoulos et al. 2010; Bayindir et al. 2015), 12-HETE (Leiria et al. 2019) as well as PGE2 (García-Alonso et al. 2016; Vegiopoulos et al. 2010) contributed higher-than-average in the murine BAT/WAT comparison (Figure 12 D). Among those, only 9- and 13-HODE consistently contributed to the discrimination of BAT and brite adipose tissue from WAT (Figure 12 D-F), suggesting an association of individual metabolites with the abundance of thermogenic competent adipocytes in a translational context. In line with this notion, the AA-derivatives 11,12-EET and 5,6-EET generated by the CYP pathway, and the LOX pathway products 15-HETE, 5-HETE and its active form 5-oxoETE contributed above-average in all three conditions (Figure 12 D-F). However, the abundance of most of these metabolites was exclusively different in murine BAT versus WAT but not in the other comparisons (Figure 13 A-C), confirming the limited discriminative potential of the oxylipin profile in these settings. Only the abundance of 13-HODE in humans and 5-oxoETE in the murine brite versus white comparison were significantly different in brown and brite adipose tissue compared to WAT, respectively (Figure 13 B & C). Interestingly, 11,12-EET, 5,6-EET and 5-HETE were significantly higher in murine BAT than in WAT (Figure 13 A), contradicting the overall trend towards higher total oxylipin abundance in WAT (Figure 11 C). This suggests an involvement of these three metabolites in regulation of BAT function. We identified 5,6-EET and 5-HETE as the only two metabolites significantly more abundant in murine BAT compared to WAT that showed at least a similar trend towards a higher abundance in murine brite and human BAT versus WAT (Figure 13 B & C). In line with this regulation, 5-oxoETE, the oxidation product of 5-HETE, also tended to be more abundant in these tissues. Consequently, 5-HETE and 5,6-EET constitute novel oxylipins associated with the abundance of brown and brite adipocytes in a translational context.

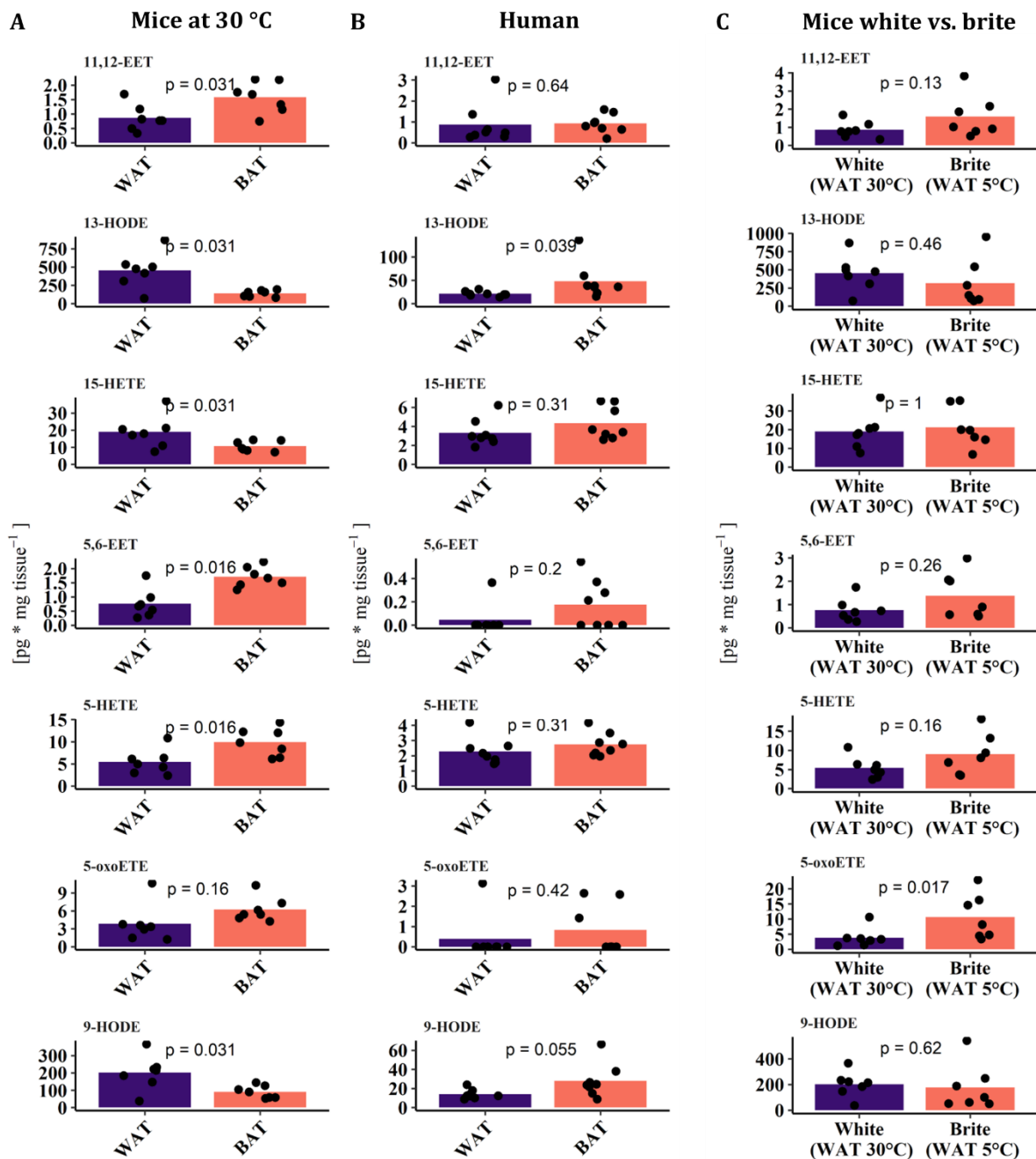


Figure 13: 5-HETE and 5,6-EET are regulated similar between adipose tissues.

The concentration of the seven higher than average contributing oxylipins in (A) murine BAT and WAT ($n = 7$), (B) human BAT and WAT ($n = 8$), and (C) murine white and brite adipose tissue ($n = 7$). Bars represent mean values and p-values are derived from paired (A,B) or unpaired (C) Wilcoxon test.

3.6 DISCUSSION

Activation of NST in BAT and brite adipose tissue increases energy expenditure and therefore is a potential therapeutic strategy to treat obesity. Within this scope, metabolites of PUFA (especially oxylipins) are discussed as potential effectors. Several studies have associated selected oxylipins with improved BAT functionality (Leiria et al. 2019; Lynes et al. 2017) or the recruitment of brite adipocytes (García-Alonso et al. 2016) in mice. However, evidence in the human context is scarce.

Only the prostaglandin PGI₂ has been shown to increase UCP1 gene expression in cultured murine and human adipocytes (Vegiopoulos et al. 2010; Ghandour et al. 2016). Therefore, we screened the abundance of 36 n6- or n3-PUFA-derived metabolites in human and murine adipose tissues to identify novel compounds associated with abundance of brown and brite adipocytes in a translational context. Based on their respective PUFA metabolite pattern, murine but not human BAT could be distinguished from WAT. Indeed, it has been argued that human supraclavicular BAT resembles murine brite adipose tissue rather than murine BAT, thus comprising a mixture of white and brite adipocytes (de Jong et al. 2019; Sharp et al. 2012). This is in line with our finding that in mice the oxylipin profiles of brite adipose tissue induced by cold exposure and WAT at thermoneutrality could also not be distinguished. We think of two possible explanations for this observation. First, the oxylipin profile could be a surrogate marker for the thermogenic activity of the respective adipose tissues, since only BAT but not WAT shows increased metabolic activity in cold acclimatized mice (Labbé et al. 2016). However, we did not measure thermogenic activity in our study, and thus lack direct experimental evidence. Second, the oxylipin profile could be a surrogate marker for the abundance of brown or brite adipocytes that markedly increase in abundance upon cold exposure in both BAT and WAT of mice, respectively. However, we speculate that the relative abundance of interspersed brown or brite adipocytes in human BAT and murine brite adipose tissue, respectively, is not sufficient to notably alter the oxylipin metabolite profiles of the whole tissue.

We therefore checked individual oxylipins with discriminative potential between murine BAT and WAT. A set of seven oxylipins with high potential to explain variability between BAT or brite adipose tissue and WAT in mice and humans was identified. Within this set, we could confirm previously reported oxylipins associated with the recruitment of BAT and browning of WAT. As such, LA-derived 9- and 13- HODE were the most abundant oxylipins in both human and murine adipose tissues and had a high discriminative potential. When used at very high concentrations, both compounds sensitize murine white adipocyte progenitors to β_3 -receptor agonist treatment, consequently increasing UCP1 gene expression in the presence of isoproterenol (Y. H. Lee et al. 2016). In our study, the abundance of 9- and 13-HODE in murine adipose tissues gradually decreased with the abundance of brown and brite adipocytes from white to brite to brown. This phenotype may indicate a coordinated regulation of 9- and 13-HODE production to contain thermogenic capacity on reasonable levels upon prolonged β -adrenergic stimulation (1 week at 5 °C). However, the sensitizing effect of 9- and 13-HODE was achieved with supraphysiological concentrations of 68 μ M (Y. H. Lee et al. 2016). Furthermore, the decreasing abundance of 9- and 13-HODE in increasingly thermogenic competent tissues might simply reflect an increased consumption of precursor fatty acids caused by the higher lipolytic and oxidative activity. Consequently, the relevance of 9- and 13-HODE in a physiological context needs further

experimental validation. Interestingly, 12-HETE and 14-Hydroxydocosaheptaenoic acid (14-HDoHE), two LOX products reported to be upregulated in murine iBAT and iWAT upon cold stimulation (Leiria et al. 2019), were also high contributors explaining variability between murine BAT and WAT in our study. In contrast to previously published observations, 14-HDoHE was not only lower at 5 °C compared to 30 °C in BAT but also lacked regulation in WAT (Figure 14). Additionally, 12-HETE concentrations were not different between 5 °C and 30 °C in BAT or WAT (Figure 14). We cannot exclude an effect of diets differing in the fatty acid composition altering the supply of oxylipin precursor fatty acids. However, we speculate that the lack of regulation of 12-HETE and 14-HDoHE especially in WAT upon cold stimulation indicates that both oxylipins are not implicated in the process of WAT browning *in vivo*.

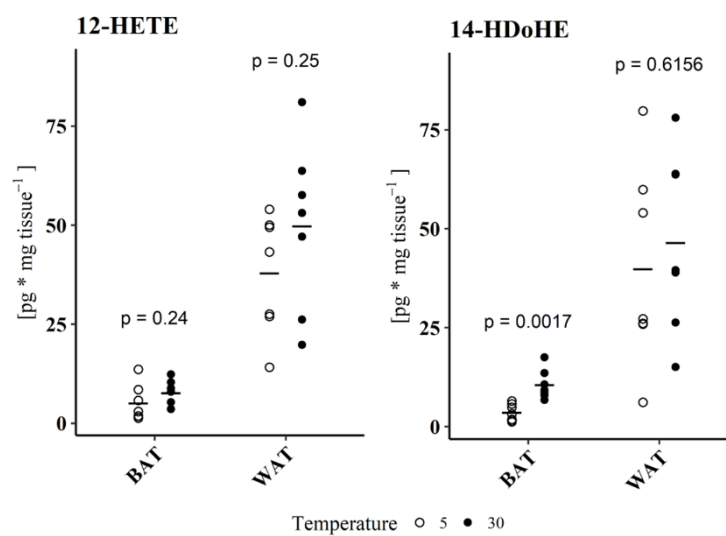


Figure 14: Changes of 12-HETE and 14-HDoHE abundance in murine BAT and WAT by ambient temperature.

Abundance of (A) 12-HETE and (B) 14-HDoHE in BAT and WAT of mice ($n = 7$) acclimatized to 5 °C or 30 °C for 1 week. P-values are derived from unpaired Student's *t*-test.

In line with the scope of our study, we could identify two novel metabolites, which have not been associated with the recruitment of brown and brite adipocytes. Following a translational pattern, the oxylipins 5-HETE and 5,6-EET were more abundant in BAT and brite adipose tissue compared to WAT in mice and humans. 5,6-EET is directly synthesized from AA via the CYP pathway and can activate transient receptor potential vanilloid 4 (TRPV4) channels (Watanabe et al. 2003). In contrast, 5-HETE synthesis from AA is a multi-step process involving 5-LOX and glutathione peroxidases (Rådmark et al. 2015). Expression of CYP isoforms responsible for 5,6-EET production has been reported for murine adipocytes (Graves et al. 2015). Further 5-LOX is expressed in human and murine adipose tissue (Mehrabian et al. 2008; Heemskerk et al. 2015; Horrillo et al. 2010). Thus, it is possible that both 5-HETE and 5,6-EET are generated endogenously in adipose tissues, although their tissue-specific abundance may be influenced by plasma levels. Considering the different number of brown adipocytes and levels of UCP1

expression in BAT and WAT, both compounds might be associated with thermogenic capacity. Indeed, both 5-HETE and 5,6-EET are linked to signaling pathways with the potential to regulate the recruitment of thermogenic capacity in adipose tissue. Although 5-HETE is a rather inactive metabolite and needs further conversion by 5-hydroxyeicosanoid dehydrogenase (5-HEDH) to the active metabolite 5-oxo-EETE, the latter one activates the OXE receptor and PPAR γ (Shiraki et al. 2005). Activation of PPAR γ is one of the strongest inducers of UCP1 expression (Petrovic et al. 2008). Consequently, 5-HETE could by conversion to 5-oxo-EETE activate PPAR γ and regulate adipogenesis and UCP1 expression. Nevertheless, not all PPAR γ agonists are able to increase UCP1 expression in brown or white adipose tissue. As such, the oxylipin and PPAR γ agonist 15-Deoxy-Delta-12,14-prostaglandin J2 (15d-PGJ2) has no effect on the recruitment of UCP1 mRNA in human adipocytes (Bartesaghi et al. 2015). This in line with our finding that 15d-PGJ2 was virtually undetectable in BAT as well as WAT and did not contribute to the variation in human adipose tissue samples. In contrast to 5-HETE, 5,6-EET could have a negative regulatory effect on the browning of adipose tissues by binding to the TRPV4 channel. This receptor constitutes a negative regulator of thermogenic capacity as mice with a knockout of TRPV4 show increased expression of UCP1 in WAT in addition to increased total energy expenditure (Ye et al. 2012). Although 5-HETE and 5,6-EET have the potential to affect browning of adipose tissues, these effects remain to be demonstrated in in vitro and in vivo studies aiming to clarify the role both oxylipins for the recruitment and function of brown and brite adipocytes.

In summary, we show that bona fide BAT versus WAT are distinguishable by their global oxylipin profile. Furthermore, we identify 5-HETE and 5,6-EET as novel compounds associated with the recruitment of brown and brite adipocytes in mice and humans. Further studies need to establish whether these oxylipins are mere markers or functional effectors of thermogenic capacity.

4 NO EFFECT OF DIETARY FISH OIL SUPPLEMENTATION ON THE RECRUITMENT OF BROWN AND BRITE ADIPOCYTES IN MICE OR HUMANS UNDER THERMONEUTRAL CONDITIONS

A similar version of this chapter was published: Maurer S. F., Dieckmann S., Lund J., Fromme T., Hess A. L., Colson C., Kjølbaek L., Astrup A., Gillum M. P., Larsen L. H., Liebisch G., Amri E.-Z., Klingenspor M. (2021) No Effect of Dietary Fish Oil Supplementation on the Recruitment of Brown and Brite Adipocytes in Mice or Humans under Thermoneutral Conditions. *Mol. Nutr. Food Res.* 65, 2000681. doi: 10.1002/mnfr.202000681

4.1 ABSTRACT

Brown and brite adipocytes within the mammalian adipose organ provide NST and thus, have an exceptional capacity to dissipate chemical energy as heat. PUFA of the n3-series, abundant in fish oil, have been repeatedly demonstrated to enhance the recruitment of thermogenic capacity in these cells, consequently affecting body adiposity and glucose tolerance. We scrutinized these effects in mice housed in a thermoneutral environment and in a human dietary intervention trial. Mice were housed in a thermoneutral environment eliminating the superimposing effect of mild cold-exposure on thermogenic adipocyte recruitment. Dietary fish oil supplementation in two different inbred mouse strains neither affected body mass trajectory nor enhanced the recruitment of brown and brite adipocytes, both in the presence and absence of a β_3 -adrenoreceptor agonist imitating the effect of cold-exposure on adipocytes. In line with these findings, dietary fish oil supplementation of persons with overweight or obesity failed to recruit thermogenic adipocytes in subcutaneous adipose tissue. Thus, our data question the hypothesized potential of n3-PUFA as modulators of adipocyte-based thermogenesis and energy balance regulation.

4.2 AUTHOR CONTRIBUTIONS

Sebastian Dieckmann planned and performed the mouse experiments corresponding to (Figure 17, Figure 18, Figure 19 and Figure 20) and conducted molecular analyses on mouse tissues of those experiments. SD analyzed data and contributed to interpretation of all murine data. SD edited the manuscript and handled the review process.

4.3 INTRODUCTION

Brown adipocytes abundantly express UCP1, a protein of the mitochondrial inner membrane that uncouples O₂ consumption from ATP production. Activation of UCP1 enhances macronutrient catabolism, mitochondrial substrate oxidation and consequently, energy expenditure in BAT. The same mechanism is provided by brite adipocytes (Y. Li et al. 2014; Shabalina et al. 2013), an inducible cell type of WAT that morphologically and functionally resembles bona fide brown adipocytes. The recruitment and activation of thermogenic brown and brite adipocytes is considered a therapeutic strategy to tackle overweight, obesity and associated disorders. In this context, the potential of nutritional components has been comprehensively explored in recent years (El Hadi et al. 2019; Yoneshiro, Matsushita, and Saito 2019; Okla et al. 2017).

PUFA influence the effect of a HFD on UCP1 expression in rodent BAT (Fromme and Klingenspor 2011). Dietary fish oil is a rich source of n₃-PUFAs abundantly providing EPA and DHA. Supplementation of mice with fish oil or EPA/DHA-enriched diets has been performed repeatedly (Table 2). Multiple studies reported increased UCP1 expression in BAT and/or WAT upon n₃-PUFA supplementation, which can affect body adiposity (Oliveira et al. 2019; Bargut, Silva-e-Silva, et al. 2016; Bargut, Souza-Mello, et al. 2016; Bhaskaran et al. 2017; M. Kim et al. 2015; Kalupahana et al. 2010; Pahlavani et al. 2017; J. Kim et al. 2016; Ludwig et al. 2013; Worsch et al. 2018; J. Villarroya et al. 2014; Zhuang et al. 2019; You et al. 2020; Ghandour et al. 2018; Bargut et al. 2019; Sato et al. 2020), while some reports found no effect on UCP1 expression (Iizuka et al. 2020; Maeda et al. 2007; Pahlavani et al. 2019; P. Flachs et al. 2011; Tsuboyama-Kasaoka et al. 1999). Increased UCP1 expression has been reproduced in cell culture studies employing human and murine models of brown and brite adipogenesis treated with EPA and DHA (J. Kim et al. 2016; Zhuang et al. 2019; Quesada-López et al. 2016; Fleckenstein-Elsen et al. 2016; Laiglesia et al. 2016; Zhao and Chen 2014). Conversely, UCP1 gene induction is attenuated or absent upon n₆-PUFA supplementation of cultured human adipocytes (Fleckenstein-Elsen et al. 2016; Pisani et al. 2014; Ghandour et al. 2018). Various direct and indirect mechanisms have been proposed to underlie these observations including interactions of n₃-PUFAs with the sympathetic nervous system, an activation of free fatty acid receptor 4, or the metabolism of dietary PUFAs into oxygenated metabolites (oxylipins, i.e. octadecanoids, eicosanoids and docosanoids) of the n₆ or n₃-series (M. Kim et al. 2015; J. Kim et al. 2016; Ghandour et al. 2018; Quesada-López et al. 2016; Maurer et al. 2019; Fan et al. 2018).

Table 2: Intervention studies investigating effects of dietary n3-PUFA supplementation on brown/brite adipocyte recruitment and body adiposity in adult wildtype mice.

Study	Mice	Housing temperature	Total fat [energy%]	n3-PUFA source	isocaloric control	Feeding duration [weeks]	n3-PUFA induced effects compared to isocaloric control diet at endpoint			
							body mass	dissected fat mass	UCP1 in BAT	UCP1 in WAT
(Oliveira et al. 2019)	C57BL/6J	25°C	60	fish oil	lard	8	↓	BAT ↔ iWAT ↓ eWAT ↓	protein ↔ mRNA ↔	protein n.a. mRNA ↑ (iWAT)
(Bargut, Silva-e-Silva, et al. 2016; Bargut, Souza-Mello, et al. 2016)	male C57BL/6 3 months	20°C	50	menhaden fish oil (low dose) menhaden fish oil (high dose)	lard	8	↓	BAT n.a. iWAT ↓ eWAT ↓	protein ↑ mRNA ↑	protein ↑ (iWAT) ↑ mRNA (iWAT)
(Bhaskaran et al. 2017)	male C57BL/6J 8 weeks	20°C	45	fish oil	lard	14	↓	BAT ↔ scWAT ↓ abdWAT ↓	n.a.	protein ↑ (eWAT) ↑ mRNA (eWAT)
(M. Kim et al. 2015)	male C57BL/6	23°C	45	DHA-enriched fish oil (low dose) EPA-enriched fish oil (low dose) DHA-enriched fish oil (high dose) EPA-enriched fish oil (high dose)	lard	10	↓	BAT ↓ iWAT ↔ abdWAT ↓ BAT ↓ iWAT ↓ abdWAT ↓	protein ↑ mRNA ↔ protein ↔ mRNA ↑ protein ↔↑ mRNA ↑ protein ↑ mRNA ↑	protein ↑ (iWAT) ↑ mRNA ↔ (iWAT) protein ↑ (iWAT) ↑ mRNA (iWAT)
(Kalupahana et al. 2010; Pahlavani et al. 2017)	male C57BL/6J 5-6 weeks	22°C	45	EPA ethyl ester	lard	11 5*	↓ ↔	BAT ↓ iWAT ↓ gWAT ↔ BAT ↔ iWAT ↔ gWAT ↔	protein ↑ mRNA ↔ protein ↔ mRNA ↔	protein ↔ mRNA ↔ (iWAT, eWAT) n.a.
(Pahlavani et al. 2019)	male C57BL/6J 5-6 weeks	28-30°C	45	AlaskOmega EPA-enriched fish oil	lard	14	↔	BAT ↔ eWAT ↔	protein ↔ mRNA ↔	n.a.

Study	Mice	Housing temperature	Total fat [energy%]	n3-PUFA source	isocaloric control	Feeding duration [weeks]	n3-PUFA induced effects compared to isocaloric control diet at endpoint			
							body mass	dissected fat mass	UCP1 in BAT	UCP1 in WAT
(J. Kim et al. 2016)	male C57BL/6 8 weeks	n.a. 8°C	50	fish oil	palm oil olive oil	12	n.a.	total*** ↓	protein ↑ mRNA ↑	n.a.
				fish oil	n.a.	2**	n.a.	n.a.	protein n.a. mRNA ↑	n.a.
(Worsch et al. 2018; Ludwig et al. 2013)	male C57BL/6J 8 weeks	22°C	48	EPAX 1050 TG	palm oil	12	↓	BAT ↓ iWAT ↓ eWAT ↓ mWAT ↓ prWAT ↔	protein ↑ mRNA ↑	n.a.
(J. Villarroya et al. 2014)	male C57BL/6J 2 months	22°C	n.a.	EPAX 1050 TG (high dose)	corn oil	3*	n.a. (gain ↓)	BAT ↓ eWAT ↓	protein n.a. ↔ mRNA ↔	protein n.a. ↑ (eWAT) mRNA
				EPAX 1050 TG (low dose)		8	n.a. (gain ↔)	BAT ↔ eWAT ↓	protein n.a. ↔ mRNA ↔	protein n.a. ↔ (eWAT) mRNA
(P. Flachs et al. 2011)	male C57BL/6J 2 months	n.a.	n.a.	EPAX 1050 TG, ad libitum	corn oil ad libitum	5*	↔ (gain ↔)	BAT ↓ scWAT ↔ abdWAT ↔	protein n.a. ↔ mRNA ↔	protein n.a. ↔ (eWAT) mRNA
				EPAX 1050 TG, caloric restriction	corn oil caloric restriction		↔ (gain ↓)	BAT ↓ scWAT ↔ abdWAT ↔	protein n.a. ↔ mRNA ↔	protein n.a. ↔ (eWAT) mRNA
(Tsuboyama-Kasaoka et al. 1999)	female C57BL/6J 8 weeks	22°C	60	tuna fish oil	safflower oil	5 months	n.a. (gain ↓)	BAT ↔ pWAT ↓	protein n.a. ↔ mRNA ↔	protein n.a. ↔ (pWAT) mRNA
(Miller et al. 2019)	male C57BL6J 10 weeks	room temperature	45	ProOmega Menhaden Oil	safflower oil safflower oil + hydrogenated coconut oil	16	↓	BAT n.a. scWAT ↓ pgWAT ↓	n.a.	protein n.a. ↓ (pgWAT) mRNA
(Zhuang et al. 2019)	C57BL/6J 4 weeks	25°C	45	unesterified EPA	milk fat	15*	↔	BAT ↑ iWAT ↔ gWAT ↔	protein ↑ mRNA n.a.	protein ↑ (iWAT) mRNA ↑ (iWAT)
				unesterified DHA				BAT ↑ iWAT ↓ gWAT ↔	protein ↑ mRNA n.a.	protein ↑ (iWAT) mRNA ↑ (iWAT)

Study	Mice	Housing temperature	Total fat [energy%]	n3-PUFA source	isocaloric control	Feeding duration [weeks]	n3-PUFA induced effects compared to isocaloric control diet at endpoint			
							body mass	dissected fat mass	UCP1 in BAT	UCP1 in WAT
(You et al. 2020)	C57BL/6 6 weeks	n.a.	45	α -linolenic acid-enriched butter	butter	10	n.a.	BAT ↓ WAT n.a.	protein ↔ mRNA ↔	n.a.
					margarine			BAT ↓ WAT n.a.	protein ↑ mRNA ↑	
(Maeda et al. 2007)	female KK-Ay 4 weeks	23°C	n.a.	fish oil	soybean oil	4	n.a. (gain ↔)	BAT ↔ abdWAT ↔	n.a.	protein ↔ mRNA n.a.
(Iizuka et al. 2020)i	male KK/Ta 7 weeks	22°C (pioglitazone)	19.7	fish oil	safflower oil	12	↓	BAT ↓ eWAT ↔	protein n.a. mRNA ↔	protein n.a. mRNA ↔
(Sato et al. 2020)	female C57BL/6 8 weeks	23°C	45	menhaden oil	lard + soybean oil	10	↓	n.a.	n.a.	n.a.
		23°C (CL-316,243)					n.a.	n.a.	n.a.	protein n.a. mRNA ↑ (scWAT)
(Ghandour et al. 2018)	male C57BL/6j 10 weeks	28°C (vehicle)	12	fatty acid ethyl esters (α -linolenate, EPA, and DHA)	oleate ethyl ester	12	↔	n.a.	protein n.a. mRNA ↑	protein ↔ (scWAT) mRNA ↔ (scWAT)
		28°C (CL-316,243)					↔ (loss ↑)	n.a. (BAT and eWAT loss ↑)	protein n.a. mRNA ↑	protein ↑ (scWAT) mRNA ↑ (scWAT)
(Bargut et al. 2019)	male C57BL/6 3 months	20°C	10	purified EPA	soy	5*	n.a.	BAT ↓ scWAT ↔ abdWAT ↔	protein ↑ mRNA ↑	protein ↑ (scWAT) ↑ mRNA (scWAT)
				purified DHA					protein ↑ mRNA ↑	protein ↑ (scWAT) ↑ mRNA (scWAT)
				purified EPA+DHA					protein ↑ mRNA ↔	protein ↑ (scWAT) mRNA ↔ (scWAT)

Studies with missing information on housing temperature are assumed to have been conducted at room temperature (~22°C). N3-PUFA sources indicated as 'low dose' and 'high dose' refers to different concentrations used within the same study. Effects induced by n3-PUFA supplementation were primarily retrieved from data that were provided with statistical analyses, and effects are depicted based on the results of statistical analyses as provided by the original studies. Data without statistics (e.g. immunohistochemical analyses without quantification) were considered in individual cases. n.a. = not available. ↑ = increased. ↔ = unchanged. ↓ = reduced. * = n3-PUFA supplementation was preceded by feeding of isocaloric control diet. ** = preceded by n3-PUFA supplementation at 25°C. *** = total fat mass determined by dual-energy X-ray absorptiometry. eWAT = epididymal WAT. scWAT = subcutaneous WAT. iWAT = inguinal WAT. pgWAT = peri-gonadal WAT. gWAT = gonadal WAT. mWAT = mesenteric WAT. prWAT = peri-renal WAT. pWAT = parametrial WAT. abdWAT = intra-abdominal WAT including combinations of different depots (eWAT, mWAT, prWAT, renal WAT, uterine WAT, retroperitoneal WAT).

Collectively, the current state of the art suggests a reciprocal effect of n3 and n6-PUFAs on thermogenic adipocyte recruitment and energy balance regulation. However, there are major limitations to this conclusion. Firstly, *in vivo* studies with mice demonstrating beneficial effects of n3 PUFA supplementation on thermogenic adipocyte recruitment have been mostly conducted under subthermoneutral conditions (Oliveira et al. 2019; Bargut, Silva-e-Silva, et al. 2016; Bargut, Souza-Mello, et al. 2016; Bhaskaran et al. 2017; M. Kim et al. 2015; Kalupahana et al. 2010; J. Kim et al. 2016; Ludwig et al. 2013; Worsch et al. 2018; J. Villarroya et al. 2014; Zhuang et al. 2019; You et al. 2020; Bargut et al. 2019; Sato et al. 2020; Iizuka et al. 2020; Maeda et al. 2007; P. Flachs et al. 2011; Tsuboyama-Kasaoka et al. 1999; Miller et al. 2019). The thermoneutral zone of common laboratory mice is ~30–32°C environmental temperature (Gordon 2012). Housing of mice below this temperature enforces UCP1-dependent thermoregulation to maintain body temperature. This process is under control of the sympathetic nervous system which influences the assessment of PUFA effects on thermogenic adipocytes and limits the translational potential to humans, living under thermoneutral conditions most of their lives (Ganeshan and Chawla 2017). Secondly, n3-PUFA supplementation effects are divergent. Studies with mice mostly reported thermogenic adipocyte recruitment in response to HFD comprising fish oil, EPA or DHA instead of lard, palm oil or dairy fat (Oliveira et al. 2019; Bargut, Silva-e-Silva, et al. 2016; Bargut, Souza-Mello, et al. 2016; M. Kim et al. 2015; Kalupahana et al. 2010; Pahlavani et al. 2017; Ludwig et al. 2013; Worsch et al. 2018; Zhuang et al. 2019), all of which are poor sources for n3-PUFAs. In rats, fish oil supplementation reduces WAT expansion and increases UCP1 gene expression in BAT in comparison to safflower oil, which is high in the n6-PUFA LA (Y. Takahashi and Ide 2000). Interestingly, the same effect occurs with borage oil versus safflower oil due to its relatively high content of the linoleic acid-derivative γ linolenic acid (Yoko Takahashi, Ide, and Fujita 2000). Thus, the effect of borage oil on the recruitment of thermogenic adipocytes may differ from that of other fat sources that are low in n3 PUFAs and/or high in n6 PUFAs. To our knowledge, brown and brite adipocyte recruitment in mice upon fish oil supplementation has not yet been compared to borage oil or any other γ linolenic acid-rich oil. Thirdly, the effect of dietary n3-PUFA supplementation on thermogenic adipocyte recruitment has not yet been investigated in a human dietary intervention trial, leaving the translational relevance of findings from cell culture and rodent *in vivo* studies unclear.

In this study, we employed two different inbred mouse strains fed with fish oil, borage oil or palm oil under thermoneutral housing conditions to explore the efficacy of dietary n3-PUFA supplementation on body mass accumulation and thermogenic adipocyte recruitment. To elucidate the translational potential of this physiology, brite adipogenesis was investigated in subcutaneous adipose tissue of human subjects supplemented with n3-PUFAs during an

intervention study. Collectively, our data demonstrate that dietary n3-PUFAs do not affect thermogenic adipocyte recruitment and body adiposity, neither in mice nor in humans.

4.4 MATERIAL AND METHODS

4.4.1 Animals and housing

All animal experimentation was performed in accordance with the German animal welfare law with permission from the district government of Upper Bavaria (Regierung von Oberbayern, reference numbers 55.2-1-54-2532-198-13 and ROB-55.2-2532.Vet_02-16-166). An overview of all animal experiments is provided in Figure 5 C-E. Male mice of the inbred strains C57BL/6J and 129S6/SvEvTac were bred and housed at RT ($23^{\circ}\text{C} \pm 1^{\circ}\text{C}$) and fed standard rodent chow-diet (Cat# V1124-300, Ssniff Spezialdiäten GmbH, Soest/Germany) prior to the beginning of experiments. At the age of 7-11 weeks, mice were transferred to climate cabinets (HPP750life, Memmert, Schwabach/Germany or UniProtect, Zoonlab, Castrop-Rauxel/Germany) conditioned to 30°C and 55% relative humidity. At the same time, mice were switched to a purified CD (Cat# S5745-E720, Ssniff Spezialdiäten GmbH, Soest/Germany) with a fat content of 50 g/kg providing ~13% energy from soybean oil (Table 1). In all experiments, *ad libitum* CD feeding was conducted prior to other experimental interventions described below. Tissues for molecular analyses were collected from mice killed by CO₂ asphyxiation.

4.4.2 Dietary PUFA supplementation of mice

Following 3-4 weeks of CD-feeding, mice were assigned to experimental groups with similar mean body mass. Mice were switched to IFD with a total fat content of 140 g/kg providing ~31% energy from soybean oil (50 g/kg) and an experimental fat source (90 g/kg borage oil, fish oil, a proportionate mixture of both, or palm oil; Table 1). Following IFD-feeding, mice were either killed for tissue dissection (Figure 5 C and D) or administered HFD with a total fat content of 250 g/kg (50 g/kg soybean oil, 110 g/kg palm oil and 90 g/kg experimental oil) providing ~48% energy from fat (Table 1, Figure 5 E). Fish-oil comprising diets were produced using a pharmaceutical marine oil preparation (Henry Lamotte Oils, Bremen/Germany) with a total n3-PUFA content of ~34% including ~18% EPA and ~12% DHA. All IFDs (S5745-E141 (90 g/kg palm oil), -E142 (90 g/kg borage oil), -E143 (90 g/kg fish oil), -E152 (80 g/kg borage oil, 10 g/kg fish oil), -E153 (60 g/kg borage oil, 30 g/kg fish oil)) and HFDs (S5745-E722 (palm oil), -E146 (borage oil) and -E147 (fish oil)) were produced by Ssniff Spezialdiäten GmbH, and supplemented with butylated hydroxytoluene and exchanged twice per week to minimize fatty acid peroxidation in a thermoneutral environment. Mice were provided *ad libitum* access to IFDs and HFDs for 4 weeks in all experiments. Food intake was assessed regularly based on the difference in feeder weights

between two time points. Body composition was determined by nuclear magnetic resonance spectroscopy (mq7.5, Bruker BioSpin GmbH, Rheinstetten/Germany).

4.4.3 CL-316,243 treatment

Intraperitoneal injection of CL-316,243 (0.2 mg/kg) was conducted once daily on 7 consecutive days at the same time of the day. Vehicle-treated mice received saline. Body composition was assessed on the day of the first injection and on the day after the last injection. Mice were killed and dissected one day after the last injection.

4.4.4 Oral glucose tolerance tests

After 6 hours of fasting, mice received an oral glucose load of 2.8 g/kg lean mass. Blood glucose levels were measured at incised tail tips before (0 min) and during 2 hours after glucose gavage (FreeStyle Lite, Abbott, Wiesbaden/Germany). Fasting and glucose tolerance tests were performed at RT ($23^{\circ}\text{C} \pm 1^{\circ}\text{C}$) to enhance glucose uptake by BAT and brite adipose tissue via mild cold-activation. Using this experimental design we previously demonstrated UCP1-dependent differences in oral glucose tolerance (Maurer et al. 2020). The total AUC of blood glucose levels was calculated by the trapezoidal method (Purves 1992). Glucose tolerance was determined at the end of IFD and HFD feeding.

4.4.5 Oxylipin analysis

Whole blood was collected in lithium heparin-coated tubes (Sarstedt, Nümbrecht/Germany) and centrifuged for 5 min with 2,000 g at RT. The plasma supernatant was transferred to fresh tubes, snap-frozen in liquid nitrogen and stored at -80°C until use. An entire lobe of deep-frozen iWAT was grinded in liquid nitrogen. Aliquots of WAT and plasma were shipped on dry ice to commercial oxylipin analysis (Metatoul platform of metabolomics and fluxomics, Toulouse/France). Oxylipin abundance was normalized to plasma volume or tissue mass, respectively.

4.4.6 Histology

IWAT and iBAT were fixed in 4% formaldehyde and stored in 70% ethanol. Following automated dehydration and paraffin-embedding, 5 μm sections were drawn to object slides, dried at 37°C and stained with hematoxylin and eosin using an automated multistainer (ST5020, Leica, Wetzlar/Germany). Sections were mounted, dried and analyzed by bright field microscopy (M8, PreciPoint, Freising/Germany).

4.4.7 SDS-PAGE and Western Blot

Interscapular BAT was homogenized with a disperser (Micra D-1, Micra GmbH, Heitersheim/Germany) in a total volume of 10 μl /mg lysis buffer (50 mM Tris, 1% NP-40, 0.25% sodium deoxycholate, 150 mM NaCl, 1 mM EDTA) containing protease and phosphatase inhibitor

cocktail (0.1% each, Sigma-Aldrich, St. Louis MO/USA). Homogenates were centrifuged with 14,000-16,000 g at 4°C. The supernatant was centrifuged again and cleared from residual fat. Total protein was resolved in a 12.5% gel and transferred to a nitrocellulose membrane. Primary antibodies were applied to detect UCP1 (~32 kDa, custom-made rabbit-anti-hamster IgG known to reliably detect murine UCP1 (C. W. E. Meyer et al. 2004)) or pan actin (~43 kDa, anti-actin clone c4, Merck Millipore, Burlington MA/USA). A molecular weight marker (PageRuler Prestained Protein Ladder, Thermo Fisher Scientific) was used to confirm the detection of target proteins. IR-dye conjugated secondary antibodies (LI-COR, Lincoln NE/USA) were applied and detected at 700 nm or 800 nm with the Odyssey imager (LI-COR, Lincoln NE/USA). Image analysis was conducted with the Odyssey software 3.0 (LI-COR) or Image Studio Lite software 5.2 (LI-COR, Lincoln NE/USA). UCP1 was normalized to pan-actin or total protein staining (REVERT Total Protein Stain, LI-COR, Lincoln NE/USA) as indicated in figure legends.

4.4.8 RNA isolation and quantitative real-time PCR of murine samples

IWAT was homogenized in TRIsure™ (Bioline, London/UK) with a dispersing instrument (Micra D-1, Micra, Heitersheim/Germany). Volumes containing precipitated RNA were transferred to spin columns (SV Total RNA Isolation System, Promega, Madison WI/USA), centrifuged for 1 min with 12,000 g and further processed according to the manufacturers protocol. RNA concentrations were determined spectrophotometrically (Infinite 200 PRO NanoQuant, Tecan, Männedorf/Switzerland). Generation of cDNA was performed with the SensiFAST cDNA Synthesis Kit (Bioline, London/UK) or QuantiTect Reverse Transcription Kit (Qiagen, Hilden/Germany). Quantitative real-time PCR was performed in a 384 well plate format with the LightCycler 480 system (Roche Diagnostics, Rotkreuz/Switzerland) and SensiMix SYBR no-ROX (Bioline, London/UK). Primers (Eurofins Genomics Germany GmbH, Ebersberg/Germany): UCP1 (TCTCTGCCAGGACAGTACCC and AGAAGCCCAATGATGTTCAG), cell death-inducing DNA fragmentation factor, alpha subunit-like effector A (Cidea) (TGCTCTTCTGTATCGCCCAGT and GCCGTGTTAAGGAATCTGCTG), cytochrome c oxidase subunit 7a isoform 1 (Cox7a1) (CCGACAATGACCTCCCAGTA and TGTTTGTCCAAGTCCTCCAA), general transcription factor IIB (Gtf2b) (TGGAGATTTGTCCACCATGA and GAATTGCCAAACTCATCAAACT), ribosomal protein lateral stalk subunit P0 (Rplp0, also known as 36b4) (CTTTATCAGCTGCACATCACTCAGA and TCCAGGCTTTGGGCATCA), tumor necrosis factor alpha (TNF α) (TGCCTATGTCTCAGCCTCTTC and GAGGCCATTTGGGAACTTCT), F4/80 (CCTGGACGAATCCTGTGAAG and GGTGGGACCACAGAGATTG). Target gene expression was normalized as indicated in figure legends.

4.4.9 Human dietary intervention study

The MyNewGut study was a 12-week randomized crossover trial that investigated diet-induced effects on gut microbiota composition and markers of MetS in individuals with overweight

(Kjølbæk et al. 2020). The study is registered at Clinical Trial (NCT02215343), was conducted according to the guidelines laid down in the Declaration of Helsinki, and carried out at the University of Copenhagen (Department of Nutrition, Exercise and Sports) in accordance with the ethical standards of the responsible regional committee on human experimentation in Denmark. In brief, the study was composed of two 4-week dietary interventions separated by a 4-week wash out period. In one of the dietary interventions, participants supplemented their diet with 10.4 g/d wheat bran extract rich in arabinoxylan oligosaccharides (AXOS). In the other dietary intervention, participants supplemented their diet with fish oil containing 3.6 g/d n3 PUFA, including 1.32 g DHA and 1.86 g EPA. Apart from increasing the intake of fish oil, the PUFA intervention also aimed at increasing PUFA intake to 10% of total energy intake by reducing the intake of saturated fatty acids. The participants had not supplemented their diet with fish oil for six weeks preceding study start. Inclusion criteria can be found elsewhere (Kjølbæk et al. 2020). Briefly, the participants baseline characteristics were: a median age of 46 years (IQR: 34 – 53 years), a median BMI of 30.0 kg/m² (IQR: 27.4 – 31.7 kg/m²), a median waist circumference of 94.3 cm (IQR: 90.3 – 102.0 cm). Besides having increased waist circumference 32.1 %, 17.9 %, 7.1 % and 3.6 % of the participants had a MetS score (International Diabetes Federation 2005) of 1,2,3 and 4, respectively.

4.4.10 Gene expression analyses in human abdominal subcutaneous adipose tissue

Subcutaneous adipose tissue was obtained from the abdominal region after an overnight fast before and after each dietary intervention. Following skin sterilization and local anaesthetization (lidocaine 1% or 2%), a small incision was made in the abdominal skin. Trained medical staff sampled ~1 g of subcutaneous fat by biopsy needles (5 mm, Pelomi, Albertslund/Denmark). Adipose samples were immediately rinsed in sterile saline and submerged in Allprotect Tissue Reagent (Qiagen, Hilden/Germany) before being frozen in liquid nitrogen and cryopreserved at -80°C until extraction of RNA. Frozen adipose tissue biopsies (~100 mg) were homogenized using a GentleMACS Dissociator (Miltenyi Biotec, Bergisch Gladbach/Germany). Total RNA was extracted using QIAzol lysis buffer and the miRNeasy Mini Kit (Qiagen, Hilden/Germany). RNA concentration and purity were determined using a NanoDrop Spectrophotometer (Thermo Fisher Scientific, Waltham MA/USA). Synthesis of cDNA was based upon 136 ng of RNA and carried out using TaqMan Reverse Transcription Reagents (Thermo Fisher Scientific) and a 7900 HT Fast Real-Time PCR Thermocycler (Applied Biosystems, Waltham MA/USA). cDNA related to the same participant was synthesized on the same plate. qPCR was performed using a 7900 HT Fast Real-Time PCR Thermocycler (Applied Biosystem, Waltham MA/USA s), TaqMan Fast Advanced Master Mix (Thermo Fisher Scientific), and TaqMan Gene Expression Assay containing primers and probes for UCP1 (Hs00222453_m1, Thermo Fisher Scientific) and adiponectin (Hs00605917_m1, Thermo Fisher Scientific). All samples from each participant were analyzed in triplicate and on

the same plate in order to avoid bias from inter-run variation. Conditions for thermal cycling were: 50°C for 2 minutes, 95°C for 20 minutes, and 50 cycles of 1 second at 95°C and 20 seconds at 60°C. Peptidylprolyl isomerase A (PPIA) (Hs04194521_s1, ThermoFisher Scientific) was chosen as the reference gene for normalization.

4.4.11 Lipidomic Analysis of human plasma

Venous blood samples were drawn after an overnight fasting period at the start and end of each dietary intervention period. Samples were collected in EDTA tubes, placed directly on ice and immediately centrifuged at 2500 g for 10 min at 4°C. Samples were stored at -80°C until shipped to University Hospital Regensburg/Germany for lipidomic analysis. Lipids were quantified by direct flow injection electrospray ionization tandem mass spectrometry (ESI-MS/MS) in positive ion mode using the analytical setup and strategy described previously (Liebisch et al. 2004). A fragment ion of m/z 184 was used for lysophosphatidylcholine (Liebisch et al. 2002). The following neutral losses were applied: PE-based plasmalogens were analyzed according to the principles described by Zemski-Berry (Zemski Berry and Murphy 2004). Cholesteryl ester were quantified using a fragment ion of m/z 369 after selective derivatization of free cholesterol (Liebisch et al. 2006). Lipid species were annotated according to the recently published proposal for shorthand notation of lipid structures that are derived from mass spectrometry (Liebisch et al. 2013).

4.4.12 Dosage Information

Doses of borage and fish oil supplemented in the mouse diets (Table 1) were chosen in order to match either the n6/n3-ratio found in modern western diets (16:1) or the recommendation for a healthy fatty acid ratio (1:1)(Simopoulos 2016). For the diets containing the highest doses of fish oil (90 g/kg) the dose was 225 mg/d based on an average food consumption of 2.5 g/d at 30 g body weight. Based on body surface area (Nair and Jacob 2016), this corresponds to a human equivalent fish oil dose of 33.7 g/d for a 60 kg person. This dose of fish oil cannot be achieved by available nutritional supplements.

The MyNewGut study aimed at providing a high amount of n3-PUFA using an intake of six daily capsules (1.32g/d EPA and 1.86 g/d DHA). This amount is at least twice the amount oftentimes applied but is in accordance with EFSA's safety guidelines stating that the combined daily intake of EPA and DHA should not exceed 5 g/d (EFSA Panel on Dietetic Products Nutrition and Allergies (NDA) 2012).

4.4.13 Statistics

Data are displayed as individual values with the group mean indicated as horizontal line, or as mean values \pm standard deviation. Statistical analyses were conducted using Prism 6 and 8 for mouse and human data, respectively (GraphPad Software Inc., La Jolla CA/USA). Murine data were

analyzed by 2-Way ANOVA (Figure 15, Figure 16, Figure 17, Figure 19, Figure 20 E-H, Figure 21 B, Figure 22 B) or 2-Way repeated measures ANOVA (Figure 20 A-D, Figure 21 A & C-H, Figure 22 A & C-H) and Holm-Sidak post-test if applicable. Significant effects are indicated by asterisks (* $p < 0.05$; ** $p < 0.01$; *** $p < 0.001$; **** $p < 0.0001$). Energy intake (Figure 20 H, Figure 21 B, Figure 22 B) is depicted as mean energy intake per cage for each mouse. PCA was calculated in R (version 3.6.3) and R-Studio (version 1.2.5033) with the packages factoextra (version 1.0.7) and FactoMineR (version 2.3) on scaled and centered data. Human data were analyzed using two-tailed Wilcoxon matched-pairs signed rank test.

4.5 RESULTS

4.5.1 Fish oil and borage oil supplementations cause divergent changes in PUFA metabolism

Dietary fish oil supplementation has been reported to recruit thermogenic adipocytes in murine BAT and WAT (Oliveira et al. 2019; Bargut, Silva-e-Silva, et al. 2016; Bargut, Souza-Mello, et al. 2016; Bhaskaran et al. 2017; M. Kim et al. 2015; Kalupahana et al. 2010; Pahlavani et al. 2017; J. Kim et al. 2016; Ludwig et al. 2013; Worsch et al. 2018; J. Villarroya et al. 2014; Zhuang et al. 2019; You et al. 2020; Ghandour et al. 2018; Bargut et al. 2019; Sato et al. 2020). To investigate this effect under thermoneutral housing conditions, two common inbred mouse strains, C57BL/6J and 129S6/SvEvTac, were subjected to dietary PUFA supplementation at 30°C (Figure 5 C). Mice of both strains received a fish oil-comprising diet rich in EPA and DHA to increase n3 PUFA uptake (dietary n6/n3 ratio = 1.0). Alternatively, mice were administered a borage oil-comprising diet rich in n6-PUFAs including γ -linolenic acid (dietary n6/n3 ratio = 23.2). A third group of mice was used as control and fed an isocaloric, palm oil-comprising diet devoid of these fatty acids (dietary n6/n3 ratio = 12.7; Figure 6). Plasma oxylipin profiling was conducted after 4 weeks of feeding to validate PUFA supplementation by the chosen fat sources. In line with respective elevated PUFA concentrations, fish oil and borage oil increased the total plasma oxylipin concentration compared to palm oil-fed mice of both mouse strains (Figure 15 A). The ratio of n6-derived to n3-derived plasma oxylipins was approximately doubled by borage oil versus palm oil supplementation, while it was strongly reduced by fish oil supplementation (Figure 15 B). Thus, borage oil promoted the systemic production of n6 derived oxylipins, while fish oil strongly enhanced n3-derived oxylipin production. This diet-induced difference in oxylipin abundance was less pronounced in iWAT, a subcutaneous fat depot with a high propensity to undergo browning. The relative increase in the total oxylipin concentration upon fish and borage oil supplementation was lower in iWAT compared to plasma in both mouse strains and even less pronounced in the 129S6/SvEvTac strain (Figure 15 A & C). Similarly, borage oil supplementation doubled the ratio of n6 derived to n3 derived iWAT oxylipins over that of palm oil fed mice in the C57BL/6J but not 129S6/SvEvTac strain, suggesting a strain specific response to n6-PUFA supplementation (Figure 15 D). Fish oil

supplementation reduced the ratio of n6 derived to n3 derived oxylipins in iWAT of both mouse strains (Figure 15 B), but within a lower order of magnitude compared to plasma (Figure 15 D).

We performed PCA analyses, which clearly separated the plasma oxylipin profiles of the diet groups (Figure 15 E). In line with a strong decrease of the n6/n3 oxylipin ratio in plasma (Figure 15 B), fish oil supplementation resulted in a positive shift along PC2 in both mouse strains (Figure 15 E). This shift was caused primarily by increased concentrations of n3-oxylipins (Table 3). Additionally, fish oil and borage oil supplementation resulted in a negative shift along PC1, separating both diets from palm oil. This shift was caused primarily by the highly abundant n3-derived hydroxy-DHA (14-HDoHE and 17-HDoHE) and n6-derived 13-HODE and 9-HODE as well as the n6-oxylipin 6k-PGF1 α (Table 3). Similarly, the PC analysis of iWAT separated the oxylipin profile of fish oil-fed mice via a negative shift along PC2 (Figure 15 F), based on the contribution of n3-derived oxylipins (Table 4). Oxylipin profile in iWAT of fish oil and borage oil supplemented animals separated from palm oil via a positive shift along PC1 (Figure 15 F). This shift was primarily caused by increasing concentrations of n6-derived CYP450 products (5,6-EET, 8,9-EET and 14,15-EET) as well as n6-derived (5-HETE, 5oxoETE and Leukotriene B4) and n3-derived (9-HODE and 13-HODE) LOX products (Table 4). Interestingly, this shift was more pronounced in iWAT of fish oil-fed C57BL/6J than in 129S6/SvEvTac mice (Figure 15 F). Thus, n3-PUFA supplementation via fish oil enhanced the abundance of all detectable n3 derived oxylipins (Table 4) but also increased n6 derived oxylipins. Taken together, borage and fish oil comprising diets abundantly provided n6 and n3-PUFAs, respectively, and efficiently modulated fatty acid metabolism.

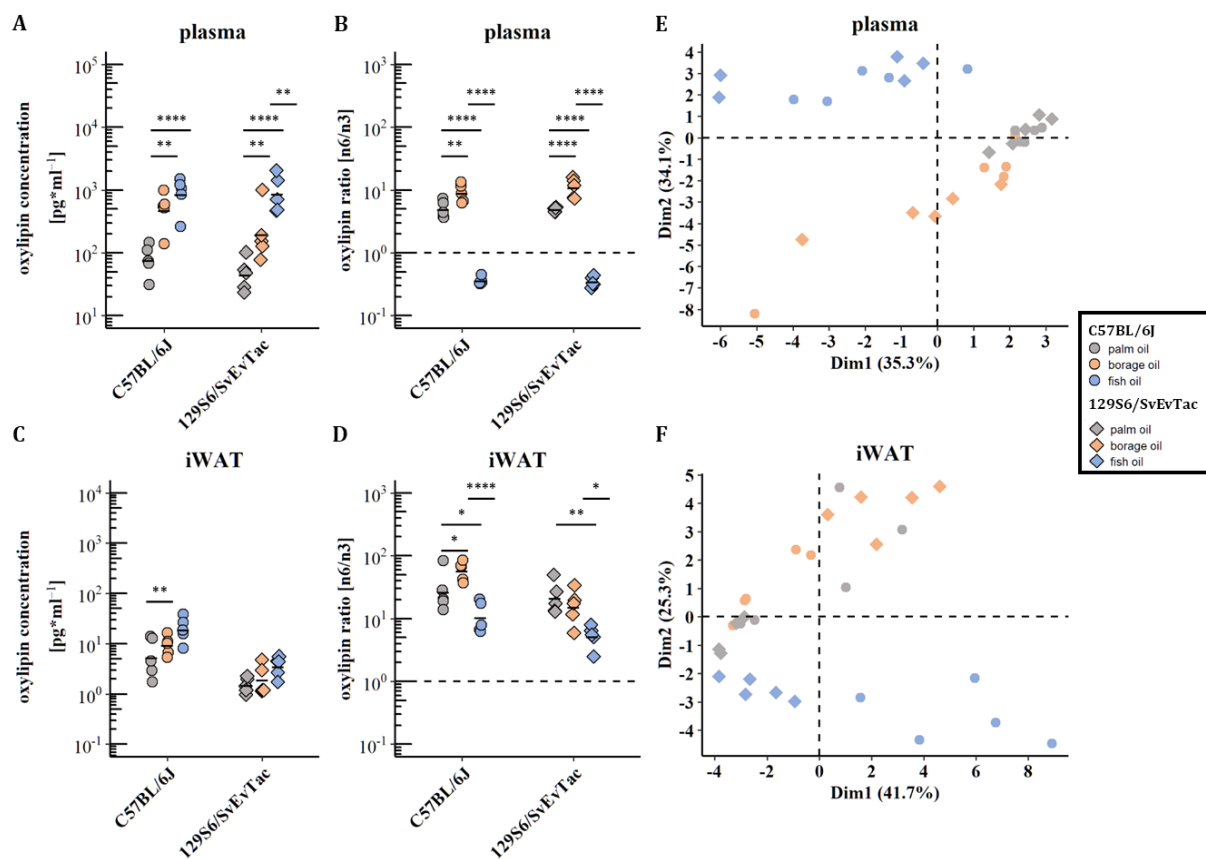


Figure 15: Effect of dietary PUFA supplementation on the oxylipin profile of plasma and iWAT in C57BL/6J and 129S6/SvEvTac mice.

(A) Total concentration of all measured oxylipins in plasma. (B) Ratio of n6-derived oxylipins in plasma. (C) Total concentration of all measured oxylipins in iWAT. (D) Ratio of n6-derived to n3-derived oxylipins in iWAT. (E) Principal component analysis of the plasma oxylipin profile. (F) Principal component analysis of the iWAT oxylipin profile. Asterisks indicate a significant effect of the fat source in C57BL/6J or 129S6/SvEvTac mice ($n = 5$).

Table 3: Plasma oxylipin concentrations [pg*ml⁻¹] of C57BL/6J and 129S6/SvEvTac mice (related to Figure 15).

Oxylipin	C57BL/6J			129S6/SvEvTac		
	palm oil	borage oil	fish oil	palm oil	borage oil	fish oil
8iso-PGA2 (n6)	82.16 ± 183.72	88.72 ± 91.85	0.00 ± 0.00	113.57 ± 67.30	211.94 ± 106.58	68.31 ± 152.74
15d-PGJ2 (n6)	0.00 ± 0.00 ^a	0.00 ± 0.00 ^a	90.11 ± 8.73 ^b	54.77 ± 53.37 ^{A,B}	0.00 ± 0.00 ^A	106.27 ± 29.90 ^B
PGF2α (n6)	0.00 ± 0.00	49.87 ± 111.51	23.46 ± 52.45	0.00 ± 0.00	49.64 ± 111.01	104.05 ± 62.19
6k-PGF1α (n6)	15.79 ± 35.32	97.31 ± 160.00	189.55 ± 191.20	18.99 ± 42.46 ^A	124.45 ± 156.99 ^{A,B}	222.90 ± 158.15 ^B
PGE3 (n3)	179.47 ± 53.76	122.16 ± 111.69	173.51 ± 111.05	64.98 ± 90.46	0.00 ± 0.00	36.05 ± 80.62
TxB2 (n6)	33.47 ± 74.84 ^a	1349.35 ± 1924.12 ^b	593.71 ± 693.03 ^{a,b}	60.26 ± 83.17	330.27 ± 451.05	392.27 ± 428.48
LTB4 (n6)	0.00 ± 0.00 ^a	111.04 ± 32.07 ^b	57.97 ± 62.33 ^{a,b}	0.00 ± 0.00 ^A	111.48 ± 71.56 ^B	96.46 ± 61.44 ^B
LTB5 (n3)	0.00 ± 0.00 ^a	0.00 ± 0.00 ^a	143.85 ± 88.37 ^b	0.00 ± 0.00 ^A	0.00 ± 0.00 ^A	153.14 ± 126.18 ^B
5-HETE (n6)	2692.44 ± 319.02 ^{a,b}	3969.62 ± 785.53 ^a	1142.07 ± 264.52 ^b	2585.75 ± 810.94 ^{A,B}	3455.12 ± 1285.49 ^A	1469.02 ± 381.65 ^B
8-HETE (n6)	1354.94 ± 347.82 ^a	4096.70 ± 1220.21 ^b	1416.25 ± 540.28 ^a	806.52 ± 492.03	2147.19 ± 1734.35	1390.69 ± 743.84
12-HETE (n6)	55685.28 ± 34024.08 ^a	472046.02 ± 277710.47 ^b	240345.64 ± 123875.22 ^{a,b}	28163.35 ± 21617.20 ^A	251251.55 ± 321561.13 ^{A,B}	238149.83 ± 154677.59 ^B
15-HETE (n6)	825.70 ± 127.81 ^{a,b}	2053.87 ± 405.44 ^a	684.30 ± 157.76 ^b	809.16 ± 321.43 ^A	1822.91 ± 1114.45 ^B	911.17 ± 383.00 ^{A,B}
18-HEPE (n3)	0.00 ± 0.00 ^a	28.28 ± 63.23 ^a	2015.86 ± 619.85 ^b	0.00 ± 0.00 ^A	0.00 ± 0.00 ^A	2560.26 ± 1254.14 ^B
5,6-EET (n6)	671.81 ± 136.00 ^a	1706.16 ± 417.33 ^b	561.10 ± 356.14 ^a	774.06 ± 168.90 ^{A,B}	1234.85 ± 738.93 ^A	403.29 ± 249.86 ^B
8,9-EET (n6)	126.97 ± 176.59	482.10 ± 115.84	291.38 ± 314.22	252.22 ± 238.63	533.19 ± 482.31	161.14 ± 220.97
14,15-EET (n6)	228.42 ± 129.18 ^{a,b}	333.39 ± 213.96 ^a	0.00 ± 0.00 ^b	334.28 ± 203.88 ^{A,B}	550.63 ± 251.13 ^A	70.88 ± 158.50 ^B
13-HODE (n6)	5415.05 ± 830.90 ^a	12912.00 ± 3722.97 ^b	13912.56 ± 6443.66 ^b	5751.47 ± 1924.59	13229.98 ± 14700.12	12012.78 ± 5123.65
9-HODE (n6)	2972.29 ± 830.39	3984.20 ± 995.47	4086.06 ± 683.99	2787.91 ± 749.77	3717.10 ± 1898.09	4484.97 ± 1559.84
7MaR1 (n3)	0.00 ± 0.00 ^a	0.00 ± 0.00 ^a	487.17 ± 331.91 ^b	0.00 ± 0.00 ^A	0.00 ± 0.00 ^A	1115.29 ± 518.28 ^B
PDx (n3)	0.00 ± 0.00 ^a	36.43 ± 49.90 ^a	583.60 ± 136.46 ^b	24.47 ± 54.71 ^A	59.82 ± 55.06 ^A	858.86 ± 369.05 ^B
17-HDoHE (n3)	1188.92 ± 355.53 ^a	1966.51 ± 580.00 ^{a,b}	33792.47 ± 14670.70 ^b	1072.21 ± 440.60 ^A	2053.69 ± 2279.31 ^A	34292.36 ± 22275.27 ^B
14-HDoHE (n3)	14418.61 ± 9963.58 ^a	55262.53 ± 26865.02 ^{a,b}	675726.69 ± 320079.88 ^b	7637.53 ± 5415.55 ^A	30862.89 ± 45337.63 ^{A,B}	729413.31 ± 505585.98 ^B

Mice of both strains were kept at 30°C and fed with diets (140 g/kg total fat content) comprising fish, borage or palm oil as fat source (90 g/kg). The plasma oxylipin profile was analyzed after 4 weeks of feeding. All listed oxylipins were identified in at least 1 sample. The compounds PGA1, PGD2, 11β-PGF2α, PGE2, LxA4, LxB4, 5oxoETE, 5,6-DiHETE, 11,12-EET, RvD1 and RvD2 were undetectable in plasma of all mice. Oxylipin concentrations are expressed as mean ± standard deviation (n=5). Oxylipin concentrations were analyzed by Kruskal-Wallis test and Dunn's multiple comparison test in each mouse strain. Different superscripted, printed characters indicate a significant effect (p<0.05) of the fat source on plasma oxylipin concentration in C57BL/6J (lowercase a, b, c) or 129S6/SvEvTac (uppercase A, B, C) mice. Uppercase are not to be compared to lowercase letters.

Table 4: iWAT oxylipin concentrations [pg*mg tissue⁻¹] of C57BL/6J and 129S6/SvEvTac mice (related to Figure 15).

Oxylipin	C57BL/6J			129S6/SvEvTac		
	palm oil	borage oil	fish oil	palm oil	borage oil	fish oil
PGA1 (n6)	2.31 ± 1.22 ^{a,b}	7.12 ± 1.32 ^a	0.00 ± 0.00 ^b	0.72 ± 0.30 ^{A,B}	2.94 ± 1.73 ^A	0.51 ± 0.42 ^B
8iso-PGA2 (n6)	24.06 ± 22.53	33.37 ± 9.47	18.04 ± 5.94	5.92 ± 3.18	16.20 ± 9.54	6.24 ± 5.37
PGD2 (n6)	0.90 ± 2.02	1.00 ± 1.20	1.23 ± 2.76	0.18 ± 0.40 ^{A,B}	1.00 ± 1.10 ^A	0.00 ± 0.00 ^B
15d-PGJ2 (n6)	1.58 ± 1.94 ^{a,b}	1.55 ± 0.78 ^a	0.00 ± 0.00 ^b	0.57 ± 0.71 ^{A,B}	0.61 ± 0.08 ^A	0.00 ± 0.00 ^B
11β-PGF2α (n6)	0.00 ± 0.00	0.00 ± 0.00	0.00 ± 0.00	0.00 ± 0.00	0.00 ± 0.00	0.22 ± 0.22
PGE2 (n6)	7.74 ± 10.51	9.09 ± 4.40	5.99 ± 3.55	2.32 ± 1.19 ^{A,B}	10.39 ± 5.91 ^A	2.61 ± 3.73 ^B
PGF2α (n6)	11.53 ± 5.25	15.20 ± 3.34	10.02 ± 6.89	4.94 ± 1.95 ^{A,B}	8.80 ± 1.72 ^A	1.39 ± 0.81 ^B
6k-PGF1α (n6)	49.97 ± 23.69 ^{a,b}	79.03 ± 27.23 ^a	23.39 ± 14.01 ^b	30.05 ± 22.79	39.00 ± 21.04	13.64 ± 15.06
PGE3 (n3)	0.00 ± 0.00 ^a	0.00 ± 0.00 ^a	8.31 ± 2.13 ^b	0.00 ± 0.00 ^A	0.00 ± 0.00 ^A	1.63 ± 1.14 ^B
TxB2 (n6)	32.12 ± 17.99 ^{a,b}	51.70 ± 18.51 ^a	18.99 ± 13.69 ^b	11.58 ± 8.17	14.03 ± 8.71	4.32 ± 2.90
LxA4 (n6)	0.00 ± 0.00	1.50 ± 1.41	0.00 ± 0.00	0.00 ± 0.00	0.19 ± 0.43	0.00 ± 0.00
LTB4 (n6)	2.32 ± 1.42 ^a	3.46 ± 0.73 ^{a,b}	7.24 ± 1.81 ^b	0.34 ± 0.32	1.16 ± 1.16	1.32 ± 0.74
LTB5 (n3)	0.00 ± 0.00	0.00 ± 0.00	0.00 ± 0.00	0.25 ± 0.24	0.16 ± 0.23	1.34 ± 1.63
5oxoETE (n6)	40.48 ± 32.73 ^a	101.55 ± 23.01 ^{a,b}	140.82 ± 75.87 ^b	6.25 ± 3.73	23.19 ± 22.82	22.24 ± 10.74
5,6-DiHETE (n6)	0.00 ± 0.00	0.00 ± 0.00	0.00 ± 0.00	0.00 ± 0.00	0.23 ± 0.24	0.00 ± 0.00
5-HETE (n6)	100.48 ± 76.49	200.48 ± 36.21	164.39 ± 54.73	17.79 ± 8.98	36.65 ± 41.37	57.55 ± 26.58
8-HETE (n6)	35.13 ± 20.38	50.94 ± 13.49	42.56 ± 13.37	8.12 ± 3.37	19.54 ± 16.64	11.52 ± 5.94
12-HETE (n6)	557.28 ± 370.10	574.11 ± 143.55	303.52 ± 145.98	170.66 ± 110.03 ^{A,B}	518.80 ± 361.51 ^A	82.62 ± 24.89 ^B
15-HETE (n6)	150.18 ± 110.54	252.70 ± 76.75	202.73 ± 72.17	36.08 ± 19.54	118.19 ± 104.48	52.82 ± 24.81
18-HEPE (n3)	1.37 ± 0.79 ^a	1.96 ± 0.54 ^{a,b}	362.53 ± 113.44 ^b	0.00 ± 0.00 ^A	0.44 ± 0.33 ^{A,B}	120.79 ± 82.25 ^B
5,6-EET (n6)	55.66 ± 45.41	105.32 ± 46.70	120.19 ± 109.29	8.49 ± 2.34	17.76 ± 16.04	19.06 ± 10.07
8,9-EET (n6)	40.41 ± 36.99	58.18 ± 30.84	106.74 ± 71.32	3.45 ± 1.13	7.94 ± 7.86	9.18 ± 5.29
11,12-EET (n6)	34.12 ± 30.39	79.76 ± 44.41	69.69 ± 50.82	3.08 ± 2.86	10.96 ± 11.19	9.11 ± 6.12
14,15-EET (n6)	15.22 ± 13.68	32.25 ± 18.15	46.94 ± 33.47	1.89 ± 1.01	4.32 ± 4.00	4.54 ± 2.64
13-HODE (n6)	3756.21 ± 3261.75	4714.66 ± 2270.13	10772.99 ± 6259.98	737.94 ± 217.81 ^{A,B}	754.53 ± 662.67 ^A	1668.83 ± 700.90 ^B
9-HODE (n6)	2039.98 ± 1782.36 ^a	3392.40 ± 1687.85 ^{a,b}	7727.27 ± 4935.09 ^b	436.12 ± 115.40 ^{A,B}	502.99 ± 474.22 ^A	1187.89 ± 533.92 ^B
7MaR1 (n3)	0.00 ± 0.00 ^a	0.00 ± 0.00 ^a	54.46 ± 15.29 ^b	0.00 ± 0.00 ^A	0.00 ± 0.00 ^A	14.05 ± 9.92 ^B
PDx (n3)	1.74 ± 0.91 ^a	1.30 ± 0.84 ^a	20.39 ± 6.54 ^b	0.44 ± 0.33 ^A	0.59 ± 0.51 ^A	5.54 ± 3.69 ^B
17-HDoHE (n3)	84.02 ± 51.07 ^a	75.18 ± 26.36 ^a	593.28 ± 189.70 ^b	30.50 ± 18.37 ^A	71.51 ± 67.77 ^{A,B}	232.64 ± 148.55 ^B
14-HDoHE (n3)	134.15 ± 94.85 ^a	84.08 ± 22.18 ^a	675.57 ± 244.40 ^b	54.27 ± 37.92 ^A	99.09 ± 97.28 ^{A,B}	277.38 ± 168.82 ^B

Mice of both strains were kept at 30°C and fed with diets (140 g/kg total fat content) comprising fish, borage or palm oil as fat source (90 g/kg). The iWAT oxylipin profile was analyzed after 4 weeks of feeding. All listed oxylipins were identified in at least 1 sample. The compounds LxB4, RvD1 and RvD2 were undetectable in iWAT of all mice. Oxylipin concentrations are expressed as mean ± standard deviation (n=5). Oxylipin concentrations were analyzed by Kruskal-Wallis test and Dunn's multiple comparison test in each mouse strain. Different superscripted, printed characters indicate a significant effect (p<0.05) of the fat source on iWAT oxylipin concentration in C57BL/6J (lowercase a, b, c) or 129S6/SvEvTac (uppercase A, B, C) mice. Uppercase are not to be compared to lowercase letters.

4.5.2 Dietary n3-PUFA supplementation does not influence the recruitment of thermogenic adipocytes in murine adipose tissues

To investigate whether dietary n3-PUFA supplementation affected the recruitment of thermogenic adipocytes, we determined UCP1 expression in BAT and WAT. Administration of n3-rich fish oil did not enhance UCP1 expression in iBAT or iWAT of either mouse strain (Figure 16 A & B). On the contrary, supplementation of n6-rich borage oil increased transcript abundance of brite adipocyte markers UCP1 and Cidea compared to palm and fish oil-fed mice of the C57BL/6J strain (Figure 16 B & C), while the expression of thermogenic marker genes was unaffected by the dietary fat source in WAT of 129S6/SvEvTac mice (Figure 16 B-D).

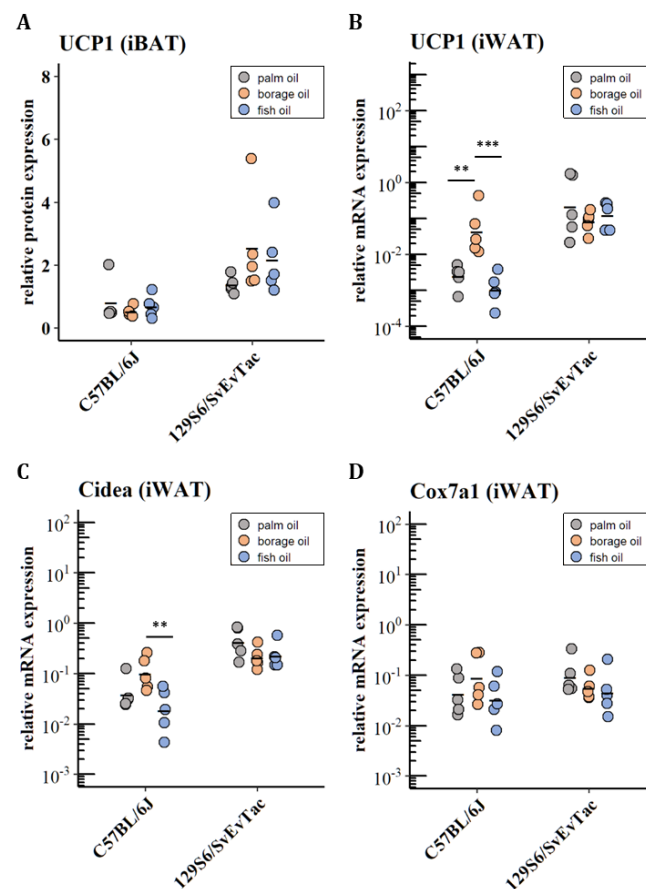


Figure 16: Effect of dietary PUFA supplementation on thermogenic adipocyte recruitment.

(A) Relative UCP1 levels in iBAT. UCP1 was normalized to pan-actin. A representative Western Blot image is displayed in Supplementary Figure 4. Relative gene expression of (B) UCP1, (C) Cidea, and (D) Cox7a1 in iWAT. Gene expression was normalized to Gtf2b. Asterisks indicate a significant effect of the fat source on C57BL/6J or 129S6/SvEvTac mice (n = 5).

In a second experiment we investigated whether the recruitment of brown and brite adipocytes is facilitated by the availability of n3-PUFAs upon adrenergic stimulation (Figure 5 D). C57BL/6J mice were fed diets with gradual increasing dietary n6/n3 ratios from ~1 (IFD1, previously “fish oil”), ~5 (IFD5), ~11 (IFD11) and ~18 (IFD18, previously “borage oil”) for 4 weeks (Figure 7). Additionally, the β 3-adrenoreceptor agonist CL-316,243 was administered on 7 consecutive days

during the last week (days 21-28) of the dietary intervention to stimulate the recruitment of brown and brite adipocytes.

In line with the ability to recruit and activate thermogenesis (Park et al. 2015; Hankir et al. 2017), CL-316,243 treatment resulted in UCP1 protein induction and a strong reduction in iBAT mass (Figure 17A and B), the latter of which was likely the consequence of concomitant UCP1 activation and lipid oxidation to fuel thermogenesis. Similarly, CL-316,243 administration resulted in a slight reduction of iWAT mass (Figure 17C) and the induction of brite adipocyte marker gene expression (Figure 17D-F). In line with these effects, CL-316,243 reversed diet-induced lipid droplet hypertrophy in brown adipocytes and promoted iWAT remodeling by brite adipogenesis (Figure 17 G). However, the dietary n6/n3 ratio neither affected thermogenic adipocyte abundance in vehicle nor in CL-316,243 treated mice. Interestingly, elevated UCP1 mRNA expression in iWAT of borage oil (IDF18) versus fish oil (IDF1)-fed mice (as observed in our previous experiment, Figure 16 B) was absent in mice of this experiment (Figure 17 D), suggesting that this effect is not robust. Based on the low gene expression levels of TNF α and F4/80 in iWAT (Figure 18) we did not see any indications of inflammation. Inhibition of UCP1 gene expression by adipose tissue inflammation and macrophage infiltration as published before (Sakamoto et al. 2016) is therefore unlikely. Collectively, the recruitment of brown and brite adipocytes was affected by CL-316,243 but not by the dietary fat source.

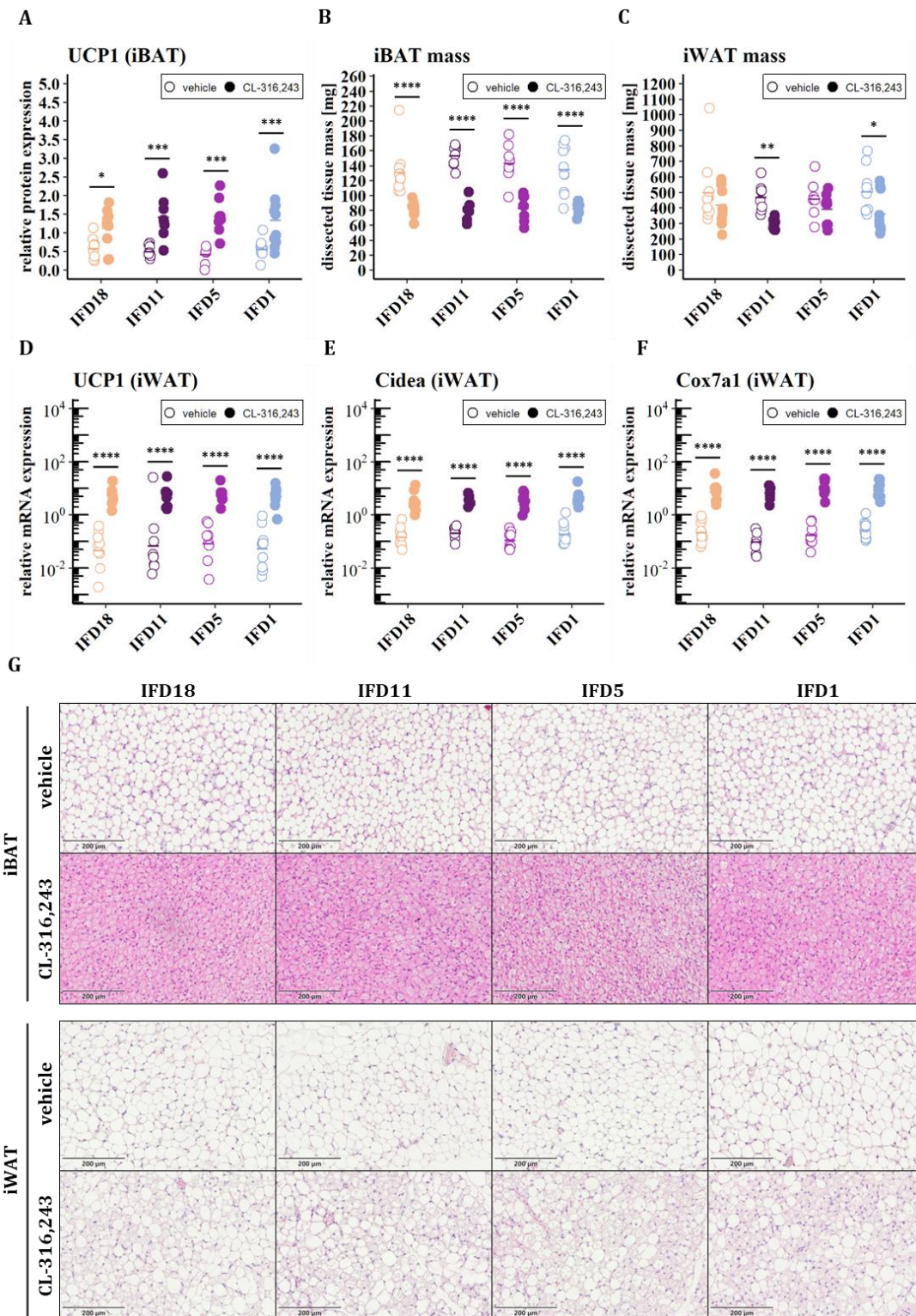


Figure 17: Effect of dietary PUFA-supplementation on the recruitment of thermogenic adipocytes in the presence and absence of β 3-agonism.

(A) Relative UCP1 protein levels. UCP1 was normalized to total protein stain (see Supplementary Figure 5). (B) Dissected iBAT mass. (C) Dissected iWAT mass. Relative gene expression of (D) UCP1, (E) Cidea, and (F) Cox7a1 in iWAT. Gene expression was normalized to Rplp0. (G) Hematoxylin/Eosin-stained iBAT and iWAT sections. Log10 transformed data was used for statistical analysis in (B) and (C) in order to meet the assumption of normal distribution. There were no significant effects of the diet among vehicle or CL-316243 treated mice. Asterisks indicate a significant effect of CL-316243 versus vehicle treatment ($n = 8-10$).

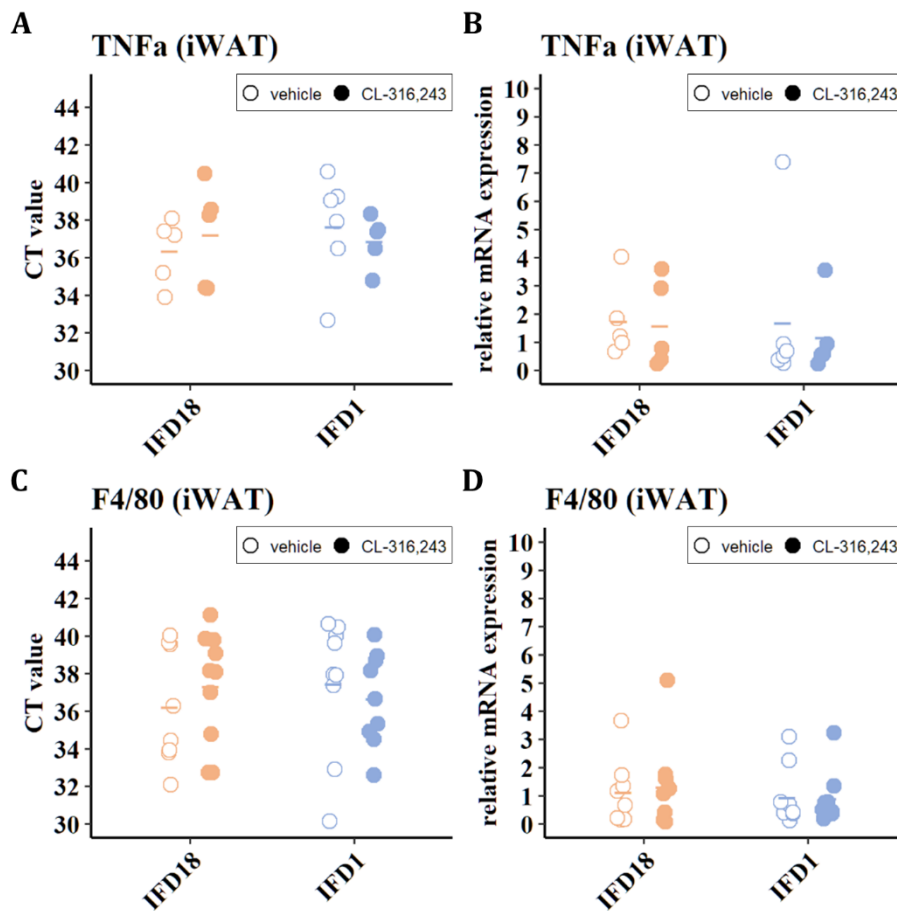


Figure 18: Effect of dietary PUFA supplementation on inflammatory marker expression in iWAT.

Gene expression of (A-B) *TNFα* and (C-D) *F4/80*, represented as CT values (A,C) or relative gene expression normalized to *Rplp0* (B,D).

Mice of all diet groups had comparable body mass and body composition at the beginning of CL-316,243 treatment following 3 weeks of PUFA supplementation (Figure 19). While body mass remained constant or tended to increase in vehicle treated mice, body mass was reduced by CL-316,243 administration initially but remained constant thereafter (Figure 20A-D). This small, -induced body mass reduction was similar for all dietary n6/n3 ratios (Figure 20E) and caused by a reduction in fat, not lean mass (Figure 20F and G). Mice fed with n3-rich IFD1 tended to show attenuated total body mass reduction in response to CL-316,243 despite significant fat mass loss (Figure 20E and F) caused by a minor gain in lean mass (Figure 20G). In line with these physiological effects, energy intake was not influenced by dietary n6/n3 ratios and comparable between vehicle and CL-316,243 treated mice (Figure 20H). Thus, thermogenic adipocyte recruitment and energy balance regulation were influenced by β_3 -adrenoreceptor agonism but not by dietary fat source.

Taken together, dietary fatty acid composition of isocaloric diets fed under thermoneutral housing conditions did not influence recruitment of murine thermogenic adipocytes, neither alone nor in synergy with the β_3 -adrenergic route of thermogenesis.

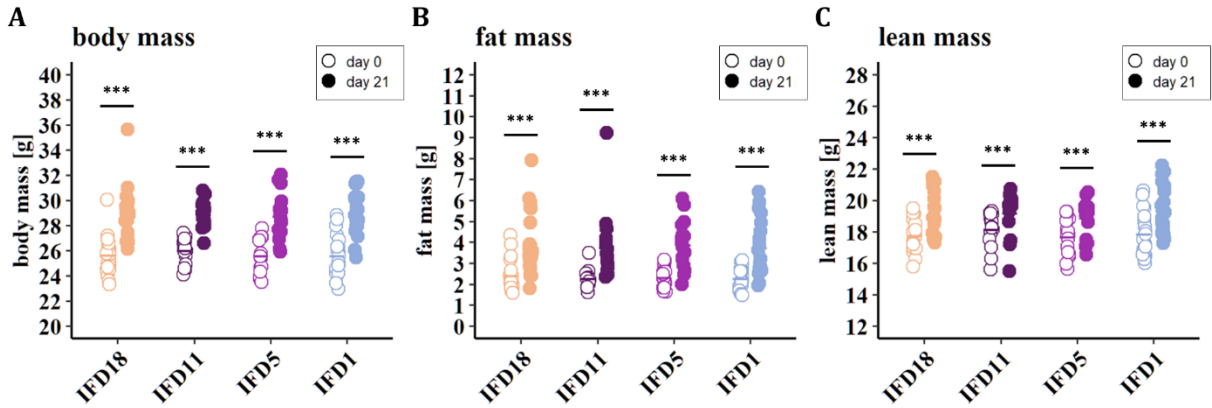


Figure 19: Effect of dietary PUFA supplementation on body mass and body composition prior to CL-316,243 administration.

(A) Body mass, (B) fat mass and (C) lean mass at the beginning of the experiment (day 0) and prior to CL-316,243 administration after three weeks of feeding (day 21; n=16-20 per diet). All datasets were analyzed by 2-Way repeated measures ANOVA and Holm-Sidak post-test. Asterisks indicate significant changes in body mass and body composition over time (***) p < 0.001). There were no significant effects of the dietary n6/n3 ratio at either timepoint.

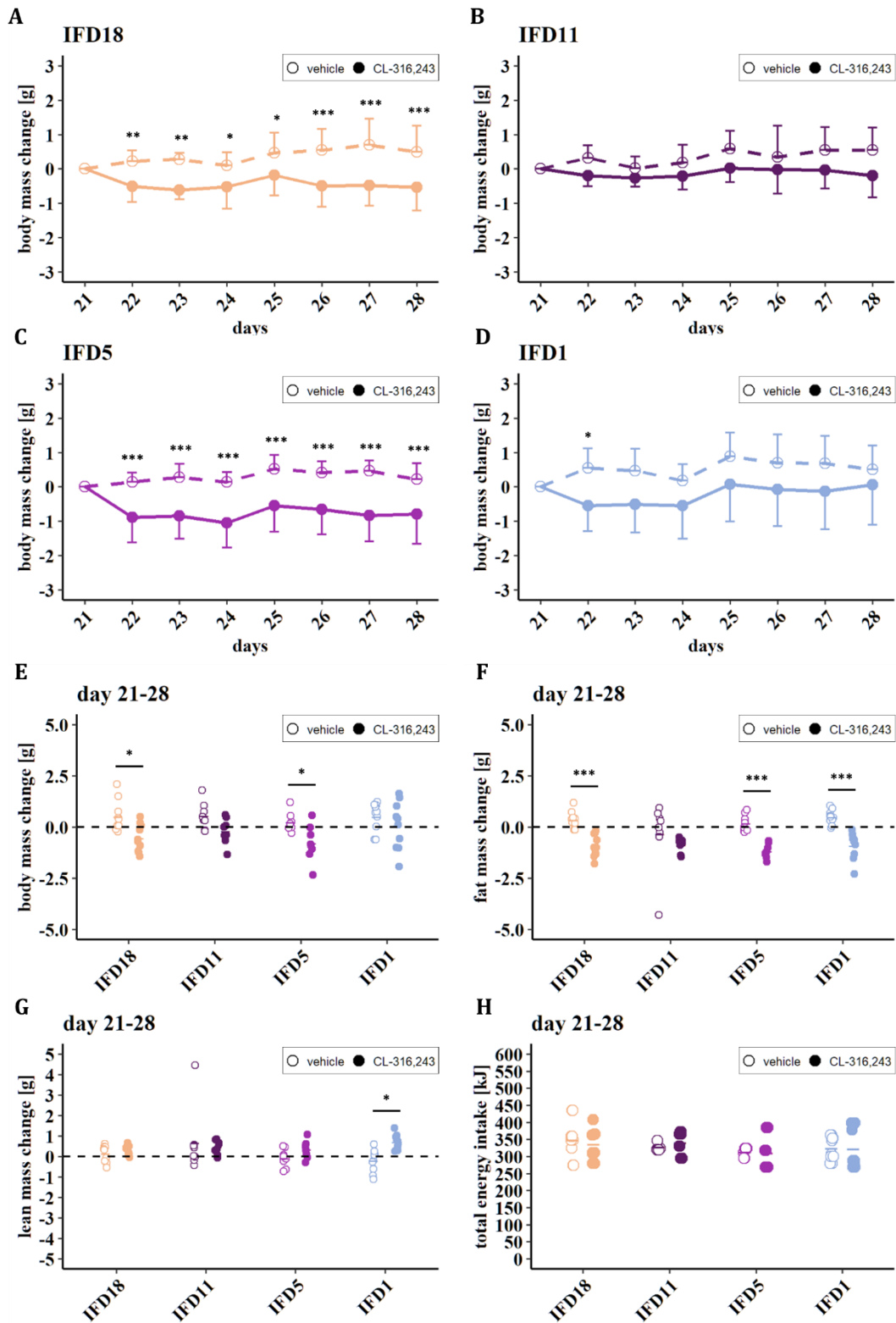


Figure 20: Effect of dietary PUFA supplementation and β 3-agonism on body mass and body composition changes.

Body mass trajectories depicting absolute changes in body mass during vehicle and CL-316243 treatment of mice fed with (A) IFD18, (B) IFD11, (C) IFD5, and (D) IFD1. Total changes in (E) body mass, (F) fat mass, and (G) lean mass during 7 days of vehicle and CL-316243 treatment. (H) Total energy intake during vehicle and CL-316243 treatment. Asterisks indicate a significant effect of CL-316243 versus vehicle treatment ($n = 8-10$). There were no significant effects of the diet among vehicle or CL-316,243 treated mice.

4.5.3 Dietary n3-PUFA supplementation does not influence the development of diet-induced obesity

The induction of thermogenic adipocytes by dietary n3-PUFAs has been associated with attenuated development of DIO and glucose intolerance (Oliveira et al. 2019; Bargut, Silva-e-Silva, et al. 2016; Bhaskaran et al. 2017; Kalupahana et al. 2010; Ludwig et al. 2013; Miller et al. 2019; Janovská et al. 2013). We assessed dietary fat source effects on these parameters in a third experiment (Figure 5 E). Mice of the C57BL/6J strain received palm oil, fish oil or borage oil comprising IFDs (140 g/kg total fat content) as conducted in the previous experiments. In line with our previous findings (Figure 20 E), body mass gain was unaffected by the dietary fat source during 4 weeks of IFD-feeding (Figure 21 A). To promote the development of DIO and glucose intolerance, IFDs were subsequently exchanged for HFD with a total fat content of 250 g/kg. The original proportion of borage and fish oil (90 g/kg) was maintained in these HFDs (Table 1). As expected, the enhanced caloric value of the HFD promoted body mass gain due to increased energy intake (Figure 21 A & B). This enhanced body mass gain during HFD feeding was caused by fat mass, not lean mass gain (Figure 21C-E). However, none of these parameters was affected by dietary fatty acid composition. We observed a similar pattern in a parallel experiment conducted with mice of the 129S6/SvEvTac strain (Figure 22 A-E).

To elucidate the effect of dietary PUFA supplementation on glucose homeostasis, mice were subjected to oral glucose tolerance tests at the end of IFD and HFD-feeding, respectively. In both mouse strains, blood glucose response after oral glucose gavage was not influenced by the dietary fat source at the end of IFD feeding (Figure 21 F & H and Figure 22F & H). In line with enhanced body mass gain, the switch from IFD to HFD impaired glucose tolerance in C57BL/6J mice. Interestingly, this diet-induced alteration was prevented by supplementation of fish oil-comprising HFD (Figure 21 G & H). Impairment of glucose tolerance by HFD was, however, absent in 129S6/SvEvTac mice (Figure 22 G & H) and thus, demonstrating a strain specific protective effect of fish oil.

In summary, dietary n3-PUFA supplementation under thermoneutral conditions did not influence body mass accretion or adiposity in mice, but attenuated diet-induced impairment of oral glucose tolerance in a strain-specific manner.

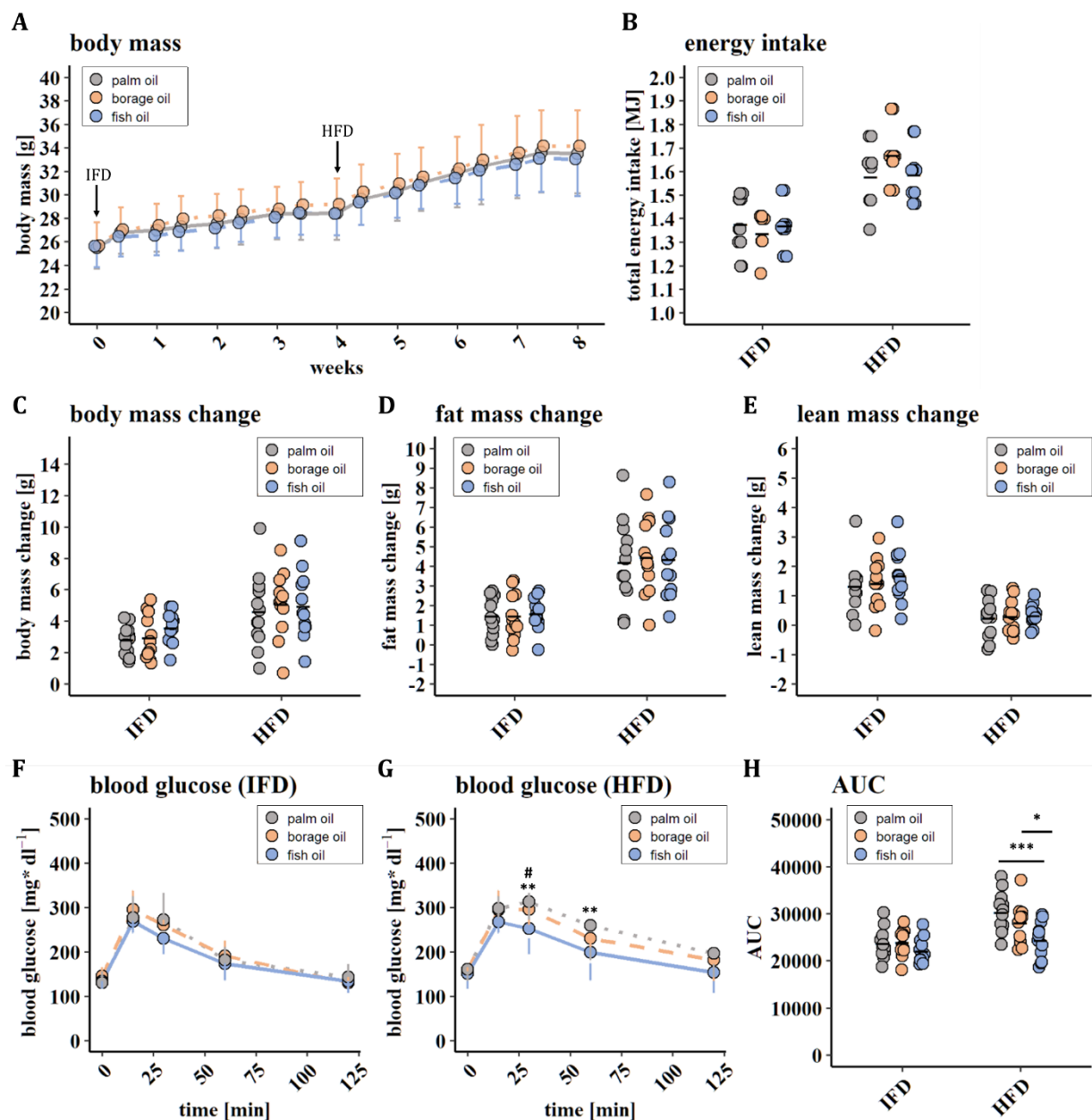


Figure 21: Effect of dietary PUFA supplementation on the development of diet-induced obesity and glucose intolerance in C57BL/6J mice.

(A) Body mass trajectories. (B) Total energy intake at the end of IFD and HFD-feeding. Changes in (C) body mass, (D) fat mass, and (E) lean mass over the course of IFD and HFD-feeding. Blood glucose trajectories of oral glucose tolerance tests conducted at the end of (F) IFD-feeding and (G) HFD-feeding. Asterisks indicate a significant effect of fish oil versus palm oil supplementation ($n = 12$). Rhombs indicate a significant effect of fish oil versus borage oil supplementation. There were no significant differences between borage oil and palm oil supplementation. (H) Total area under the curve (AUC) of blood glucose levels. Asterisks indicate a significant effect of the dietary fat source during HFD-feeding ($n = 12$).

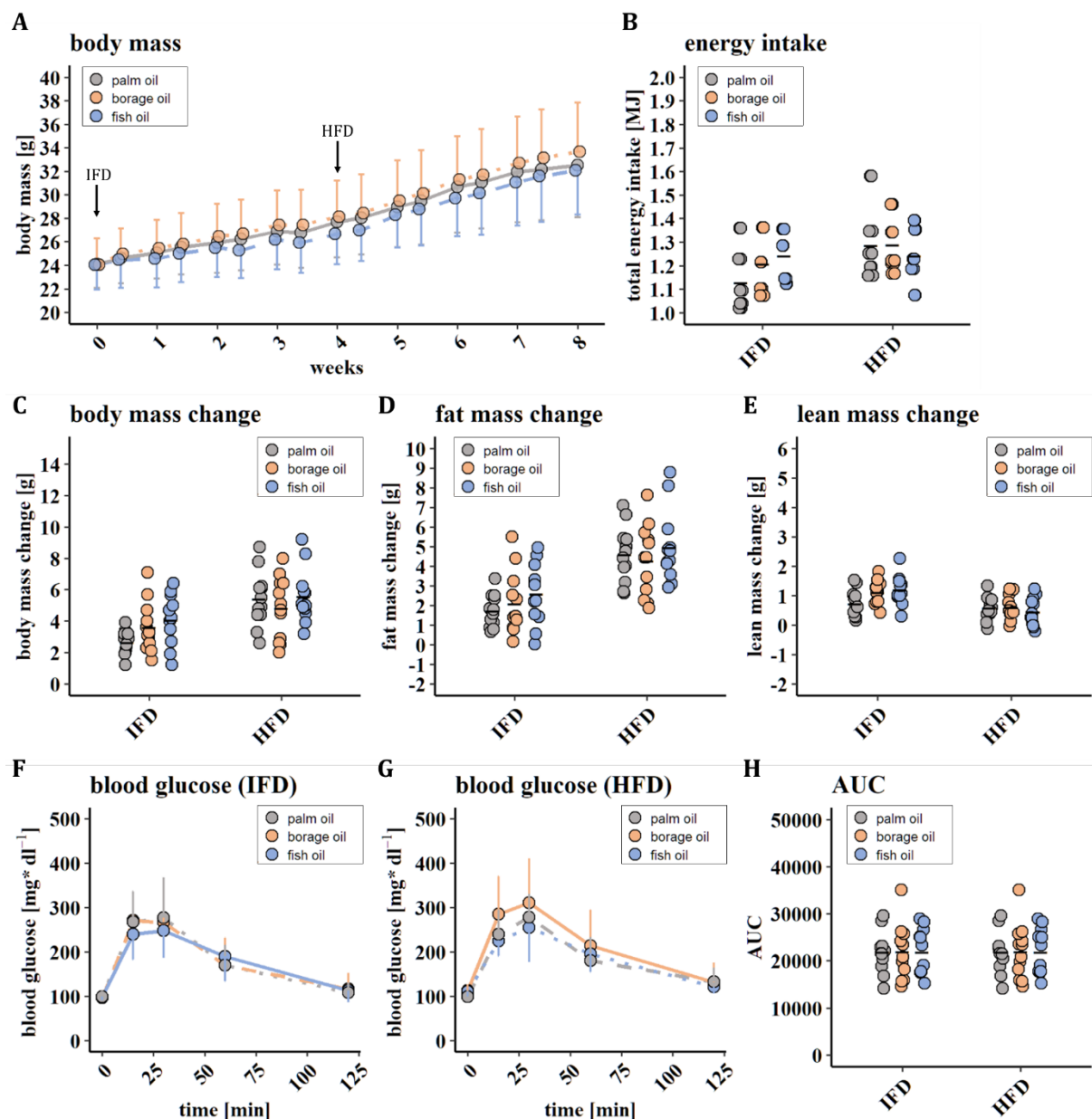


Figure 22: Effect of dietary PUFA supplementation on the development of diet-induced obesity and glucose intolerance in 129S6/SvEvTac mice.

(A) Body mass trajectories. (B) Total energy intake at the end of IFD and HFD-feeding. Energy intake is depicted as mean energy intake per cage for each mouse. (C-E) Changes in (C) body mass, (D) fat mass and (E) lean mass over the course of IFD and HFD-feeding. (F, G) Blood glucose trajectories of oral glucose tolerance tests conducted at the end of (F) IFD-feeding and (G) HFD-feeding. (H) Total area under the curve (AUC) of blood glucose levels. There were no significant effects of the dietary fat source on either parameter during IFD or HFD-feeding ($n = 12$).

4.5.4 Dietary n3-PUFA supplementation does not promote browning of WAT in human subjects

Supplementation of n3-PUFAs affects brite adipogenesis of cultured human adipocytes (Ghandour et al. 2018; Fleckenstein-Elsen et al. 2016; Laiglesia et al. 2016). To investigate whether such in vitro effects translate into WAT browning in vivo, we took advantage of the MyNewGut study, a 12-week randomized crossover trial investigating the effects of a dietary intervention on subjects with overweight and obesity (Kjølbaek et al. 2020). Twenty-nine participants supplemented their

diet either with a wheat bran extract rich in arabinoxylan oligosaccharides (AXOS intervention) or fish oil to consume EPA and DHA at a dose of 3.6 g per day (PUFA intervention). Lipidomic analysis of plasma samples revealed increased levels of cholesteryl esters and other lipids derived from DHA and EPA in response to PUFA but not AXOS supplementation, thus substantiating the efficacy of the dietary intervention (Figure 23A-D, Figure 24). The effect of PUFA supplementation on browning of WAT was investigated based on subcutaneous fat biopsies. As expected, mRNA encoding the adipose-derived hormone adiponectin was abundantly expressed (average Ct-values of 23) confirming the biopsies as adipose tissue (Figure 23E & F). In contrast, UCP1 mRNA was barely expressed (average Ct-values of 38) and only detectable in a subset of biopsies obtained prior to the start of dietary interventions (Figure 23G & H). Both the PUFA and the AXOS intervention failed to enhance this very low UCP1 gene expression (Figure 23G & H). Again, the inhibitory effect of inflammation on UCP1 gene expression could be excluded based on the lack of effect of fish oil supplementation on systemic inflammation markers (high sensitive C-reactive protein and white blood cell count, as previously published (Kjølbæk et al. 2020), and the stable expression of adiponectin as an anti-inflammatory marker before and after PUFA supplementation (Figure 23F). Thus, dietary n3-PUFA supplementation did not affect WAT browning in humans in vivo.

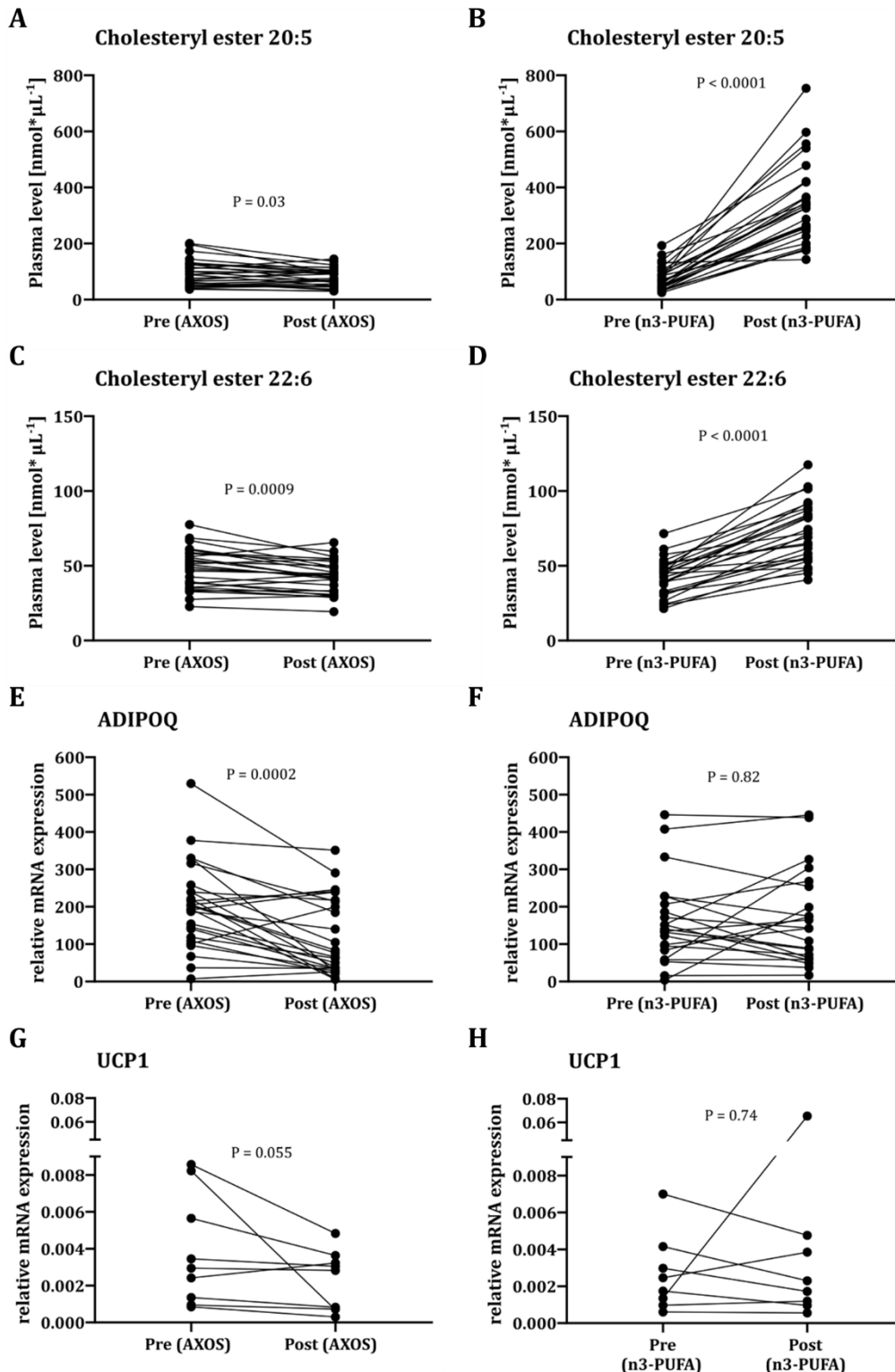


Figure 23: Effect of dietary PUFA supplementation on (A,B) plasma levels of cholesteryl ester 20:5, (C,D) cholesteryl ester 22:6 and gene expression in human WAT of (E,F) adiponectin (ADIPOQ) and (G,H) UCP1.

Overweight and obese subjects supplemented their diet with A,C,E,G) arabinoxylan oligosaccharides (AXOS) or B,D,F,H) fish oil (n3-PUFA) over 4 weeks during a randomized crossover trial. Both dietary interventions were separated by a 4-week washout period. Blood plasma and abdominal subcutaneous fat was collected before (pre) and after (post) each dietary intervention. All datasets were analyzed by two tailed, nonparametric Wilcoxon matched-pairs signed rank test with p-values indicated (n = 8–26).

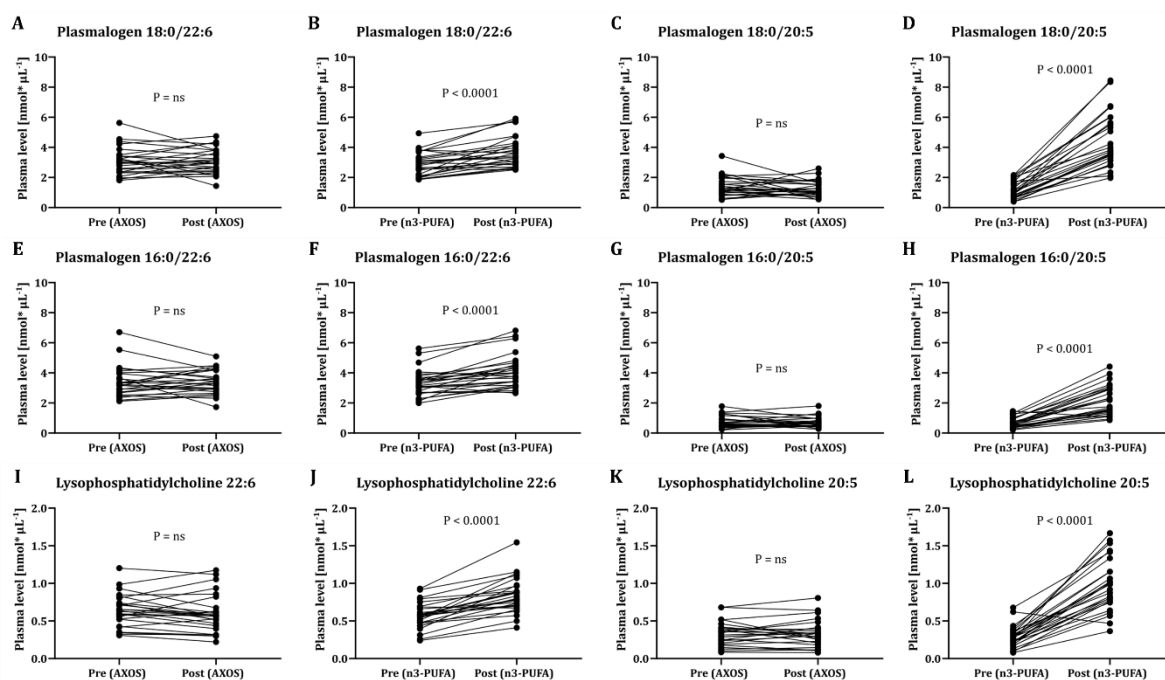


Figure 24: Effect of dietary PUFA supplementation on plasma levels of selected plasmalogens (A-H) and Lysophosphatidylcholine (I-L) (n=8-26).

Overweight and obese subjects supplemented their diet with (A, C, E, G, I, H) arabinoxylan oligosaccharides (AXOS) or (B, D, F, H, J, L) fish oil (n3-PUFA) over 4 weeks during a randomized crossover trial. Both dietary interventions were separated by a 4-week washout period. Blood plasma was collected before (pre) and after (post) each dietary intervention.

4.5.5 Discussion

Global obesity prevalence has dramatically increased over the last decades entailing a pronounced risk for associated health burdens (Bentham et al. 2017; Pi-Sunyer 2009). The potential for intervention by nutritional compounds has been comprehensively explored and a number of candidates with anti-obesogenic potential has been identified (Trigueros et al. 2013; Jayarathne et al. 2017; Lu et al. 2018; Sun, Wu, and Chau 2016). Among these are PUFAs of the n3-series (Albracht-Schulte et al. 2018), rendering dietary fat quality a potential modulator of body mass development. Indeed, the proportionate consumption of n3 PUFAs has decreased in modern societies (Simopoulos 2016), suggesting the effect of energy dense food on adiposity to be exacerbated by the excessive intake of other types of fatty acids. Conversely, an increase in dietary n3 PUFA uptake has been hypothesized to counteract this effect by the ability of n3-PUFAs to affect the recruitment of brown and brite adipocytes within the mammalian adipose organ via several different mechanisms (Maurer et al. 2019; Fernández-Galilea et al. 2020; Lund, Larsen, and Lauritzen 2018; Fan, Koehler, and Chung 2019). In this study, we rigorously tested this hypothesis in mice and man.

Previous studies mostly reported brown and/or brite adipocyte recruitment upon dietary n3-PUFA supplementation in mice kept under subthermoneutral conditions (Miller et al. 2019; Tsuboyama-Kasaoka et al. 1999; P. Flachs et al. 2011; Pahlavani et al. 2019; J. Kim et al. 2016;

Ludwig et al. 2013; Worsch et al. 2018; J. Villarroya et al. 2014; Zhuang et al. 2019; You et al. 2020; Oliveira et al. 2019; Bargut, Silva-e-Silva, et al. 2016; Bargut, Souza-Mello, et al. 2016; Bhaskaran et al. 2017; M. Kim et al. 2015; Kalupahana et al. 2010). Ambient temperatures below 30°C have a considerable influence on thermogenic adipocyte recruitment as small rodents rely on UCP1 to maintain their body temperature (Enerbäck et al. 1997). This regulation is mediated via the sympathetic nervous system. Importantly, the adrenergic influence on human BAT must be assumed minimal due to clothing and heating systems minimizing heat loss. In mice, dietary n3 PUFAs have been reported to directly influence the activity of the sympathetic nervous system via activation of gastrointestinal afferent pathways, and to synergize the effect of adrenergic stimulation on the recruitment of brown and brite adipocytes (M. Kim et al. 2015; J. Kim et al. 2016; Ghandour et al. 2018; Sato et al. 2020). To investigate the significance of adrenergic stimulation, our mice were housed under thermoneutral conditions (i.e. at 30°C) and subjected to β 3-agonist treatment during dietary PUFA supplementation. Brown and brite adipocyte recruitment were, in the presence and absence of β 3-agonism, not affected by dietary n3-PUFA supplementation in two different mouse strains. Thus, our findings, together with a previous study (Pahlavani et al. 2019), suggest thermoneutral housing temperature to impede the effect of n3-PUFAs on thermogenic adipocytes. However, our results do not corroborate previous findings demonstrating enhanced recruitment of brown and brite adipocytes upon adrenergic stimulation in mice receiving an n3-PUFA supplemented diet (M. Kim et al. 2015; J. Kim et al. 2016; Ghandour et al. 2018; Sato et al. 2020).

Interestingly, borage oil supplementation upregulated UCP1 transcript abundance in C57BL/6J mice in one experiment but not in a second, suggesting an influence by changes in the experimental framework including different food batches. Obviously, effects of dietary PUFA supplementation are, in the presence and absence of adrenergic stimulation, insufficiently robust and easily superimposed by confounding factors of experimental setup.

Oxylipin profiling of WAT and plasma revealed profound changes in systemic fatty acid metabolism, corroborating the efficacy of dietary n3 PUFA supplementation in our study. The absence of brite adipocytes in WAT of fish oil fed mice has recently been associated with n3-PUFA-derived oxylipins formed by non-enzymatic reactions that accumulate in WAT due to lipid peroxidation of fish oil supplemented foods (Miller et al. 2019). Indeed, levels of 18 hydroxy-EPA (18-HEPE, an EPA-derived n3-peroxide) were increased in both plasma and WAT of our fish oil-fed mice. Moreover, the ability of dietary n3 PUFAs to recruit brown and brite adipocytes has been associated with a local downregulation of inhibitory, n6-derived oxylipins (Ghandour et al. 2018). In fact, the n6-derived oxylipins 9 HODE and 13-HODE were very abundant in WAT of n3-PUFA supplemented, fish oil fed mice. Interestingly, 9 HODE and 13-HODE enhance the recruitment of brite cells in vitro (Y. H. Lee et al. 2016). However, our own findings point towards a function for

these two metabolites as negative regulators of thermogenic adipocytes *in vivo* (Dieckmann et al. 2020), possibly due to their function as ligands for PPAR γ , the master regulator of adipogenesis (Umeno et al. 2020). Thus, high WAT levels of 9-HODE, 13 HODE and 18-HEPE may at least partially explain the inability of n3-PUFA supplemented diets to recruit brown and brite adipocytes in mice of our study.

In rodents, fish oil has been reported to have beneficial metabolic effects and to protect against the development of DIO (Buckley and Howe 2009; J. J. Li, Huang, and Xie 2008; Kuda, Rossmeisl, and Kopecky 2018). Several studies reported a remarkable impact of n3 PUFA supplementation during HFD-feeding leading to significantly lower body mass during the entire feeding period in comparison to mice fed isocaloric control diets (Oliveira et al. 2019; Bhaskaran et al. 2017; Kalupahana et al. 2010). In an independent study conducted in our facility, small reductions in body mass became significant after 12 weeks of feeding a HFD that contained fish oil instead of palm oil (Ludwig et al. 2013). This effect was absent in the present study. Interestingly, the overall composition of our HFDs was highly similar to the HFDs used by Ludwig and coworkers (Ludwig et al. 2013), suggesting differences in study design (consecutive IFD and HFD-feeding versus continuous HFD-feeding), feeding duration (n3-PUFA supplementation during 8 weeks versus 12 weeks) and the source of n3-PUFAs (marine fish oil preparation with EPA>DHA versus EPAX concentrate with DHA>EPA) as possible confounders. We question a major influence of the fat source since n3-PUFA-comprising HFDs affect body adiposity and thermogenic adipocyte recruitment irrespective of EPA and DHA abundance (M. Kim et al. 2015; Zhuang et al. 2019). Further, inappropriate dosage of n3-PUFA can be excluded as a factor influencing our results, as the amount of n3-PUFA (90 mg/kg fish oil including ~20 mg/kg total n3-PUFA) administered are well in line with previously used doses of fish oil (mean dose 108 mg/kg (Oliveira et al. 2019; Bargut, Silva-e-Silva, et al. 2016; Bhaskaran et al. 2017; M. Kim et al. 2015; Pahlavani et al. 2019)) and isolated n3-PUFA (mean dose 20 mg/kg (Kalupahana et al. 2010; Pahlavani et al. 2017; Ludwig et al. 2013; Zhuang et al. 2019; Ghandour et al. 2018; Bargut et al. 2019)). In line with our findings, dietary n3-PUFA supplementation of mice at thermoneutral housing temperature and in the absence of CL-316,243 reportedly failed to attenuate body mass gain, or required extremely long feeding duration (Ghandour et al. 2018; Pahlavani et al. 2019; Janovská et al. 2013). Thus, the housing temperature of mice seems to be one crucial confounder influencing the response to dietary n3-PUFA supplementation. Moreover, attenuated body mass gain upon n3-PUFA supplementation even occurs in UCP1-ablated mice (Oliveira et al. 2019; Pahlavani et al. 2019), suggesting a possible, causal contribution by BAT and WAT via means of other mechanisms such as lipid cycling rather than UCP1-dependent thermogenesis (Worsch et al. 2018; Pavel Flachs et al. 2013). In conclusion, the protective effect of n3-PUFA supplementation on DIO is abrogated by thermoneutral housing and not influenced by adipocyte-based, UCP1-dependent thermogenesis.

Mice of the C57BL/6J strain display a high propensity to develop glucose intolerance (Kless et al. 2015). In our study, these mice were protected from HFD-induced glucose intolerance when supplemented with fish oil. A similar protection has been observed in UCP1-ablated mice (Oliveira et al. 2019; Pahlavani et al. 2019). Although the recruitment of UCP1-independent thermogenic mechanisms can account for increased postprandial glucose disposal (Maurer et al. 2020), we speculate that glucose tolerance improvements are more likely to have a different origin. In fact, n3 PUFAs can affect insulin release and insulin sensitivity via various mechanisms, cumulating in an improvement of whole-body glucose tolerance (X. Wang and Chan 2015; P. Flachs, Rossmeisl, and Kopecky 2014). Of note, the translational significance of such beneficial fish oil supplementation effects on glucose tolerance, as frequently observed in rodents, seems to have limited relevance for humans (P. Flachs, Rossmeisl, and Kopecky 2014; Lalia and Lanza 2016).

While a number of studies have investigated effects in rodents *in vivo*, the thermogenic recruitment of human adipocytes upon n3-PUFA supplementation has to date only been demonstrated in cultured cells. To overcome this limitation, we took advantage of abdominal subcutaneous adipose tissue specimens collected during a human intervention study assessing effects of dietary n3-PUFA supplementation in persons with overweight and obesity (Kjølbaek et al. 2020). Importantly, EPA-treatment can increase the expression of thermogenic marker genes in cultured adipocytes from subcutaneous adipose tissue of overweight subjects (Laiglesia et al. 2016). Moreover, human subcutaneous adipocytes have a browning potential *in vivo* (Xu et al. 2016; Otero-Díaz et al. 2018; Patsouris et al. 2015; Sidossis et al. 2015; Finlin et al. 2018; Kern et al. 2014; Harms et al. 2019). In agreement with several other human interventions (A. L. Carey et al. 2006; Cheung et al. 2013; Norheim et al. 2014; Naja Z. Jespersen et al. 2019), our gene expression data show that UCP1 transcripts are barely detectable in subcutaneous abdominal fat. Fully in line with our experiments in mice, fish oil supplementation of the study participants over the course of 4 weeks did not at all affect this very low UCP1 mRNA expression, suggesting that an increased intake of n3-PUFAs for one month do not promote WAT browning in humans *in vivo*, at least in overweight subjects. In line with this observation, resting energy expenditure of the same subjects was not affected by fish oil supplementation (Kjølbaek et al. 2020). This human intervention study has several limitations. First, it is important to emphasize that changes in adipose gene expression were part of the exploratory outcomes of the MyNewGut study. Secondly, we cannot exclude that four weeks of fish oil supplementation is insufficient for inducing browning of human subcutaneous WAT. Yet, previous studies have demonstrated that this fat depot in humans has the capacity to undergo browning *in vivo* and suggests that this might occur even in response to acute cold exposure (Finlin et al. 2018; Kern et al. 2014; Finlin et al. 2017). Moreover, adrenergic stimuli and phosphodiesterase inhibition can promote UCP1 expression and brite adipogenesis in human subcutaneous white fat within 1-4 weeks (Sidossis et al. 2015;

Patsouris et al. 2015; S. Li et al. 2018). Taken together with our human lipidomics data and the high dose of n3-PUFA applied in the MyNewGut study (3.6 g/d), these observations suggest that fish oil, in physiologically relevant doses, does not promote browning of abdominal subcutaneous white fat of subjects with overweight. Fish oil supplementation, however, may stimulate adipose browning in other anatomical areas. Given that body adiposity is associated with an impaired browning capacity (Kern et al. 2014; Andrew L. Carey et al. 2014; Chung et al. 2017), fish oil supplementation may also be hypothesized to be more efficient at inducing browning in lean individuals.

In conclusion, dietary n3-PUFA supplementation did not affect thermogenic adipocyte recruitment or body mass accretion, neither in mice nor in humans. We thus propose disregarding dietary fish oil and n3-PUFAs as translationally relevant agents to modulate energy balance regulation via adipocyte-based thermogenesis.

5 SUSCEPTIBILITY TO DIET-INDUCED OBESITY AT THERMONEUTRAL CONDITIONS IS INDEPENDENT OF UCP1

A similar version of this chapter is in preparation: Dieckmann S., Strohmeyer A., Willershäuser M., Wurst W., Worthmann A., Fuh M. M., Heeren J., Köhler N., Pauling J., Klingenspor M.

5.1 ABSTRACT

Activation of UCP1 in BAT upon cold stimulation leads to substantial increase in energy expenditure to defend body temperature. Increases in energy expenditure after a high caloric food intake, termed diet-induced thermogenesis, are also attributed to BAT. These properties render BAT a potential target to combat DIO. However, studies investigating the role of UCP1 to protect against DIO are controversial and rely on the phenotyping of a single constitutive UCP1-knockout model. To address this issue, we generated a novel UCP1-knockout model by Cre-mediated deletion of Exon 2 in the UCP1 gene. We studied the effect of constitutive UCP1-KO on metabolism and the development of DIO. UCP1-KO and wildtype mice were housed at 30°C and fed a CD for 4-weeks followed by 8-weeks of HFD. Body weight and food intake were monitored continuously over the course of the study and indirect calorimetry was used to determine energy expenditure during both feeding periods. Based on western blot analysis, thermal imaging and NA test, we confirmed the lack of functional UCP1 in knockout mice. However, body weight gain, food intake and energy expenditure were not affected by deletion of UCP1 gene function during both feeding periods. Conclusively, we show that UCP1 does not protect against DIO at thermoneutrality. Further we introduce a novel UCP1-KO mouse enabling the generation of conditional UCP1-knockout mice to scrutinize the contribution of UCP1 to energy metabolism in different cell types or life stages.

5.2 AUTHORS CONTRIBUTION

Sebastian Dieckmann conceived the study design, planned, and performed the mouse experiments, conducted molecular analyses, analyzed data (Figure 25, Figure 26, Figure 27, Figure 28, Figure 31, Figure 32), interpreted data, and wrote the manuscript.

5.3 INTRODUCTION

Thermogenic BAT is the main contributor to NST, the process to maintain normothermia in a variety of small mammals. NST is mediated by the UCP1, which enables high rates of oxygen consumption by the mitochondrial electron transport chain without ATP production. The most potent stimulation of UCP1 and NST is mediated by the sympathetic innervation of BAT with the neurotransmitter NA triggering beta-3-adrenergic receptor signaling in brown adipocytes. Furthermore, meal-associated thermogenesis in BAT is activated upon food intake (Glick, Teague, and Bray 1981) by the prandial surge of the gut peptide hormone secretin (Y. Li et al. 2018). Other activators of BAT thermogenesis have been reported (Zietak and Kozak 2016; Gnad et al. 2014) and recent findings suggest that brown fat conveys effects on systemic metabolism and energy balance by means of paracrine intercellular and endocrine interorgan crosstalk. The beneficial metabolic effects of BAT clearly go beyond the combustion of calories (Kajimura, Spiegelman, and Seale 2015). Activation of meal-associated thermogenesis in BAT initiates meal termination and thereby contributes to the control of energy intake (Schnabl, Li, and Klingenspor 2020). Together with the potential of BAT to impact energy balance and systemic metabolism by clearing glucose from circulation, these characteristics render UCP1 and BAT potential targets to improve cardiometabolic health and the treatment of type 2 diabetes (Becher et al. 2021).

In this context the question whether UCP1 can protect against DIO has been studied repeatedly. Standard housing temperature (20-23°C) represents a mild cold challenge for laboratory mice resulting in a two-fold increase of daily energy expenditure (Fischer, Cannon, and Nedergaard 2018). BAT is the source for this thermoregulatory heat production. UCP1-KO mice when kept at standard housing temperature do not develop DIO (Bond and Ntambi 2018) and even seem to be protected, having lower body weight than WT mice (Liu et al. 2003; T. Wang et al. 2008; Keipert et al. 2020). It has been proposed that this is due to alternative thermogenic mechanisms less efficient than UCP1-dependent thermogenesis (Liu et al. 2003; T. Wang et al. 2008; Keipert et al. 2020), that are recruited to cope with the need for thermoregulatory heat production in UCP1-KO mice. Housing mice at higher temperatures (27°C – 30°C), corresponding to their thermoneutral zone eliminates this heat sink. Since UCP1 in BAT is inactive at thermoneutrality, the lack of thermogenic BAT function should be without consequences for energy balance. Indeed, several studies using the established UCP1-KO mouse model originally generated by Leslie Kozak and coworkers confirmed this expectation (Enerbäck et al. 1997; Liu et al. 2003; Zietak and Kozak 2016; Winn et al. 2017; Maurer et al. 2020). In contrast, other studies reported that UCP1-KO mice are more susceptible to DIO at thermoneutrality (Feldmann et al. 2009; von Essen et al. 2017; Rowland et al. 2016; Luijten et al. 2019; Pahlavani et al. 2019). One explanation for the increased susceptibility to DIO in UCP1-KO mice may be adaptations in metabolism, leading to a more efficient metabolism or the lack of diet-induced thermogenesis in UCP1-KO mice (von Essen et al.

2017). However, recent data from a UCP1 knockdown model (H. Wang et al. 2021) demonstrate that UCP1 abundance alone does not protect against DIO at thermoneutrality. Despite having remarkable reduced but still activatable UCP1 levels, these mice are not more or less prone to DIO compared to wildtype littermates with normal functional levels of UCP1.

This showcases the urgent need for new UCP1-KO models to scrutinize the role of UCP1 on energy balance and metabolism. So far two UCP1-KO models are available (Enerbäck et al. 1997; Bond and Ntambi 2018). Other transgenic mice with impaired UCP1 expression include knockdown models (Chen, Hsu, and Huang 2018; H. Wang et al. 2019) or diphtheria toxin chain A induced depletion of UCP1 expressing cells (Lowell et al. 1993; Rosenwald et al. 2013).

In the present study we therefore introduce and validate a novel Cre-mediated UCP1-KO model and demonstrate that deletion of UCP1 has no effect on energy balance regulation at thermoneutrality.

5.4 MATERIAL AND METHODS

5.4.1 Animal model

The UCP1-KO mouse line was generated in frame of the EUCOMM program and is a constitutive UCP1-KO model on a C57BL/6N background. It originates from the UCP1^{tm1a} mouse, carrying a lacZ & neomycin cassette, two FLP sites and three loxP sites (Figure 1 A). Through crossing with a FLP mouse, the lacZ and neomycin cassette as well as one FLP site and one loxP site are removed, resulting in a UCP1^{tm1c} (UCP1-WT) mouse. Cross breeding this mouse with a Rosa26-CRE mouse results in the UCP1^{tm1d} (UCP1-KO) mouse carrying a germline deletion of the exon 2 of the UCP1 gene. UCP1-KO and UCP1-WT mice were crossed to generate UCP1-HET mice. The UCP1-KO line is maintained by crossing male and female UCP1-HET mice. All studied mice were derived of our heterozygous maintenance breeding. Mice were bred and housed at 23°C ambient temperature with a 12/12 h light/dark cycle and had *ad libitum* access to water and chow diet.

All animal experiments were performed according to the German animal welfare law and approved by the district government of Upper Bavaria (Regierung von Oberbayern, reference number ROB-55.2-2532.Vet_02-15-128).

5.4.1.1 HFD feeding at thermoneutrality

Male wildtype (n = 7) and knockout (n = 7) mice for the HFD feeding experiment were obtained from our heterozygous maintenance breeding. At the age of 8 weeks, mice were switched from chow to a chemically defined CD with a fat content of 50 g/kg (~13 kJ% from Fat, 15.3 MJ/kg, Sniff Cat# S5745-E702). Simultaneously, mice were single caged and transferred to climate cabinets with an ambient temperature of 30 °C and 55 % RH. After an acclimatization phase of 4 weeks, mice were switched from CD to a HFD with a fat content of 250 g/kg (~48 kJ% from fat,

19.6 MJ/kg, Sniff Cat# S5745-E712). After 8 weeks of HFD feeding, mice were killed by CO₂ asphyxiation. Whole blood was taken by cardiac puncture, collected in lithium heparin-coated tubes (Sarstedt, Nümbrecht/Germany) and centrifuged at 4°C for 10 min with 1500 x g. The plasma supernatant was transferred to fresh tubes and snap frozen in liquid nitrogen. Subsequently, cecal content and tissues were dissected, weighed, and immediately snap frozen in liquid nitrogen. Cecal content, tissues and plasma were stored at -80°C until further processing. Body weight and food intake were determined twice a week between 12.00 PM and 4.00 PM. Additionally, body composition was determined every other week by nuclear magnetic resonance spectroscopy (mq7.5, Bruker BioSpin GmbH, Rheinstetten/Germany). Mice were maintained on a 12/12 h light/dark cycle and had *ad libitum* access to water and the respective diets during the whole experiment. Food was replaced completely twice a week to avoid rancidity of the HFD at 30°C. Energy expenditure, energy intake, energy excretion and metabolic efficiency of CD and HFD-fed mice were assessed as described below.

5.4.2 Indirect calorimetry, basal metabolic rate and NA tests

Indirect calorimetry was performed based on an open respirometer system (LabMaster System; TSE Systems, Bad Homburg/Germany) similar to a previously described methods (Maurer et al. 2015). O₂ consumption and CO₂ production were determined after 2.5 weeks of feeding CD and after 4 weeks of HFD. Mice were transferred in specially equipped cages in a climate cabinet (KPK 600, Feutron/Germany) set to 30 °C after determining body weight and body composition in the afternoon (2.00 – 5.00 PM). The measurement was started on the next day at 6.00 AM (CD) or 12.00 PM (HFD) and continued two (CD) or three (HFD) dark phases. The air from the cages was extracted over a period of 1 min every 4-6 min. Heat production was calculated according to (Heldmaier 1975) as: $heat\ production\ [mW] = (4.44 + 1.43 * respiratory\ exchange\ ratio) * oxygen\ consumption\ [ml/h]$

BMR was determined immediately after the last night phase of the indirect calorimetry measurement of the HFD period. Mice were deprived of food between 7.00 – 8.00 AM for at least 4 hours. BMR was calculated as the mean of the four lowest consecutive heat production measurements during the last 90 minutes of fasting, similar to a previous published method (Fromme et al. 2019). Subsequently, NA tests were performed between 10.00 AM – 5.00 PM at 26°C to avoid NA induced hypothermia. Noradrenaline (1 mg/kg, Arterenol®, Sanofi) was injected intraperitoneally. Air was extracted continuously from the cages with a measurement period of 1 min over 60 min.

5.4.3 Collection of food spillage and faeces

Embedding material was collected from cages after indirect calorimetry for each mouse separately, to correct food intake for spillage and to determine energy loss by faecal excretion.

The material was dried at room air under a chemical flow hood for at least 1 week. Subsequently, cage material was fractionated based on size by shaking the material on a sieve shaker (EML 200 Digital Plus T, Haver & Boecker, Oelde/Germany) for 5 min with an interval of 0.5 min at an amplitude of 1.4, through sieves with different mesh sizes (4, 3.15, 2.5, 1.25 and 1 mm, VWR International GmbH, Darmstadt/Germany). Flowthrough of the 1 mm sieve was collected in a pan. Each sieve was scanned for spilled food and faeces (the majority of faeces will be present in the 1.25 mm sieve). If applicable, food and faeces were picked with tweezers and collected for weighing and determination of energy content by bomb calorimetry. Food intake (in grams) during the indirect calorimetry sessions was corrected for the amount of collected food spillage (in grams).

5.4.4 Determination of energy content of food and faeces by bomb calorimetry

The energy content of the diets and the faecal pellets collected during indirect calorimetry was determined with an isoperibolic bomb calorimeter (Model Nr. 6400, Parr Instrument Company, IL/USA). Energy content of the diets was determined on food samples collected at different time points during the experiment (CD n = 9, HFD n = 10). Energy intake was calculated by multiplying the mean energy content of the diets (kJ/g) with the amount of food intake (in grams).

The collected faeces was weighed and grinded with metal balls for 2.5 min at 30 Hz (Tissue Lyser II, Retsch GmbH, Haan/Germany). Grinded faeces was pressed into a pellet, weighed, and subjected to bomb calorimetry. Benzoic acid (~0.7 g) was added as combustion aid. The energy lost via faeces was calculated for each mouse by multiplying the total amount of faeces collected (in grams, see 2.4) by the energy content (kJ/g) determined by bomb calorimetry.

5.4.5 Thermal imaging

Thermal imaging was performed as described previously (Maurer et al. 2015) with 1-3 day old new-born pups. In brief, at least 3 serial pictures were taken of each litter in 6-well cell culture plates (T890 thermal imager, Testo, Lenzkirch/Germany). Image analysis was performed with the IRSoft Software (version 4.6, Testo, Lenzkirch/Germany) and the temperature above the iBAT depot (interscapular skin surface temperature, iSST) was determined.

5.4.6 Genotyping

Genotyping was performed on earpieces obtained during tagging of the animals. Tissues were lysed (10 mM TRIS, 50 mM KCl, 0.45 % Nonidet P40, 0.45 % Tween-20, 10 % gelatin in H₂O at pH 8.3% with 0.2 mg/ml Proteinase K) for 4 h at 65°C and vigorous shaking. Proteinase K was inactivated by heating for 10 min at 95 °C. PCR (denaturation: 5 min / 95°C followed by 39 amplification cycles with 30s / 95°C, 45 / 54 °C, 45 / 72°C and a final elongation 10 min / 72°C) was performed with three primers (Figure 1A, “a”: AAGGCGCATAACGATACCAC, “b”: TACAATGCAGGCTCCAAACAC, “c”: CGAGCACAGGAAGTTCAACA, Eurofins Genomics,

Ebersberg/Germany) and the ImmoMix™ kit (Cat# BIO-25020, Bioline, London/UK) according to the manufacturer's instructions.

5.4.7 RNA isolation and cDNA synthesis and sequencing

RNA precipitation was performed with TRIsure™ (Bioline, London/UK) following the manufacturer's instructions, from deep-frozen iBAT. Precipitated RNA was loaded to spin columns (SV Total RNA Isolation System, Promega, Cat# Z3105), centrifuged for 1 min with 12,000 x g and further processed according to the supplier's instructions. RNA concentration was determined spectrophotometrically (Infinite 200 PRO NanoQuant, Tecan). cDNA synthesis was performed with 1 µg RNA (SensiFAST™ cDNA Synthesis Kit, Cat# BIO-65053, Bioline, London/UK), according to the manufacturer's instructions. PCR (denaturation: 10 min / 95°C followed by 30 amplification cycles with 1 min / 95°C, 30s / 54 °C, 40s / 72°C and a final elongation 5 min / 72°C) was performed with primers ("d": cggagtttcagcttgctggca, "e": tcgcacagcttggtacgcttg, Eurofins Genomics, Ebersberg/Germany, Figure 1A) and products were separated by gel electrophoresis on a 1 % agarose gel. Separated PCR products were visualized under a UV light, cut, immediately weighed and stored at -20°C. PCR products were purified with the Wizard SV Genomic DNA Purification System (Promega, Cat# A2361), and sent in to a commercial sequencing platform (Eurofins Genomics, Ebersberg/Germany). Analysis of sequencing results was performed with the "Benchling" platform (<https://www.benchling.com/>).

5.4.8 Protein expression analysis by SDS-Page and Western Blot

Protein was isolated from iBAT, homogenized in 10 µl/mg isolation buffer (50 mM Tris, 1% NP-40, 0.25% sodium deoxycholate, 150 mM NaCl, 1 mM EDTA) containing 0.1 % phosphatase (Sigma-Aldrich, St. Louis MO/USA) and 0.1 % protease inhibitor cocktail (Sigma-Aldrich, St. Louis MO/USA) with a dispersing device (Micra D-1, Micra GmbH, Heitersheim/Germany). The homogenized samples were centrifuged 15 min at 4°C with 14.000 rcf. The clear layer of the supernatant was isolated by pipetting and centrifuged again. Samples were cleared from residual fat by a second extraction of the clear phase with a syringe. Protein concentrations were determined with the Pierce™ BCA Protein Assay Kit (ThermoScientific, Rockford IL/USA) according to the manufacturer's instructions. For protein detection, 30 µg protein were separated in a 12.5 % SDS-PAGE and transferred to a nitrocellulose membrane. Subsequently, primary antibody was applied to detect UCP1 (Cat# ab23841, abcam, London/UK, 1:5000) followed by primary antibody detection using an IR-dye conjugated secondary antibody (IRDye 800CW, LI-COR, Lincoln NE/USA, 1:20000). The IR signal was detected with the Azure Sapphire™ biomolecular imager (azure biosystems, Dublin CA/USA). Image analysis was conducted with the Image Studio™ Lite software version 5.2.

5.4.9 DNA Extraction and 16S rRNA Sequencing

Cecal contents were collected together with other tissues and immediately snap frozen in liquid nitrogen and stored at -80°C. DNA isolation, library preparation and sequencing were performed at the ZIEL – Core Facility Microbiome of the Technical University of Munich. Briefly, DNA was extracted using previously published protocols (Klindworth et al. 2013). For the assessment of bacterial communities primers specifically targeting the V3-V4 region of the bacterial 16S rRNA (Forward-Primer (341F- CCTACGGGNGGCWGCAG; Reverse-Primer (785r-ovh): GACTACHVGGGTATCTAATCC) gene including a forward and reverse illumine specific overhang and a barcode were used. Sequencing was performed using an Illumina MiSeq DNA platform. Obtained multiplexed sequencing files have been analyzed using the IMNGS platform, which is based on the UPARSE approach for sequence quality check, chimera filtering and cluster formation (Edgar 2013; Lagkouvardos et al. 2016). For the analysis standard values for barcode mismatches, trimming, expected errors and abundance cutoff have been used and only sequences between 300 and 600 bp were considered for analysis. Downstream analysis of the IMNGS platform output files were performed using the RHEA R pipeline (Lagkouvardos et al. 2017). In brief, obtained abundances have been normalized and quality of obtained sequences was assessed using rarefaction curves (McMurdie and Holmes 2014). Analysis of alpha diversity, beta diversity and group comparisons have been performed using default settings. Exceptions have been applied for group comparisons for zero-radius operational taxonomic unit (zOTUs) and taxonomic levels (abundance cutoff 0.5 and exclusion of alpha diversity measures). Graphical output was modified for presentation using inkscape (<https://inkscape.org>). Assignment of zOTUs to taxons has been performed using the SILVA database (Version 138.1 (Quast et al. 2013)). Assignment of species to specific zOTUs with EZBioCloud (Yoon et al. 2017).

5.4.10 Lipid Extraction and Mass Spectrometry Analysis

Lipid extraction for quantitative analysis using Lipidyzer™ platform (SCIEX, Framingham MA/USA.) was done using an adapted Methyl-tert-butyl-ether (MTBE) extraction protocol. Lipidyzer™ internal standards mixture was prepared according to the manufacturer's instruction but dissolved in MTBE. To each 50 µL plasma aliquot, 50 µL water; 50 µL Internal Standard, 500 µL MTBE and 160 µL Methanol was added, shortly vortexed and incubated on a mixer for 30 minutes. 200 µL of water was added and centrifuged at 16000g. The supernatant was transferred in vials and the residual phase re-extracted using MTBE: Methanol: Water in the ratio 3:1:1. The collected supernatants were evaporated with a vacuum centrifuge and resuspended in 250 µL of 10 mM ammonium acetate in Dichloromethane: Methanol (50:50 (v/v)).

Samples were analysed using a QTRAP 5500 (AB SCIEX) equipped with Differential Mobility Spectrometer (DMS) interface (Schneider et al. 2010) operating with SelexION technology, coupled to a Shimadzu Nexera X2 liquid chromatography system. The Lipidyzer platform™ is

operated via the software Analyst version 1.6.8 and Lipidomics workflow manager (SCIEX, Framingham MA/USA). A detailed description of this shotgun approach has been previously reported (Lintonen et al. 2014). The Lipidyzer™ Platform was tuned using the SelexION Tuning Kit (SCIEX) according to the manufacturer's recommendations and a system suitability test was performed using the System Suitability Kit (SCIEX) according to the manufacturer's instructions. The Lipidyzer™ Platform uses 10 mM ammonium acetate in Dichloromethane: Methanol (50:50 (v/v)) as running buffer, Dichloromethane: Methanol (50:50 (v/v)) as rinse 0&1, 2-propanol as rinses 2&3, and 1-propanol as a DMS modifier. 50µl of samples are injected for each of the two MRM methods: One with a DMS on and one with DMS off. MRM data acquisition, processing, and quantification is performed automatically by the lipidyzer lipidomics workflow manager. Lipid concentrations are given in nmol/ml.

5.4.11 Data analysis and statistics

General data analysis was performed with R (version 4.0.3) within R-Studio (version 1.3.1093). Unless otherwise indicated data are represented as means ± sd or with single values for each mouse. Student's t-tests were performed with the package "ggpubr" (version 0.4.0). ANOVA, and linear model analysis with the package "stats" (version 4.0.3). Trapezoid AUC were calculated using the AUC function of the package "DescTools" (version 0.99.38).

Analysis of alpha diversity was performed with Prism 6 (GraphPad Software Inc., La Jolla CA/USA) using non-parametric Mann-Whitney U test. Beta diversity is visualized using non-metric multi-dimensional scaling based on generalized UniFrac and tested for significance using PERMANOVA. Differences in zOTUs have been determined using Kruskal-Wallis rank sum test with adjustments for multiple testing using the Benjamini & Hochberg method.

Multi-omics analysis was performed using R (version 4.0.4) and python (version 3.8.5). Multi-omics factor analysis (MOFA) (Argelaguet et al. 2018; 2020) was used for unsupervised data integration of the lipidome and microbiome data. The mofapy2 python package (version 0.5.8) and the MOFA2 R package (version 1.0.1) (for downstream analysis) were used together with custom visualization tools. Data integration analysis for biomarker discovery using latent variable approaches for 'omics studies (DIABLO) (Singh et al. 2019) was used as a supervised analysis framework. DIABLO generalizes (sparse) partial least-squares discriminant analysis (PLS-DA) for the integration of multiple datasets measured on the same samples. For DIABLO analyses the mixOmics R package (version 6.14.0) (Rohart et al. 2017) was used along with custom code for randomized performance estimation.

5.5 RESULTS

5.5.1 Deletion of UCP1 Exon 2 leads to a loss of protein expression

The original mouse used to generate the knockout of UCP1 in the mice used in this study was generated in frame of the EUCOMM program via a “knockout first allele” approach (Skarnes et al. 2011; Pettitt et al. 2009). In order to generate WT (UCP1^{tm1c}), the lacZ and the neomycin resistance cassette were removed from the UCP1^{tm1a} allele, by cross breeding with flippase expressing mice (Figure 25 A1), thus generating WT (UCP1^{tm1c}) mice. These mice containing only one flippase recognition target (frt) and two lox P sites flanking exon 2 of the UCP1 gene were crossed with mice expressing Cre-recombinase under the control of the rosa26 promotor (Rosa26Cre/+) (Figure 25 A2). This results in a constitutive germline deletion exon 2 of the UCP1 gene and the generation of KO (UCP1^{tm1d}) mice (Figure 25 A3). The deletion of exon 2 of the UCP1 gene was first confirmed by PCR on genomic DNA with one forward and two reverse primers binding to distinct sites of the UCP1 gene (Figure 25 A2 & A3).

As predicted, this resulted in a short (263 bp) product for WT mice (Figure 25 B, primers a-b) and a longer (388 bp) product for KO (Figure 25 B, primers a-c), while HET mice showed both products. Of note, the 1255 bp product generated by the primers a and c in WT and HET is not seen, as the elongation period of the PCR protocol is too short to produce a product of this size. To further investigate the consequences of exon 2 deletion, we performed a RT-PCR on RNA isolated from BAT of both WT and KO mice. For the primer pair binding in exon 1 (d) and exon 5 (e) of the UCP1 gene (Figure 25 A), KO showed a smaller product size (~500 bp) compared to WT mice (~700 bp), as predicted by in-silico PCR (KO: 508 bp, WT: 707 bp, <https://genome.ucsc.edu/cgi-bin/hgPcr>) (Figure 25 C). Subsequent sequencing of the WT and KO PCR-products revealed that the deletion of exon 2 causes a frame shift, leading to a premature stop codon in exon 3 (Supplementary Figure 6). Consequently, KO mice do not express UCP1 protein, as confirmed by western blot analysis (Figure 25 1D).

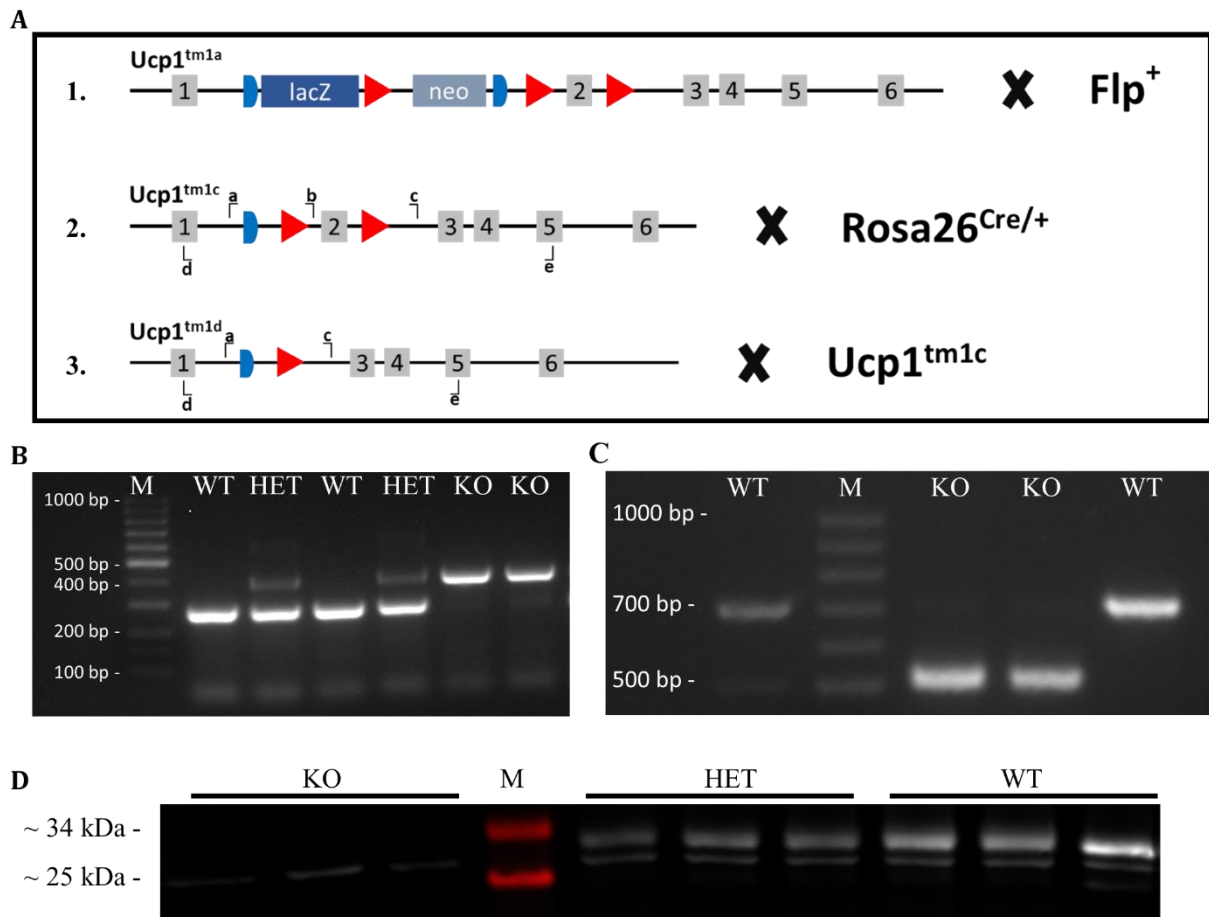


Figure 25: Overview and validation of the UCP1 knockout strategy.

(A) Breeding scheme for the generation of the UCP1 knockout. (A1) $Ucp1^{tm1a}$ mice containing three loxP sites (red), two frt sites (blue) as well as a lacZ and a neo cassette were crossed with mice expressing flippase (Flp^+). (A2) The resulting $Ucp1^{tm1c}$ (WT) mouse is crossed with a $Rosa26^{Cre/+}$ mouse, deleting exon 2 of the *ucp1* gene, generating $Ucp1^{tm1d}$ (KO) mice. (A3) $Ucp1^{tm1c}$ and $Ucp1^{tm1d}$ mice are crossed to generate HET mice. Lower case letters indicating binding positions of primers used for PCR (a-c) and RT-PCR (d&e). (B) PCR of gDNA from tissue samples of WT, HET and KO mice. (C) RT-PCR products from iBAT of WT and KO mice. (D) Representative western blot analysis for UCP1 (~33 kDa) in KO, HET and WT mice. See Supplementary Figure 7 for the uncropped version of the western blot.

5.5.2 Thermogenic deficiency leads to decreased body weight in young KO mice

The loss of the major protein responsible for NST resulted in a clear reduction of iSST in newborn KO compared to WT mice (Figure 26 A & B). The loss of one functional UCP1 allele in heterozygous (HET) mice on the other hand had no implication on iSST in newborn pups compared to WT mice (Figure 26 A & B). The genotype distribution of offspring from HET/HET breeding pairs (generation F2-F3) did not significantly deviate from the mendelian distribution of 1:2:1 (Figure 26 C, Table 5). However, KO mice had lower body weight at weaning (at the age of ~3-4 weeks) compared to HET and WT mice (Figure 26 D), a phenotype that could be confirmed in the conventional UCP1-KO mouse on 129S1/SvImJ- but not on C57Bl/6J-background (Supplementary Figure 8 A & C). Irrespectively of the knockout model bodyweight of all three genotypes were similar at ~8 weeks of age (Figure 26 E, Supplementary Figure 8 B & D).

In summary this suggests a strain specific effect of UCP1 depletion on early body weight that recovers with age.

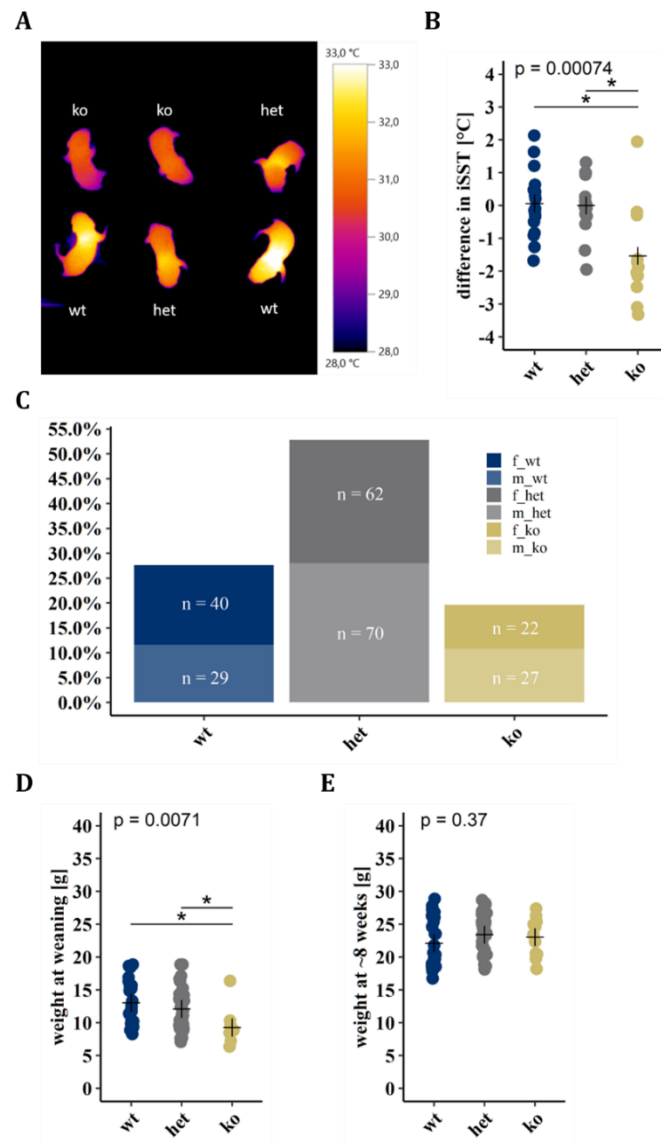


Figure 26: Lack of UCP1 leads to phenotypic alterations in young mice.

(A) Representative thermal image of newborn pups (2-3 days) of a UCP1-HET breeding pair. (B) Analysis of interscapular skin surface temperature (iSST, $n(\text{wt}) = 17$, $n(\text{het}) = 17$, $n(\text{ko}) = 11$, $N = 45$ of 5 litters). (C) Offspring genotype distribution of UCP1-HET breeding pairs ($n = 15$) at 23 °C ambient temperature ($N = 250$). (D-E) Body weight of female and male UCP1-WT ($n = 23$), UCP1-HET ($n = 33$) and UCP1-KO ($n = 11$) mice (D) at weaning and (E) at the age of 8-weeks ($N = 67$ of 9 litters). (B,D,E) Crosses indicating group means. 1-Way ANOVA and t-test with bonferroni adjusted p-value, * = p-value < 0.05.

Table 5: Offspring genotype distribution of heterozygous breeding pairs.

Genotype	N	Observed (%)	Expected (%)	P (X ² test)
UCP1-WT	69	27.6	25	0.1364
UCP1-HET	132	52.8	50	
UCP1-KO	49	19.6	25	

5.5.3 UCP1-KO and WT mice have similar susceptibility to DIO at thermoneutrality

The susceptibility UCP1-KO mice to DIO under thermoneutral conditions is still a matter of debate. We addressed this controversial question using our novel UCP1-KO model by feeding mice at thermoneutrality a CD for 4 weeks followed by 8 weeks of HFD. At the start of the experiment at the age of 8 weeks, mice of both genotypes had similar body weights (data not shown). Cumulative body weight gain increased with time but was similar between both genotypes (Figure 27 A) as indicated by linear model analysis during CD (Duration $P < 0.001$, Genotype $P = 0.491$) and HFD (Duration $P < 0.001$, Genotype $P = 0.188$) feeding. In line, total energy intake between both genotypes was similar during CD and HFD feeding (Figure 27 B & C).

We determined body composition in terms of lean and fat mass different timepoints of the experiment. Both lean mass (Figure 27 D) and fat mass (Figure 27 E) correlated well with body weight during both feeding regimes, with fat mass being the main contributor to the increase in body weight during HFD feeding ($R^2 > 0.9$), in both WT and KO mice (Figure 27 D & E).

UCP1-KO mice have been described to be metabolically more efficient (Feldmann et al. 2009; von Essen et al. 2017; Luijten et al. 2019), thus incorporating more fat mass per unit of energy intake. We addressed this question by linear model analysis of cumulative fat mass gain versus cumulative energy intake over the experimental period (Figure 27 F). There was no difference in the correlation of fat mass gain and energy intake between genotypes, consequently both UCP1-WT and UCP1-KO mice showed similar metabolic efficiency. Of note, this result was confirmed by determining metabolic efficiency as the percentage of food energy stored as fat mass described previously (von Essen et al. 2017) (Figure 27 G & H). The similarity in fat mass of both UCP1-WT and UCP1-KO determined by NMR was reinforced by dissected weights of iWAT, eWAT and iBAT (Figure 27 I-K). Collectively this data indicates that UCP1 does not affect body adiposity at thermoneutral conditions.

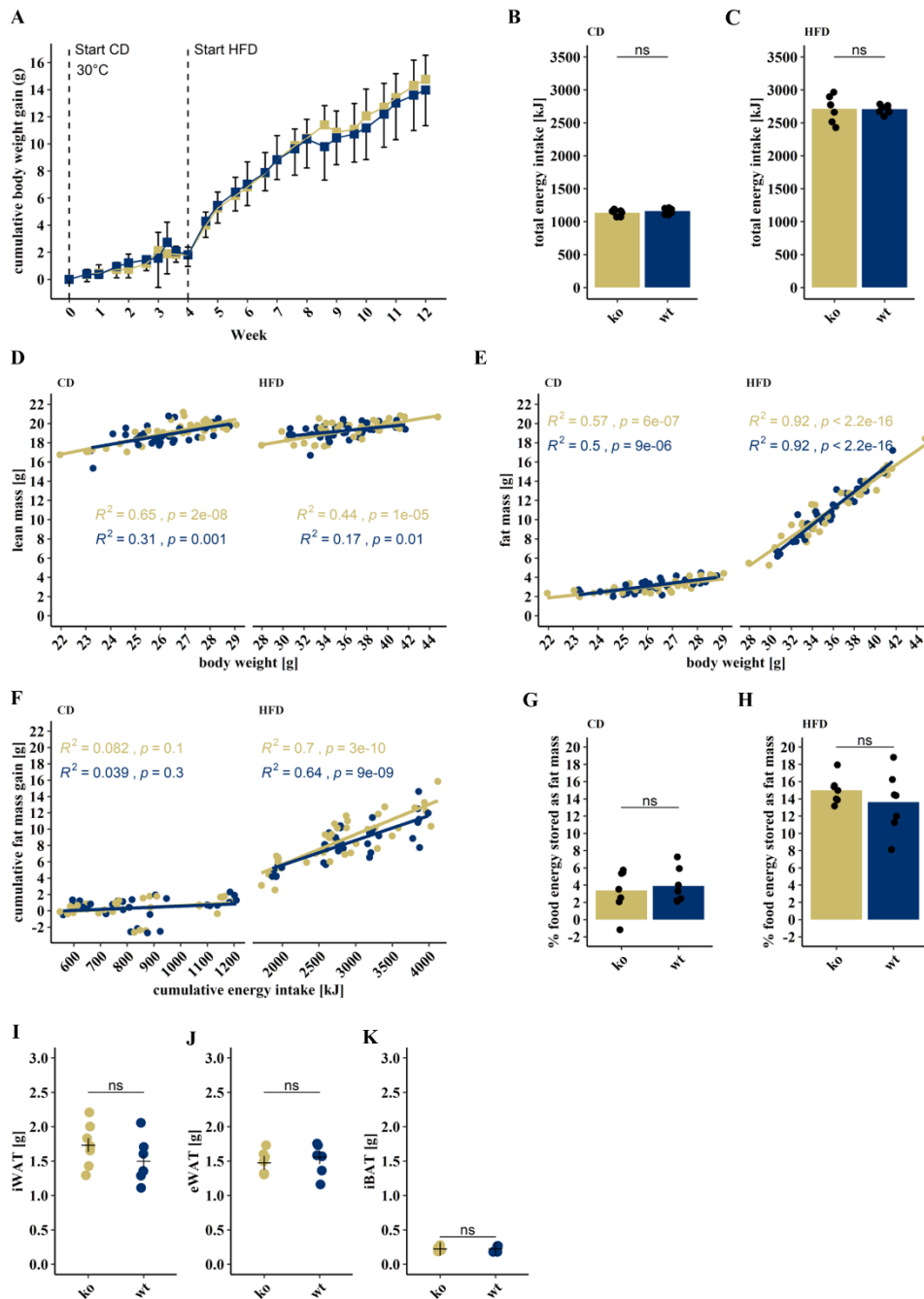


Figure 27: Similar susceptibility to diet-induced obesity in UCP1-KO and WT mice.

(A) Body weight of *Ucp1*-WT (*wt*, $n = 7$) and *Ucp1*-KO (*ko*, $n = 7$) mice at 30°C fed a control (CD) or high-fat diet (HFD). Total energy intake of mice during (B) CD and (C) HFD feeding. (D&E) Pearson correlation coefficient between measurements of (D) lean mass and body weight and (E) fat mass and body weight during CD (left) and HFD (right) feeding. (F) Metabolic efficiency in terms of correlation (Persons' correlation coefficient) between cumulative fat mass gain and cumulative energy intake for CD (left panel) and HFD (right panel). Metabolic efficiency expressed as percent of the total food energy consumed stored as fat mass during (G) CD and (H) HFD feeding. Student's *t*-test between *Ucp1*-WT (*wt* $n = 7$) and *Ucp1*-KO (*ko* $n = 7$), $ns = p > 0.5$, bars indicate group means. Metabolic efficiency expressed as percentage of food energy stored as fat mass was calculated according to (von Essen et al. 2017). Briefly total fat mass gain (g) during each period was multiplied by 37.4 kJ/g and divided by food intake (kJ). Weights of dissected (I) inguinal white adipose tissue (iWAT), (J) epididymal white adipose tissue (eWAT) and (K) interscapular brown adipose tissue (iBAT) at the end of HFD feeding. (B,C,G-I) Student's *t*-test $ns = p\text{-value} > 0.05$. Group means indicated as (B,C) bars and (G-I) crosses.

5.5.4 Plasma lipid composition of UCP1-KO and UCP1-WT mice is comparable

Activated BAT can clear substantial amounts of lipids from circulation (Berbeé et al. 2015; Bartelt et al. 2011). Thus, we investigated if ablation of UCP1 affected systemic lipid metabolism, by targeted lipidomics on plasma samples. Lipid class composition was similar between both genotypes. Only cholesteryl esters (CE) were significantly more abundant in UCP1-WT compared to UCP1-KO mice (Figure 28 A). Concentration of CE, ceramides (CER), hexosylceramides (HCER) and sphingomyelins (SM) were significantly higher in UCP1-WT mice (Figure 28 B). However, fold changes (FC) between to UCP1-KO were rather small (CE, $FC_{wt/ko} = 1.13$; CER, $FC_{wt/ko} = 1.17$; HCER $FC_{wt/ko} = 1.16$; SM, $FC_{wt/ko} = 1.1$). The similarity of plasma lipid composition between both genotypes was confirmed by PCA of composition (Figure 28 C) and concentration (Figure 28 D) on a lipid species level.

Collectively, these data indicate that ablation of UCP1 does not affect the systemic lipid metabolism at thermoneutrality.

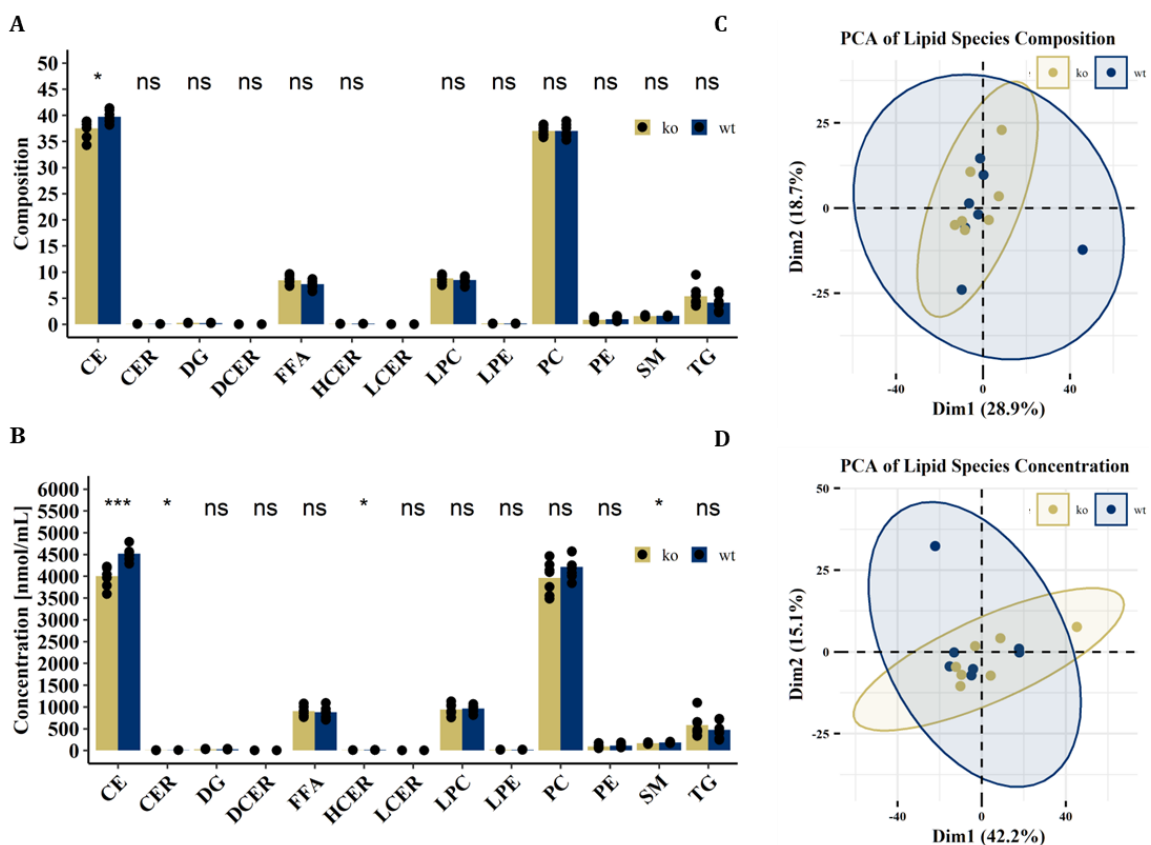


Figure 28: Plasma lipid profiles are comparable between UCP1-KO and UCP1-WT.

(A) Composition and (B) concentration of lipid classes in plasma of UCP1-KO (ko, $n = 7$) and UCP1-WT (wt, $n = 7$) mice housed at 30°C after 8 weeks of high-fat diet feeding. Principal component analysis (PCA) of lipid species (C) composition and (D) concentration. Cholesteryl esters (CE), ceramides (CER), diacylglycerols (DG), dihydroceramides (DCER), free fatty acids (FFA), hexosylceramides (HCER), lactosylceramides (LCER), lysophosphatidylcholines (LPC), lysophosphatidylethanolamines (LPE), phosphatidylcholines (PC), phosphatidylethanolamines (PE), sphingomyelins (SM), triacylglycerols (TG). (A&B) Student's *t*-test ns = p -value > 0.05, * = p -value < 0.05, *** = p -value < 0.001. Group means indicated as (A&B) bars.

5.5.5 Lack of UCP1 is associated with the abundance of specific microbial genera

The gut microbiome influences host metabolism (Tremaroli and Bäckhed 2012) and studies demonstrate an effect of microbiome composition on UCP1 expression (T.-R. Wu et al. 2019) and thermogenesis (Ziętak et al. 2016). Consequently, we investigated whether UCP1 expression alters microbiome composition, by comparing the cecal microbiomes of UCP1-WT and UCP1-KO mice. Similar microbial richness (alpha-diversity) was observed between genotypes by 16S rRNA analysis (Figure 29 A). However, deletion of UCP1 affected cecal microbial composition demonstrated by differences in beta-diversity between genotypes (Figure 29 B). Detailed analysis of the microbial composition revealed four zOTU significantly different between UCP1-KO and UCP1-WT based on unadjusted Kruskal-Wallis rank sum test (Figure 29 C-F). After adjustment for multiple comparisons two of these zOTU demonstrated a trend to higher abundance in UCP1-KO while the other were significantly more abundant in UCP1-WT mice. These zOTUs could be assigned to *Parabacteroides golsteinii* (zOTU3 & zOTU4) and *Desulfovibrio fairfieldensis* (zOTU17 and zOTU19), respectively. Interestingly, *P. golsteinii* has previously been reported to decrease HFD induced obesity and diabetes and increase UCP1 expression in iBAT and iWAT in C57BL/6J mice (T.-R. Wu et al. 2019). These data indicate a connection between UCP1 expression and the gut microbiota and confirm *P. goldsteinii* as a potential species associated to UCP1.

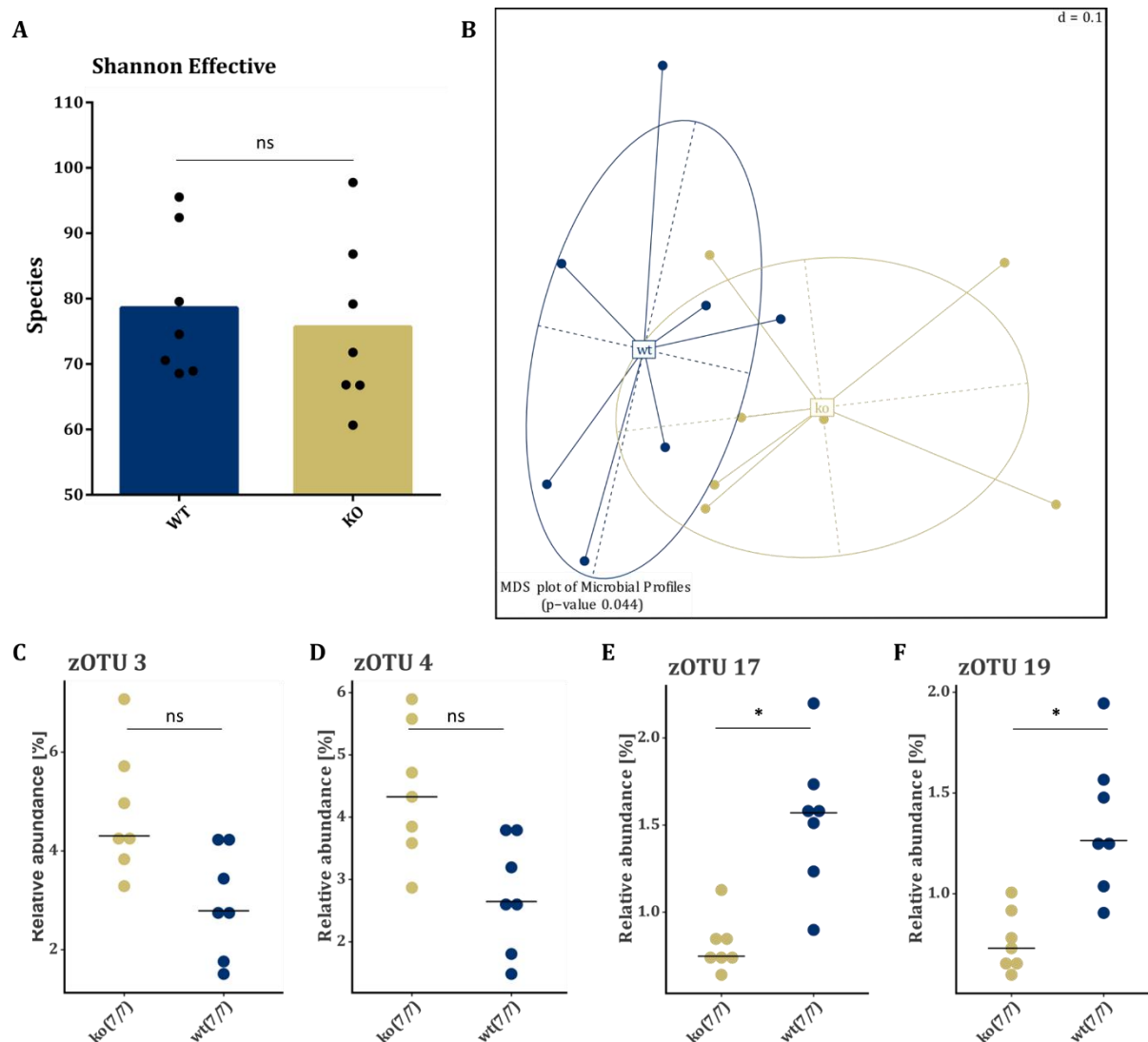


Figure 29: Single cecal microbial genera are associated with the presence of UCP1.

Analysis of cecal microbiome of UCP1-KO (ko, n = 7) and UCP1-WT (wt, n = 7) mice housed at 30°C after 8 weeks of high-fat diet feeding. Comparison of (A) alpha-diversity determined by Shannon effective index and (B) beta-diversity assessed by principal coordinates analysis. (C-F) Relative abundance of zOTU identified by statistically different unadjusted Kruskal-Wallis rank sum test between WT and KO mice. Statistical differences tested by (A) non-parametric Mann-Whitney U test $ns = p\text{-value} > 0.05$, (B) Permutational multivariate analysis of variance, (C-F) Kruskal-Wallis rank sum test with the Benjamini & Hochberg adjustment $ns = p\text{-value} > 0.05$, $* = p\text{-value} < 0.05$, Group means indicated as (A) bars, (C-F) lines.

The microbiome can substantially influence host lipid metabolism (Schoeler and Caesar 2019). As we identified small changes in both lipid metabolism and microbiome composition, we investigated potential interactions between microbiome and lipidome. Therefore, we analyzed the combined lipidome and microbiome data set using supervised (DIABLO PLS-DA) and unsupervised (MOFA) approaches. DIABLO sparse PLS-DA revealed two sets of features that discriminated between UCP1-KO and UCP1-WT mice (Figure 30 A). However, quality assessment by repeated analysis of the dataset with randomly assigned groups (1000 iterations) demonstrated similar good discrimination as between UCP1-KO and UCP1-WT mice (Figure 30

A). Consequently, it was not possible to discriminate the observed difference between UCP1-KO and UCP1-WT from random differences between samples. This assumption was confirmed by unsupervised MOFA demonstrating no separation of the two genotypes by the two factor groups explaining the highest proportion of variance between UCP1-KO and UCP1-WT mice (Figure 30 B).

Consequently, no genotype specific interactions between plasma lipid composition and the microbiome could be identified.

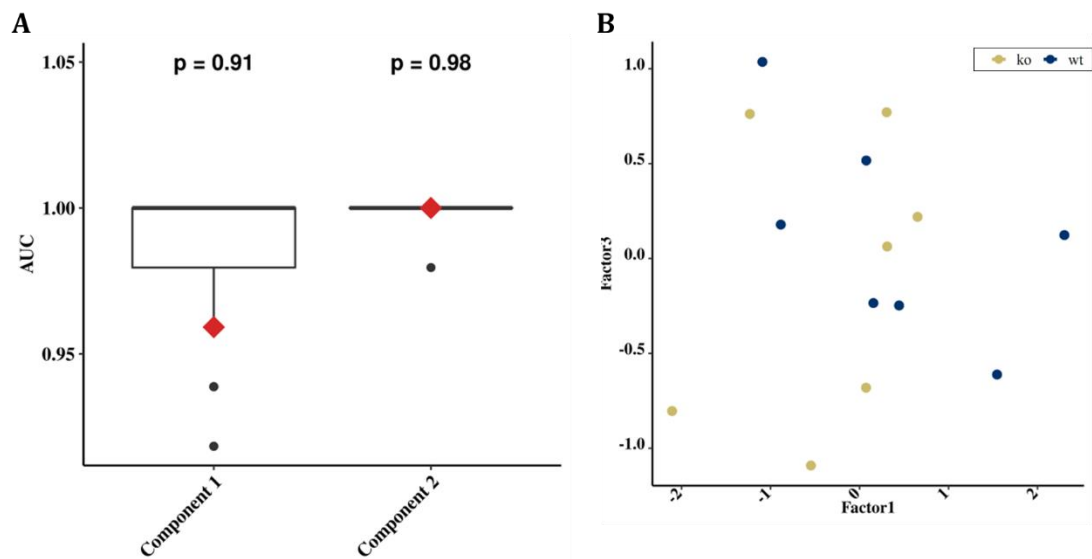


Figure 30: Multi-omics reveal no interaction between microbiome and lipidome explaining differences between UCP1-KO and UCP1-WT mice.

Integrated analysis of the combined lipidome and microbiome data sets. (A) Receiver operating characteristic area under the curve (AUC) of data integration analysis for biomarker discovery using a latent components partial least squares discriminant analysis (DIABLO PLS-DA). Red diamonds indicate results of supervised DIABLO PLS-DA of the components 1 and 2 (Comp1, Comp2). Box plots indicate results of 1000 randomized DIABLO PLS-DA analyses. $P\text{-value} = \#(AUC_{\text{supervised}} < AUC_{\text{random}}) / 1000$. (B) Visualization of the two factors explaining most of the variance between UCP1-KO and UCP1-WT mice based on multi-omics factor analysis (MOFA).

5.5.6 UCP1-KO mice have similar energy balance at thermoneutrality

The effect of UCP1 knockout on energy balance regulation was investigated in detail by indirect calorimetry measurements 3-4 weeks after the start of CD or HFD feeding. We observed a clear diurnal pattern of the respiratory exchange ratio during CD feeding, being higher during the dark phase compared to the light phase (Figure 31 A-B) indicating that mice utilized more carbohydrates during the dark, feeding phase while relying more on fatty acid metabolism during the lighted, fasting phase. During HFD feeding the respiratory exchange ratio was generally reduced compared to the CD period, demonstrating a shift in substrate utilization towards fatty acid oxidation based in the high-fat content of the diet (Figure 31 C & D). However, no differences in respiratory exchange ratio between KO and WT mice were detected during either feeding period (Figure 31 B & D).

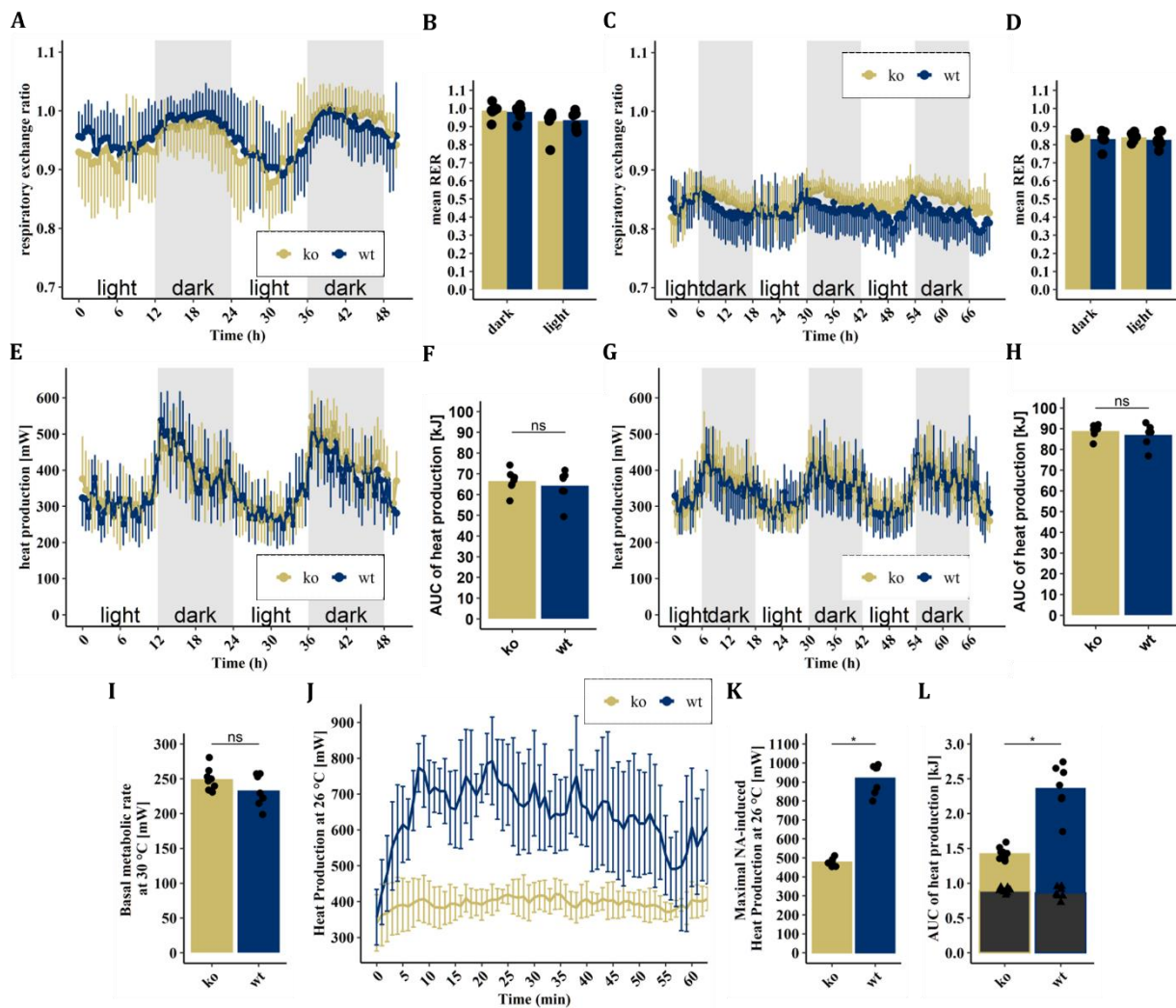


Figure 31: Energy expenditure at thermoneutrality is comparable between UCP1-KO and UCP1-WT mice.

(A) Respiratory exchange ratio of UCP1-KO (ko, $n = 7$) and UCP1-WT (wt, $n = 7$) mice during CD feeding. (B) mean respiratory exchange ratio (RER) of dark and light phases corresponding to (A). (C) Respiratory exchange ratio of mice during HFD feeding. (D) mean respiratory exchange ratio (RER) of dark and light phases corresponding to (C). (E) Heat production during CD feeding and (F) the respective area under the curve (AUC). (G) Heat production during HFD feeding and (H) the respective AUC. (I) Mean basal metabolic rate (mean of the four consecutive lowest values after at least 3h of fasting) at 30 °C. (J) Heat production curve of mice injected with NA at 26 °C. (K) Maximal heat production during the 80 minutes measurement interval shown in (J). (L) AUC of heat production corresponding to (J). Grey bars and triangles indicating contribution of basal metabolic rate. (F,H,I,K,L) Students t -test, $ns = p > 0.5$, $* = p < 0.5$, bars indicate group means; (A,C,E,G) data represented as means and standard deviation, averaged over a period of 30 min; (J) data represented as means and standard deviation, averaged over a period of 10 min.

The activation of BAT thermogenesis by feeding (diet-induced thermogenesis) might contribute to total energy expenditure and thus protect WT mice from DIO (von Essen et al. 2017). To scrutinize these findings, we investigated whether knockout of UCP1 affected energy expenditure in the new mouse model. As expected metabolic rate in terms of O_2 consumption, CO_2 production and heat production were subject to diurnal alterations during CD and HFD feeding, increasing during the active dark phase and decreasing during the inactive light phase (Figure 31 E & G and

Supplementary Figure 9 A-G). However, energy expenditure (area under the heat production curve) during the measurements were similar between WT and KO mice at all times (Figure 31 F & H and Supplementary Figure 9 E & F) but decreased upon HFD feeding (Supplementary Figure 9 G). Consequently, knockout of UCP1 did not affect energy expenditure at thermoneutral conditions.

Subsequent to the energy expenditure measurement during HFD feeding, we investigated basal metabolic rate and NA induced heat production in fasted mice. KO and WT mice had similar basal metabolic rates (Figure 31 I) and increased metabolic rates after NA injection, similar to previous observations (Granneman et al. 2003; C. W. Meyer et al. 2010). However, WT showed a remarkably higher response upon NA injection compared to (Figure 31 J-L), indicating the contribution of UCP1 mediated thermogenesis.

In addition to energy expenditure, we measured energy intake and fecal energy excretion during the calorimetry sessions. Faecal energy content was higher during HFD compared to CD feeding, reflecting the increased energy content of the HFD (not shown). However, there was no difference between genotypes in either feeding period (Figure 32 A & B). This was also true for excreted (Figure 32 C & D) and ingested (Figure 32 E & F) energy during the calorimetry sessions. Consequently, energy balance (ingested energy – excreted energy – AUC of heat production) was unaffected by the deletion of UCP1 under thermoneutral conditions (Figure 32 G & H).

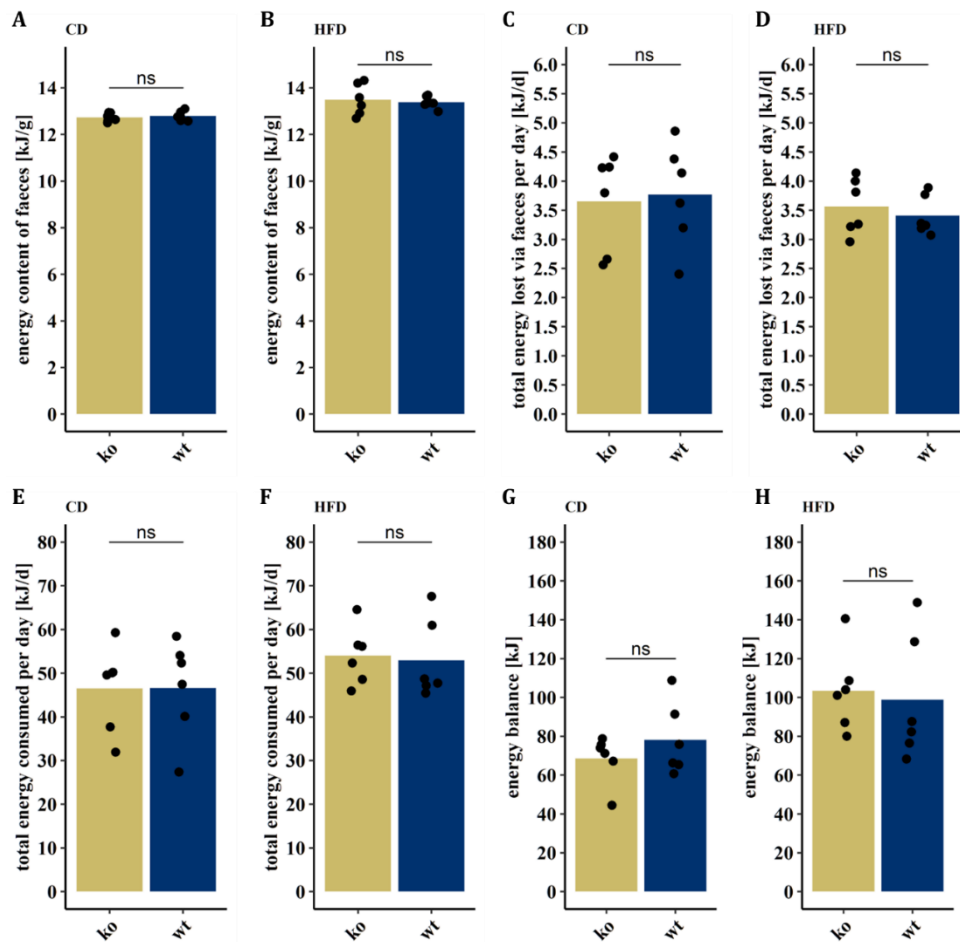


Figure 32: Knockout of UCP1 does not influence energy balance at thermoneutrality.

Faecal energy content of UCP1-WT (n = 6) and UCP1-KO (n = 6) fed (A) CD or (B) HFD. Total energy lost via faeces of mice fed (C) CD or (D) HFD. Energy consumption of mice fed (E) CD or (F) HFD. Energy balance of mice during (G) CD or (H) HFD feeding. One mouse (wt) was removed as it did not eat during the calorimetry session. Another one (ko) was removed from the analysis as the faecal samples did not combust completely. Students t-test, ns = $p > 0.5$, bars indicate group means.

5.6 DISCUSSION

We characterized for the first time a novel UCP1-KO model, as an alternative to the established UCP1-KO mouse, generated by Leslie Kozak and coworkers (Enerbäck et al. 1997). The introduction of novel UCP1-KO models is important since, due to a lack of alternatives, studies investigating the role of UCP1 in context of DIO rely exclusively on this established UCP1-KO model. Only recently a second UCP1-KO mouse model has been described, lacking functional UCP1 due to a SNP at nucleotide 38 of exon 5 of the UCP1 gene (Bond and Ntambi 2018).

The aims of the study were to provide a basal characterization of the constitutive UCP1-KO mouse and to validate this model by comparison with the results of previous studies on the established UCP1-KO mouse, especially in light of the still ongoing debate whether (Feldmann et al. 2009; von Essen et al. 2017; Rowland et al. 2016; Luijten et al. 2019; Pahlavani et al. 2019) or not (Enerbäck

et al. 1997; Liu et al. 2003; Zietak and Kozak 2016; Winn et al. 2017; Maurer et al. 2020) the knockout of UCP1 renders mice more susceptible to DIO at thermoneutral conditions.

At standard housing conditions (~23°C ambient temperature) mice rely on constantly active thermogenesis to maintain normothermia. Mice lacking UCP1 recruit other thermogenic mechanisms to defend body temperature at these conditions and thus in contrast to WT mice are protected against DIO obesity (Keipert et al. 2020; T. Wang et al. 2008; Liu et al. 2003). Similarly, UCP1-KO pups showed decreased body temperature (iSST) in the present study and decreased weight after weaning, confirming the significance of UCP1 as an efficient mechanism to defend body temperature in early life. Interestingly, differences in body weight after weaning could be seen in pups of the conventional UCP1-KO mouse on a 129S1/SvImJ but not on a C57BL/6J background. Indeed, the effect of UCP1 knockout depends on the genetic background since congenic 129S1/SvImJ or C57BL/6J UCP1-KO mice are cold sensitive, while their F1-hybrids are not (Hofmann et al. 2001).

Once the need for thermoregulatory heat production is eliminated by housing mice in their thermoneutral zone (27-30°C) the effect of UCP1 deletion becomes inconclusive. Results from several studies suggest that at thermoneutrality UCP1-KO mice are more susceptible to DIO due to the lack of diet-induced thermogenesis (von Essen et al. 2017; Feldmann et al. 2009; Rowland et al. 2016; Luijten et al. 2019), a mechanism activating BAT thermogenesis enabling rodents to increase their energy expenditure to avoid excessive weight gain caused by overfeeding (Bachman et al. 2002; Rothwell and Stock 1979). Thus, it seems plausible that mice lacking UCP1 are more susceptible to DIO at thermoneutrality (Feldmann et al. 2009; Luijten et al. 2019; von Essen et al. 2017; Rowland et al. 2016) considering UCP1 as the main contributor to BAT thermogenesis. We investigated this phenomenon by comprehensive metabolic analysis of our novel UCP1-KO model. Total energy expenditure was similar in both KO and WT mice and did not differ during the nightly feeding period, indicating no effect of UCP1 deletion to diet-induced thermogenesis. Further, considering the similarities in body weight gain, food intake and metabolic efficiency between KO and WT animals, there is no evidence for a more DIO susceptible phenotype of UCP1-KO mice. These findings are in line with various studies on the established UCP1-KO mouse (Enerbäck et al. 1997; Zietak and Kozak 2016; Winn et al. 2017; Maurer et al. 2020) and a second recently described UCP1-KO mouse (Bond and Ntambi 2018). Based on the combined evidence of different UCP1-KO models we conclude that energy balance regulation and the development of DIO are not affected by the presence of UCP1 at thermoneutrality.

For future studies, a major advantage and the novelty of our mouse model compared to other available UCP1-KO models (Enerbäck et al. 1997; Bond and Ntambi 2018) is the option to induce conditional Cre-mediated deletion of Exon 2 of the UCP1 gene, using tamoxifen- or digitonin-inducible Cre-systems. Although, we described the constitutive UCP1-KO, this system allows to

conditionally knock-out UCP1 in specific tissues or a time dependent manner. This is of significance to investigate the role of alternative mechanisms for NST that might be recruited due to the lack of UCP1 in early life stages. So far, the only available inducible model was the UCP1-DTR mouse, expressing the diphtheria toxin receptor (DTR) under control of the UCP1 promotor, thus depleting UCP1 expressing cells (Rosenwald et al. 2013; Challa et al. 2020). This provided first insights about the contribution of brite adipocytes to energy expenditure (Challa et al. 2020). In contrast, our model will allow the activation independent knockout of UCP1 in distinct cell types while leaving cells otherwise functional. Further research on inducible UCP1-KO mice based on our knockout strategy will help to study the recruitment of alternative thermogenic mechanism and to clarify the role of individual thermogenic adipocytes to NST.

In summary we provide evidence that the abundance of UCP1 does not influence energy metabolism at thermoneutrality and provide a new mouse model as foundation for a better understanding of the contribution of UCP1 in different cell types or life stages to energy metabolism.

6 SPATIAL RECRUITMENT OF CARDIOLIPINS IN WHITE ADIPOSE TISSUE AFTER COLD STIMULATION IS INDEPENDENT OF UCP1

A similar version of this chapter has been submitted: Dieckmann S., Maurer S., Kleigrew K., Klingenspor M.

6.1 ABSTRACT

Brown and brite adipocytes are the key cells performing UCP1 dependent NST induced by cold exposure. Several lipid species are associated to NST in brown and white adipose tissue. Studies investigating the association of the lipid profile with NST rely on the analysis of whole organ homogenates or on the differentiation of pre-adipocytes *in vitro*. These approaches have so far not addressed the heterogeneity of WAT. Aim of this study was to characterize the lipid composition of WAT on a region-specific level in an *in vivo* context.

We applied MALDI-MSI in combination with IHC and high-resolution mass spectrometry on sections of iWAT of 129S6/SvEvTac and C57BL6/N-UCP1-KO and wildtype mice acclimatized to cold to identify lipids specific to areas of UCP1 expression.

Based on the analysis of cold exposed 129S6/SvEvTac mice we identified cardiolipins (CL) and DG species to be specific for areas expressing UCP1 and TG to be the main lipid class characteristic for UCP1 negative regions within iWAT. Investigation of C57BL6/N-UCP1-KO and wildtype mice housed at either RT or acclimatized to cold, demonstrated that CL content in WAT is increased upon cold stimulation, independent of UCP1.

We introduce a MALDI-MSI based approach to identify lipids associated to thermogenic adipocytes in adipose tissues demonstrating a clear regional cold dependent upregulation of CL independent of UCP1.

6.2 AUTHORS CONTRIBUTION

Sebastian Dieckmann designed the study, performed mouse experiments, sectioning, IHC, data analysis, interpreted the results and drafted the manuscript.

6.3 INTRODUCTION

BAT is the main organ responsible for NST. The distinctive cell type of BAT are brown adipocytes that are characterized by high expression levels of UCP1, the key mediator of heat production. NST capacity and UCP1 expression, however, are not restricted to BAT but are also recruited in brite adipocytes that emerge within iWAT upon prolonged β_3 -adrenergic signaling in a process termed “browning”. The thermogenic function of brown and brite adipocytes is not only linked to UCP1 expression but also architecture of these adipocytes. Both cell types contain multilocular lipid droplets, in contrast to the mostly unilocular appearance of lipid droplets in white adipocytes, the main cell type for storing excessive energy in form of triglycerides. Brown and brite adipocytes are packed with mitochondria that are required to enable high rates of ATP-independent uncoupled respiration but also ATP-dependent futile cycles (Kazak et al. 2015). In contrast to white adipocytes, brown and brite adipocytes exhibit high capacities for de novo lipogenesis, beta-oxidation, lipolysis and re-esterification of fatty acids. Consequently, quantitative lipidomics revealed differences of brown and brite compared to white adipocytes like higher levels of distinct phospholipid classes, DG and cardiolipins (CL) in these thermogenic adipocytes (Schweizer et al. 2019; Sustarsic et al. 2018; Lynes et al. 2018; He et al. 2019). CL are an essential component of the inner mitochondrial membrane. They are composed of two phosphatidylglycerols linked by glycerol, forming a dimeric phospholipid with four acyl chains. Bound to several mitochondrial membrane proteins, CL are a signature lipid of mitochondria and play a pivotal role in mitochondrial functionality (Paradies et al. 2019). Pathological alterations in CL metabolism are linked to several diseases such as Barth syndrome, myocardial ischemia, Parkinson’s disease or diabetes (Paradies et al. 2019). The importance of CL in mitochondrial bioenergetics results from the interaction with enzymes of the electron transport chain or the ATP synthase. Further, CL are an integral part of NST, a process induced in brown adipocytes upon β_3 -adrenergic signaling and essential for small rodents to defend body core temperature. Stimulation of brown and brite adipocytes by β_3 -adrenergic receptor agonists lead to increased CL content in brite and brown adipocytes *in vitro* as well as iWAT and BAT *in vivo* (Schweizer et al. 2019; Sustarsic et al. 2018; Lynes et al. 2018; He et al. 2019). The association between CL and UCP1 is further demonstrated by the stabilizing effect of CL on UCP1 (Hoang, Smith, and Jelokhani-Niaraki 2013; Y. Lee et al. 2015), facilitating its function. In line, adipose tissue specific knockout of cardiolipin synthase 1 impairs the β_3 -adrenergic induced recruitment of UCP1 (Sustarsic et al. 2018).

Although the significance of CL for UCP1 function is well established, we are unaware of studies demonstrating the effect of UCP1 on CL abundance. Further, the studies investigating changes in lipid composition and the association between CL and BAT activity or UCP1 rely on the analysis of whole organ homogenates (Lynes et al. 2018; Sustarsic et al. 2018; He et al. 2019) or on the differentiation of pre-adipocytes *in vitro* (Schweizer et al. 2019). Considering the heterogeneity

of WAT (Barreau et al. 2016) these approaches might neglect region-specific differences in lipid metabolism. Consequently, we asked whether changes in the lipid profile in respect to CL occur ubiquitously in WAT (WAT) or in a spatial pattern coinciding with the presence of brite adipocytes. Therefore, the aim of our study was to characterize the lipid composition of adipose tissue and to demonstrate the association between CL and UCP1 on a region-specific level in an *in vivo* context. We present MALDI-MSI in combination with IHC and high-resolution LC-MS/MS as a suitable approach to identify lipids associated to specific functions like the cold induced recruitment of thermogenic adipocytes.

6.4 MATERIAL AND METHODS

6.4.1 Animals

All animals were bred and housed in a specific-pathogen-free facility at 23°C ambient temperature. The experiments were performed according to the German animal welfare law with permission from the district government of Upper Bavaria (Regierung von Oberbayern, reference number ROB-55.2-2532.Vet_02-16-166). At the age of 8-weeks, male mice were single caged, transferred to climate cabinets set to 23°C and 55% relative humidity. Simultaneously, mice were switched to a CD (Sniff Cat# S5745-E702) and divided into two groups based on bodyweight.

129S6/SvEvTac: After 3 weeks at 23°C, one group (5°C) was directly transferred into a second climate cabinet set to 5 °C ambient temperature and 55 % relative humidity for one week.

UCP1-KO: UCP1 knockout (UCP1-KO) and wildtype (UCP1-WT) mice on a C57BL6/N background were generated as described previously (Dieckmann et al in submission) and acclimatized to cold as followed. After 1-week at 23 °C, one group was maintained at 23 °C (23°C) for 4-weeks. The second group (5°C) was gradually acclimatized to cold by decreasing the temperature every week to 20 °C, 15 °C, 10 °C and finally 5 °C.

All mice were killed by CO₂ asphyxiation and pinching of the diaphragm after 1-week at 5°C. Inguinal WAT was dissected, weighed, and immediately embedded in 1% CMC on dry ice. Tissues were stored at -80 °C until further processing.

6.4.2 Cryosectioning

Cryosections of iWAT were generated with a Leica CM2505 Cryostat set to -35 °C chamber temperature and -30 °C specimen temperature. To obtain sections of similar regions within the tissue, approximately 20-25x 16 µm thick sections were discarded until the lymph node was visible in the sections. Subsequently 6x consecutive 16 µm sections were obtained. The first was thaw mounted on a chilled conductive ITO-slide (Bruker Daltonik, Bremen/Germany). The second was thaw mounted on a polysine-coated slide for IHC. The third and fourth section were combined

and transferred into a glass vial for LC-MS/MS analysis. A fifth and sixth section were discarded before repeating sectioning to the next replicate. Samples on ITO-Slides and in glass vials were kept within the cryostat. Samples for IHC and H&E staining were kept at RT. After preparation of all samples, teaching points were drawn on the ITO-slide with a correction pen (Tipp-Ex, Cat# 8022921, BIC, France). An image of the dried ITO-slide was acquired with a digital single-lens reflex camera (Nikon D5600) for alignment with the MALDI instrument. Subsequently, all slides were placed in a vacuum desiccator, evacuated for 10 min, closed and dried for additional 20 min at RT. The ITO-slide was immediately processed further for MALDI-MSI (matrix application), while all other slides were stored at -20 °C until staining. Samples in glass vials were stored at -80 °C until further processing.

6.4.3 Matrix application

The HCCA matrix (7 g/l HCCA, 0.2 % TFA in 60 % ACN) was applied on ITO-slides by spraying (ImagePrep, Bruker Daltonik, Bremen/Germany) and the following program: (1) Initialization, (2) 0.07 V, 1 cycle, 0.05 V, (3) 0.07 V, 2 cycle, 0.1 V, (4) 0.2 V, 3 cycle, 0.2 V, (5) 0.6/-0.5 V, 4 cycle, 0.3 V.

6.4.4 MALDI-MSI

MALDI-MSI was performed on the MALDI ultrafleXtreme (Bruker Daltonik, Bremen/Germany) with a Smartbeam2-Laser set to “4 large” and a raster size of 100 µm in positive ionization mode.

6.4.5 Immunohistochemistry

Samples on polysine-coated slides were washed 5 min in TBS and fixed for 10 min in ice-cold methanol/acetone (1:1). Fixed samples were washed twice in TBS for 5 min. Blocking was performed for 2 h at RT (TBST with 10% donkey serum, 1% bovine serum albumin) before application of the primary antibody against UCP1 (1:800, Cat# ab23841, abcam, London/UK) for 2 h at RT or overnight at 4 °C. After primary antibody incubation, samples were washed three times in TBST for 5 min before applying the secondary antibody (1:500, Cat# A10040, Thermo Fisher) overnight at 4 °C or 2 h at RT. Secondary antibody solution was removed and samples stained with Hoechst33342 (1:500, Cat# 14533, Sigma-Aldrich, St. Louis MO/USA) for 10 min at RT. Finally, samples were washed three times in TBST for 5 min, supplied with mounting medium (Cat# VEC-H-1000-10, Biozol, Eching/Germany), covered by a cover slide and sealed with nail polish. Whole slide scans were performed immediately after staining with a fluorescence microscope (Leica AF000 LX, Filters: Y3 ET, Cat# 11504169 and DAPI ET, Cat# 11504203). Merged slide scans were exported from the LAS X software and subsequently opened and edited identically in ImageJ (Version 1.53c).

6.4.6 LC-MS/MS Analysis

The tissue section was extracted with 0.5 mL chloroform/methanol (1:1, v:v) in an analytical glass vial. First, each tissue section was vortexed for 30 sec with a centrifugation step for 1 min at 1200 rpm. Afterwards the samples were sonicated for 15 min and shaken for 30 min. After centrifugation for 5 min at 3000 rpm, 200 μ L of the supernatant was dried in a Concentrator plus (Eppendorf) and dissolved in 20 μ L chloroform/methanol (1:1, v:v) which was used for analysis.

The lipid analysis was performed using a Nexera UHPLC system (Shimadzu) coupled to a Q-TOF mass spectrometer (TripleTOF 6600, AB Sciex) according to a published analytical method (Witting et al. 2014): Separation of the lipid extract was performed using a UPLC BEH C18 2.1x100, 1.7 μ m analytical column (Waters Corp.) with 300 μ L/min flow rate. The mobile phase was water/acetonitrile (40:60, v:v) with 10 mM ammonium formiate and 0.1% formic acid (eluent A) and isopropanol/acetonitrile (90:10, v:v) with 10 mM ammonium formiate and 0.1% formic acid (eluent B). The gradient profile was 32% B from 0 to 1.5 min raising to 97% B at 21 min which was held for 4 min. Afterward the column was equilibrated at starting conditions. A volume of 5 μ L per sample was injected. The autosampler was cooled to 10°C and the column oven heated to 40°C. The samples have been measured in the Information Dependent Acquisition (IDA) mode. MS settings in the positive mode were as follows: Gas 1 55, Gas 2 65, Curtain gas 35, Temperature 500°C, Ion Spray Voltage 5500, declustering potential 80. The mass range of the TOF MS and MS/MS scans were 100 - 2000 m/z and the collision energy set to 35 V with a 15 V spread. MS settings in the negative mode were as follows: Gas 1 55, Gas 2 65, Cur 35, Temperature 500°C, Ion Spray Voltage -4500, declustering potential -80. The mass range of the TOF MS and MS/MS scans were 100 - 2000 m/z and the collision energy set to -35 V with a 15 V spread. Mass to charge ratios identified by MALDI were added to the inclusion list to obtain a respective MS/MS-spectra for lipid annotation by MS-DIAL (Tsugawa et al. 2020).

6.4.7 Data Analysis

Analysis of data acquired by MALDI-MSI was performed with the SCiLS software (Bruker Daltonik, Bremen/Germany, Version 2016b) and the tools provided with the software. Sections of one measurement were loaded as individual regions in a combined dataset, applying convolution baseline correction. Data was normalized to the total ion count for data analysis and image representation. Segmentation was performed on medium denoised data. Identification of discriminative m/z intervals by receiver operating characteristic (ROC) analysis was performed on individual spectra and the aligned peaks resulting from the combined segmentation of all sections of one experiment. Initial annotation of m/z intervals was based on the bulk search option of the LIPID MAPS® Structure Database (LMSD) considering only $[M+H]^+$ ions with a mass tolerance of ± 0.5 Da (https://www.lipidmaps.org/resources/tools/bulk_structure_searches.php)

[?database=LMSD](#)). LC-MS Data was analyzed with the MS-Dial software (Version 4.48, (Tsugawa et al. 2020)).

6.5 RESULTS

6.5.1 MALDI-MSI yields reproducible results within different sections of iWAT

The iWAT is a heterogeneous tissue, showing region specific degrees of browning (Barreau et al. 2016). Due to this heterogeneity studies on whole tissue homogenates cannot resolve regional changes in the lipidomic profile induced by various treatment conditions. Aim of our study was to address this issue by applying MALDI-MSI on sections of iWAT. The heterogeneity within the tissue also might limit the interpretation of results, reproducibility and the comparison of sections taken in different depths in the tissue. We established the reproducibility and comparability on iWAT of 129S6/SvEvTac mice acclimatized to 5°C for one week. Mice of the 129S6/SvEvTac strain were used due to their high propensity to browning. As a first step to reduce the heterogeneity between measurements, we restricted the area of interest to sections around the lymph node, that is clearly visible to the eye in iWAT. In a second step we checked the homogeneity within this area by measuring, four sections of a single iWAT, spanning a range of ~280 µm (Figure 33 A) in a single run. The similarity of sections was examined by spatial segmentation of the spectra. The resulting segmentation map demonstrated a high similarity between the iWAT sections of a single mouse (Figure 33 A). This observation was confirmed in two other 129S6/SvEvTac mice (Figure 33 B & C). These results demonstrate that no general methodological bias was introduced by our sectioning protocol substantiating the comparability and reproducibility of sections in a defined region of iWAT. Additionally, the segmentation of regional spectra also demonstrates the heterogeneity within iWAT (Figure 33 A-C), indicating regional specificity of lipid species.

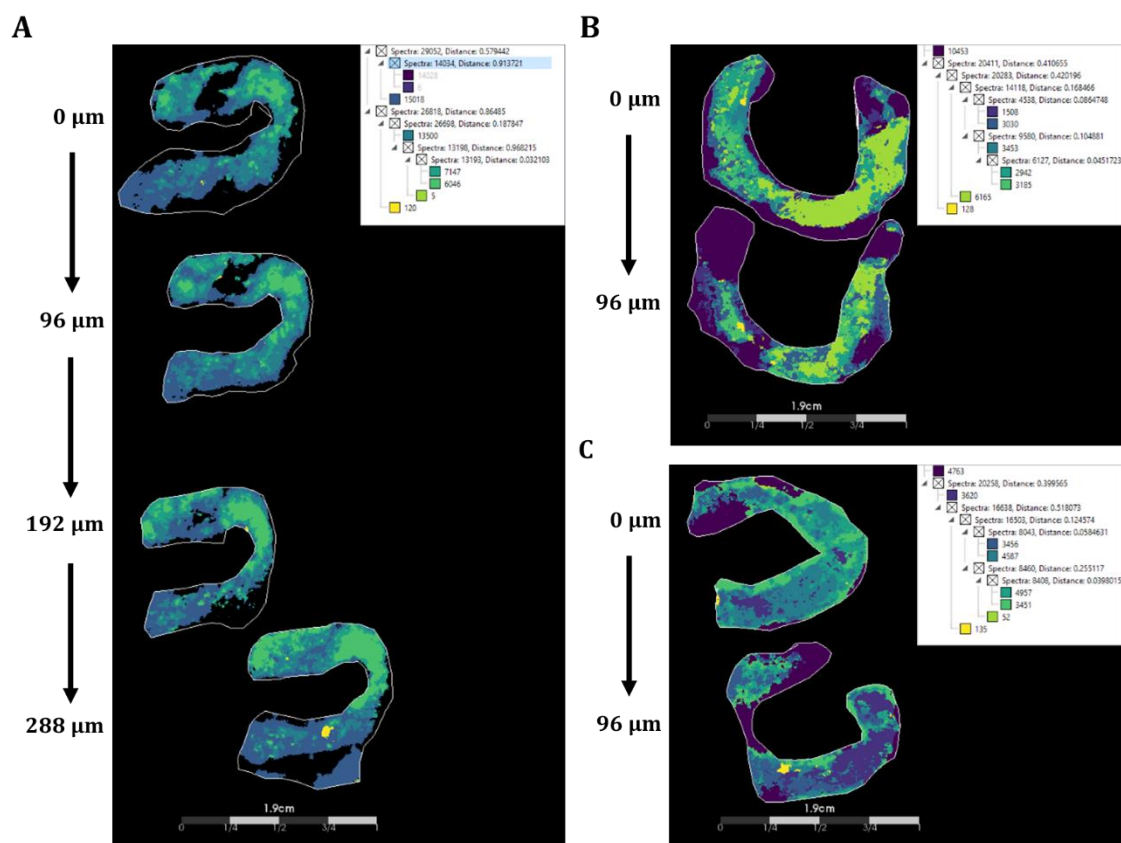


Figure 33: High similarity between different sections.

Segmentation results of inguinal white adipose tissue of three (A-C) 129S6/SvEvTac mice acclimatized to 5°C for 1 week. Sections spanning a range of (B&C) ~100 μm up to (A) ~280 μm subjected to MALDI-MSI with subsequent spatial segmentation based on bisecting k-means in combination with correlation distance. Identical colors indicate similar spectra. Insets show segmentation trees. Scale bars 1.9 cm.

6.5.2 Identification and annotation of region-specific *m/z* intervals

After demonstrating the reliability of our MALDI-MSI approach, we asked the question whether the structural differences in the lipid composition correspond to specific functional regions within iWAT (Figure 33). Since several lipids are associated to cold induced NST on a whole tissue level (Lynes et al. 2018; Sustarsic et al. 2018; Hoene et al. 2014; Lynes et al. 2017), we investigated, if these changes of the lipidome observed upon cold stimulation appear ubiquitously in iWAT or are associated to clusters of thermogenic adipocytes. Therefore, we combined the MALDI-MSI data with IHC staining against UCP1, the major marker of brite adipocytes, and high-resolution LC-MS/MS (Figure 34 A), to validate the findings of the MALDI-MSI on a global level. Staining of UCP1 in iWAT of cold acclimatized 129S6/SvEvTac mice demonstrated the expected cluster of UCP1-expressing cells around the lymph node (Figure 34 B, additional mouse examples Supplementary Figure 10 & Supplementary Figure 11 A) (Barreau et al. 2016). As seen before (Figure 33) the similar spectra clustered in specific regions and could be expanded until one matched the UCP1 expression pattern (Figure 34 B & C, additional mouse examples Supplementary Figure 10 & Supplementary Figure 11 A & B). To identify which *m/z* intervals discriminated between the

regions overlapping with UCP1 expression (UCP1-positive) and those without overlap (UCP1-negative), we performed ROC-analysis between these two regions (Figure 34 D, additional mouse examples Supplementary Figure 10 & Supplementary Figure 11 C) in a total of $n = 8$ sections (3 mice with 2-4 sections). For each mouse, a mean ROC of ≥ 0.75 was considered characteristic for UCP1-positive regions, a mean ROC of ≤ 0.25 for the UCP1-negative regions and a mean ROC between 0.45 and 0.55 to be not characteristic for any of the two regions. Using this approach, we identified 24 m/z intervals associated to UCP1 expression (Table 6), 28 m/z intervals to UCP1-negative regions (Table 7) and 63 m/z intervals not specific for any of the two regions (Table 8). Visual inspection of the m/z intervals confirmed the discrimination potential of our approach (Figure 34 E, additional mouse examples Supplementary Figure 10 & Supplementary Figure 11 D). Within the set of m/z intervals not discriminating between the regions of interest, we identified some to be ubiquitously present (e.g. m/z 749.422, Figure 34 F) and some to be associated to the lymph node (e.g. m/z 774.388, Supplementary Figure 10 & Supplementary Figure 11 F). These m/z intervals were annotated to potential lipid species utilizing the bulk search option in the LMSD. In 8 instances no matching $[M+H]^+$ ion could be assigned to the entered m/z interval, resulting in 20 and 28 annotated m/z intervals for the UCP1-positive (Table 6) and UCP1-negative (Table 7) regions, respectively. Of the non-discriminating m/z intervals, 59 could be annotated to potential lipid species. Due to the broad mass tolerance (± 0.5 Da) of the MALDI-measurement, we received 1-14 potential annotations for each m/z interval, corresponding to a variety of different lipid classes (Table 6, Table 7, Table 8).

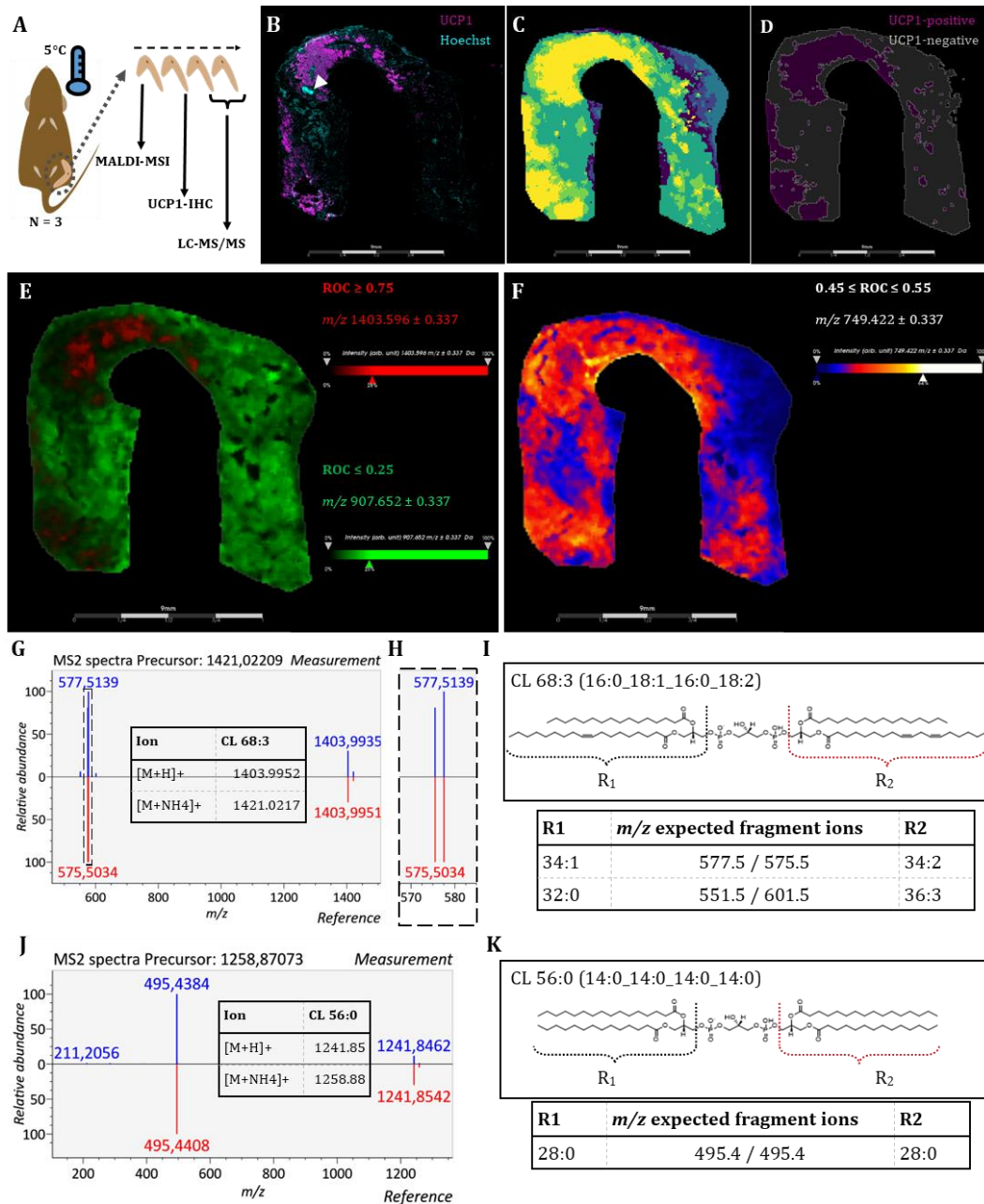


Figure 34: Identification and validation of region-specific lipid species.

(A) Overview of the experimental setup. 129S6/SvEvTac mice were housed at 5°C for 1 week. Inguinal white adipose tissue (iWAT) was dissected (grey dashed circle). Four consecutive sections were prepared, the first used for MALDI-MSI, the second for immunohistochemistry (IHC) staining of UCP1 and the last two for LC-MS/MS analysis. (B) IHC of iWAT stained for UCP1 (magenta) and Hoechst (cyan). White arrowhead indicating the position of the lymph node. (C) Segmentation map of the MALDI-data expanded to several levels to match the UCP1 pattern in B. (D) UCP1-pos (magenta) and UCP1-neg (grey) adipose tissue regions assigned based on the segmentation used for ROC-analysis. (E) MALDI images of two examples m/z intervals identified to be specific for the UCP1-negative (green, ROC ≤ 0.25) and UCP1-positive (red, ROC ≥ 0.75) regions depicted in D. (F) MALDI image of one example m/z interval not specific for any of the two regions assigned in D (0.45 ≤ ROC ≤ 0.55). (G) MS2 spectra used to validate the region-specific m/z intervals exemplified on m/z 1403.596. Inlet shows the theoretical molecular masses of two different ions for CL 68:3 annotated by LIPID MAPS® Structure database search. (H) Detailed view of MS2 spectra of the m/z interval indicated by the dashed box in (G). (I) Structure of CL 68:3 and fragments based on different acyl chain composition. (J) MS2 spectra of a commercial CL standard (CL 56:0). (K) Structure of CL 56:0 and fragments based on acyl chain composition.

Table 6: Overview of m/z intervals associated to UCP1-positive regions.

	MALDI		LIPID MAPS®			LC-MS/MS			
	m/z	match mass	delta	name	formula	ion	RT (min)	measured mass	delta (mDa)
1	1404.608	1404.8461	.2381	Hex(5)-Cer 38:1;O2	C68H125NO28				
2	1403.596	1403.9952	.3992	CL 68:3	C77H144O17P2	NH4+	19.7	1424.02051	1.22
3	1401.572	1401.8464	.2744	Hex(3)-HexNAc- Fuc-Cer 36:1;O2	C68H124N2O27				
		1401.9795	.4075	CL 68:4	C77H142O17P2	NH4+	19.3	1418.99646	9.64
4	1400.560	1400.826	.2660	Hex(2)-HexNAc- NeuGc-Cer 36:1;O2	C67H121N3O27				
5	1373.570	1373.8151	.2451	Hex(3)-HexNAc- Fuc-Cer 34:1;O2	C66H120N2O27				
6	619.195	619.2878	.0928	LPI 20:5	C29H47O12P				
		619.3606	.1656	PA 28:3;O2	C31H55O10P				
		619.3841	.1891	ST 35:5;O9	C35H54O9				
		619.4333	.2383	PA 30:1	C33H63O8P				
		619.4446	.2496	EPC 30:2;O3	C32H63N2O7P				
		619.4697	.2747	PA O-31:1	C34H67O7P				
		619.5296	.3346	DG 36:3	C39H70O5	NH4+	15.4	636.55463	1.58
		619.5449	.3499	CE 16:3	C43H70O2				
		619.6388	.4438	WE 42:1	C42H82O2				
7	618.183	618.3402	.1572	PE 25:4;O2	C30H52N010P				
		618.4857	.3027	CerP 34:1;O2	C34H68N06P				
8	617.171	617.4177	.2467	PA 30:2	C33H61O8P				
		617.4541	.2831	PA O-31:2	C34H65O7P				
		617.5139	.3429	DG 36:4	C39H68O5	NH4+	15	634.53876	1.77
		617.5503	.3793	DG O-37:4	C40H72O4				
9	615.146	615.3316	.1856	TG 35:13;O	C38H46O7				
		615.3504	.2044	LPI 19:0	C28H55O12P				
		615.3868	.2408	LPI O-20:0	C29H59O11P				
		615.402	.2560	PA 30:3	C33H59O8P				
		615.4983	.3523	DG 36:5	C39H66O5	NH4+	13.95	632.52106	3.84
10	571.287	571.2878	.0008	LPI 16:1	C25H47O12P				
11	570.275	570.2826	.0076	LPS 22:6	C28H44N09P				
		570.3554	.0804	LPC 22:5	C30H52N07P				
		570.3765	.1015	LPS O-21:0;O	C27H56N09P				
		570.5092	.2342	Cer 34:1;O4	C34H67N05				
		570.5456	.2706	Cer 35:0;O3	C35H71N04				
12	569.263	569.3085	.0455	PG 20:1;O	C26H49O11P				
		569.332	.0690	ST 24:1;O4;GlcA	C30H48O10				
		569.3813	.1183	LPG 22:0	C28H57O9P				
		569.5139	.2509	DG 32:0	C35H68O5	NH4+	16.2	589.534	6.53
		569.5292	.2662	CE 12:0	C39H68O2				
13	567.239	567.2929	.0539	PA 23:2;O3	C26H47O11P				
		567.3528	.1138	ST 31:3;O9	C31H50O9				
		567.3656	.1266	LPG 22:1	C28H55O9P				
		567.4983	.2593	DG 32:1	C35H66O5	NH4+	15.2	584.52185	3.05
		567.5347	.2957	FAHFA 36:1;O	C36H70O4				
		567.5711	.3321	FA 37:0;O	C37H74O3				
14	559.142	559.2538	.1118	ST 30:8;O10	C30H38O10				
		559.2878	.1458	LPI 15:0	C24H47O12P				
		559.3242	.1822	LPI O-16:0	C25H51O11P				
		559.3265	.1845	ST 32:6;O8	C32H46O8				
		559.4357	.2937	DG 32:5	C35H58O5				
		559.4721	.3301	FAHFA 36:5;O	C36H62O4				
		559.5449	.4029	FA 38:3	C38H70O2				
		559.5449	.4029	WE 38:3	C38H70O2				
15	558.130	558.319	.1890	PC 20:4	C28H48N08P				
		558.3459	.2159	ST 27:1;O5;T	C29H51N07S				
		558.3554	.2254	LPC 21:4	C29H52N07P				
16	557.117	557.2381	.1211	ST 30:9;O10	C30H36O10				
		557.2721	.1551	LPI 15:1	C24H45O12P				

MALDI		LIPID MAPS®				LC-MS/MS			
m/z	match mass	delta	name	formula	ion	RT (min)	measured mass	delta (mDa)	
	557.2874	.1704	LPG 22:6	C28H45O9P					
	557.3085	.1915	LPI O-16:1	C25H49O11P					
	557.3109	.1939	ST 32:7;08	C32H44O8					
	557.5292	.4122	FA 38:4	C38H68O2					
17	511.234	511.2667	.0327	PA 20:1;02	C23H43O10P				
		511.2902	.0562	FA 27:6;07	C27H42O9				
		511.2902	.0562	MGMG 18:5	C27H42O9				
		511.303	.0690	LPG 18:1	C24H47O9P				
		511.3265	.0925	ST 28:2;08	C28H46O8				
		511.4357	.2017	DG 28:1	C31H58O5	NH4+	8.8	528.46045	1.83
		511.4721	.2381	FAHFA 32:1;0	C32H62O4				
		511.4721	.2381	FA 32:1;02	C32H62O4				
	511.5085	.2745	FA 33:0;0	C33H66O3					
18	511.909	512.2619	.3529	PS 16:0	C22H42NO10P				
		512.2983	.3893	LPS O-17:1;0	C23H46NO9P				
		512.2983	.3893	LPS 17:0	C23H46NO9P				
		511.5085	.4005	FA 33:0;0	C33H66O3				
		512.3347	.4257	LPS O-18:0	C24H50NO8P				
		511.4721	.4369	FAHFA 32:1;0	C32H62O4				
		511.4721	.4369	FA 32:1;02	C32H62O4				
		512.3711	.4621	LPC O-17:0;0	C25H54NO7P				
	512.3711	.4621	LPE O-20:0;0	C25H54NO7P					
	511.4357	.4733	DG 28:1	C31H58O5	NH4+	12.8	528.46045	1.83	
19	498.076	498.2826	.2066	LPS 16:0	C22H44NO9P				
		498.2826	.2066	LPS O-16:1;0	C22H44NO9P				
		498.3554	.2794	LPE O-19:0;0	C24H52NO7P				
		498.4881	.4121	Cer 31:0;02	C31H63NO3				
20	485.931	486.2826	.3516	LPS O-15:0;0	C21H44NO9P				
		485.4928	.4382	FOH 31:0;02	C31H64O3				
		485.4564	.4746	FA 30:0;02	C30H60O4				
21	1375.594	No HIT							
22	1374.582	No HIT							
23	1402.584	No HIT							
24	616.158	No HIT							

M/z intervals associated to UCP1-positive regions. by MALDI-MSI (m/z), their matches to the LIPID MAPS® structure data base bulk search (mass, delta, name and formula). If applicable the ion, retention time (RT), exact MS1 mass (measured mass) and delta to the matched reference mass are given for lipids that could be identified in the LC-MS/MS data by exact mass measurement and data base hits for their respective MS2 fragmentation.

Table 7: Overview of m/z intervals associated to UCP1-negative regions.

MALDI		LIPID MAPS®				LC-MS/MS			
m/z	match mass	delta	name	formula	ion	RT (min)	measured mass	delta (mDa)	
1	472.436	472.3996	0.0364	CAR 20:0;0	C27H53NO5				
		472.3421	0.0939	CAR 22:6	C29H45NO4				
2	519.331	519.3316	0.0006	ST 30:4;07	C30H46O7				
		519.4044	0.0734	ST 32:2;05	C32H54O5				
		519.4408	0.1098	FAHFA 33:4;0	C33H58O4				
		519.5136	0.1826	FA 35:2	C35H66O2				
3	637.413	637.4075	0.0055	PG 26:1	C32H61O10P				
		637.3711	0.0419	PA 28:2;03	C31H57O11P				
		637.4826	0.0696	DG 38:8	C41H64O5	Na+	16.21	659.46533	0.73
		637.3347	0.0783	PG 24:3;02	C30H53O12P				
		637.5554	0.1424	DG dO-40:8	C43H72O3				
		637.5765	0.1635	DG 37:1	C40H76O5				
		637.5918	0.1788	CE 17:1	C44H76O2				
	637.6493	0.2363	FA 42:0;0	C42H84O3					
4	672.838	672.5409	0.2971	HexCer 32:1;02	C38H73NO8				
		672.4599	0.3781	PE 31:3	C36H66NO8P				

	MALDI	LIPID MAPS®				LC-MS/MS			
	m/z	match mass	delta	name	formula	ion	RT (min)	measured mass	delta (mDa)
5	679.248	679.3453	0.0973	PG 26:4;O3	C32H55O13P				
		679.3688	0.1208	ST 30:5;O7;Hex	C36H54O12				
		679.4333	0.1853	PA 35:6	C38H63O8P				
		679.4545	0.2065	PG 29:1	C35H67O10P				
		679.4697	0.2217	PA O-36:6	C39H67O7P				
		679.4908	0.2428	PG O-30:1	C36H71O9P				
		679.5871	0.3391	TG 39:1	C42H78O6				
		679.6235	0.3755	DG 40:1	C43H82O5				
		679.6388	0.3908	CE 20:1	C47H82O2				
		679.6963	0.4483	FA 45:0;O	C45H90O3				
6	680.26	680.3406	0.0806	PS 25:3;O3	C31H54NO13P				
		680.4133	0.1533	PE 28:2;O3	C33H62NO11P				
		680.4497	0.1897	PS 28:0	C34H66NO10P				
		680.4861	0.2261	PS O-29:0	C35H70NO9P				
		680.4861	0.2261	LPS O-29:1;O	C35H70NO9P				
		680.6551	0.3951	Cer 43:1;O3	C43H85NO4				
		680.6915	0.4315	Cer 44:0;O2	C44H89NO3				
7	734.578	734.5694	0.0086	PE 35:0	C40H80NO8P				
		734.5694	0.0086	PC 32:0	C40H80NO8P	H+	14.56	734.56848	0.92
		734.6058	0.0278	PC O-33:0	C41H84NO7P				
		734.6058	0.0278	PE O-36:0	C41H84NO7P				
		734.533	0.045	PS O-33:1	C39H76NO9P				
		734.4967	0.0813	PS 32:1	C38H72NO10P				
		734.4755	0.1025	PE 36:7	C41H68NO8P				
		734.4239	0.1541	PS 30:3;O2	C36H64NO12P				
		734.7385	0.1605	Cer 48:1;O2	C48H95NO3				
8	851.648	851.6008	0.0472	PI O-36:1	C45H87O12P				
		851.5913	0.0567	SQDG 36:0	C45H86O12S				
		851.7123	0.0643	TG 52:6	C55H94O6	NH4+	18.52	868.73773	1.16
		851.5797	0.0683	PG 42:6	C48H83O10P				
		851.5644	0.0836	PI 35:1	C44H83O13P				
		851.4705	0.1775	PI 36:8	C45H71O13P				
		852.1436	0.4956	CoA 4:1;O	C25H40N7O18P3S				
9	852.66	852.6477	0.0123	PE 44:4	C49H90NO8P				
		852.6477	0.0123	PC 41:4	C49H90NO8P				
		852.6841	0.0241	PC O-42:4	C50H94NO7P				
		852.6113	0.0487	PS O-42:5	C48H86NO9P				
		852.5865	0.0735	SHexCer 38:1;O3	C44H85NO12S				
		852.5749	0.0851	PS 41:5	C47H82NO10P				
		852.5538	0.1062	PC 42:11	C50H78NO8P				
		852.8378	0.1778	Cer 54:0;O4	C54H109NO5				
		852.18	0.48	CoA 5:0	C26H44N7O17P3S				
10	853.672	853.6164	0.0556	PI O-36:0	C45H89O12P				
		853.728	0.056	TG 52:5	C55H96O6	NH4+	18.52	870.74457	9.95
		853.5953	0.0767	PG 42:5	C48H85O10P				
		853.5801	0.0919	PI 35:0	C44H85O13P				
		853.5613	0.1107	TG 51:14;O2	C54H76O8				
		853.4862	0.1858	PI 36:7	C45H73O13P				
		854.1229	0.4509	CoA 3:1;O2	C24H38N7O19P3S				
		854.1593	0.4873	CoA 4:0;O	C25H42N7O18P3S				
11	854.684	854.6997	0.0157	PC O-42:3	C50H96NO7P				
		854.6633	0.0207	PC 41:3	C49H92NO8P				
		854.6633	0.0207	PE 44:3	C49H92NO8P				
		854.6269	0.0571	PS O-42:4	C48H88NO9P				
		854.6117	0.0723	IPC 38:0;O3	C44H88NO12P				
		854.5906	0.0934	PS 41:4	C47H84NO10P				
		854.5694	0.1146	PC 42:10	C50H80NO8P	H+	11.6	854.5672	2.2
		854.4967	0.1873	PS 42:11	C48H72NO10P				
12	855.696	855.7436	0.0476	TG 52:4	C55H98O6	NH4+	18.96	872.75848	11.72
		855.611	0.085	PG 42:4	C48H87O10P				
		855.5018	0.1942	PI 36:6	C45H75O13P				

	MALDI		LIPID MAPS®			LC-MS/MS				
	m/z	match mass	delta	name	formula	ion	RT (min)	measured mass	delta (mDa)	
13	875.601	875.6008	0.0002	PI O-38:3	C47H87O12P					
		875.5797	0.0213	PG 44:8	C50H83O10P					
		875.5644	0.0366	PI 37:3	C46H83O13P					
		875.5456	0.0554	TG 53:17;O2	C56H74O8					
		875.6736	0.0726	PG 43:1	C49H95O10P					
		875.7123	0.1113	TG 54:8	C57H94O6		NH4+	18.29	892.72992	8.97
		875.8062	0.2052	TG 53:1	C56H106O6		NH4+	20.96	892.83044	2.38
14	876.951	876.6688	0.2822	PS 42:0	C48H94NO10P					
		876.6477	0.3033	PC 43:6	C51H90NO8P					
15	877.626	877.6164	0.0096	PI O-38:2	C47H89O12P					
		877.6528	0.0268	SLBPA 42:0	C48H93O11P					
		877.5953	0.0307	PG 44:7	C50H85O10P					
		877.5801	0.0459	PI 37:2	C46H85O13P					
		877.6892	0.0632	PG 43:0	C49H97O10P					
		877.728	0.102	TG 54:7	C57H96O6		NH4+	18.56	894.75409	0.43
		877.4862	0.1398	PI 38:9	C47H73O13P					
		877.8219	0.1959	TG 53:0	C56H108O6		NH4+	21.27	894.83875	9.64
		877.8582	0.2322	FA 57:1;O3	C57H112O5					
		878.1229	0.4969	CoA 5:3;O2	C26H38N7O19P3S					
16	878.638	878.5906	0.0474	PS 43:6	C49H84NO10P					
		878.6997	0.0617	PC O-44:5	C52H96NO7P					
		878.5694	0.0686	PC 44:12	C52H80NO8P		H+	11.17	878.55914	10.26
		878.1957	0.4423	CoA 7:1	C28H46N7O17P3S					
		878.1593	0.4787	CoA 6:2;O	C27H42N7O18P3S					
17	879.65	879.6321	0.0179	PI O-38:1	C47H91O12P					
		879.611	0.039	PG 44:6	C50H87O10P					
		879.5957	0.0543	PI 37:1	C46H87O13P					
		879.5769	0.0731	TG 53:15;O2	C56H78O8					
		879.7436	0.0936	TG 54:6	C57H98O6		NH4+	20.92	896.76385	6.35
		879.5018	0.1482	PI 38:8	C47H75O13P					
		880.1385	0.4885	CoA 5:2;O2	C26H40N7O19P3S					
18	880.662	880.679	0.017	PC 43:4	C51H94NO8P					
		880.6178	0.0442	SHexCer 40:1;O3	C46H89NO12S					
		880.7154	0.0534	PC O-44:4	C52H98NO7P					
		880.5123	0.1497	PS 44:12	C50H74NO10P					
		880.2113	0.4507	CoA 7:0	C28H48N7O17P3S					
		880.1749	0.4871	CoA 6:1;O	C27H44N7O18P3S					
19	881.674	881.6477	0.0263	PI O-38:0	C47H93O12P					
		881.6266	0.0474	PG 44:5	C50H89O10P					
		881.6114	0.0626	PI 37:0	C46H89O13P					
		881.5926	0.0814	TG 53:14;O2	C56H80O8					
		881.7593	0.0853	TG 54:5	C57H100O6		NH4+	20.13	898.78156	4.27
		881.5175	0.1565	PI 38:7	C47H77O13P					
		882.1542	0.4802	CoA 5:1;O2	C26H42N7O19P3S					
20	882.686	882.643	0.043	IPC 40:0;O3	C46H92NO12P					
		882.731	0.045	PC O-44:3	C52H100NO7P					
		882.6219	0.0641	PS 43:4	C49H88NO10P					
		882.6007	0.0853	PC 44:10	C52H84NO8P					
		882.1906	0.4954	CoA 6:0;O	C27H46N7O18P3S					
21	901.579	901.5801	0.0011	PI 39:4	C48H85O13P					
		901.6164	0.0374	PI O-40:4	C49H89O12P					
		901.6552	0.0762	TG 54:11;O2	C57H88O8		NH4+	18.3	918.66998	11.72
		901.728	0.149	TG 56:9	C59H96O6		NH4+	18.44	918.74487	9.65
		901.8219	0.2429	TG 55:2	C58H108O6		NH4+	20.88	918.84668	1.71
		901.931	0.352	FA 61:1;O	C61H120O3					
22	902.591	902.6845	0.0935	PS 44:1	C50H96NO10P					
		902.7572	0.1662	PC 44:0	C52H104NO8P					
		902.8899	0.2989	ACer 59:1;O2	C59H115NO4					
23	903.604	903.5957	0.0083	PI 39:3	C48H87O13P					
		903.6321	0.0281	PI O-40:3	C49H91O12P					
		903.5018	0.1022	PI 40:10	C49H75O13P					

MALDI		LIPID MAPS®				LC-MS/MS			
m/z	match mass	delta	name	formula	ion	RT (min)	measured mass	delta (mDa)	
	903.7436	0.1396	TG 56:8	C59H98O6	NH4+	19.07	920.76611	4.09	
	903.8375	0.2335	TG 55:1	C58H110O6	NH4+	21.3	920.85712	6.95	
24	904.616	904.7001	0.0841	PS 44:0	C50H98NO10P				
	905.6114	0.0166	PI 39:2	C48H89O13P					
	905.6477	0.0197	PI 0-40:2	C49H93O12P					
	905.5175	0.1105	PI 40:9	C49H77O13P					
25	905.628	905.7593	0.1313	TG 56:7	C59H100O6	NH4+	19.23	922.78302	2.81
	905.8532	0.2252	TG 55:0	C58H112O6	NH4+	21.52	922.87195	7.75	
	905.8895	0.2615	FA 59:1;O3	C59H116O5					
26	906.64	906.6335	0.0065	SHexCer 42:2;O3	C48H91N012S				
	907.6634	0.0114	PI 0-40:1	C49H95O12P					
	907.627	0.025	PI 39:1	C48H91O13P					
27	907.652	907.5331	0.1189	PI 40:8	C49H79O13P				
	907.7749	0.1229	TG 56:6	C59H102O6	NH4+	19.61	924.79584	5.67	
	908.6491	0.0149	SHexCer 42:1;O3	C48H93N012S					
28	908.664	908.2426	0.4214	CoA 9:0	C30H52N7O17P3S				
	908.2062	0.4578	CoA 8:1;O	C29H48N7O18P3S					
	908.1698	0.4942	CoA 7:2;O2	C28H44N7O19P3S					

M/z intervals associated to UCP1-negative regions by MALDI-MSI (m/z), their matches to the LIPID MAPS® structure data base bulk search (mass, delta, name and formula). If applicable the ion, retention time (RT), exact MS1 mass (measured mass) and delta to the matched reference mass are given for lipids that could be identified in the LC-MS/MS data by exact mass measurement and data base hits for their respective MS2 fragmentation.

Table 8: Overview of m/z intervals not discriminative between UCP1-positive and UCP1-negative regions.

MALDI		LIPID MAPS®				LC-MS/MS			
m/z	match mass	delta	Name	Formula	ion	RT (min)	measured mass	delta (mDa)	
1	303.747	303.2682	0.4788	ST 21:1;O	C21H34O				
		303.253	0.494	MG 0-14:1;O	C17H34O4				
		303.253	0.494	FA 17:0;O2	C17H34O4				
2	407.997	408.2744	0.2774	NA 23:5;O4	C23H37NO5				
		408.3472	0.3502	NA 25:3;O2	C25H45NO3				
3	440.048	440.2772	0.2292	LPE 0-15:1;O	C20H42NO7P				
		440.2772	0.2292	LPC 12:0	C20H42NO7P				
		440.2772	0.2292	LPE 15:0	C20H42NO7P				
		440.3135	0.2655	LPE 0-16:0	C21H46NO6P				
		440.3159	0.2679	NA 28:8;O2	C28H41NO3				
		440.337	0.289	CAR 18:2;O	C25H45NO5				
4	441.06	441.2999	0.2399	ST 28:5;O4	C28H40O4				
		441.3363	0.2763	ST 29:4;O3	C29H44O3				
		441.3727	0.3127	FA 30:6	C30H48O2				
		441.3727	0.3127	ST 30:3;O2	C30H48O2				
		441.3938	0.3338	FA 27:1;O2	C27H52O4				
		441.3938	0.3338	FAHFA 27:1;O	C27H52O4				
		441.4091	0.3491	ST 31:2;O	C31H52O				
		441.4302	0.3702	FA 28:0;O	C28H56O3				
		441.4666	0.4066	FOH 29:0;O	C29H60O2				
5	442.072	442.22	0.148	LPS 12:0	C18H36NO9P				
		442.2928	0.2208	LPE 0-15:0;O	C20H44NO7P				
		442.3316	0.2596	NA 28:7;O2	C28H43NO3				
		442.3527	0.2807	CAR 18:1;O	C25H47NO5				
		443.1734	0.0894	ST 21:3;O5;S	C21H30O8S				
6	443.084	443.2041	0.1201	PG 12:0	C18H35O10P				
		443.2404	0.1564	LPG 13:0	C19H39O9P				
		443.2428	0.1588	ST 26:6;O6	C26H34O6				
		443.2792	0.1952	ST 27:5;O5	C27H38O5				
		443.3003	0.2163	WE 24:3;O5	C24H42O7				
		443.352	0.268	ST 29:3;O3	C29H46O3				

	MALDI m/z	LIPID MAPS®				LC-MS/MS			
		match mass	delta	Name	Formula	ion	RT (min)	measured mass	delta (mDa)
		443.3884	0.3044	ST 30:2;O2	C30H50O2				
		443.3884	0.3044	FA 30:5	C30H50O2				
		444.3683	0.2723	CAR 18:0;O	C25H49NO5				
7	467.038	467.2639	0.2259	FA 25:6;O6	C25H38O8				
		467.2639	0.2259	ST 19:1;O2;GlcA	C25H38O8				
		467.2792	0.2412	ST 29:7;O5	C29H38O5				
		467.3132	0.2752	LPA 20:0	C23H47O7P				
		467.319	0.281	ST 27:1;O;S	C27H46O4S				
		467.3367	0.2987	ST 27:1;O6	C27H46O6				
		467.3731	0.3351	ST 28:0;O5	C28H50O5				
		467.4459	0.4079	FA 29:1;O	C30H58O3				
		467.4823	0.4443	WE 31:0	C31H62O2				
		467.4823	0.4443	FA 31:0	C31H62O2				
		467.5186	0.4806	FOH 32:0	C32H66O				
		483.2506	0.3556	LPA 22:6	C25H39O7P				
8	482.895	483.2589	0.3639	ST 19:1;O3;GlcA	C25H38O9				
		483.2717	0.3767	LPG 16:1	C22H43O9P				
		483.3139	0.4189	ST 27:1;O2;S	C27H46O5S				
		482.4568	0.4382	Cer 30:1;O2	C30H59NO3				
9	487.28	487.2819	0.0019	LPA 22:4	C25H43O7P				
		487.2902	0.0102	MGMG 16:3	C25H42O9				
		487.269	0.011	ST 28:6;O7	C28H38O7				
		487.3054	0.0254	ST 29:5;O6	C29H42O6				
10	495.377	495.3445	0.0325	LPA 22:0	C25H51O7P				
		495.3316	0.0454	ST 28:2;O7	C28H46O7				
		495.3105	0.0665	ST 31:7;O5	C31H42O5				
		495.2952	0.0818	ST 27:3;O8	C27H42O8				
		495.2717	0.1053	PA 20:1;O	C23H43O9P				
		495.2717	0.1053	LPG 17:2	C23H43O9P				
		495.5136	0.1366	FA 33:0	C33H66O2				
		495.5136	0.1366	WE 33:0	C33H66O2				
		495.5499	0.1729	FOH 34:0	C34H70O				
11	499.426	499.451	0.025	WE 34:5	C34H58O2				
		499.451	0.025	FA 34:5	C34H58O2				
		499.3394	0.0866	LPG 0-18:0	C24H51O8P				
		499.3054	0.1206	ST 30:6;O6	C30H42O6				
		499.303	0.123	LPG 17:0	C23H47O9P				
		499.2724	0.1536	ST 26:2;O4;S	C26H42O7S				
		499.2667	0.1593	PG 16:0	C22H43O10P				
12	500.101	500.2772	0.1762	LPE 20:5	C25H42NO7P				
		500.2983	0.1973	LPS 0-16:0;O	C22H46NO9P				
		500.304	0.203	ST 24:1;O4;T	C26H45NO6S				
13	502.125	502.2564	0.1314	PC 16:4	C24H40NO8P				
		502.2928	0.1678	LPE 20:4	C25H44NO7P	H+	2.53	502.29153	1.2
14	504.149	504.3085	0.1595	LPE 20:3	C25H46NO7P				
		504.4081	0.2591	NAT 26:0	C28H57NO4S				
		506.3241	0.1501	LPE 20:2	C25H48NO7P				
		506.3241	0.1501	LPC 17:2	C25H48NO7P				
		506.3605	0.1865	LPC 0-18:2	C26H52NO6P				
		506.3605	0.1865	CerP 26:1;O2	C26H52NO6P				
		506.4568	0.2828	Cer 32:3;O2	C32H59NO3				
15	514.271	514.3139	0.0429	LPS 0-17:0;O	C23H48NO9P				
16	515.283	515.3003	0.0173	ST 30:6;O7	C30H42O7				
		515.3037	0.0207	ST 27:1;O4;S	C27H46O7S				
17	522.368	522.3554	0.0126	PC 0-18:1	C26H52NO7P				
		522.3554	0.0126	LPC 18:1	C26H52NO7P	H+	3.4	552.35437	1.04
		522.4517	0.0837	Cer 32:3;O3	C32H59NO4				
		522.2826	0.0854	LPS 18:2	C24H44NO9P				
		522.4881	0.1201	Cer 33:2;O2	C33H63NO3				
		522.5244	0.1564	Cer 34:1;O	C34H67NO2				
18	525.404	525.4513	0.0473	DG 29:1	C32H60O5	Na+	30.69	447.41901	14.28

MALDI	m/z	LIPID MAPS®				LC-MS/MS			
		match mass	delta	Name	Formula	ion	RT (min)	measured mass	delta (mDa)
		525.3551	0.0489	LPG O-20:1	C26H53O8P				
		525.4666	0.0626	WE 36:6	C36H60O2				
		525.4666	0.0626	FA 36:6	C36H60O2				
		525.4877	0.0837	FAHFA 33:1;O	C33H64O4				
		525.3187	0.0853	LPG 19:1	C25H49O9P				
		525.5241	0.1201	FA 34:0;O	C34H68O3				
		525.2823	0.1217	PA 21:1;O2	C24H45O10P				
19	526.079	526.2928	0.2138	LPE 22:6	C27H44N07P				
		526.3139	0.2349	LPS 18:0	C24H48N09P				
		526.3139	0.2349	LPS O-18:1;O	C24H48N09P				
		526.3867	0.3077	LPE O-21:0;O	C26H56N07P				
		526.483	0.404	Cer 32:1;O3	C32H63N04				
		526.5194	0.4404	Cer 33:0;O2	C33H67N03				
20	534.176	534.2826	0.1066	LPE 20:4;O2	C25H44N09P				
		534.3554	0.1794	LPE 22:2	C27H52N07P				
		534.3554	0.1794	LPC 19:2	C27H52N07P				
		534.4881	0.3121	Cer 34:3;O2	C34H63N03				
21	544.297	544.267	0.03	LPS 20:5	C26H42N09P				
		544.3398	0.0428	LPC 20:4	C28H50N07P	H+	2.44	544.3344	5.37
22	562.178	562.4231	0.2451	CerP 30:1;O2	C30H60N06P				
		562.5194	0.3414	Cer 36:3;O2	C36H67N03				
23	564.202	564.3296	0.1276	PE 22:2;O	C27H50N09P				
		564.366	0.164	PC 20:1	C28H54N08P				
		564.4024	0.2004	PC O-21:1	C29H58N07P				
		564.4024	0.2004	LPE 24:1	C29H58N07P				
		564.535	0.333	Cer 36:2;O2	C36H69N03	H+	14.66	564.53223	2.74
24	623.918	623.5762	0.3419	CE 16:1	C43H74O2	NH4+	19.89	640.6145	11.78
		623.5609	0.3571	DG 36:1	C39H74O5	NH4+	16.99	640.586	1.52
		624.3143	0.3963	PS 22:2;O2	C28H50N012P				
		623.5034	0.4146	DG O-38:8	C41H66O4				
		623.4881	0.4299	FOH 37:5;O6	C37H66O7				
		624.3507	0.4327	PE 24:2;O3	C29H54N011P				
		624.3871	0.4691	PS 24:0	C30H58N010P				
		624.3871	0.4691	PE 25:1;O2	C30H58N010P				
25	625.942	625.5918	0.3502	CE 16:0	C43H76O2				
		625.5765	0.3655	DG 36:0	C39H76O5	Na+	19.23	647.54938	9.09
		625.4826	0.4594	DG 37:7	C40H64O5	Na+	15.63	647.46136	3.24
		626.4391	0.4971	LPS O-25:0;O	C31H64N09P				
26	634.039	634.3351	0.2961	PE 25:4;O3	C30H52N011P				
		634.3715	0.3325	PE 26:3;O2	C31H56N010P				
		634.3715	0.3325	PC 23:3;O2	C31H56N010P				
		634.4078	0.3688	PE 27:2;O	C32H60N09P				
		634.4442	0.4052	PE 28:1	C33H64N08P				
		634.4806	0.4416	CerP 34:1;O3	C34H68N07P				
		634.4806	0.4416	PE O-29:1	C34H68N07P				
		634.4806	0.4416	LPE O-29:2;O	C34H68N07P				
		633.5452	0.4938	DG 37:3	C40H72O5				
27	647.197	647.3919	0.1949	PA 30:3;O2	C33H59O10P				
		647.4646	0.2676	PA 32:1	C35H67O8P				
		647.4759	0.2789	EPC 32:2;O3	C34H67N2O7P				
		647.501	0.304	PA O-33:1	C36H71O7P				
		647.5122	0.3152	EPC 33:1;O2	C35H71N2O6P				
		647.5122	0.3152	SM 30:1;O2	C35H71N2O6P				
		647.5609	0.3639	DG 38:3	C41H74O5	NH4+	16.23	664.58398	3.54
		647.5762	0.3792	CE 18:3	C45H74O2				
28	651.246	651.3504	0.1044	PG 25:3;O2	C31H55O12P				
		651.4232	0.1772	PG 27:1	C33H63O10P				
		651.4595	0.2135	PG O-28:1	C34H67O9P				
		651.4983	0.2523	DG 39:8	C42H66O5				
		651.5072	0.2612	EPC 32:0;O3	C34H71N2O7P				
		651.5347	0.2887	DG O-40:8	C43H70O4				

MALDI	m/z	LIPID MAPS®				LC-MS/MS			
		match mass	delta	Name	Formula	ion	RT (min)	measured mass	delta (mDa)
		651.5922	0.3462	DG 38:1	C41H78O5				
		651.6075	0.3615	CE 18:1	C45H78O2	NH4+	17.78	668.63171	2.26
		651.6286	0.3826	WD 42:1;O2	C42H82O4				
		651.665	0.419	FA 43:0;O	C43H86O3				
29	654.282	654.3249	0.0429	PS 23:2;O3	C29H52N013P				
		654.6031	0.3211	Cer 40:1;O4	C40H79N05				
		654.6395	0.3575	Cer 41:0;O3	C41H83N04				
30	703.876	703.6388	0.2373	CE 22:3	C49H82O2				
		703.6235	0.2525	DG 42:3	C45H82O5				
		703.5748	0.3012	EPC 37:1;O2	C39H79N2O6P				
		703.5748	0.3012	SM 34:1;O2	C39H79N2O6P	H+	13.53	703.57416	0.73
		703.5636	0.3124	PA 0-37:1	C40H79O7P				
		703.5385	0.3375	EPC 36:2;O3	C38H75N2O7P				
		703.5355	0.3405	MGDG 30:0	C39H74O10				
		703.5272	0.3488	PA 36:1	C39H75O8P				
31	704.889	704.4545	0.4215	PG 31:3	C37H67O10P				
		704.6915	0.1975	Cer 46:2;O2	C46H89N03				
		704.5589	0.3301	PE 0-34:1	C39H78N07P				
		704.5589	0.3301	PC 0-31:1	C39H78N07P				
		704.5225	0.3665	PE 33:1	C38H74N08P	H+	14.53	704.53235	9.83
		704.5225	0.3665	PC 30:1	C38H74N08P	Na+	12.09	726.50067	3.72
		704.4861	0.4029	PS 0-31:2	C37H70N09P				
		704.4497	0.4393	PS 30:2	C36H66N010P				
32	729.18	704.4497	0.4393	PC 28:3;O2	C36H66N010P				
		704.4133	0.4757	PE 30:4;O3	C35H62N011P				
		729.3457	0.1657	PI 23:2;O3	C32H57O16P				
		729.4701	0.2901	PG 33:4	C39H69O10P				
		729.5065	0.3265	PG 0-34:4	C40H73O9P				
		729.5429	0.3629	PA 38:2	C41H77O8P				
		729.5511	0.3711	MGDG 32:1	C41H76O10				
		729.5541	0.3741	EPC 38:3;O3	C40H77N2O7P				
		729.5793	0.3993	PA 0-39:2	C42H81O7P				
		729.5905	0.4105	SM 36:2;O2	C41H81N2O6P	H+	13.78	729.58661	3.91
33	749.422	729.5905	0.4105	EPC 39:2;O2	C41H81N2O6P				
		729.6028	0.4228	TG 43:4	C46H80O6	NH4+	16.7	746.56885	0.55
		729.6391	0.4591	DG 44:4	C47H84O5				
		749.3719	0.0501	LPIM1 17:0	C32H61O17P				
		749.5116	0.0896	PA 40:6	C43H73O8P				
		749.5327	0.1107	PG 34:1	C40H77O10P				
		749.5327	0.1107	LBPA 34:1	C40H77O10P				
34	750.434	749.5691	0.1471	PG 0-35:1	C41H81O9P				
		749.6654	0.2434	TG 44:1	C47H88O6	NH4+	18.96	766.68427	7.62
		750.4188	0.0152	PS 30:3;O3	C36H64N013P				
		750.5068	0.0728	PC 34:6	C42H72N08P				
		750.5068	0.0728	PE 37:6	C42H72N08P				
		750.528	0.094	PS 33:0	C39H76N010P				
		750.5432	0.1092	PE 0-38:6	C43H76N07P				
		750.5643	0.1303	PS 0-34:0	C40H80N09P				
35	751.447	750.7334	0.2994	Cer 48:1;O3	C48H95N04				
		750.7698	0.3358	Cer 49:0;O2	C49H99N03				
		751.4392	0.0078	PI 28:2	C37H67O13P				
		751.5272	0.0802	PA 40:5	C43H75O8P				
		751.3664	0.0806	PI 26:4;O2	C35H59O15P				
		751.5484	0.1014	PG 34:0	C40H79O10P				
36	752.459	751.5847	0.1377	PG 0-35:0	C41H83O9P				
		751.681	0.234	TG 44:0	C47H90O6	NH4+	19.43	768.69922	8.36
		752.4497	0.0093	PS 34:6	C40H66N010P				
		752.5072	0.0482	IPC 32:1;O2	C38H74N011P				
		752.5225	0.0635	PC 34:5	C42H74N08P				
		752.5225	0.0635	PE 37:5	C42H74N08P	H+	13.08	752.51648	6.04
		752.5589	0.0999	PE 0-38:5	C43H78N07P				

	MALDI	LIPID MAPS®				LC-MS/MS			
	m/z	match mass	delta	Name	Formula	ion	RT (min)	measured mass	delta (mDa)
		752.6035	0.1445	HexCer 38:3;O2	C44H81N08				
		752.7126	0.2536	Cer 47:1;O4	C47H93N05				
		752.749	0.29	Cer 48:0;O3	C48H97N04				
37	774.388	774.5068	0.1188	PC 36:8	C44H72N08P	Na+	15.13	796.505	16.23
		774.5068	0.1188	PE 39:8	C44H72N08P				
		774.528	0.14	PS 35:2	C41H76N010P				
		774.5432	0.1552	PE O-40:8	C45H76N07P				
		774.5643	0.1763	PS O-36:2	C42H80N09P				
		774.5796	0.1916	PC dO-38:8	C46H80N06P				
		774.5878	0.1998	DGCC 36:5	C46H79N08				
		774.6007	0.2127	PE 38:1	C43H84N08P				
		774.6007	0.2127	PC 35:1	C43H84N08P	H+	15.26	774.60187	1.16
		774.609	0.221	HexCer 37:1;O4	C43H83N010				
		774.6371	0.2491	PE O-39:1	C44H88N07P				
774.6371	0.2491	PC O-36:1	C44H88N07P						
774.6454	0.2574	HexCer 38:0;O3	C44H87N09						
38	775.400	775.3876	0.0124	LPIM1 19:1	C34H63O17P				
		775.4392	0.0392	PI 30:4	C39H67O13P				
		775.4627	0.0627	MGDG 34:8;O2	C43H66O12				
		775.4908	0.0908	PG O-38:9	C44H71O9P				
		775.5272	0.1272	PA 42:7	C45H75O8P				
		775.5355	0.1355	MGDG 36:6	C45H74O10				
		775.5484	0.1484	PG 36:2	C42H79O10P	NH4+	13.73	792.5838	8.91
		775.5484	0.1484	LBPA 36:2	C42H79O10P				
		775.5847	0.1847	PG O-37:2	C43H83O9P				
		775.6211	0.2211	PA 41:0	C44H87O8P				
		775.6575	0.2575	PA O-42:0	C45H91O7P				
775.6687	0.2687	SM 39:0;O2	C44H91N2O6P						
		775.681	0.281	TG 46:2	C49H90O6	NH4+	18.94	792.70148	6.1
39	786.534	786.528	0.006	PS 36:3	C42H76N010P				
		786.5432	0.0092	PC O-38:9	C46H76N07P				
		786.5068	0.0272	PE 40:9	C45H72N08P				
		786.5643	0.0303	PS O-37:3	C43H80N09P				
		786.6007	0.0667	PE 39:2	C44H84N08P				
		786.6007	0.0667	PC 36:2	C44H84N08P	H+	14.86	786.59955	1.16
		786.6371	0.1031	PC O-37:2	C45H88N07P				
		786.6371	0.1031	PE O-40:2	C45H88N07P				
		786.6454	0.1114	HexCer 39:1;O3	C45H87N09				
786.6817	0.1477	HexCer 40:0;O2	C46H91N08						
40	792.269	792.481	0.212	PS 37:7	C43H70N010P				
		792.5174	0.2484	PS O-38:7	C44H74N09P				
		792.5538	0.2848	PE 40:6	C45H78N08P	H+	14.43	792.55573	1.96
		792.5538	0.2848	PC 37:6	C45H78N08P				
		792.5538	0.2848	PE O-40:7;O	C45H78N08P				
		792.5749	0.3059	PS 36:0	C42H82N010P				
		792.5902	0.3212	PC O-38:6	C46H82N07P				
		792.6113	0.3423	PS O-37:0	C43H86N09P				
		792.6841	0.4151	PE dO-40:0	C45H94N07P				
41	794.293	794.4967	0.2037	PS 37:6	C43H72N010P				
		794.533	0.24	PS O-38:6	C44H76N09P				
		794.5694	0.2764	PE 40:5	C45H80N08P	H+	15.13	794.56653	2.87
		794.5694	0.2764	PC 37:5	C45H80N08P	Na+	14.14	816.54889	2.5
		794.6058	0.3128	PC O-38:5	C46H84N07P	H+	14.17	794.60223	3.54
794.7596	0.4666	Cer 50:1;O4	C50H99N05						
42	796.318	796.5123	0.1943	PS 37:5	C43H74N010P				
		796.5239	0.2059	SHexCer 34:1;O3	C40H77N012S				
		796.5487	0.2307	PS O-38:5	C44H78N09P				
		796.5851	0.2671	PE 40:4	C45H82N08P				
		796.5851	0.2671	PC 37:4	C45H82N08P				
		796.6215	0.3035	PC O-38:4	C46H86N07P				
		796.6661	0.3481	HexCer 41:2;O2	C47H89N08				

	MALDI	LIPID MAPS®				LC-MS/MS			
	m/z	match mass	delta	Name	Formula	ion	RT (min)	measured mass	delta (mDa)
43	797.33	796.7752	0.4572	Cer 50:0;04	C50H101N05				
		797.4083	0.0783	PI 28:3;03	C37H65O16P				
		797.5116	0.1816	PA 44:10	C47H73O8P				
		797.5175	0.1875	PI 31:0	C40H77O13P				
		797.5198	0.1898	MGDG 38:9	C47H72O10				
		797.5198	0.1898	FA 47:11;08	C47H72O10				
		797.5327	0.2027	PG 38:5	C44H77O10P				
		797.5538	0.2238	PI O-32:0	C41H81O12P				
		797.5562	0.2262	FA 48:10;07	C48H76O9				
		797.6654	0.3354	TG 48:5	C51H88O6				
44	798.342	798.528	0.186	PS 37:4	C43H76N010P				
		798.5491	0.2071	IPC 34:0;03	C40H80N012P				
		798.5643	0.2223	PS O-38:4	C44H80N09P				
		798.5643	0.2223	PC 36:4;0	C44H80N09P				
		798.6007	0.2587	PC 37:3	C45H84N08P				
		798.6007	0.2587	PE 40:3	C45H84N08P	H+	15.73	796.58105	4.03
		798.6371	0.2951	PC O-38:3	C46H88N07P				
		798.6454	0.3034	HexCer 40:2;03	C46H87N09				
		798.6817	0.3397	HexCer 41:1;02	C47H91N08	H-H2O	17.17	780.6665	4.7
45	802.391	802.4654	0.0744	PS 38:9	C44H68N010P				
		802.5381	0.1471	PC 38:8	C46H76N08P	H+	15.89	802.55225	14.16
		802.5593	0.1683	PS 37:2	C43H80N010P				
		802.5956	0.2046	PS O-38:2	C44H84N09P				
		802.6109	0.2199	PC dO-40:8	C48H84N06P				
		802.632	0.241	PE 40:1	C45H88N08P				
		802.632	0.241	PC 37:1	C45H88N08P	H+	15.85	802.62744	4.58
		802.6684	0.2774	PC O-38:1	C46H92N07P	H+	15.83	802.65314	15.26
		802.6684	0.2774	PE O-41:1	C46H92N07P				
46	803.403	803.4705	0.0675	PI 32:4	C41H71O13P				
		803.494	0.091	MGDG 36:8;02	C45H70O12				
		803.5221	0.1191	PG dO-40:10;1	C46H75O9P				
		803.5585	0.1555	PA 44:7	C47H79O8P				
		803.5797	0.1767	PG 38:2	C44H83O10P				
		803.616	0.213	PG O-39:2	C45H87O9P				
		803.6524	0.2494	PA 43:0	C46H91O8P				
		803.7	0.297	SM 41:0;02	C46H95N2O6P				
		803.7123	0.3093	TG 48:2	C51H94O6	NH4+	19.47	830.73541	3.48
47	818.247	818.4967	0.2497	PS 39:8	C45H72N010P				
		818.5694	0.3224	PC 39:7	C47H80N08P	Na+	9.79	840.57007	18.68
		818.5694	0.3224	PE 42:7	C47H80N08P	H+	14.36	818.56311	6.29
		818.5906	0.3436	PS 38:1	C44H84N010P	H+	11.19	840.57062	1.89
		818.6058	0.3588	PC O-40:7	C48H84N07P	H+	13.71	818.5929	12.87
		818.6269	0.3799	PS O-39:1	C45H88N09P				
		817.8371	0.4099	FA 55:1;0	C55H108O3				
		818.6633	0.4163	PE 41:0	C46H92N08P				
		818.6633	0.4163	PC 38:0	C46H92N08P				
		818.6633	0.4163	PE-NMe 40:0	C46H92N08P				
		818.6716	0.4246	HexCer 40:0;04	C46H91N010				
		818.6997	0.4527	PE O-42:0	C47H96N07P				
		818.6997	0.4527	PC O-39:0	C47H96N07P	H+	15.83	818.69971	3.3
		818.7361	0.4891	PC dO-40:0	C48H100N06P				
48	820.271	820.5123	0.2413	PS 39:7	C45H74N010P				
		820.5487	0.2777	PS O-40:7	C46H78N09P				
		820.5851	0.3141	PC 39:6	C47H82N08P				
		820.5851	0.3141	PE 42:6	C47H82N08P	H+	15.34	820.57391	11.17
		820.6062	0.3352	PS 38:0	C44H86N010P				
		820.6215	0.3505	PC O-40:6	C48H86N07P	H+	14.08	820.61121	10.31
		820.6426	0.3716	PS O-39:0	C45H90N09P				
49	821.284	821.5175	0.2335	PI 33:2	C42H77O13P				
		821.5327	0.2487	PG 40:7	C46H77O10P				
		821.5538	0.2698	PI O-34:2	C43H81O12P				

MALDI		LIPID MAPS®				LC-MS/MS			
m/z	match mass	delta	Name	Formula	ion	RT (min)	measured mass	delta (mDa)	
	821.6266	0.3426	PG 39:0	C45H89O10P					
	821.663	0.379	PG O-40:0	C46H93O9P					
	821.6654	0.3814	TG 50:7	C53H88O6	NH4+	17.44	838.69379	1.9	
	820.8116	0.4724	Cer 53:1;O3	C53H105NO4					
	821.7593	0.4753	TG 49:0	C52H100O6	NH4+	20.6	838.78217	3.66	
50	822.633	822.6371	0.0041	PC O-40:5	C48H88N07P				
		822.6007	0.0323	PC 39:5	C47H84N08P				
		822.6007	0.0323	PE 42:5	C47H84N08P				
		822.5643	0.0687	PS O-40:6	C46H80N09P				
		822.528	0.105	PS 39:6	C45H76N010P				
		822.7909	0.1579	Cer 52:1;O4	C52H103NO5				
		822.1331	0.4999	CoA 3:1	C24H38N7O17P3S				
51	828.369	828.481	0.112	PS 40:10	C46H70N010P				
		828.5385	0.1695	PC 36:5;O3	C44H78N011P				
		828.5538	0.1848	PC 40:9	C48H78N08P	H+	11.06	828.54846	5.31
		828.5749	0.2059	PS 39:3	C45H82N010P				
		828.6113	0.2423	PS O-40:3	C46H86N09P				
		828.6477	0.2787	PC 39:2	C47H90N08P				
		828.6477	0.2787	PE 42:2	C47H90N08P				
		828.6841	0.3151	PC O-40:2	C48H94N07P				
828.6923	0.3233	HexCer 42:1;O3	C48H93NO9	H-H2O	17.4	810.67603	5.67		
52	829.381	829.4862	0.1052	PI 34:5	C43H73O13P				
		829.499	0.118	PGP 34:1	C40H78O13P2				
		829.5097	0.1287	FA 47:11;O10	C47H72O12				
		829.5953	0.2143	PG 40:3	C46H85O10P				
		829.7157	0.3347	SM 43:1;O2	C48H97N2O6P	H+	17.82	829.70935	6.35
		829.728	0.347	TG 50:3	C53H96O6	NH4+	18.9	846.7442	10.32
53	830.393	830.4967	0.1037	PS 40:9	C46H72N010P				
		830.5542	0.1612	PC 36:4;O3	C44H80N011P				
		830.5694	0.1764	PC 40:8	C48H80N08P	Na+	11.95	852.55157	0.18
		830.5906	0.1976	PS 39:2	C45H84N010P				
		830.6269	0.2339	PS O-40:2	C46H88N09P				
		830.6633	0.2703	PE 42:1	C47H92N08P				
		830.6633	0.2703	PC 39:1	C47H92N08P				
		830.6997	0.3067	PC O-40:1	C48H96N07P				
54	845.237	845.5175	0.2805	PI 35:4	C44H77O13P				
		845.5327	0.2957	PG 42:9	C48H77O10P				
		845.5538	0.3168	PI O-36:4	C45H81O12P				
		845.6266	0.3896	PG 41:2	C47H89O10P				
		845.663	0.426	PG O-42:2	C48H93O9P				
		845.6654	0.4284	TG 52:9	C55H88O6	Na+	17.4	867.62848	18.8
55	846.25	846.6007	0.3507	PC 41:7	C49H84N08P				
		846.6007	0.3507	PE 44:7	C49H84N08P				
		846.6219	0.3719	PS 40:1	C46H88N010P	H+	16.49	846.61298	8.91
		845.8684	0.3816	FA 57:1;O	C57H112O3				
		846.6371	0.3871	PC O-42:7	C50H88N07P				
		846.6582	0.4082	PS O-41:1	C47H92N09P				
		846.6946	0.4446	PE 43:0	C48H96N08P				
		846.6946	0.4446	PC 40:0	C48H96N08P				
		846.731	0.481	PC O-41:0	C49H100N07P				
		845.7593	0.4907	TG 51:2	C54H100O6	NH4+	20.15	862.78339	2.44
56	862.106	861.7906	0.3154	TG 52:1	C55H104O6	NH4+	20.81	878.81641	0.67
		861.6967	0.4093	TG 53:8	C56H92O6	NH4+	18.63	894.72723	9.15
		861.6579	0.4481	PG 42:1	C48H93O10P				
		862.5593	0.4533	PS 42:7	C48H80N010P				
57	863.118	862.6895	0.4285	PS O-42:0	C48H96N09P				
		863.5644	0.4464	PI 36:2	C45H83O13P	NH4+	13.61	880.58563	5.37
		862.6532	0.4648	PS 41:0	C47H92N010P				
		863.6008	0.4828	PI O-37:2	C46H87O12P				
		862.632	0.486	PC 42:6	C50H88N08P				
		862.625	0.493	Hex2Cer 34:1;O2	C46H87N013				

	MALDI	LIPID MAPS®				LC-MS/MS			
	m/z	match mass	delta	Name	Formula	ion	RT (min)	measured mass	delta (mDa)
58	914.062	914.1593	0.0973	CoA 9:5;0	C30H42N7O18P3S				
		913.8219	0.2401	TG 56:3	C59H108O6	NH4+	18.32	930.83075	17.64
		913.728	0.334	TG 57:10	C60H96O6	Na+	20.03	935.71002	0.12
		913.5801	0.4819	PI 40:5	C49H85O13P				
59	955.222	955.5331	0.3111	PI 44:12	C53H79O13P				
		954.7885	0.4335	PC 48:2	C56H108N08P				
60	444.096	No HIT							
61	506.174	No HIT							
62	913.05	No HIT							
63	915.074	No HIT							

M/z intervals not discriminative between UCP1-positive and UCP1-negative regions by MALDI-MSI (m/z), their matches to the LIPID MAPS® structure data base bulk search (mass, delta, name and formula). If applicable the ion, retention time (RT), exact MS1 mass (measured mass) and delta to the matched reference mass are given for lipids that could be identified in the LC-MS/MS data by exact mass measurement and data base hits for their respective MS2 fragmentation.

6.5.3 Validation of annotated lipid species by high resolution LC-MS/MS

To limit the possible lipids per *m/z* interval we validated the presence of the lipids in our LC-MS/MS dataset generated on the second and third consecutive section of each MALDI sample. Candidates were validated by searching for their LMSD annotated metabolite name in the LC-MS/MS dataset, considering their exact mass and their respective MS2 fragmentation pattern (Figure 34 G&H). For example, CL demonstrates a characteristic fragmentation pattern where the diacylglycerol group is cleaved of the phosphatic backbone which can be used for the annotation of the correct carbon and double bond number of the diacyl side chains indicating that CL 68:3 consists of a C34:1 and a C34:2 diacyl chain (Figure 34 I). The general fragmentation pattern of CL was confirmed by analysis of a commercially available CL standard (CL 56:0) (Figure 34 J & K). Based on this approach we could confirm the presence of 8 of the annotated lipid species for the UCP1-positive and 22 for the UCP1-negative region, respectively (Table 6, Table 7). Concerning the UCP1-negative region these were primarily TG, as well as diacylglycerophosphocholines (PC) and DG. The UCP1-positive regions were exclusively represented by DG and the two cardiolipins CL 68:3 and CL 68:3. This pattern supports our approach as TG are the main storage lipid, while CL are associated with thermogenic function in iWAT (Lynes et al. 2018) and like UCP1 constitutes a mitochondrial marker, almost exclusively present in mitochondrial membranes. In summary, the combined MALDI-MSI, IHC, LC-MS/MS approach allowed us to identify region-specific lipids linked to thermogenesis in form of UCP1 expressing brite adipocytes.

6.5.4 CL 68:3 and CL 68:4 are upregulated by cold independent of UCP1

We identified the cardiolipin species CL 68:3 and CL 68:4 to be associated with UCP1 expression in iWAT of cold acclimatized 129S6/SvEvTac mice. Since lack of CL in adipose tissue leads to attenuated expression of UCP1 (Sustarsic et al. 2018), we asked if vice versa lack of UCP1 expression would affect CL metabolism. Therefore, we housed UCP1-WT and UCP1-KO mice at 23°C or acclimatized mice to 5°C (Figure 35 A). Subsequently we investigated the presence and

distribution both CL 68:3 and CL 68:4 applying our MALDI-MSI protocol. The UCP1-IHC staining revealed the expected increase in UCP1 expression upon cold stimulation in UCP1-WT mice while no UCP1 could be detected in UCP1-KO mice in both conditions (Figure 35 B, additional mouse examples Supplementary Figure 12 & Supplementary Figure 13). Analysis of the MALDI images for CL 68:4 (m/z 1401,805 \pm 0.338 Da) and CL 68:3 (m/z 1403,834 \pm 0.338 Da) confirmed the high similarity with the expression pattern of UCP1 in wildtype animals (Figure 35 C & D, additional mouse examples Supplementary Figure 12 & Supplementary Figure 13). The relative intensities of both CL species were increased in cold acclimatized compared to RT acclimatized animals (Figure 35 C & D, additional mouse examples Supplementary Figure 12 & Supplementary Figure 13). Interestingly, both CL species were also increased in cold acclimatized UCP1-KO animals. Their intensities tended to be even higher than in cold acclimatized UCP1-WT mice. The MALDI images revealed that even in UCP1 ablated mice the increased abundance of CLs was not ubiquitous but demonstrated a spatial pattern similar to that of UCP1-WT mice.

Conclusively, we could demonstrate that the cardiolipins CL 68:3 and CL 68:4 are upregulated by cold exposure in iWAT of mice, independently of UCP1.

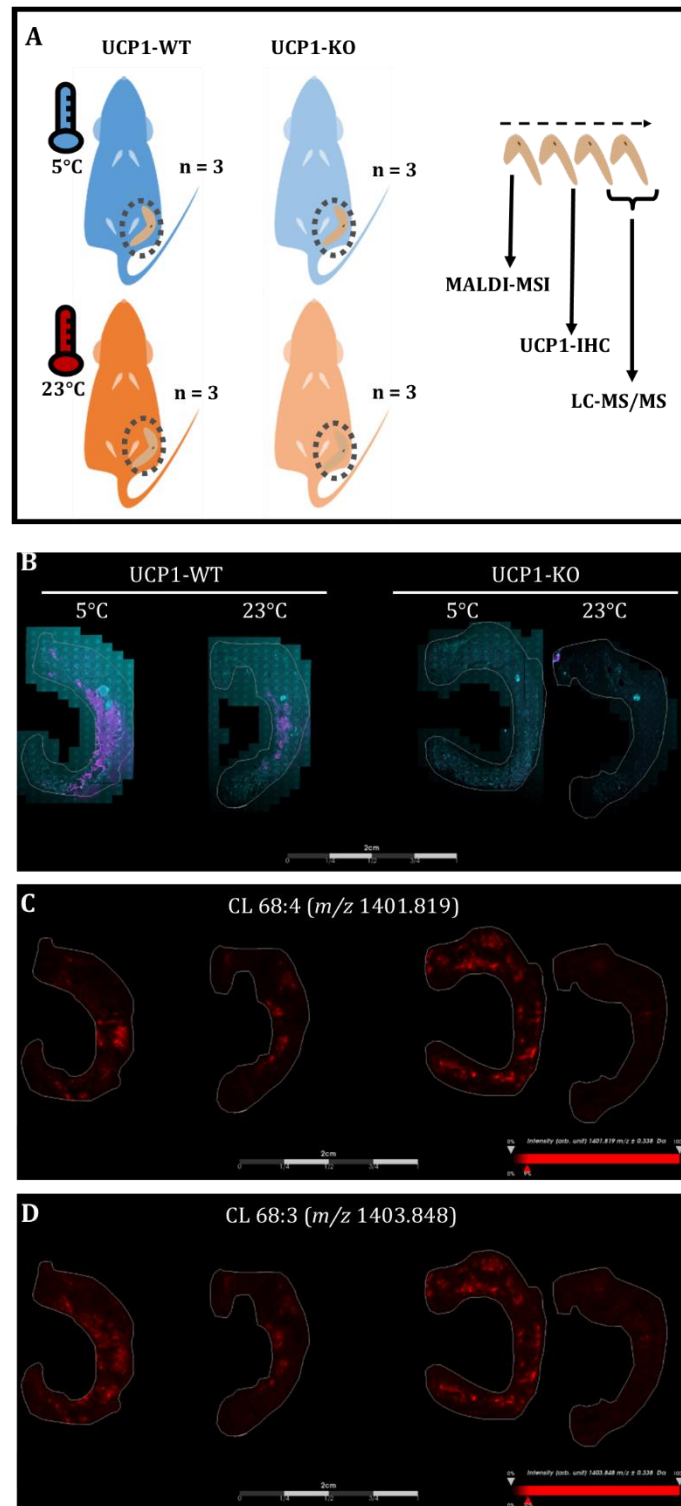


Figure 35: CL 68:4 and CL 68:3 abundance is associated to cold, independent of UCP1.

(A) Overview of the experimental setup. UCP1 knockout (UCP1-KO) and UCP1 wildtype (UCP1-WT) mice were either housed at 23°C or acclimatized to 5°C. Inguinal white adipose tissue was dissected (grey dashed circle). Four consecutive sections were prepared, the first used for MALDI-MSI, the second for immunohistochemistry staining of UCP1 and the last two for LC-MS/MS analysis. **(B)** Immunohistochemistry staining against UCP1 (magenta) and a Hoechst nuclear stain (cyan) of UCP1-WT and UCP1-KO mice. **(C-D)** MALDI images of **(C)** m/z 1401.819 \pm 0.338 Da representing CL 68:4 and **(D)** m/z 1403.848 \pm 0.338 Da representing CL 68:3.

6.6 DISCUSSION

Aim of this study was to characterize the lipid composition of WAT on a region-specific level in an *in vivo* context. Inguinal WAT is a highly heterogeneous tissue (Barreau et al. 2016) a factor that is so far unaddressed by most lipidomic studies using whole tissue homogenates (Sustarsic et al. 2018; Lynes et al. 2018) or *in vitro* differentiated pre-adipocytes (Schweizer et al. 2019). We made use of the MALDI-MSI technology, enabling the local acquisition of mass spectra on tissue sections to address this shortcoming. The feasibility of MALDI-MSI to investigate adipose tissue metabolism has recently been demonstrated on WAT of rats (Fernández-Vega et al. 2020). We demonstrate that the lipid composition of iWAT is highly regional resembling the heterogeneous spatial distribution of white and brite adipocytes and UCP1 expression in the tissue (Barreau et al. 2016). Combining MALDI-MSI with IHC and high-resolution LC-MS/MS, we could demonstrate that the lipid species CL 68:3 and CL 68:4 highly correlate with the expression of UCP1 in cold acclimatized 129S6/SvEvTac mice. However, investigation of UCP1-WT and UCP1-KO mice housed at 23°C or acclimatized to cold demonstrated that the cold induced upregulation of CL in iWAT is independent of UCP1.

We detected several *m/z* intervals with overall highly similar regional distribution in different measurement runs and biological replicates, demonstrating the reliability of our MALDI-MSI approach. In line with the fat storing function of adipose tissue, the main verified lipid species were DG and TG. As such, we identified TG 44:1 (*m/z* 749.422) as a lipid species not specific to UCP1-positive or UCP1-negative regions but rather ubiquitously distributed. Additionally, *m/z* 774.388 showed a highly regional localization and was associated to the lymph node. This mass could be mapped to two potential glycerophospholipids (PC 36:8, PS 35:2) based on our LC-MS/MS data. Further we demonstrate that TG are associated to UCP1-negative regions while DG are associated to regions with detectable UCP1 expression. This might reflect differences in metabolic activity and function with “inert” UCP1-negative storage regions being rich in TG while increased DG content might be caused by high lipolytic activity of UCP1 expressing adipocytes as UCP1 dependent thermogenesis is activated and fueled by free fatty acids derived from lipolysis (Cannon and Nedergaard 2004). Additionally, our findings are in line with a study of *in vitro* differentiated adipocytes reporting two DG associated to UCP1 in our study (DG 32:0 & DG 32:1) to be more abundant in white compared to brite adipocytes (Schweizer et al. 2019).

The upregulation of CL in cold acclimatized mice and its association to thermogenesis is well established (Sustarsic et al. 2018; Lynes et al. 2018; Schweizer et al. 2019; He et al. 2019). Further CL are bound to UCP1 and are important for its stability in the mitochondrial membrane, facilitating its function (Hoang, Smith, and Jelokhani-Niaraki 2013; Y. Lee et al. 2015). Thus, it is plausible that we detected CL 68:3 and CL 68:4 to be closely associated with UCP1 expression in iWAT of cold acclimatized 129S6/SvEvTac mice. However, applying our combined MALDI-

MSI/UCP1-IHC/LC-MS/MS approach on UCP1-KO and UCP1-WT mice we demonstrate for the first time that the cold induced upregulation of CL is independent of UCP1. Although we did not study other functional/cell specific marker we speculate that CL 68:3 and CL 68:4 are rather associated to multilocular brite adipocytes, that emerge in WAT upon cold or β 3-adrenergic stimulation (Anunciado-Koza et al. 2008; Granneman et al. 2003). These cells have increased mitochondrial content and occur in greater number in UCP 1-KO compared to UCP1-WT mice (Anunciado-Koza et al. 2008; Granneman et al. 2003). Subsequent studies with additional mitochondrial, brite adipocyte or general morphological marker like citrate synthase, Cidea or perilipin are needed to confirm this assumption.

A major limitation of our study is the low resolution of our MALDI-MSI device. In most instances this resulted in the annotation of multiple possible lipid species for a single m/z interval. While we are confident about the annotation of the DG and TG based on their high abundance, this is a major limitation for low abundant or regionally very restricted lipids. These might be below the detection limit for the LC-MS/MS due to the dilution in the whole section homogenate. Other reasons, for a lack of annotation or detection by LC-MS/MS include that m/z intervals provided by the MALDI-MSI do not necessarily reflect lipid species but peptide fragments. Additionally, a lack of annotated database references might further explain why for some m/z intervals none of the annotated lipid species could be identified in our LC-MS/MS data set. These issues are already addressed by the advancement of MALD-MSI instrumentation with higher resolution, MS2 spectra and ion mobility.

Conclusively, we demonstrate that MALDI-MSI is a powerful tool to investigate the relationship of lipid metabolism and functional characteristics of adipose tissue in an *in vivo* context.

7 GENERAL DISCUSSION

Background and aim

In the last decade BAT has emerged as a promising target to tackle the obesity epidemic due to its energy consuming properties (Tseng, Cypess, and Kahn 2010; Yoneshiro et al. 2013). However, major obstacles persist including the negative association between BAT volume and BMI (van Marken Lichtenbelt et al. 2009) as well as the innate inactivity of UCP1 (Y. Li et al. 2014). Consequently, means to increase BAT volume and activate UCP1 are of high interest.

Aim of the present work was to investigate the association between lipid derived metabolites and the recruitment of brown and brite adipocytes. On the one hand, a focus was placed on the investigation of a specific group of lipid derivatives termed oxylipins (Chapter 3&4). On the other hand, two new tools to investigate the association between UCP1 and lipid derivatives on a broader level were established (Chapter 5&6).

Regulation of UCP1 by oxylipins

Lipids and their derivatives are potent signaling molecules implied in various physiological pathways. In this light, oxylipins as one class of n6- and n3-PUFA derived metabolites are discussed to modulate the activity of brown and brite adipocytes. *In vitro* several oxylipins are suggested to be implemented in the control of brown and brite adipocyte activity (Maurer et al. 2019). However, so far PGI₂ is the only oxylipin that has been demonstrated to induce UCP1 gene expression in murine and human cell cultures (Vegiopoulos et al. 2010; Ghandour et al. 2016). Additionally, evidence *in vivo* about the functional involvement of oxylipins especially in humans is limited. So far only the oxylipins PGE₂ and 12,13-DiHOME are associated to UCP1 or brown fat activity in humans *in vivo*. For example 12,13-DiHOME increases fatty acid uptake into BAT and was identified to be increased in serum of humans exposed to cold (Lynes et al. 2017; Kulterer et al. 2020). Nevertheless, these studies did not address the oxylipin profile in adipose tissues but investigate the lipid profiles in plasma samples. Although it is possible that oxylipins are distributed by systemic circulation they can also be produced by adipocytes or adipose tissue residing cells as has been shown for 9- and 13-HODE (Y. H. Lee et al. 2016) and primarily act in a paracrine manner. In this line, key enzymes producing PGI₂ and PGE₂ like PGHS, prostaglandin E synthase and prostaglandin I synthase as well as several receptors involved in oxylipin signaling are expressed in human adipocytes (Michaud et al. 2014; Barquissau et al. 2017). Thus, oxylipins associated to cold induced BAT activity by plasma analyses not necessarily reflect the situation in BAT but rather a general systemic modulation of lipid metabolism. The data presented in chapter 3 addresses this issue by investigating the oxylipin profiles of human brown and white adipose tissue. The global oxylipin profile was distinguishable between murine BAT and WAT. However, no global changes in oxylipin profile between human WAT and BAT could be identified.

The discrepancies between mouse and human may be explained by the mixed phenotype of brown adipocytes of human supraclavicular fat, that rather resemble murine brite adipocytes (J. Wu et al. 2012; Sharp et al. 2012; Lidell et al. 2013; Shinoda et al. 2015; Naja Zenius Jespersen et al. 2013). This is in line with the lack of discriminating potential of the oxylipin profile between murine brite and white adipose tissue, suggesting that the proportion of interspersed thermogenic cells in white adipose tissue may be too small to detect notable changes in the global oxylipin profile.

Nevertheless, despite investigating a heterogenous cell population, an association between single oxylipins and the presence of brown adipocytes was observed. The oxylipins 5,6-EET and 5-HETE were significantly increased in murine BAT vs. WAT and tended to be increased in human BAT. This substantiates the possible contribution of oxylipins to the recruitment of brown and brite adipocytes but needs complementary research *in vivo* and *in vitro*. Unfortunately, our panel did not include recently described oxylipins like 12,13-DiHOME (Lynes et al. 2017). Consequently, no conclusion about the presence of a potential association of this oxylipin and UCP1 expression in adipose tissues could be made.

As mentioned before, little reproducible evidence about the functional involvement of oxylipins in the recruitment of UCP1 or brite and brown adipocytes is available. This holds true for 5,6-EET and 5-HETE, demonstrating a high variability in their effect on UCP1 expression in *in vitro* differentiated brown and brite adipocytes. One explanation may be the nature of oxylipins as highly unstable metabolites that undergo rapid enzymatic conversion or oxidation. This prompt degradation is important, as oxylipins elicit a remarkable bioactivity and are key regulators in diverse signaling pathways, including inflammatory signals. Appropriate handling and storage of the study material is therefore crucial to avoid oxidation of the compounds (Koch et al. 2020). Nevertheless, oxidation of oxylipins is inevitable once the compounds are supplemented to the cells in aqueous solutions at 37 °C. Thus, to cope with the loss of active metabolites through autoxidation, supraphysiological doses might be used. However, oxidation products of oxylipins like 5-oxo-EET often are bioactive compounds themselves and thus may elicit unpredictable effects on the cells that influence the experimental readout. These issues can be circumvented by the use of stable analogues as has been demonstrated for PGI₂ (Vegiopoulos et al. 2010). However, while these stable analogues are an important component to elucidate functional pathways *in vitro* their physiological significance *in vivo* is questionable. Due to their role in a plethora of signaling pathways, administration of stable oxylipin derivatives will presumably lead to unspecific systemic side effects, thus will have no additional benefit over currently available pharmacological activators of BAT like mirabegron (Cypess et al. 2015). Consequently, injection of stable compounds is not a suitable option to utilize the potential stimulating effects of oxylipins

on UCP1 expression and activity. However, oxylipins as a group of lipid derived metabolites have a key benefit – their abundance can be modulated via nutritional intervention.

Dietary intake of the respective precursor fatty acids of oxylipins and other lipid derivatives increases their abundance in circulation and adipose tissue depots (Balvers et al. 2012; Ostermann and Schebb 2017; Schebb et al. 2014). Furthermore, the dietary n6/n3-PUFA ratio affects health (Simopoulos 2016). In line feeding of diets rich in n6- and n3-PUFA substantially changed the global oxylipin pattern like expected by increasing n6- or n3-PUFA derived oxylipins in murine WAT and BAT, respectively. This substantiates the feasibility of the approach to modulate oxylipin concentration by supplementation of the respective precursor fatty acid. However, no robust effect on the recruitment of brown or brite adipocytes was observed upon n6- and n3-PUFA supplementation. Consequently, supplementation of the corresponding precursor fatty acids may influence the concentration of oxylipins in BAT and WAT. However sole increase in oxylipins may not per se lead to the activation or recruitment of brown and brite adipocytes, respectively. However, the sensitivity towards UCP1 recruiting stimuli may still be increased by dietary modulation of the respective n6- and n3-PUFA derivatives.

Of note, these statements may only apply to the fairly limited number of oxylipins that were detected in the present studies. Improvement of currently available tools and the development of cost-efficient methods will increase the amount of detectable lipid derivatives. Together with the discovery of novel metabolites the knowledge of how these metabolites impact energy balance regulation will be complemented and thus accelerate the development of precise intervention strategies.

MALDI-MSI as novel tool to study the link between lipid derived metabolites and UCP1

Methods to investigate the role of lipid derived metabolites in energy balance regulation are currently largely relying on the analysis of whole tissue homogenates or isolated primary cells. As discussed previously, the small proportion of brite and brown adipocytes in murine brite and human BATs may limit the detection of changes in lipid composition by analyzing whole tissue homogenates. Consequently, less pronounced changes in a single cell type might be too small to be robustly detected or masked by high concentrations of lipids of the predominant cell types. Additionally, once changes in lipid composition are observed in heterogenous cell populations, these cannot be linked to the respective cell type. One option to address this is for example the investigation of isolated primary cells *in vitro* (Schweizer et al. 2019). While this is a compelling method to perform functional assays to elucidate the specific treatment effects on lipid composition, it lacks the *in vivo* context. MALDI-MSI is a feasible complementary tool to identify changes in lipid composition in cell subsets in conjunction with morphological markers like UCP1 in an *in vivo* context. The additional information increases sensitivity as specific regions of interest can be assigned retrospectively based on several structural cues. Like this the relationship

between several lipid derivatives and regions of UCP1 expressing cells could be demonstrated in iWAT of cold acclimatized mice. The method was substantiated by the strong correlation between UCP1 and the cardiolipins CL 68:3 and 68:4. This class of lipids is a well-known mitochondrial membrane lipid, functionally implied in the cold-induced activity of BAT (Sustarsic et al. 2018; Lynes et al. 2018). Of note, both CL species were upregulated in iWAT of cold acclimatized UCP1-KO mice, indicating increased mitochondrial biogenesis independent of UCP1. This is in line with elevated abundance of brite adipose tissue in UCP1-KO compared to wildtype mice (Anunciado-Koza et al. 2008; Granneman et al. 2003) and may indicate the recruitment of alternative thermogenic mitochondrial dependent mechanisms like creatine-dependent substrate cycling (Kazak et al. 2015). Of note, the current MALDI-MSI approach was used as a showcase to demonstrate the general feasibility of the method. The experimental protocol and the low accuracy of the MALDI-MS did not allow the identification of unstable lipid derivatives such as oxylipins. However dedicated experimental protocols and improvements in the accuracy and MALDI-MSI may enable follow up research on even this class of metabolites.

Collectively, the data demonstrates that MALD-MSI is a valuable tool that should be implemented in scientific workflows studying the spatial connection between lipid metabolism and thermogenic adipocytes.

Environmental temperature: a crucial factor studying UCP1-dependent thermogenesis

The observation, that supplementation of n3-PUFA does not lead to the recruitment of brown or brite adipocytes conflicts with several published studies demonstrating a positive effect of n3-PUFA supplementation on adiposity and markers of BAT function e.g. UCP1 (Table 2). There is however one key difference between data presented in this work and these studies – the thermal environment. Almost all studies demonstrating a beneficial effect of n3-PUFA on UCP1 expression of BAT function have been performed at RT thus below the thermoneutral zone of mice. Consequently, results of these studies are biased by a constitutively active BAT initialized by the mild cold exposure leading to a ~1.8 fold increase in energy expenditure (Fischer, Cannon, and Nedergaard 2018). This does not reflect the human thermal environment nor the activity status of UCP1 in BAT, which is inherently inactive (Y. Li et al. 2014) and thus limits the translatability of the obtained results from mouse to human. Besides studying mice at a human-like thermal environment, a major strength of the data on oxylipin profiles and the nutritional intervention studies presented in this project is the inclusion of human data. Like in mice, supplementation of n3-PUFA did not alter UCP1 gene expression in subcutaneous adipose tissue of humans. Consequently, increased abundance of oxylipins or n3-PUFA supplementation does not per se increase the recruitment of brown or brite adipocytes. Nevertheless, this does not exclude a facilitating effect of n3-PUFA and the derived oxylipins in conjunction with other activators like mild cold exposure as suggested by studies in mice housed at RT (Table 2). On the one hand, the

lack of differences between UCP1 expression in murine BAT and WAT of mice treated with the β 3-adrenergic receptor agonist CL-316,243 and control mice are arguing against this. On the other hand, it is possible that the 1-week of chronic CL-316,243 injection may have recruited the maximal capacity of UCP1 and thus masked a positive effect of the n3-PUFA supplementation. Consequently, these observations do show that the dietary n6- or n3-PUFA supplementation does not alter the total capacity to recruit UCP1.

The importance to consider the thermal environment for studying the impact of UCP1 on the development of DIO is substantiated by the presented data on a novel UCP1-KO mouse. Housing these UCP1-KO mice at thermoneutrality did not alter energy balance regulation in terms of energy expenditure or intake compared to wildtype mice. These data corroborate the collective data on the most widely studied UCP1-KO model that the presence of UCP1 alone does not protect against DIO (Enerbäck et al. 1997; Liu et al. 2003; Zietak and Kozak 2016; Winn et al. 2017; Maurer et al. 2020). Consequently, similar to human physiology, UCP1 is inactive at thermoneutral environmental conditions in mice and does not contribute to energy balance. Recently physiological “humanized” mice have been reported by housing middle-aged mice at TNZ on an energy-rich diet (de Jong et al. 2019). Endeavors like this are vital for further research aiming to assess UCP1 or BAT activity in a translational context.

Sole presence of UCP1 is not generating heat

The observation that presence of UCP1 is not sufficient to impact the development of DIO is important in the respect of scientific workflows to assess beneficial effects of brown and brite adipocytes on metabolic health. Most studies focus on the investigation of UCP1 mRNA or protein expression levels as surrogate marker of BAT functionality. Thereby the inactivity of UCP1 is neglected as UCP1 alone does not produce heat (Nedergaard and Cannon 2013). Consequently, sole investigation of UCP1 abundance will not help to understand whether BAT can be utilized to fight the obesity epidemic.

Additional, functional parameters need to be considered in order to characterize the effect of oxylipins or other compounds putatively affecting activity of UCP1. In this respect properly performed respiratory assays *in vitro* on isolated cells (Oeckl et al. 2020) and *in vivo* in form of indirect calorimetry (Virtue and Vidal-Puig 2013) are powerful tools to assess UCP1 activity. Inclusion of UCP1-KO models will in this respect also facilitate the interpretation in light of whether the observed effects rely on the thermogenic activity of brown or brite adipocytes or are mediated by alternative mechanisms. Of note, increased energy expenditure mediated by thermogenic activity of BAT is not the only beneficial effect that BAT can exert on metabolic health (Kajimura, Spiegelman, and Seale 2015). The oxylipin 12,13-DiHOME for example does not directly induce the thermogenic capacity of BAT by recruiting and activating UCP1. Instead, it facilitates the uptake of fatty acids from circulation into BAT thus fuels thermogenesis and BAT

mediated glucose uptake (Lynes et al. 2017). This example clearly demonstrates that extended functional markers besides the assessment of UCP1 expression should be utilized to assess activation of BAT.

Conclusion and outlook

Collectively, the results obtained in frame of this project clearly demonstrate the interactions between lipid derived metabolites and the presence of UCP1. However, considering the thermal environment the role of oxylipins on the recruitment of thermogenic capacity needs to be reconsidered. Studying mice in conditions as closely as possible to the human environment will facilitate the understanding of BAT to fight the obesity epidemic and the improvement of metabolic health. As demonstrated, changes in the abundance of oxylipins did not affect the recruitment or induction of NST capacity at thermoneutrality. However, considering the accumulating evidence of studies demonstrating an effect of oxylipins on the recruitment of NST capacity at temperatures below thermoneutrality, it needs to be concluded that oxylipins may rather promote the sensitivity to other stimulants such as chronic mild cold exposure.

Future research should focus on this potentially sensitizing effect of oxylipins, always considering the appropriate thermal environment. Sensitizing brown and brite adipocytes to other stimuli may reduce the effective doses of other NST stimulating agents such as β_3 -adrenergic receptor agonists, thus limiting systemic side effects.

In summary, the modulation of lipid composition, e.g. by dietary intervention, should remain a focus of follow up research aiming to utilize the health promoting effects of active BAT in order to tackle the obesity epidemic.

8 REFERENCES

- Albracht-Schulte, Kembra, Nishan Sudheera Kalupahana, Latha Ramalingam, Shu Wang, Shaikh Mizanoor Rahman, Jacalyn Robert-McComb, and Naima Moustaid-Moussa. 2018. "Omega-3 Fatty Acids in Obesity and Metabolic Syndrome: A Mechanistic Update." *Journal of Nutritional Biochemistry* 58 (2017): 1–16. <https://doi.org/10.1016/j.jnutbio.2018.02.012>.
- Anderson, James W, Elizabeth C Konz, Robert C Frederich, and Constance L Wood. 2001. "Long-Term Weight-Loss Maintenance: A Meta-Analysis of US Studies." *The American Journal of Clinical Nutrition* 74 (5): 579–84. <https://doi.org/10.1093/ajcn/74.5.579>.
- Anunciado-Koza, Rea, Jozef Ukropec, Robert A. Koza, and Leslie P. Kozak. 2008. "Inactivation of UCP1 and the Glycerol Phosphate Cycle Synergistically Increases Energy Expenditure to Resist Diet-Induced Obesity." *Journal of Biological Chemistry* 283 (41): 27688–97. <https://doi.org/10.1074/jbc.M804268200>.
- Argelaguet, Ricard, Damien Arnol, Danila Bredikhin, Yonatan Deloro, Britta Velten, John C. Marioni, and Oliver Stegle. 2020. "MOFA+: A Statistical Framework for Comprehensive Integration of Multi-Modal Single-Cell Data." *Genome Biology* 21 (1): 111. <https://doi.org/10.1186/s13059-020-02015-1>.
- Argelaguet, Ricard, Britta Velten, Damien Arnol, Sascha Dietrich, Thorsten Zenz, John C Marioni, Florian Buettner, Wolfgang Huber, and Oliver Stegle. 2018. "Multi-Omics Factor Analysis—a Framework for Unsupervised Integration of Multi-omics Data Sets." *Molecular Systems Biology* 14 (6). <https://doi.org/10.15252/msb.20178124>.
- Bachman, Eric S., Harveen Dhillon, Chen Yu Zhang, Saverio Cinti, Antonio C. Bianco, Brian K. Kobilka, and Bradford B. Lowell. 2002. "BAR Signaling Required for Diet-Induced Thermogenesis and Obesity Resistance." *Science* 297 (5582): 843–45. <https://doi.org/10.1126/science.1073160>.
- Bajzer, M., M. Olivieri, M. K. Haas, P. T. Pfluger, I. J. Magrisso, M. T. Foster, M. H. Tschöp, K. A. Krawczewski-Carhuatanta, D. Cota, and S. Obici. 2011. "Cannabinoid Receptor 1 (CB1) Antagonism Enhances Glucose Utilisation and Activates Brown Adipose Tissue in Diet-Induced Obese Mice." *Diabetologia* 54 (12): 3121–31. <https://doi.org/10.1007/s00125-011-2302-6>.
- Balvers, Michiel G.J., Kitty C.M. Verhoeckx, Sabina Bijlsma, Carina M. Rubingh, Jocelijn Meijerink, Heleen M. Wortelboer, and Renger F. Witkamp. 2012. "Fish Oil and Inflammatory Status Alter the N-3 to n-6 Balance of the Endocannabinoid and Oxylinpin Metabolomes in Mouse Plasma and Tissues." *Metabolomics* 8 (6): 1130–47. <https://doi.org/10.1007/s11306-012-0421-9>.

- Bargut, Thereza Cristina Lonzezzetti, Fabiane Ferreira Martins, Larissa Pereira Santos, Marcia Barbosa Aguila, and Carlos A. Mandarim-de-Lacerda. 2019. "Administration of Eicosapentaenoic and Docosahexaenoic Acids May Improve the Remodeling and Browning in Subcutaneous White Adipose Tissue and Thermogenic Markers in Brown Adipose Tissue in Mice." *Molecular and Cellular Endocrinology* 482 (December 2018): 18–27. <https://doi.org/10.1016/j.mce.2018.12.003>.
- Bargut, Thereza Cristina Lonzezzetti, Anna Carolina Alves Gomes Silva-e-Silva, Vanessa Souza-Mello, Carlos Alberto Mandarim-de-Lacerda, and Marcia Barbosa Aguila. 2016. "Mice Fed Fish Oil Diet and Upregulation of Brown Adipose Tissue Thermogenic Markers." *European Journal of Nutrition* 55 (1): 159–69. <https://doi.org/10.1007/s00394-015-0834-0>.
- Bargut, Thereza Cristina Lonzezzetti, Vanessa Souza-Mello, Carlos Alberto Mandarim-De-Lacerda, and Marcia Barbosa Aguila. 2016. "Fish Oil Diet Modulates Epididymal and Inguinal Adipocyte Metabolism in Mice." *Food and Function* 7 (3): 1468–76. <https://doi.org/10.1039/c5fo00909j>.
- Barquissau, Valentin, Rayane A. Ghandour, Gérard Ailhaud, Martin Klingenspor, Dominique Langin, Ez Zoubir Amri, and Didier F. Pisani. 2017. "Control of Adipogenesis by Oxylipins, GPCRs and PPARs." *Biochimie* 136 (May): 3–11. <https://doi.org/10.1016/j.biochi.2016.12.012>.
- Barreau, Corinne, Elodie Labit, Christophe Guissard, Jacques Rouquette, Marie Laure Boizeau, Souleymane Gani Koumassi, Audrey Carrière, et al. 2016. "Regionalization of Browning Revealed by Whole Subcutaneous Adipose Tissue Imaging." *Obesity* 24 (5): 1081–89. <https://doi.org/10.1002/oby.21455>.
- Bartelt, Alexander, Oliver T. Bruns, Rudolph Reimer, Heinz Hohenberg, Harald Ittrich, Kersten Peldschus, Michael G. Kaul, et al. 2011. "Brown Adipose Tissue Activity Controls Triglyceride Clearance." *Nature Medicine* 17 (2): 200–206. <https://doi.org/10.1038/nm.2297>.
- Bartesaghi, Stefano, Stefan Hallen, Li Huang, Per Arne Svensson, Remi A. Momo, Simonetta Wallin, Eva K. Carlsson, Anna Forslöw, Patrick Seale, and Xiao Rong Peng. 2015. "Thermogenic Activity of UCP1 in Human White Fat-Derived Beige Adipocytes." *Molecular Endocrinology* 29 (1): 130–39. <https://doi.org/10.1210/me.2014-1295>.
- Bayindir, Irem, Rohollah Babaeikelishomi, Silvia Kocanova, Isabel Sofia Sousa, Sarah Lerch, Olaf Hardt, Stefan Wild, et al. 2015. "Transcriptional Pathways in CPG12-Induced Adipocyte Progenitor Activation for Browning." *Frontiers in Endocrinology* 6: 129. <https://doi.org/10.3389/fendo.2015.00129>.
- Becher, Tobias, Srikanth Palanisamy, Daniel J. Kramer, Mahmoud Eljalby, Sarah J. Marx, Andreas

- G. Wibmer, Scott D. Butler, et al. 2021. "Brown Adipose Tissue Is Associated with Cardiometabolic Health." *Nature Medicine* 27 (1): 58–65. <https://doi.org/10.1038/s41591-020-1126-7>.
- Bentham, James, Mariachiara Di Cesare, Ver Bilano, Honor Bixby, Bin Zhou, Gretchen A. Stevens, Leanne M. Riley, et al. 2017. "Worldwide Trends in Body-Mass Index, Underweight, Overweight, and Obesity from 1975 to 2016: A Pooled Analysis of 2416 Population-Based Measurement Studies in 128·9 Million Children, Adolescents, and Adults." *The Lancet* 390 (10113): 2627–42. [https://doi.org/10.1016/S0140-6736\(17\)32129-3](https://doi.org/10.1016/S0140-6736(17)32129-3).
- Berbeé, Jimmy F.P., Mariëtte R. Boon, P. Padmini S.J. Khedoe, Alexander Bartelt, Christian Schlein, Anna Worthmann, Sander Kooijman, et al. 2015. "Brown Fat Activation Reduces Hypercholesterolaemia and Protects from Atherosclerosis Development." *Nature Communications* 6 (1): 1–11. <https://doi.org/10.1038/ncomms7356>.
- Bertholet, Ambre M., and Yuriy Kirichok. 2019. "The Mechanism FA-Dependent H⁺ Transport by UCP1." In *Handbook of Experimental Pharmacology*, 251:143–59. Springer New York LLC. https://doi.org/10.1007/164_2018_138.
- Bhaskaran, Shylesh, Archana Unnikrishnan, Rojina Ranjit, Rizwan Qaisar, Gavin Pharaoh, Stephanie Matyi, Michael Kinter, and Sathyaseelan S. Deepa. 2017. "A Fish Oil Diet Induces Mitochondrial Uncoupling and Mitochondrial Unfolded Protein Response in Epididymal White Adipose Tissue of Mice." *Free Radical Biology and Medicine* 108 (April): 704–14. <https://doi.org/10.1016/j.freeradbiomed.2017.04.028>.
- Bond, Laura M., and James M. Ntambi. 2018. "UCP1 Deficiency Increases Adipose Tissue Monounsaturated Fatty Acid Synthesis and Trafficking to the Liver." *Journal of Lipid Research* 59 (2): 224–36. <https://doi.org/10.1194/jlr.M078469>.
- Boon, Mariëtte R., Sander Kooijman, Andrea D. Van Dam, Leonard R. Pelgrom, Jimmy F.P. Berbé, Cheryl A.R. Visseren, Robin C. Van Aggele, et al. 2014. "Peripheral Cannabinoid 1 Receptor Blockade Activates Brown Adipose Tissue and Diminishes Dyslipidemia and Obesity." *FASEB Journal* 28 (12): 5361–75. <https://doi.org/10.1096/fj.13-247643>.
- Buckley, J. D., and P. R.C. Howe. 2009. "Anti-Obesity Effects of Long-Chain Omega-3 Polyunsaturated Fatty Acids." *Obesity Reviews* 10 (6): 648–59. <https://doi.org/10.1111/j.1467-789X.2009.00584.x>.
- Burgess, E., P. Hassmén, and K. L. Pumpa. 2017. "Determinants of Adherence to Lifestyle Intervention in Adults with Obesity: A Systematic Review." *Clinical Obesity* 7 (3): 123–35. <https://doi.org/10.1111/cob.12183>.
- Cannon, Barbara, and Jan Nedergaard. 2004. "Brown Adipose Tissue: Function and Physiological

- Significance." *Physiological Reviews*. American Physiological Society. <https://doi.org/10.1152/physrev.00015.2003>.
- Carey, A. L., E. Wolk Petersen, C. R. Bruce, R. J. Southgate, H. Pilegaard, J. A. Hawley, B. K. Pedersen, and M. A. Febbraio. 2006. "Discordant Gene Expression in Skeletal Muscle and Adipose Tissue of Patients with Type 2 Diabetes: Effect of Interleukin-6 Infusion." *Diabetologia* 49 (5): 1000–1007. <https://doi.org/10.1007/s00125-006-0178-7>.
- Carey, Andrew L., Camilla Vorlander, Medini Reddy-Luthmoodoo, Alaina K. Natoli, Melissa F. Formosa, David A. Bertovic, Mitchell J. Anderson, Stephen J. Duffy, and Bronwyn A. Kingwell. 2014. "Reduced UCP-1 Content in in Vitro Differentiated Beige/ Brite Adipocytes Derived from Preadipocytes of Human Subcutaneous White Adipose Tissues in Obesity." *PLoS ONE* 9 (3). <https://doi.org/10.1371/journal.pone.0091997>.
- Challa, Tenagne D., Dianne H. Dapito, Elisabeth Kulenkampff, Elke Kiehlmann, Caroline Moser, Leon Straub, Wenfei Sun, and Christian Wolfrum. 2020. "A Genetic Model to Study the Contribution of Brown and Brite Adipocytes to Metabolism." *Cell Reports* 30 (10): 3424–3433.e4. <https://doi.org/10.1016/j.celrep.2020.02.055>.
- Chaudhry, Archana, and James G. Granneman. 1999. "Differential Regulation of Functional Responses by β -Adrenergic Receptor Subtypes in Brown Adipocytes." *American Journal of Physiology-Regulatory, Integrative and Comparative Physiology* 277 (1): R147–53. <https://doi.org/10.1152/ajpregu.1999.277.1.R147>.
- Chechi, Kanta, Wouter Van Marken Lichtenbelt, and Denis Richard. 2018. "Brown and Beige Adipose Tissues: Phenotype and Metabolic Potential in Mice and Men." *Journal of Applied Physiology* 124 (2): 482–96. <https://doi.org/10.1152/jappphysiol.00021.2017>.
- Chen, Hui-Feng, Chen-Ming Hsu, and Yi-Shuian Huang. 2018. "CPEB 2-dependent Translation of Long 3'-UTR Ucp1 mRNA Promotes Thermogenesis in Brown Adipose Tissue ." *The EMBO Journal* 37 (20). <https://doi.org/10.15252/embj.201899071>.
- Cheung, L., J. Gertow, O. Werngren, L. Folkersen, N. Petrovic, J. Nedergaard, A. Franco-Cereceda, P. Eriksson, and R. M. Fisher. 2013. "Human Mediastinal Adipose Tissue Displays Certain Characteristics of Brown Fat." *Nutrition and Diabetes* 3 (MAY): e66-9. <https://doi.org/10.1038/nutd.2013.6>.
- Chondronikola, Maria, Elena Volpi, E. Borsheim, Craig Porter, Palam Annamalai, S. Enerback, Martin E. Lidell, et al. 2014. "Brown Adipose Tissue Improves Whole-Body Glucose Homeostasis and Insulin Sensitivity in Humans." *Diabetes* 63 (12): 4089–99. <https://doi.org/10.2337/db14-0746>.
- Chung, Kyoung Jin, Antonios Chatzigeorgiou, Matina Economopoulou, Ruben Garcia-Martin,

- Vasileia I. Alexaki, Ioannis Mitroulis, Marina Nati, et al. 2017. "A Self-Sustained Loop of Inflammation-Driven Inhibition of Beige Adipogenesis in Obesity." *Nature Immunology* 18 (6): 654–64. <https://doi.org/10.1038/ni.3728>.
- Cypess, Aaron M., Sanaz Lehman, Gethin Williams, Ilan Tal, Dean Rodman, Allison B. Goldfine, Frank C. Kuo, et al. 2009. "Identification and Importance of Brown Adipose Tissue in Adult Humans." *New England Journal of Medicine* 360 (15): 1509–17. <https://doi.org/10.1056/nejmoa0810780>.
- Cypess, Aaron M., Lauren S. Weiner, Carla Roberts-Toler, Elisa Franquet Elía, Skyler H. Kessler, Peter A. Kahn, Jeffrey English, et al. 2015. "Activation of Human Brown Adipose Tissue by a B3-Adrenergic Receptor Agonist." *Cell Metabolism* 21 (1): 33–38. <https://doi.org/10.1016/j.cmet.2014.12.009>.
- Dieckmann, Sebastian, Stefanie Maurer, Tobias Fromme, Cécilia Colson, Kirsi A. Virtanen, Ez Zoubir Amri, and Martin Klingenspor. 2020. "Fatty Acid Metabolite Profiling Reveals Oxylipins as Markers of Brown but Not Brite Adipose Tissue." *Frontiers in Endocrinology* 11 (February). <https://doi.org/10.3389/fendo.2020.00073>.
- Edgar, Robert C. 2013. "UPARSE: Highly Accurate OTU Sequences from Microbial Amplicon Reads." *Nature Methods* 10 (10): 996–98. <https://doi.org/10.1038/nmeth.2604>.
- EFSA Panel on Dietetic Products Nutrition and Allergies (NDA). 2012. "Scientific Opinion on the Tolerable Upper Intake Level of Eicosapentaenoic Acid (EPA), Docosahexaenoic Acid (DHA) and Docosapentaenoic Acid (DPA)." *EFSA Journal* 10 (7). <https://doi.org/10.2903/j.efsa.2012.2815>.
- Enerbäck, Sven, Anders Jacobsson, Elizabeth M. Simpson, Carmen Guerra, Hitoshi Yamashita, Mary Ellen Harper, and Leslie P. Kozak. 1997. "Mice Lacking Mitochondrial Uncoupling Protein Are Cold-Sensitive but Not Obese." *Nature* 387 (6628): 90–94. <https://doi.org/10.1038/387090a0>.
- Essen, Gabriella von, Erik Lindsund, Barbara Cannon, and Jan Nedergaard. 2017. "Adaptive Facultative Diet-Induced Thermogenesis in Wild-Type but Not in UCP1-Ablated Mice." *American Journal of Physiology - Endocrinology and Metabolism* 313 (5): E515–27. <https://doi.org/10.1152/ajpendo.00097.2017>.
- Fan, Rong, Karsten Koehler, and Soonkyu Chung. 2019. "Adaptive Thermogenesis by Dietary N-3 Polyunsaturated Fatty Acids: Emerging Evidence and Mechanisms." *Biochimica et Biophysica Acta - Molecular and Cell Biology of Lipids* 1864 (1): 59–70. <https://doi.org/10.1016/j.bbalip.2018.04.012>.
- Fan, Rong, Ashley Mulcahy Toney, Yura Jang, Seung Hyun Ro, and Soonkyu Chung. 2018. "Maternal

- N-3 PUFA Supplementation Promotes Fetal Brown Adipose Tissue Development through Epigenetic Modifications in C57BL/6 Mice." *Biochimica et Biophysica Acta - Molecular and Cell Biology of Lipids* 1863 (12): 1488–97. <https://doi.org/10.1016/j.bbaliip.2018.09.008>.
- Fedorenko, Andriy, Polina V. Lishko, and Yuriy Kirichok. 2012. "Mechanism of Fatty-Acid-Dependent UCP1 Uncoupling in Brown Fat Mitochondria." *Cell* 151 (2): 400–413. <https://doi.org/10.1016/j.cell.2012.09.010>.
- Feldmann, Helena M., Valeria Golozoubova, Barbara Cannon, and Jan Nedergaard. 2009. "UCP1 Ablation Induces Obesity and Abolishes Diet-Induced Thermogenesis in Mice Exempt from Thermal Stress by Living at Thermoneutrality." *Cell Metabolism* 9 (2): 203–9. <https://doi.org/10.1016/j.cmet.2008.12.014>.
- Fernández-Galilea, Marta, Elisa Félix-Soriano, Ignacio Colón-Mesa, Xavier Escoté, and Maria J. Moreno-Aliaga. 2020. *Omega-3 Fatty Acids as Regulators of Brown/Beige Adipose Tissue: From Mechanisms to Therapeutic Potential. Journal of Physiology and Biochemistry*. Vol. 76. Springer. <https://doi.org/10.1007/s13105-019-00720-5>.
- Fernández-Vega, A., E. Chicano-Gálvez, B. M. Prentice, D. Anderson, F. Priego-Capote, M. A. López-Bascón, M. Calderón-Santiago, et al. 2020. "Optimization of a MALDI-Imaging Protocol for Studying Adipose Tissue-Associated Disorders." *Talanta*. <https://doi.org/10.1016/j.talanta.2020.121184>.
- Finlin, Brian S., Hasiyet Memetimin, Amy L. Confides, Ildiko Kasza, Beibei Zhu, Hemendra J. Vekaria, Brianna Harfmann, et al. 2018. "Human Adipose Beiging in Response to Cold and Mirabegron." *JCI Insight* 3 (15): 1–15. <https://doi.org/10.1172/jci.insight.121510>.
- Finlin, Brian S., Beibei Zhu, Amy L. Confides, Philip M. Westgate, Brianna D. Harfmann, Esther E. Dupont-Versteegden, and Philip A. Kern. 2017. "Mast Cells Promote Seasonal White Adipose Beiging in Humans." *Diabetes* 66 (5): 1237–46. <https://doi.org/10.2337/db16-1057>.
- Fischer, Alexander W., Barbara Cannon, and Jan Nedergaard. 2018. "Optimal Housing Temperatures for Mice to Mimic the Thermal Environment of Humans: An Experimental Study." *Molecular Metabolism* 7 (January): 161–70. <https://doi.org/10.1016/j.molmet.2017.10.009>.
- Flachs, P., M. Rossmeisl, and J. Kopecky. 2014. "The Effect of N-3 Fatty Acids on Glucose Homeostasis and Insulin Sensitivity." *Physiological Research* 63 (SUPPL.): S93-118. <https://doi.org/10.33549/physiolres.932715>.
- Flachs, P., R. Rühl, M. Hensler, P. Janovska, P. Zouhar, V. Kus, Z. MacEk Jilkova, et al. 2011. "Synergistic Induction of Lipid Catabolism and Anti-Inflammatory Lipids in White Fat of Dietary Obese Mice in Response to Calorie Restriction and n-3 Fatty Acids." *Diabetologia* 54

- (10): 2626–38. <https://doi.org/10.1007/s00125-011-2233-2>.
- Flachs, Pavel, Martin Rossmeisl, Ondrej Kuda, and Jan Kopecky. 2013. “Stimulation of Mitochondrial Oxidative Capacity in White Fat Independent of UCP1: A Key to Lean Phenotype.” *Biochimica et Biophysica Acta - Molecular and Cell Biology of Lipids* 1831 (5): 986–1003. <https://doi.org/10.1016/j.bbali.2013.02.003>.
- Fleckenstein-Elsen, Manuela, Daniela Dinnies, Tomas Jelenik, Michael Roden, Tania Romacho, and Jürgen Eckel. 2016. “Eicosapentaenoic Acid and Arachidonic Acid Differentially Regulate Adipogenesis, Acquisition of a Brite Phenotype and Mitochondrial Function in Primary Human Adipocytes.” *Molecular Nutrition & Food Research* 60 (9): 2065–75. <https://doi.org/10.1002/mnfr.201500892>.
- Forster, Brigitte, Dimitri Van De Ville, Jesse Berent, Daniel Sage, and Michael Unser. 2004. “Extended Depth-of-Focus for Multi-Channel Microscopy Images: A Complex Wavelet Approach.” In *2004 2nd IEEE International Symposium on Biomedical Imaging: Macro to Nano*. <https://doi.org/10.1109/isbi.2004.1398624>.
- Fromme, Tobias, Kristina Hüttinger, Stefanie Maurer, Yongguo Li, Thomas Gantert, Jarlei Fiamoncini, Hannelore Daniel, Sören Westphal, and Martin Klingenspor. 2019. “Bile Acid Supplementation Decreases Body Mass Gain in C57BL/6J but Not 129S6/SvEvTac Mice without Increasing Energy Expenditure.” *Scientific Reports* 9 (1): 131. <https://doi.org/10.1038/s41598-018-37464-z>.
- Fromme, Tobias, and Martin Klingenspor. 2011. “Uncoupling Protein 1 Expression and High-Fat Diets.” *American Journal of Physiology - Regulatory Integrative and Comparative Physiology* 300 (1): R1–8. <https://doi.org/10.1152/ajpregu.00411.2010>.
- Gabbs, Melissa, Shan Leng, Jessay G. Devassy, Md Monirujjaman, and Harold M. Aukema. 2015. “Advances in Our Understanding of Oxylipins Derived from Dietary PUFAs.” *Advances in Nutrition* 6 (5): 513–40. <https://doi.org/10.3945/an.114.007732>.
- Ganeshan, Kirthana, and Ajay Chawla. 2017. “Warming the Mouse to Model Human Diseases.” *Nature Reviews Endocrinology* 13 (8): 458–65. <https://doi.org/10.1038/nrendo.2017.48>.
- García-Alonso, Verónica, Esther Titos, Jose Alcaraz-Quiles, Bibiana Rius, Aritz Lopategi, Cristina López-Vicario, Per Johan Jakobsson, Salvadora Delgado, Juanjo Lozano, and Joan Clària. 2016. “Prostaglandin E2 Exerts Multiple Regulatory Actions on Human Obese Adipose Tissue Remodeling, Inflammation, Adaptive Thermogenesis and Lipolysis.” Edited by Patricia T. Bozza. *PLoS ONE* 11 (4): e0153751. <https://doi.org/10.1371/journal.pone.0153751>.
- Ghandour, Rayane A., Cecilia Colson, Maude Giroud, Stefanie Maurer, Samah Rekima, Gérard Ailhaud, Martin Klingenspor, Ez Zoubir Amri, and Didier F. Pisani. 2018. “Impact of Dietary

- Ω 3 Polyunsaturated Fatty Acid Supplementation on Brown and Brite Adipocyte Function.” *Journal of Lipid Research* 59 (3): 452–61. <https://doi.org/10.1194/jlr.M081091>.
- Ghandour, Rayane A., Maude Giroud, Alexandros Vegiopoulos, Stephan Herzig, Gérard Ailhaud, Ez Zoubir Amri, and Didier F. Pisani. 2016. “IP-Receptor and PPARs Trigger the Conversion of Human White to Brite Adipocyte Induced by Carbaprostacyclin.” *Biochimica et Biophysica Acta - Molecular and Cell Biology of Lipids* 1861 (4): 285–93. <https://doi.org/10.1016/j.bbalip.2016.01.007>.
- Glick, Z., R. J. Teague, and G. A. Bray. 1981. “Brown Adipose Tissue: Thermic Response Increased by a Single Low Protein, High Carbohydrate Meal.” *Science* 213 (4512): 1125–27. <https://doi.org/10.1126/science.7268419>.
- Gnad, Thorsten, Saskia Scheibler, Ivar Von Kugelgen, Camilla Scheele, Ana Kilic, Anja Glode, Linda S. Hoffmann, et al. 2014. “Adenosine Activates Brown Adipose Tissue and Recruits Beige Adipocytes via A2A Receptors.” *Nature* 516 (7531): 395–99. <https://doi.org/10.1038/nature13816>.
- Gordon, C. J. 2012. “Thermal Physiology of Laboratory Mice: Defining Thermoneutrality.” *Journal of Thermal Biology* 37 (8): 654–85. <https://doi.org/10.1016/j.jtherbio.2012.08.004>.
- Granneman, J. G., M. Burnazi, Z. Zhu, and L. A. Schwamb. 2003. “White Adipose Tissue Contributes to UCP1-Independent Thermogenesis.” *American Journal of Physiology - Endocrinology and Metabolism* 285 (6 48-6): E1230–36. <https://doi.org/10.1152/ajpendo.00197.2003>.
- Graves, Joan P., Artiom Gruzdev, J. Alyce Bradbury, Laura M. DeGraff, Huiling Li, John S. House, Samantha L. Hoopes, Matthew L. Edin, and Darryl C. Zeldin. 2015. “Quantitative Polymerase Chain Reaction Analysis of the Mouse Cyp2j Subfamily: Tissue Distribution and Regulation.” *Drug Metabolism and Disposition* 43 (8): 1169–80. <https://doi.org/10.1124/dmd.115.064139>.
- Hadi, Hamza El, Angelo Di Vincenzo, Roberto Vettor, and Marco Rossato. 2019. “Food Ingredients Involved in White-to-Brown Adipose Tissue Conversion and in Calorie Burning.” *Frontiers in Physiology* 10 (JAN): 1954. <https://doi.org/10.3389/fphys.2018.01954>.
- Hall, Kevin D., and Scott Kahan. 2018. “Maintenance of Lost Weight and Long-Term Management of Obesity.” *Medical Clinics of North America* 102 (1): 183–97. <https://doi.org/10.1016/j.mcna.2017.08.012>.
- Hankir, Mohammed K., Mathias Kranz, Susanne Keipert, Juliane Weiner, Sille G. Andreasen, Matthias Kern, Marianne Patt, et al. 2017. “Dissociation between Brown Adipose Tissue 18F-FDG Uptake and Thermogenesis in Uncoupling Protein 1-Deficient Mice.” *Journal of Nuclear Medicine* 58 (7): 1100–1103. <https://doi.org/10.2967/jnumed.116.186460>.

- Harms, Matthew J., Qian Li, Sunjae Lee, Cheng Zhang, Bengt Kull, Stefan Hallen, Anders Thorell, et al. 2019. "Mature Human White Adipocytes Cultured under Membranes Maintain Identity, Function, and Can Transdifferentiate into Brown-like Adipocytes." *Cell Reports* 27 (1): 213-225.e5. <https://doi.org/10.1016/j.celrep.2019.03.026>.
- He, Ping, Biyu Hou, Yanliang Li, Chunyang Xu, Peng Ma, Sin Man Lam, Victoria Gil, et al. 2019. "Lipid Profiling Reveals Browning Heterogeneity of White Adipose Tissue by B3-Adrenergic Stimulation." *Biomolecules* 9 (9): 444. <https://doi.org/10.3390/biom9090444>.
- Heemskerk, Mattijs M., Martin Giera, Fatiha el Bouazzaoui, Mirjam A. Lips, Hanno Pijl, Ko Willems van Dijk, and Vanessa van Harmelen. 2015. "Increased PUFA Content and 5-Lipoxygenase Pathway Expression Are Associated with Subcutaneous Adipose Tissue Inflammation in Obesewomen with Type 2 Diabetes." *Nutrients* 7 (9): 7676-90. <https://doi.org/10.3390/nu7095362>.
- Heldmaier, Gerhard. 1975. "Metabolic and Thermoregulatory Responses to Heat and Cold in the Djungarian Hamster, *Phodopus Sungorus*." *Journal of Comparative Physiology* B 102 (2): 115-22. <https://doi.org/10.1007/BF00691297>.
- Hoang, Tuan, Matthew D. Smith, and Masoud Jelokhani-Niaraki. 2013. "Expression, Folding, and Proton Transport Activity of Human Uncoupling Protein-1 (Ucp1) in Lipid Membranes." *Journal of Biological Chemistry* 288 (51): 36244-58. <https://doi.org/10.1074/jbc.M113.509935>.
- Hoene, Miriam, Jia Li, Hans Ulrich Häring, Cora Weigert, Guowang Xu, and Rainer Lehmann. 2014. "The Lipid Profile of Brown Adipose Tissue Is Sex-Specific in Mice." *Biochimica et Biophysica Acta - Molecular and Cell Biology of Lipids* 1841 (10): 1563-70. <https://doi.org/10.1016/j.bbailip.2014.08.003>.
- Hofmann, Wolfgang E., Xiaotuan Liu, Christie M. Bearden, Mary Ellen Harper, and Leslie P. Kozak. 2001. "Effects of Genetic Background on Thermoregulation and Fatty Acid-Induced Uncoupling of Mitochondria in UCP1-Deficient Mice." *Journal of Biological Chemistry* 276 (15): 12460-65. <https://doi.org/10.1074/jbc.M100466200>.
- Horrillo, Raquel, Ana González-Pérez, Marcos Martínez-Clemente, Marta López-Parra, Natàlia Ferré, Esther Títos, Eva Morán-Salvador, Ramon Deulofeu, Vicente Arroyo, and Joan Clària. 2010. "5-Lipoxygenase Activating Protein Signals Adipose Tissue Inflammation and Lipid Dysfunction in Experimental Obesity." *The Journal of Immunology* 184 (7): 3978-87. <https://doi.org/10.4049/jimmunol.0901355>.
- Iizuka, Yuzuru, Kanako Chiba, Hyounju Kim, Satoshi Hirako, Masahiro Wada, and Akiyo Matsumoto. 2020. "Impact of Discontinuation of Fish Oil after Pioglitazone-Fish Oil

- Combination Therapy in Diabetic KK Mice.” *Journal of Nutritional Biochemistry* 76 (February): 108265. <https://doi.org/10.1016/j.jnutbio.2019.108265>.
- International Diabetes Federation. 2005. “The IDF Consensus Worldwide Definition of the Metabolic Syndrome.” *Obesity and Metabolism* 2 (3): 47–49. <https://doi.org/10.14341/2071-8713-4854>.
- Janovská, P., P. Flachs, L. Kazdová, and J. Kopecký. 2013. “Anti-Obesity Effect of n-3 Polyunsaturated Fatty Acids in Mice Fed High-Fat Diet Is Independent of Cold-Induced Thermogenesis.” *Physiological Research* 62 (2): 153–61. <https://doi.org/10.33549/physiolres.932464>.
- Jayarathne, Shasika, Iurii Koboziev, Oak Hee Park, Wilna Oldewage-Theron, Chwan Li Shen, and Naima Moustaid-Moussa. 2017. “Anti-Inflammatory and Anti-Obesity Properties of Food Bioactive Components: Effects on Adipose Tissue.” *Preventive Nutrition and Food Science* 22 (4): 251–62. <https://doi.org/10.3746/pnf.2017.22.4.251>.
- Jespersen, Naja Z., Amir Feizi, Eline S. Andersen, Sarah Heywood, Helle B. Hattel, Søren Daugaard, Lone Peijs, et al. 2019. “Heterogeneity in the Perirenal Region of Humans Suggests Presence of Dormant Brown Adipose Tissue That Contains Brown Fat Precursor Cells.” *Molecular Metabolism* 24 (March): 30–43. <https://doi.org/10.1016/j.molmet.2019.03.005>.
- Jespersen, Naja Zenius, Therese Juhlin Larsen, Lone Peijs, Søren Daugaard, Preben Homøe, Annika Loft, Jasper de Jong, et al. 2013. “A Classical Brown Adipose Tissue mRNA Signature Partly Overlaps with Brite in the Supraclavicular Region of Adult Humans.” *Cell Metabolism* 17 (5): 798–805. <https://doi.org/10.1016/j.cmet.2013.04.011>.
- Jong, Jasper M.A. de, Wenfei Sun, Nuno D. Pires, Andrea Frontini, Miroslav Balaz, Naja Z. Jespersen, Amir Feizi, et al. 2019. “Human Brown Adipose Tissue Is Phenocopied by Classical Brown Adipose Tissue in Physiologically Humanized Mice.” *Nature Metabolism* 1 (8): 830–43. <https://doi.org/10.1038/s42255-019-0101-4>.
- Kajimura, Shingo, Bruce M. Spiegelman, and Patrick Seale. 2015. “Brown and Beige Fat: Physiological Roles beyond Heat Generation.” *Cell Metabolism*. Cell Press. <https://doi.org/10.1016/j.cmet.2015.09.007>.
- Kalupahana, Nishan S., Kate Claycombe, Shelley J. Newman, Taryn Stewart, Nalin Siriwardhana, Nirupa Matthan, Alice H. Lichtenstein, and Naima Moustaid-Moussa. 2010. “Eicosapentaenoic Acid Prevents and Reverses Insulin Resistance in High-Fat Diet-Induced Obese Mice via Modulation of Adipose Tissue Inflammation.” *Journal of Nutrition* 140 (11): 1915–22. <https://doi.org/10.3945/jn.110.125732>.
- Kazak, Lawrence, Edward T. Chouchani, Mark P. Jedrychowski, Brian K. Erickson, Kosaku Shinoda,

- Paul Cohen, Ramalingam Vetrivelan, et al. 2015. "A Creatine-Driven Substrate Cycle Enhances Energy Expenditure and Thermogenesis in Beige Fat." *Cell* 163 (3): 643–55. <https://doi.org/10.1016/j.cell.2015.09.035>.
- Keipert, Susanne, Dominik Lutter, Bjoern O. Schroeder, Daniel Brandt, Marcus Ståhlman, Thomas Schwarzmayr, Elisabeth Graf, et al. 2020. "Endogenous FGF21-Signaling Controls Paradoxical Obesity Resistance of UCP1-Deficient Mice." *Nature Communications* 11 (1): 624. <https://doi.org/10.1038/s41467-019-14069-2>.
- Kern, Philip A., Brian S. Finlin, Beibei Zhu, Neda Rasouli, Robert E. McGehee, Philip M. Westgate, and Esther E. Dupont-Versteegden. 2014. "The Effects of Temperature and Seasons on Subcutaneous White Adipose Tissue in Humans: Evidence for Thermogenic Gene Induction." *Journal of Clinical Endocrinology and Metabolism* 99 (12): E2772–79. <https://doi.org/10.1210/jc.2014-2440>.
- Kim, Jiyoung, Meshail Okla, Anjeza Erickson, Timothy Carr, Sathish Kumar Natarajan, and Soonkyu Chung. 2016. "Eicosapentaenoic Acid Potentiates Brown Thermogenesis through FFAR4-Dependent up-Regulation of MiR-30b and MiR-378." *Journal of Biological Chemistry* 291 (39): 20551–62. <https://doi.org/10.1074/jbc.M116.721480>.
- Kim, Minji, Tsuyoshi Goto, Rina Yu, Kunitoshi Uchida, Makoto Tominaga, Yuriko Kano, Nobuyuki Takahashi, and Teruo Kawada. 2015. "Fish Oil Intake Induces UCP1 Upregulation in Brown and White Adipose Tissue via the Sympathetic Nervous System." *Scientific Reports* 5 (1): 18013. <https://doi.org/10.1038/srep18013>.
- Kjellberg, Jakob, Arendse Tange Larsen, Rikke Ibsen, and Betina Højgaard. 2017. "The Socioeconomic Burden of Obesity." *Obesity Facts* 10 (5): 493–502. <https://doi.org/10.1159/000480404>.
- Kjølbæk, Louise, Alfonso Benítez-Páez, Eva M. Gómez del Pulgar, Lena K. Brahe, Gerhard Liebisch, Silke Matysik, Simone Rampelli, et al. 2020. "Arabinoxylan Oligosaccharides and Polyunsaturated Fatty Acid Effects on Gut Microbiota and Metabolic Markers in Overweight Individuals with Signs of Metabolic Syndrome: A Randomized Cross-over Trial." *Clinical Nutrition* 39 (1): 67–79. <https://doi.org/10.1016/j.clnu.2019.01.012>.
- Kless, Caroline, Veronika Maria Müller, Valentina Luise Schüppel, Martina Lichtenegger, Michael Rychlik, Hannelore Daniel, Martin Klingenspor, and Dirk Haller. 2015. "Diet-Induced Obesity Causes Metabolic Impairment Independent of Alterations in Gut Barrier Integrity." *Molecular Nutrition and Food Research* 59 (5): 968–78. <https://doi.org/10.1002/mnfr.201400840>.
- Klindworth, Anna, Elmar Pruesse, Timmy Schweer, Jörg Peplies, Christian Quast, Matthias Horn, and Frank Oliver Glöckner. 2013. "Evaluation of General 16S Ribosomal RNA Gene PCR

- Primers for Classical and Next-Generation Sequencing-Based Diversity Studies." *Nucleic Acids Research* 41 (1). <https://doi.org/10.1093/nar/gks808>.
- Koch, Elisabeth, Malwina Mainka, Céline Dalle, Annika I. Ostermann, Katharina M. Rund, Laura Kutzner, Laura Fabienne Froehlich, Justine Bertrand-Michel, Cécile Gladine, and Nils Helge Schebb. 2020. "Stability of Oxylipins during Plasma Generation and Long-Term Storage." *Talanta* 217 (September). <https://doi.org/10.1016/j.talanta.2020.121074>.
- Krott, Lucia M., Fabiana Piscitelli, Markus Heine, Simona Borrino, Ludger Scheja, Cristoforo Silvestri, Joerg Heeren, and Vincenzo Di Marzo. 2016. "Endocannabinoid Regulation in White and Brown Adipose Tissue Following Thermogenic Activation." *Journal of Lipid Research* 57 (3): 464–73. <https://doi.org/10.1194/jlr.M065227>.
- Kuda, Ondrej, Martin Rossmeisl, and Jan Kopecky. 2018. "Omega-3 Fatty Acids and Adipose Tissue Biology." *Molecular Aspects of Medicine* 64 (December): 147–60. <https://doi.org/10.1016/j.mam.2018.01.004>.
- Kulterer, Oana C., Laura Niederstaetter, Carsten T. Herz, Alexander R. Haug, Andrea Bileck, Dietmar Pils, Alexandra Kautzky-Willer, Christopher Gerner, and Florian W. Kiefer. 2020. "The Presence of Active Brown Adipose Tissue Determines Cold-Induced Energy Expenditure and Oxylipin Profiles in Humans." *Journal of Clinical Endocrinology and Metabolism* 105 (7): 1–24. <https://doi.org/10.1210/clinem/dgaa183>.
- Labbé, Sébastien M., Alexandre Caron, Kanta Chechi, Mathieu Laplante, Roger Lecomte, and Denis Richard. 2016. "Metabolic Activity of Brown, 'Beige,' and White Adipose Tissues in Response to Chronic Adrenergic Stimulation in Male Mice." *American Journal of Physiology - Endocrinology and Metabolism* 311 (1): E260–68. <https://doi.org/10.1152/ajpendo.00545.2015>.
- Lagkouvardos, Ilias, Sandra Fischer, Neeraj Kumar, and Thomas Clavel. 2017. "Rhea: A Transparent and Modular R Pipeline for Microbial Profiling Based on 16S rRNA Gene Amplicons." *PeerJ* 2017 (1): e2836. <https://doi.org/10.7717/peerj.2836>.
- Lagkouvardos, Ilias, Divya Joseph, Martin Kapfhammer, Sabahattin Giritli, Matthias Horn, Dirk Haller, and Thomas Clavel. 2016. "IMNGS: A Comprehensive Open Resource of Processed 16S rRNA Microbial Profiles for Ecology and Diversity Studies." *Scientific Reports* 6 (1): 1–9. <https://doi.org/10.1038/srep33721>.
- Laiglesia, L. M., S. Lorente-Cebrián, P. L. Prieto-Hontoria, M. Fernández-Galilea, S. M.R. Ribeiro, N. Sáinz, J. A. Martínez, and M. J. Moreno-Aliaga. 2016. "Eicosapentaenoic Acid Promotes Mitochondrial Biogenesis and Beige-like Features in Subcutaneous Adipocytes from Overweight Subjects." *Journal of Nutritional Biochemistry* 37 (November): 76–82.

<https://doi.org/10.1016/j.jnutbio.2016.07.019>.

- Lalia, Antigoni Z., and Ian R. Lanza. 2016. "Insulin-Sensitizing Effects of Omega-3 Fatty Acids: Lost in Translation?" *Nutrients* 8 (6): 329. <https://doi.org/10.3390/nu8060329>.
- Lans, Anouk A.J.J. van der, Joris Hoeks, Boudewijn Brans, Guy H.E.J. Vijgen, Mariëlle G.W. Visser, Maarten J. Vosselman, Jan Hansen, et al. 2013. "Cold Acclimation Recruits Human Brown Fat and Increases Nonshivering Thermogenesis." *Journal of Clinical Investigation* 123 (8): 3395–3403. <https://doi.org/10.1172/JCI68993>.
- Lass, Achim, Robert Zimmermann, Guenter Haemmerle, Monika Riederer, Gabriele Schoiswohl, Martina Schweiger, Petra Kienesberger, Juliane G. Strauss, Gregor Gorkiewicz, and Rudolf Zechner. 2006. "Adipose Triglyceride Lipase-Mediated Lipolysis of Cellular Fat Stores Is Activated by CGI-58 and Defective in Chanarin-Dorfman Syndrome." *Cell Metabolism* 3 (5): 309–19. <https://doi.org/10.1016/j.cmet.2006.03.005>.
- Lee, Yang, Chrissie Willers, Edmund R.S. Kunji, and Paul G. Crichton. 2015. "Uncoupling Protein 1 Binds One Nucleotide per Monomer and Is Stabilized by Tightly Bound Cardiolipin." *Proceedings of the National Academy of Sciences of the United States of America* 112 (22): 6973–78. <https://doi.org/10.1073/pnas.1503833112>.
- Lee, Yun Hee, Sang Nam Kim, Hyun Jung Kwon, Krishna Rao Maddipati, and James G. Granneman. 2016. "Adipogenic Role of Alternatively Activated Macrophages in β -Adrenergic Remodeling of White Adipose Tissue." *American Journal of Physiology - Regulatory Integrative and Comparative Physiology* 310 (1): R55–65. <https://doi.org/10.1152/ajpregu.00355.2015>.
- Lee, Yun Hee, Anelia P. Petkova, Anish A. Konkar, and James G. Granneman. 2015. "Cellular Origins of Cold-Induced Brown Adipocytes in Adult Mice." *FASEB Journal* 29 (1): 286–99. <https://doi.org/10.1096/fj.14-263038>.
- Leiria, Luiz Osório, Chih Hao Wang, Matthew D. Lynes, Kunyan Yang, Farnaz Shamsi, Mari Sato, Satoru Sugimoto, et al. 2019. "12-Lipoxygenase Regulates Cold Adaptation and Glucose Metabolism by Producing the Omega-3 Lipid 12-HEPE from Brown Fat." *Cell Metabolism* 30 (4): 768-783.e7. <https://doi.org/10.1016/j.cmet.2019.07.001>.
- Li, Jing Jing, Chang J. Huang, and Dong Xie. 2008. "Anti-Obesity Effects of Conjugated Linoleic Acid, Docosahexaenoic Acid, and Eicosapentaenoic Acid." *Molecular Nutrition and Food Research* 52 (6): 631–45. <https://doi.org/10.1002/mnfr.200700399>.
- Li, Shuguang, Yixiang Li, Lin Xiang, Jing Dong, Min Liu, and Guangda Xiang. 2018. "Sildenafil Induces Browning of Subcutaneous White Adipose Tissue in Overweight Adults." *Metabolism: Clinical and Experimental* 78 (January): 106–17. <https://doi.org/10.1016/j.metabol.2017.09.008>.

- Li, Yongguo, Tobias Fromme, Sabine Schweizer, Theresa Schöttl, and Martin Klingenspor. 2014. "Taking Control over Intracellular Fatty Acid Levels Is Essential for the Analysis of Thermogenic Function in Cultured Primary Brown and Brite/Beige Adipocytes." *EMBO Reports* 15 (10): 1069–76. <https://doi.org/10.15252/embr.201438775>.
- Li, Yongguo, Katharina Schnabl, Sarah Madeleine Gabler, Monja Willershäuser, Josefine Reber, Angelos Karlas, Sanna Laurila, et al. 2018. "Secretin-Activated Brown Fat Mediates Prandial Thermogenesis to Induce Satiation." *Cell* 175 (6): 1561-1574.e12. <https://doi.org/10.1016/j.cell.2018.10.016>.
- Lidell, Martin E., Matthias J. Betz, Olof Dahlqvist Leinhard, Mikael Heglind, Louise Elander, Marc Slawik, Thomas Mussack, et al. 2013. "Evidence for Two Types of Brown Adipose Tissue in Humans." *Nature Medicine* 19 (5): 631–34. <https://doi.org/10.1038/nm.3017>.
- Liebisch, Gerhard, Marion Binder, Rainer Schifferer, Thomas Langmann, Berta Schulz, and Gerd Schmitz. 2006. "High Throughput Quantification of Cholesterol and Cholesteryl Ester by Electrospray Ionization Tandem Mass Spectrometry (ESI-MS/MS)." *Biochimica et Biophysica Acta - Molecular and Cell Biology of Lipids* 1761 (1): 121–28. <https://doi.org/10.1016/j.bbalip.2005.12.007>.
- Liebisch, Gerhard, Wolfgang Drobnik, Bernd Lieser, and Gerd Schmitz. 2002. "High-Throughput Quantification of Lysophosphatidylcholine by Electrospray Ionization Tandem Mass Spectrometry." *Clinical Chemistry* 48 (12): 2217–24. <https://doi.org/10.1093/clinchem/48.12.2217>.
- Liebisch, Gerhard, Bernd Lieser, Jan Rathenberg, Wolfgang Drobnik, and Gerd Schmitz. 2004. "High-Throughput Quantification of Phosphatidylcholine and Sphingomyelin by Electrospray Ionization Tandem Mass Spectrometry Coupled with Isotope Correction Algorithm." *Biochimica et Biophysica Acta - Molecular and Cell Biology of Lipids* 1686 (1–2): 108–17. <https://doi.org/10.1016/j.bbalip.2004.09.003>.
- Liebisch, Gerhard, Juan Antonio Vizcaíno, Harald Köfeler, Martin Trötz Müller, William J. Griffiths, Gerd Schmitz, Friedrich Spener, and Michael J.O. Wakelam. 2013. "Shorthand Notation for Lipid Structures Derived from Mass Spectrometry." *Journal of Lipid Research* 54 (6): 1523–30. <https://doi.org/10.1194/jlr.M033506>.
- Lintonen, Tuulia P.I., Paul R.S. Baker, Matti Suoniemi, Baljit K. Ubhi, Kaisa M. Koistinen, Eva Duchoslav, J. Larry Campbell, and Kim Ekroos. 2014. "Differential Mobility Spectrometry-Driven Shotgun Lipidomics." *Analytical Chemistry*. <https://doi.org/10.1021/ac5021744>.
- Liu, Xiaotuan, Martin Rossmeisl, Jennifer McClaine, and Leslie P. Kozak. 2003. "Paradoxical Resistance to Diet-Induced Obesity in UCP1-Deficient Mice." *Journal of Clinical Investigation*

111 (3): 399–407. <https://doi.org/10.1172/jci15737>.

Lowell, Bradford B., Vedrana S-Susulic, Andreas Hamann, Joel A. Lawitts, Jean Himms-Hagen, Bert B. Boyer, Leslie P. Kozak, and Jeffrey S. Flier. 1993. "Development of Obesity in Transgenic Mice after Genetic Ablation of Brown Adipose Tissue." *Nature* 366 (6457): 740–42. <https://doi.org/10.1038/366740a0>.

Lu, Muwen, Yong Cao, Jie Xiao, Mingyue Song, and Chi Tang Ho. 2018. "Molecular Mechanisms of the Anti-Obesity Effect of Bioactive Ingredients in Common Spices: A Review." *Food and Function* 9 (9): 4569–81. <https://doi.org/10.1039/c8fo01349g>.

Ludwig, Tobias, Stefanie Worsch, Mathias Heikenwalder, Hannelore Daniel, Hans Hauner, and Bernhard L. Bader. 2013. "Metabolic and Immunomodulatory Effects of N-3 Fatty Acids Are Different in Mesenteric and Epididymal Adipose Tissue of Diet-Induced Obese Mice." *American Journal of Physiology - Endocrinology and Metabolism* 304 (11): E1140–56. <https://doi.org/10.1152/ajpendo.00171.2012>.

Luijten, Ineke H.N., Helena M. Feldmann, Gabriella von Essen, Barbara Cannon, and Jan Nedergaard. 2019. "In the Absence of UCP1-Mediated Diet-Induced Thermogenesis, Obesity Is Augmented Even in the Obesity-Resistant 129S Mouse Strain." *American Journal of Physiology - Endocrinology and Metabolism* 316 (5): E729–40. <https://doi.org/10.1152/ajpendo.00020.2019>.

Lund, Jens, Lesli Hingstrup Larsen, and Lotte Lauritzen. 2018. "Fish Oil as a Potential Activator of Brown and Beige Fat Thermogenesis." *Adipocyte* 7 (2): 88–95. <https://doi.org/10.1080/21623945.2018.1442980>.

Lynes, Matthew D., Luiz O. Leiria, Morten Lundh, Alexander Bartelt, Farnaz Shamsi, Tian Lian Huang, Hirokazu Takahashi, et al. 2017. "The Cold-Induced Lipokine 12,13-DiHOME Promotes Fatty Acid Transport into Brown Adipose Tissue." *Nature Medicine* 23 (5): 631–37. <https://doi.org/10.1038/nm.4297>.

Lynes, Matthew D., Farnaz Shamsi, Elahu Gosney Sustarsic, Luiz O. Leiria, Chih Hao Wang, Sheng Chiang Su, Tian Lian Huang, et al. 2018. "Cold-Activated Lipid Dynamics in Adipose Tissue Highlights a Role for Cardiolipin in Thermogenic Metabolism." *Cell Reports* 24 (3): 781–90. <https://doi.org/10.1016/j.celrep.2018.06.073>.

Maeda, Hayato, Masashi Hosokawa, Tokutake Sashima, and Kazuo Miyashita. 2007. "Dietary Combination of Fucoxanthin and Fish Oil Attenuates the Weight Gain of White Adipose Tissue and Decreases Blood Glucose in Obese/Diabetic KK-A y Mice." *Journal of Agricultural and Food Chemistry* 55 (19): 7701–6. <https://doi.org/10.1021/jf071569n>.

Marken Lichtenbelt, Wouter D. van, Joost W. Vanhommerig, Nanda M. Smulders, Jamie M.A.F.L.

- Drossaerts, Gerrit J. Kemerink, Nicole D. Bouvy, Patrick Schrauwen, and G.J. Jaap Teule. 2009. "Cold-Activated Brown Adipose Tissue in Healthy Men." *New England Journal of Medicine* 360 (15): 1500–1508. <https://doi.org/10.1056/nejmoa0808718>.
- Matias, Isabel, and Vincenzo Di Marzo. 2007. "Endocannabinoids and the Control of Energy Balance." *Trends in Endocrinology and Metabolism* 18 (1): 27–37. <https://doi.org/10.1016/j.tem.2006.11.006>.
- Maurer, Stefanie F., Sebastian Dieckmann, Karin Kleigrew, Cécilia Colson, Ez Zoubir Amri, and Martin Klingenspor. 2019. "Fatty Acid Metabolites as Novel Regulators of Non-Shivering Thermogenesis." In *Handbook of Experimental Pharmacology*, 251:183–214. Springer, Berlin, Heidelberg. https://doi.org/10.1007/164_2018_150.
- Maurer, Stefanie F., Sebastian Dieckmann, Jens Lund, Tobias Fromme, Anne Lundby Hess, Cécilia Colson, Louise Kjølbaek, et al. 2021. "No Effect of Dietary Fish Oil Supplementation on the Recruitment of Brown and Brite Adipocytes in Mice or Humans under Thermoneutral Conditions." *Molecular Nutrition and Food Research* 65 (2): 2000681. <https://doi.org/10.1002/mnfr.202000681>.
- Maurer, Stefanie F., Tobias Fromme, Lawrence I. Grossman, Maik Hüttemann, and Martin Klingenspor. 2015. "The Brown and Brite Adipocyte Marker Cox7a1 Is Not Required for Non-Shivering Thermogenesis in Mice." *Scientific Reports* 5 (1): 17704. <https://doi.org/10.1038/srep17704>.
- Maurer, Stefanie F., Tobias Fromme, Sabine Mocek, Anika Zimmermann, and Martin Klingenspor. 2020. "Uncoupling Protein 1 and the Capacity for Nonshivering Thermogenesis Are Components of the Glucose Homeostatic System." *American Journal of Physiology - Endocrinology and Metabolism* 318 (2): E198–215. <https://doi.org/10.1152/ajpendo.00121.2019>.
- McMurdie, Paul J., and Susan Holmes. 2014. "Waste Not, Want Not: Why Rarefying Microbiome Data Is Inadmissible." Edited by Alice Carolyn McHardy. *PLoS Computational Biology* 10 (4): e1003531. <https://doi.org/10.1371/journal.pcbi.1003531>.
- Mehrabian, M., F. T. Schulthess, M. Nebohacova, L. W. Castellani, Z. Zhou, J. Hartiala, J. Oberholzer, A. J. Lusis, K. Maedler, and H. Allayee. 2008. "Identification of ALOX5 as a Gene Regulating Adiposity and Pancreatic Function." *Diabetologia* 51 (6): 978–88. <https://doi.org/10.1007/s00125-008-1002-3>.
- Meyer, Carola W., Monja Willershäuser, Martin Jastroch, Bryan C. Rourke, Tobias Fromme, Rebecca Oelkrug, Gerhard Heldmaier, and Martin Klingenspor. 2010. "Adaptive Thermogenesis and Thermal Conductance in Wild-Type and UCP1-KO Mice." *American*

- Journal of Physiology - Regulatory Integrative and Comparative Physiology* 299 (5): R1396–1406. <https://doi.org/10.1152/ajpregu.00021.2009>.
- Meyer, Carola W.E., Dirk Korthaus, Wolfgang Jagla, Emmanuelle Cornali, Johannes Grosse, Helmut Fuchs, Martin Klingenspor, et al. 2004. "A Novel Missense Mutation in the Mouse Growth Hormone Gene Causes Semidominant Dwarfism, Hyperghrelinemia, and Obesity." *Endocrinology* 145 (5): 2531–41. <https://doi.org/10.1210/en.2003-1125>.
- Michaud, Andréanne, Nicolas Lacroix-Pépin, Mélissa Pelletier, Marleen Daris, Laurent Biertho, Michel A. Fortier, and André Tchernof. 2014. "Expression of Genes Related to Prostaglandin Synthesis or Signaling in Human Subcutaneous and Omental Adipose Tissue: Depot Differences and Modulation by Adipogenesis." *Mediators of Inflammation* 2014: 1–13. <https://doi.org/10.1155/2014/451620>.
- Miller, James L., Magdalena Blaszkiwicz, Cordell Beaton, Cory P. Johnson, Stephen Waible, Amanda L. Dubois, Amanda Klemmer, Michael Kiebish, and Kristy L. Townsend. 2019. "A Peroxidized Omega-3-Enriched Polyunsaturated Diet Leads to Adipose and Metabolic Dysfunction." *Journal of Nutritional Biochemistry* 64 (February): 50–60. <https://doi.org/10.1016/j.jnutbio.2018.10.010>.
- Mina, Amir I., Raymond A. LeClair, Katherine B. LeClair, David E. Cohen, Louise Lantier, and Alexander S. Banks. 2018. "CalR: A Web-Based Analysis Tool for Indirect Calorimetry Experiments." *Cell Metabolism* 28 (4): 656-666.e1. <https://doi.org/10.1016/j.cmet.2018.06.019>.
- Mukherjee, Jogeshwar, Aparna Baranwal, and Kimberly N. Schade. 2016. "Classification of Therapeutic and Experimental Drugs for Brown Adipose Tissue Activation: Potential Treatment Strategies for Diabetes and Obesity." *Current Diabetes Reviews* 12 (4): 414–28. <https://doi.org/10.2174/1573399812666160517115450>.
- Nair, AnroopB, and Shery Jacob. 2016. "A Simple Practice Guide for Dose Conversion between Animals and Human." *Journal of Basic and Clinical Pharmacy* 7 (2): 27. <https://doi.org/10.4103/0976-0105.177703>.
- Nedergaard, Jan, Tore Bengtsson, and Barbara Cannon. 2007. "Unexpected Evidence for Active Brown Adipose Tissue in Adult Humans." *American Journal of Physiology - Endocrinology and Metabolism* 293 (2): E444–52. <https://doi.org/10.1152/ajpendo.00691.2006>.
- Nedergaard, Jan, and Barbara Cannon. 2013. "UCP1 mRNA Does Not Produce Heat." *Biochimica et Biophysica Acta (BBA) - Molecular and Cell Biology of Lipids* 1831 (5): 943–49. <https://doi.org/10.1016/j.bbalip.2013.01.009>.
- Norheim, Frode, Torgrim Mikal Langleite, Marit Hjorth, Torgeir Holen, Anders Kielland, Hans

- Kristian Stadheim, Hanne Løvdal Gulseth, Kåre Inge Birkeland, Jørgen Jensen, and Christian A. Drevon. 2014. "The Effects of Acute and Chronic Exercise on PGC-1 α , Irisin and Browning of Subcutaneous Adipose Tissue in Humans." *FEBS Journal* 281 (3): 739–49. <https://doi.org/10.1111/febs.12619>.
- OECD. 2019. *The Heavy Burden of Obesity: The Economics of Prevention*. OECD Health Policy Studies. OECD. <https://doi.org/10.1787/67450d67-en>.
- Oeckl, Josef, Andrea Bast-Habersbrunner, Tobias Fromme, Martin Klingenspor, and Yongguo Li. 2020. "Isolation, Culture, and Functional Analysis of Murine Thermogenic Adipocytes." *STAR Protocols* 1 (3): 100118. <https://doi.org/10.1016/j.xpro.2020.100118>.
- Okla, Meshail, Jiyoung Kim, Karsten Koehler, and Soonkyu Chung. 2017. "Dietary Factors Promoting Brown and Beige Fat Development and Thermogenesis." *Advances in Nutrition* 8 (3): 473–83. <https://doi.org/10.3945/an.116.014332>.
- Oliveira, Tiago E., Ériqúe Castro, Thiago Belchior, Maynara L. Andrade, Adriano B. Chaves-Filho, Albert S. Peixoto, Mayara F. Moreno, et al. 2019. "Fish Oil Protects Wild Type and Uncoupling Protein 1-Deficient Mice from Obesity and Glucose Intolerance by Increasing Energy Expenditure." *Molecular Nutrition and Food Research* 63 (7): 1800813. <https://doi.org/10.1002/mnfr.201800813>.
- Ostermann, Annika I., and Nils Helge Schebb. 2017. "Effects of Omega-3 Fatty Acid Supplementation on the Pattern of Oxylipins: A Short Review about the Modulation of Hydroxy-, Dihydroxy-, and Epoxy-Fatty Acids." *Food and Function* 8 (7): 2355–67. <https://doi.org/10.1039/c7fo00403f>.
- Ostermann, Annika I., Patrick Waindok, Moritz J. Schmidt, Cheng Ying Chiu, Christopher Smyl, Nadine Rohwer, Karsten H. Weylandt, and Nils Helge Schebb. 2017. "Modulation of the Endogenous Omega-3 Fatty Acid and Oxylipin Profile in Vivo - A Comparison of the Fat-1 Transgenic Mouse with C57BL/6 Wildtype Mice on an Omega-3 Fatty Acid Enriched Diet." Edited by Olivier Barbier. *PLoS ONE* 12 (9): e0184470. <https://doi.org/10.1371/journal.pone.0184470>.
- Otero-Díaz, Berenice, Marcela Rodríguez-Flores, Verónica Sánchez-Muñoz, Fernando Monraz-Preciado, Samuel Ordoñez-Ortega, Vicente Becerril-Elias, Guillermina Baay-Guzmán, et al. 2018. "Exercise Induces White Adipose Tissue Browning Across the Weight Spectrum in Humans." *Frontiers in Physiology* 9 (December). <https://doi.org/10.3389/fphys.2018.01781>.
- Pahlavani, Mandana, Latha Ramalingam, Emily K. Miller, Shane Scoggin, Kalhara R. Menikdiwela, Nishan S. Kalupahana, William T. Festuccia, and Naima Moustaid-Moussa. 2019. "Eicosapentaenoic Acid Reduces Adiposity, Glucose Intolerance and Increases Oxygen

- Consumption Independently of Uncoupling Protein 1." *Molecular Nutrition and Food Research* 63 (7): 1800821. <https://doi.org/10.1002/mnfr.201800821>.
- Pahlavani, Mandana, Fitia Razafimanjato, Latha Ramalingam, Nishan S. Kalupahana, Hanna Moussa, Shane Scoggin, and Naima Moustaid-Moussa. 2017. "Eicosapentaenoic Acid Regulates Brown Adipose Tissue Metabolism in High-Fat-Fed Mice and in Clonal Brown Adipocytes." *Journal of Nutritional Biochemistry* 39 (January): 101–9. <https://doi.org/10.1016/j.jnutbio.2016.08.012>.
- Paradies, Giuseppe, Valeria Paradies, Francesca M. Ruggiero, and Giuseppe Petrosillo. 2019. "Role of Cardiopilin in Mitochondrial Function and Dynamics in Health and Disease: Molecular and Pharmacological Aspects." *Cells* 8 (7): 728. <https://doi.org/10.3390/cells8070728>.
- Park, Jin Won, Kyung Ho Jung, Jin Hee Lee, Cung Hoa Thien Quach, Seung Hwan Moon, Young Seok Cho, and Kyung Han Lee. 2015. "18F-FDG PET/CT Monitoring of B3 Agonist-Stimulated Brown Adipocyte Recruitment in White Adipose Tissue." *Journal of Nuclear Medicine* 56 (1): 153–58. <https://doi.org/10.2967/jnumed.114.147603>.
- Patsouris, David, Peter Qi, Abdikarim Abdullahi, Mile Stanojcic, Peter Chen, Alexandra Parousis, Saeid Amini-Nik, and Marc G. Jeschke. 2015. "Burn Induces Browning of the Subcutaneous White Adipose Tissue in Mice and Humans." *Cell Reports* 13 (8): 1538–44. <https://doi.org/10.1016/j.celrep.2015.10.028>.
- Petrovic, Natasa, Irina G. Shabalina, James A. Timmons, Barbara Cannon, and Jan Nedergaard. 2008. "Thermogenically Competent Nonadrenergic Recruitment in Brown Preadipocytes by a PPAR γ Agonist." *American Journal of Physiology - Endocrinology and Metabolism* 295 (2): E287–96. <https://doi.org/10.1152/ajpendo.00035.2008>.
- Pettitt, Stephen J., Qi Liang, Xin Y. Rairdan, Jennifer L. Moran, Haydn M. Prosser, David R. Beier, Kent C. Lloyd, Allan Bradley, and William C. Skarnes. 2009. "Agouti C57BL/6N Embryonic Stem Cells for Mouse Genetic Resources." *Nature Methods* 6 (7): 493–95. <https://doi.org/10.1038/nmeth.1342>.
- Pi-Sunyer, Xavier. 2009. "The Medical Risks of Obesity." *Postgraduate Medicine* 121 (6): 21–33. <https://doi.org/10.3810/pgm.2009.11.2074>.
- Pisani, Didier F., Rayane A. Ghandour, Guillaume E. Beranger, Pauline Le Faouder, Jean Claude Chambard, Maude Giroud, Alexandros Vegiopoulos, et al. 2014. "The Ω 6-Fatty Acid, Arachidonic Acid, Regulates the Conversion of White to Brite Adipocyte through a Prostaglandin/Calcium Mediated Pathway." *Molecular Metabolism* 3 (9): 834–47. <https://doi.org/10.1016/j.molmet.2014.09.003>.
- Plourde, Mélanie, and Stephen C. Cunnane. 2007. "Extremely Limited Synthesis of Long Chain

- Polyunsaturates in Adults: Implications for Their Dietary Essentiality and Use as Supplements." *Applied Physiology, Nutrition and Metabolism* 32 (4): 619–34. <https://doi.org/10.1139/H07-034>.
- Pucci, A., and R. L. Batterham. 2019. "Mechanisms Underlying the Weight Loss Effects of RYGB and SG: Similar, yet Different." *Journal of Endocrinological Investigation*. Springer International Publishing. <https://doi.org/10.1007/s40618-018-0892-2>.
- Purves, Robert D. 1992. "Optimum Numerical Integration Methods for Estimation of Area-under-the-Curve (AUC) and Area-under-the-Moment-Curve (AUMC)." *Journal of Pharmacokinetics and Biopharmaceutics* 20 (3): 211–26. <https://doi.org/10.1007/BF01062525>.
- Quast, Christian, Elmar Pruesse, Pelin Yilmaz, Jan Gerken, Timmy Schweer, Pablo Yarza, Jörg Peplies, and Frank Oliver Glöckner. 2013. "The SILVA Ribosomal RNA Gene Database Project: Improved Data Processing and Web-Based Tools." *Nucleic Acids Research* 41 (D1). <https://doi.org/10.1093/nar/gks1219>.
- Quesada-López, Tania, Rubén Cereijo, Jean Valery Turatsinze, Anna Planavila, Montserrat Cairó, Aleix Gavaldà-Navarro, Marion Peyrou, et al. 2016. "The Lipid Sensor GPR120 Promotes Brown Fat Activation and FGF21 Release from Adipocytes." *Nature Communications* 7 (1): 13479. <https://doi.org/10.1038/ncomms13479>.
- R Core Team. 2020. "R: A Language and Environment for Statistical Computing." *R: A Language and Environment for Statistical Computing*. R Foundation for Statistical Computing, Vienna, Austria. <https://www.r-project.org/>.
- Rådmark, Olof, Oliver Werz, Dieter Steinhilber, and Bengt Samuelsson. 2015. "5-Lipoxygenase, a Key Enzyme for Leukotriene Biosynthesis in Health and Disease." *Biochimica et Biophysica Acta - Molecular and Cell Biology of Lipids* 1851 (4): 331–39. <https://doi.org/10.1016/j.bbailip.2014.08.012>.
- Rim, Jong S., and Leslie P. Kozak. 2002. "Regulatory Motifs for CREB-Binding Protein and Nfe212 Transcription Factors in the Upstream Enhancer of the Mitochondrial Uncoupling Protein 1 Gene." *Journal of Biological Chemistry* 277 (37): 34589–600. <https://doi.org/10.1074/jbc.M108866200>.
- Rohart, Florian, Benoît Gautier, Amrit Singh, and Kim-Anh Lê Cao. 2017. "MixOmics: An R Package for 'omics Feature Selection and Multiple Data Integration." Edited by Dina Schneidman. *PLOS Computational Biology* 13 (11): e1005752. <https://doi.org/10.1371/journal.pcbi.1005752>.
- Rosenbaum, Michael, Jules Hirsch, Dymrna A. Gallagher, and Rudolph L. Leibel. 2008. "Long-Term Persistence of Adaptive Thermogenesis in Subjects Who Have Maintained a Reduced Body

- Weight." *American Journal of Clinical Nutrition* 88 (4): 906–12. <https://doi.org/10.1093/ajcn/88.4.906>.
- Rosenwald, Matthias, Alike Perdikari, Thomas Rüllicke, and Christian Wolfrum. 2013. "Bi-Directional Interconversion of Brite and White Adipocytes." *Nature Cell Biology* 15 (6): 659–67. <https://doi.org/10.1038/ncb2740>.
- Rothwell, Nancy J., and Michael J. Stock. 1979. "A Role for Brown Adipose Tissue in Diet-Induced Thermogenesis." *Nature* 281 (5726): 31–35. <https://doi.org/10.1038/281031a0>.
- Rowland, Leslie A., Santosh K. Maurya, Naresh C. Bal, Leslie Kozak, and Muthu Periasamy. 2016. "Sarcolipin and Uncoupling Protein 1 Play Distinct Roles in Diet-Induced Thermogenesis and Do Not Compensate for One Another." *Obesity* 24 (7): 1430–33. <https://doi.org/10.1002/oby.21542>.
- Ruban, Aruchuna, Kostadin Stoenchev, Hutan Ashrafian, and Julian Teare. 2019. "Current Treatments for Obesity." *Clinical Medicine, Journal of the Royal College of Physicians of London*. Royal College of Physicians. <https://doi.org/10.7861/clinmedicine.19-3-205>.
- Sakamoto, Tomoya, Takahiro Nitta, Koji Maruno, Yu Sheng Yeh, Hidetoshi Kuwata, Koichi Tomita, Tsuyoshi Goto, Nobuyuki Takahashi, and Teruo Kawada. 2016. "Macrophage Infiltration into Obese Adipose Tissues Suppresses the Induction of UCP1 Level in Mice." *American Journal of Physiology - Endocrinology and Metabolism* 310 (8): E676–87. <https://doi.org/10.1152/ajpendo.00028.2015>.
- Sato, Hiroyasu, Yoshitaka Taketomi, Yoshimi Miki, Remi Murase, Kei Yamamoto, and Makoto Murakami. 2020. "Secreted Phospholipase PLA2G2D Contributes to Metabolic Health by Mobilizing Ω 3 Polyunsaturated Fatty Acids in WAT." *Cell Reports* 31 (5): 107579. <https://doi.org/10.1016/j.celrep.2020.107579>.
- Schebb, Nils Helge, Annika I. Ostermann, Jun Yang, Bruce D. Hammock, Andreas Hahn, and Jan Philipp Schuchardt. 2014. "Comparison of the Effects of Long-Chain Omega-3 Fatty Acid Supplementation on Plasma Levels of Free and Esterified Oxylipins." *Prostaglandins and Other Lipid Mediators* 113–115: 21–29. <https://doi.org/10.1016/j.prostaglandins.2014.05.002>.
- Schindelin, Johannes, Ignacio Arganda-Carreras, Erwin Frise, Verena Kaynig, Mark Longair, Tobias Pietzsch, Stephan Preibisch, et al. 2012. "Fiji: An Open-Source Platform for Biological-Image Analysis." *Nature Methods* 9 (7): 676–82. <https://doi.org/10.1038/nmeth.2019>.
- Schnabl, Katharina, Yongguo Li, and Martin Klingenspor. 2020. "The Gut Hormone Secretin Triggers a Gut–Brown Fat–Brain Axis in the Control of Food Intake." *Experimental Physiology* 105 (8): 1206–13. <https://doi.org/10.1113/EP087878>.

- Schneider, Bradley B., Thomas R. Covey, Stephen L. Coy, Evgeny V. Krylov, and Erkinjon G. Nazarov. 2010. "Planar Differential Mobility Spectrometer as a Pre-Filter for Atmospheric Pressure Ionization Mass Spectrometry." *International Journal of Mass Spectrometry*. <https://doi.org/10.1016/j.ijms.2010.01.006>.
- Schoeler, Marc, and Robert Caesar. 2019. "Dietary Lipids, Gut Microbiota and Lipid Metabolism." *Reviews in Endocrine and Metabolic Disorders*. Springer. <https://doi.org/10.1007/s11154-019-09512-0>.
- Schweizer, Sabine, Gerhard Liebisch, Josef Oeckl, Marcus Hoering, Claudine Seeliger, Carolin Schiebel, Martin Klingenspor, and Josef Ecker. 2019. "The Lipidome of Primary Murine White, Brite, and Brown Adipocytes—Impact of Betaadrenergic Stimulation." *PLoS Biology* 17 (8): e3000412. <https://doi.org/10.1371/journal.pbio.3000412>.
- Shabalina, Irina G., Natasa Petrovic, Jasper M.A. deJong, Anastasia V. Kalinovich, Barbara Cannon, and Jan Nedergaard. 2013. "UCP1 in Brite/Beige Adipose Tissue Mitochondria Is Functionally Thermogenic." *Cell Reports* 5 (5): 1196–1203. <https://doi.org/10.1016/j.celrep.2013.10.044>.
- Sharp, Louis Z., Kosaku Shinoda, Haruya Ohno, David W. Scheel, Emi Tomoda, Lauren Ruiz, Houchun Hu, et al. 2012. "Human BAT Possesses Molecular Signatures That Resemble Beige/Brite Cells." Edited by Hironori Waki. *PLoS ONE* 7 (11): e49452. <https://doi.org/10.1371/journal.pone.0049452>.
- Shih, Mei Fen, and Peter V. Taberner. 1995. "Selective Activation of Brown Adipocyte Hormone-Sensitive Lipase and CAMP Production in the Mouse by B3-Adrenoceptor Agonists." *Biochemical Pharmacology* 50 (5): 601–8. [https://doi.org/10.1016/0006-2952\(95\)00185-3](https://doi.org/10.1016/0006-2952(95)00185-3).
- Shinoda, Kosaku, Ineke H.N. Luijten, Yutaka Hasegawa, Haemin Hong, Si B. Sonne, Miae Kim, Ruidan Xue, et al. 2015. "Genetic and Functional Characterization of Clonally Derived Adult Human Brown Adipocytes." *Nature Medicine* 21 (4): 389–94. <https://doi.org/10.1038/nm.3819>.
- Shiraki, Takuma, Narutoshi Kamiya, Sayaka Shiki, Takashi S. Kodama, Akira Kakizuka, and Hisato Jingami. 2005. "α,β-Unsaturated Ketone Is a Core Moiety of Natural Ligands for Covalent Binding to Peroxisome Proliferator-Activated Receptor γ." *Journal of Biological Chemistry* 280 (14): 14145–53. <https://doi.org/10.1074/jbc.M500901200>.
- Sidossis, Labros S., Craig Porter, Manish K. Saraf, Elisabet Børsheim, Ravi S. Radhakrishnan, Tony Chao, Arham Ali, et al. 2015. "Browning of Subcutaneous White Adipose Tissue in Humans after Severe Adrenergic Stress." *Cell Metabolism* 22 (2): 219–27. <https://doi.org/10.1016/j.cmet.2015.06.022>.

- Simopoulos, Artemis P. 2016. "An Increase in the Omega-6/Omega-3 Fatty Acid Ratio Increases the Risk for Obesity." *Nutrients* 8 (3): 128. <https://doi.org/10.3390/nu8030128>.
- Singh, Amrit, Casey P. Shannon, Benoît Gautier, Florian Rohart, Michaël Vacher, Scott J. Tebbutt, and Kim-Anh Lê Cao. 2019. "DIABLO: An Integrative Approach for Identifying Key Molecular Drivers from Multi-Omics Assays." Edited by Inanc Birol. *Bioinformatics* 35 (17): 3055–62. <https://doi.org/10.1093/bioinformatics/bty1054>.
- Skarnes, William C., Barry Rosen, Anthony P. West, Manousos Koutsourakis, Wendy Bushell, Vivek Iyer, Alejandro O. Mujica, et al. 2011. "A Conditional Knockout Resource for the Genome-Wide Study of Mouse Gene Function." *Nature* 474 (7351): 337–44. <https://doi.org/10.1038/nature10163>.
- Sun, Nan Nong, Tsung Yen Wu, and Chi Fai Chau. 2016. "Natural Dietary and Herbal Products in Anti-Obesity Treatment." *Molecules* 21 (10): 1351. <https://doi.org/10.3390/molecules21101351>.
- Sustarsic, Elahu G., Tao Ma, Matthew D. Lynes, Michael Larsen, Iuliia Karavaeva, Jesper F. Havelund, Carsten H. Nielsen, et al. 2018. "Cardiolipin Synthesis in Brown and Beige Fat Mitochondria Is Essential for Systemic Energy Homeostasis." *Cell Metabolism* 28 (1): 159–174.e11. <https://doi.org/10.1016/j.cmet.2018.05.003>.
- Takahashi, Y., and T. Ide. 2000. "Dietary N-3 Fatty Acids Affect mRNA Level of Brown Adipose Tissue Uncoupling Protein 1, and White Adipose Tissue Leptin and Glucose Transporter 4 in the Rat." *British Journal of Nutrition* 84 (2): 175–84. <https://doi.org/10.1017/s0007114500001409>.
- Takahashi, Yoko, Takashi Ide, and Hiroyuki Fujita. 2000. "Dietary Gamma-Linolenic Acid in the Form of Borage Oil Causes Less Body Fat Accumulation Accompanying an Increase in Uncoupling Protein 1 mRNA Level in Brown Adipose Tissue." *Comparative Biochemistry and Physiology - B Biochemistry and Molecular Biology* 127 (2): 213–22. [https://doi.org/10.1016/S0305-0491\(00\)00254-6](https://doi.org/10.1016/S0305-0491(00)00254-6).
- Tremaroli, Valentina, and Fredrik Bäckhed. 2012. "Functional Interactions between the Gut Microbiota and Host Metabolism." *Nature*. Nature Publishing Group. <https://doi.org/10.1038/nature11552>.
- Trigueros, L., S. Peña, A. V. Ugidos, E. Sayas-Barberá, J. A. Pérez-Álvarez, and E. Sendra. 2013. "Food Ingredients as Anti-Obesity Agents: A Review." *Critical Reviews in Food Science and Nutrition* 53 (9): 929–42. <https://doi.org/10.1080/10408398.2011.574215>.
- Tseng, Yu-Hua, Aaron M. Cypess, and C. Ronald Kahn. 2010. "Cellular Bioenergetics as a Target for Obesity Therapy." *Nature Reviews Drug Discovery* 9 (6): 465–82.

<https://doi.org/10.1038/nrd3138>.

- Tsuboyama-Kasaoka, Nobuyo, Mayumi Takahashi, Hyounju Kim, and Osamu Ezaki. 1999. "Up-Regulation of Liver Uncoupling Protein-2 mRNA by Either Fish Oil Feeding or Fibrate Administration in Mice." *Biochemical and Biophysical Research Communications* 257 (3): 879–85. <https://doi.org/10.1006/bbrc.1999.0555>.
- Tsugawa, Hiroshi, Kazutaka Ikeda, Mikiko Takahashi, Aya Satoh, Yoshifumi Mori, Haruki Uchino, Nobuyuki Okahashi, et al. 2020. "A Lipidome Atlas in MS-DIAL 4." *Nature Biotechnology* 38 (10): 1159–63. <https://doi.org/10.1038/s41587-020-0531-2>.
- U Din, Mueez, Teemu Saari, Juho Raiko, Nobu Kudomi, Stefanie F. Maurer, Minna Lahesmaa, Tobias Fromme, et al. 2018. "Postprandial Oxidative Metabolism of Human Brown Fat Indicates Thermogenesis." *Cell Metabolism* 28 (2): 207-216.e3. <https://doi.org/10.1016/j.cmet.2018.05.020>.
- Umeno, Aya, Mami Sakashita, Sakiko Sugino, Kazutoshi Murotomi, Tsugumi Okuzawa, Naoki Morita, Kentaro Tomii, et al. 2020. "Comprehensive Analysis of PPAR γ Agonist Activities of Stereo-, Regio-, and Enantio-Isomers of Hydroxyoctadecadienoic Acids." *Bioscience Reports* 40 (4). <https://doi.org/10.1042/BSR20193767>.
- Vegiopoulos, Alexandras, Karin Müller-Decker, Daniela Strzoda, Iris Schmitt, Evgeny Chichelnitskiy, Anke Ostertag, Mauricio Berriel Diaz, et al. 2010. "Cyclooxygenase-2 Controls Energy Homeostasis in Mice by de Novo Recruitment of Brown Adipocytes." *Science* 328 (5982): 1158–61. <https://doi.org/10.1126/science.1186034>.
- Villarroya, Francesc, Marion Peyrou, and Marta Giralt. 2017. "Transcriptional Regulation of the Uncoupling Protein-1 Gene." *Biochimie* 134 (March): 86–92. <https://doi.org/10.1016/j.biochi.2016.09.017>.
- Villarroya, Joan, Pavel Flachs, Ibon Redondo-Angulo, Marta Giralt, Dasa Medrikova, Francesc Villarroya, Jan Kopecky, and Anna Planavila. 2014. "Fibroblast Growth Factor-21 and the Beneficial Effects of Long-Chain n-3 Polyunsaturated Fatty Acids." *Lipids* 49 (11): 1081–89. <https://doi.org/10.1007/s11745-014-3948-x>.
- Virtanen, Kirsi A., Martin E. Lidell, Janne Orava, Mikael Heglind, Rickard Westergren, Tarja Niemi, Markku Taittonen, et al. 2009. "Functional Brown Adipose Tissue in Healthy Adults." *New England Journal of Medicine* 360 (15): 1518–25. <https://doi.org/10.1056/nejmoa0808949>.
- Virtue, Sam, and Antonio Vidal-Puig. 2013. "Assessment of Brown Adipose Tissue Function." *Frontiers in Physiology* 4 (June): 128. <https://doi.org/10.3389/fphys.2013.00128>.
- Wang, Hui, Monja Willershäuser, Angelos Karlas, Dimitris Gorpas, Josefine Reber, Vasilis Ntziachristos, Stefanie Maurer, Tobias Fromme, Yongguo Li, and Martin Klingenspor. 2019.

- “A Dual Ucp1 Reporter Mouse Model for Imaging and Quantitation of Brown and Brite Fat Recruitment.” *Molecular Metabolism* 20 (February): 14–27. <https://doi.org/10.1016/j.molmet.2018.11.009>.
- Wang, Hui, Monja Willershäuser, Yongguo Li, Tobias Fromme, Katharina Schnabl, Andrea Bast-Habersbrunner, Samira Ramisch, Sabine Mocek, and Martin Klingenspor. 2021. “Uncoupling Protein-1 Expression Does Not Protect Mice from Diet-Induced Obesity.” *American Journal of Physiology-Endocrinology and Metabolism* 320 (2): E333–45. <https://doi.org/10.1152/ajpendo.00285.2020>.
- Wang, Ting, Youxue Wang, Yasuhide Kontani, Yoshinori Kobayashi, Yuzo Sato, Nozomu Mori, and Hitoshi Yamashita. 2008. “Evodiamine Improves Diet-Induced Obesity in a Uncoupling Protein-1-Independent Manner: Involvement of Antiadipogenic Mechanism and Extracellularly Regulated Kinase/Mitogen-Activated Protein Kinase Signaling.” *Endocrinology* 149 (1): 358–66. <https://doi.org/10.1210/en.2007-0467>.
- Wang, Xiaofeng, and Catherine B. Chan. 2015. “N-3 Polyunsaturated Fatty Acids and Insulin Secretion.” *Journal of Endocrinology* 224 (3): R97–106. <https://doi.org/10.1530/JOE-14-0581>.
- Watanabe, Hiroyuki, Joris Vriens, Jean Prenen, Guy Droogmans, Thomas Voets, and Bernd Nillus. 2003. “Anandamide and Arachidonic Acid Use Epoxyeicosatrienoic Acids to Activate TRPV4 Channels.” *Nature* 424 (6947): 434–38. <https://doi.org/10.1038/nature01807>.
- Wickham, Hadley. 2016. *Ggplot2: Elegant Graphics for Data Analysis*. Use R! Cham: Springer International Publishing. <https://doi.org/10.1007/978-3-319-24277-4>.
- Winn, Nathan C., Victoria J. Vieira-Potter, Michelle L. Gastecki, Rebecca J. Welly, Rebecca J. Scroggins, Terese M. Zidon, T’Keaya L. Gaines, et al. 2017. “Loss of UCP1 Exacerbates Western Diet-Induced Glycemic Dysregulation Independent of Changes in Body Weight in Female Mice.” *American Journal of Physiology - Regulatory Integrative and Comparative Physiology* 312 (1): R74–84. <https://doi.org/10.1152/ajpregu.00425.2016>.
- Witting, Michael, Tanja Verena Maier, Steve Garvis, and Philippe Schmitt-Kopplin. 2014. “Optimizing a Ultrahigh Pressure Liquid Chromatography-Time of Flight-Mass Spectrometry Approach Using a Novel Sub-2µm Core-Shell Particle for in Depth Lipidomic Profiling of *Caenorhabditis Elegans*.” *Journal of Chromatography A*. <https://doi.org/10.1016/j.chroma.2014.07.021>.
- Worsch, Stefanie, Mathias Heikenwalder, Hans Hauner, and Bernhard L. Bader. 2018. “Dietary N-3 Long-Chain Polyunsaturated Fatty Acids Upregulate Energy Dissipating Metabolic Pathways Conveying Anti-Obesogenic Effects in Mice.” *Nutrition and Metabolism* 15 (1): 1–

16. <https://doi.org/10.1186/s12986-018-0291-x>.
- Wu, Jun, Pontus Boström, Lauren M. Sparks, Li Ye, Jang Hyun Choi, An Hoa Giang, Melin Khandekar, et al. 2012. "Beige Adipocytes Are a Distinct Type of Thermogenic Fat Cell in Mouse and Human." *Cell* 150 (2): 366–76. <https://doi.org/10.1016/j.cell.2012.05.016>.
- Wu, Tsung-Ru, Chuan-Sheng Lin, Chih-Jung Chang, Tzu-Lung Lin, Jan Martel, Yun-Fei Ko, David M. Ojcius, Chia-Chen Lu, John D. Young, and Hsin-Chih Lai. 2019. "Gut Commensal Parabacteroides Goldsteinii Plays a Predominant Role in the Anti-Obesity Effects of Polysaccharides Isolated from Hirsutiella Sinensis." *Gut* 68 (2): 248–62. <https://doi.org/10.1136/gutjnl-2017-315458>.
- Xu, Hu, Jia Lin Fu, Yi Fei Miao, Chun Jiong Wang, Qi Fei Han, Sha Li, Shi Zheng Huang, et al. 2016. "Prostaglandin E2 Receptor EP3 Regulates Both Adipogenesis and Lipolysis in Mouse White Adipose Tissue." *Journal of Molecular Cell Biology* 8 (6): 518–29. <https://doi.org/10.1093/jmcb/mjw035>.
- Ye, L., Sandra Kleiner, Jun Wu, Rajan Sah, Rana K. Gupta, Alexander S. Banks, Paul Cohen, et al. 2012. "TRPV4 Is a Regulator of Adipose Oxidative Metabolism, Inflammation, and Energy Homeostasis." *Cell* 151 (1): 96–110. <https://doi.org/10.1016/j.cell.2012.08.034>.
- Yoneshiro, Takeshi, Sayuri Aita, Mami Matsushita, Takashi Kayahara, Toshimitsu Kameya, Yuko Kawai, Toshihiko Iwanaga, and Masayuki Saito. 2013. "Recruited Brown Adipose Tissue as an Antiobesity Agent in Humans." *Journal of Clinical Investigation* 123 (8): 3404–8. <https://doi.org/10.1172/JCI67803>.
- Yoneshiro, Takeshi, Mami Matsushita, and Masayuki Saito. 2019. "Translational Aspects of Brown Fat Activation by Food-Derived Stimulants." In *Handbook of Experimental Pharmacology*, 251:359–79. https://doi.org/10.1007/164_2018_159.
- Yoon, Seok Hwan, Sung Min Ha, Soonjae Kwon, Jeongmin Lim, Yeseul Kim, Hyungseok Seo, and Jongsik Chun. 2017. "Introducing EzBioCloud: A Taxonomically United Database of 16S RRNA Gene Sequences and Whole-Genome Assemblies." *International Journal of Systematic and Evolutionary Microbiology*. <https://doi.org/10.1099/ijsem.0.001755>.
- You, Mikyoung, Rong Fan, Judy Kim, Seung Ho Shin, and Soonkyu Chung. 2020. "Alpha-Linolenic Acid-Enriched Butter Promotes Fatty Acid Remodeling and Thermogenic Activation in the Brown Adipose Tissue." *Nutrients* 12 (1): 136. <https://doi.org/10.3390/nu12010136>.
- Zemski Berry, Karin A., and Robert C. Murphy. 2004. "Electrospray Ionization Tandem Mass Spectrometry of Glycerophosphoethanolamine Plasmalogen Phospholipids." *Journal of the American Society for Mass Spectrometry* 15 (10): 1499–1508. <https://doi.org/10.1016/j.jasms.2004.07.009>.

- Zhao, Ming, and Xiaoli Chen. 2014. "Eicosapentaenoic Acid Promotes Thermogenic and Fatty Acid Storage Capacity in Mouse Subcutaneous Adipocytes." *Biochemical and Biophysical Research Communications* 450 (4): 1446–51. <https://doi.org/10.1016/j.bbrc.2014.07.010>.
- Zhuang, Pan, Yanhua Lu, Qiyang Shou, Lei Mao, Lilin He, Jun Wang, Jingnan Chen, Yu Zhang, and Jingjing Jiao. 2019. "Differential Anti-Adipogenic Effects of Eicosapentaenoic and Docosahexaenoic Acids in Obesity." *Molecular Nutrition and Food Research* 63 (14): 1801135. <https://doi.org/10.1002/mnfr.201801135>.
- Ziętak, Marika, Petia Kovatcheva-Datchary, Lidia H. Markiewicz, Marcus Ståhlman, Leslie P. Kozak, and Fredrik Bäckhed. 2016. "Altered Microbiota Contributes to Reduced Diet-Induced Obesity upon Cold Exposure." *Cell Metabolism* 23 (6): 1216–23. <https://doi.org/10.1016/j.cmet.2016.05.001>.
- Ziętak, Marika, and Leslie P. Kozak. 2016. "Bile Acids Induce Uncoupling Protein 1-Dependent Thermogenesis and Stimulate Energy Expenditure at Thermoneutrality in Mice." *American Journal of Physiology - Endocrinology and Metabolism* 310 (5): E346–54. <https://doi.org/10.1152/ajpendo.00485.2015>.
- Zimmermann, Robert, Juliane G. Strauss, Guenter Haemmerle, Gabriele Schoiswohl, Ruth Birner-Gruenberger, Monika Riederer, Achim Lass, et al. 2004. "Fat Mobilization in Adipose Tissue Is Promoted by Adipose Triglyceride Lipase." *Science* 306 (5700): 1383–86. <https://doi.org/10.1126/science.1100747>.

EIDESSTATTLICHE ERKLÄRUNG

Ich erkläre des Eides statt, dass ich die bei der promotionsführenden Einrichtung der TUM zur Promotionsprüfung vorgelegte Arbeit mit dem Titel:

The relationship between lipid metabolites and the recruitment of uncoupling protein 1

Am Lehrstuhl für molekulare Ernährungsmedizin unter der Anleitung und Betreuung durch: Prof. Dr. Martin Klingenspor ohne sonstige Hilfe erstellt und bei der Abfassung nur die gemäß § 6 Ab. Und 7 Satz 2 angebotenen Hilfsmittel benutzt habe.

Ich habe keine Organisation eingeschaltet, die gegen Entgelt Betreuerinnen und Betreuer für die Anfertigung von Dissertationen sucht, oder die mir obliegenden Pflichten hinsichtlich der Prüfungsleistungen für mich ganz oder teilweise erledigt.

Ich habe die Dissertation in dieser oder ähnlicher Form in keinem anderen Prüfungsverfahren als Prüfungsleistung vorgelegt.

Die vollständige Dissertation wurde noch nicht veröffentlicht.

Ich habe den angestrebten Doktorgrad noch nicht erworben und bin nicht in einem früheren Promotionsverfahren für den angestrebten Doktorgrad gescheitert.

Die öffentlich zugängliche Promotionsordnung der TUM ist mir bekannt, insbesondere habe ich die Bedeutung von § 28 (Nichtigkeit der Promotion) und § 29 (Entzug des Doktorgrades) zur Kenntnis genommen. Ich bin mir der Konsequenzen einer falschen Eidesstattlichen Erklärung bewusst.

Mit der Aufnahme meiner personenbezogenen Daten in die Alumni-Datei bei der TUM bin ich einverstanden.

Weinheim, den _____

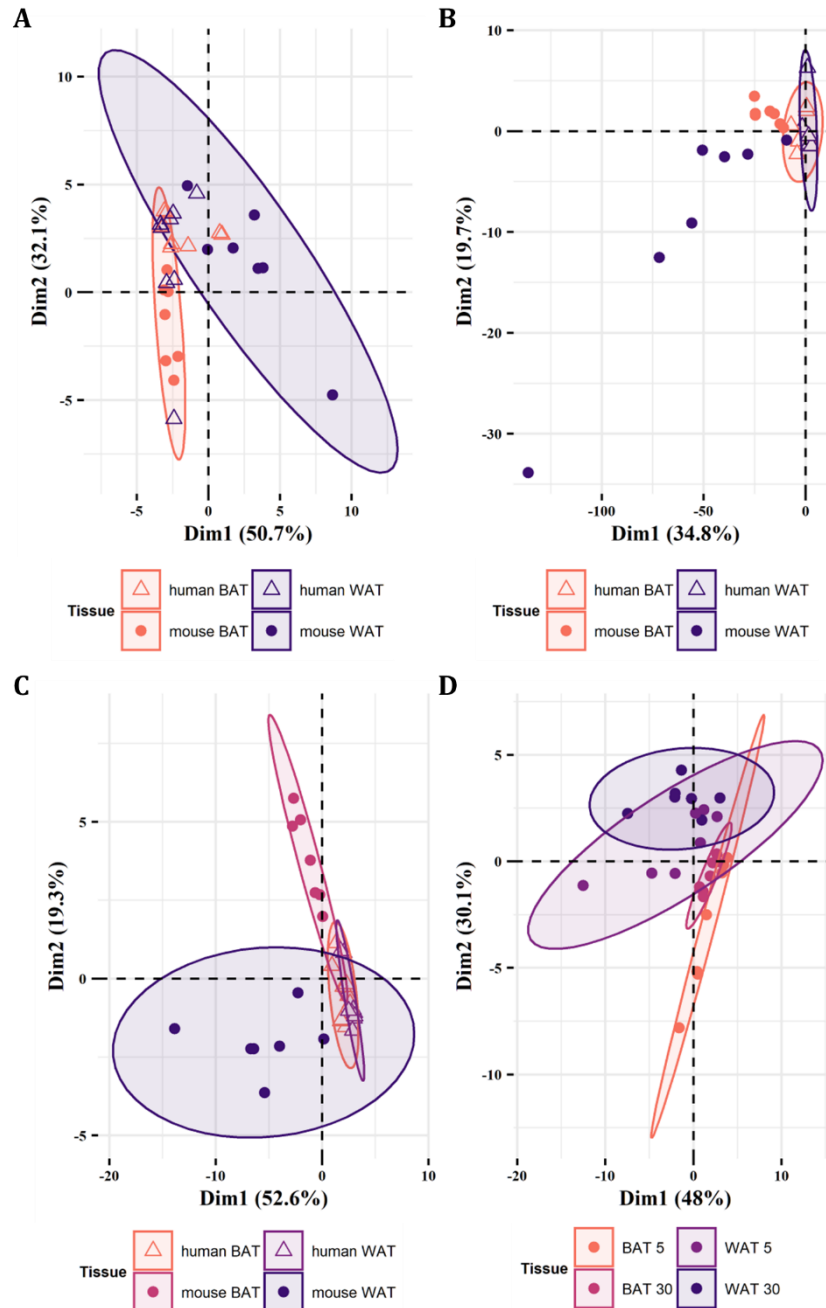
Sebastian Dieckmann

PUBLICATION LIST

- Maurer, S. F., Dieckmann, S., Kleigrewe, K., Colson, C., Amri, E. Z., & Klingenspor, M. (2019). Fatty acid metabolites as novel regulators of non-shivering thermogenesis. In *Handbook of Experimental Pharmacology* (Vol. 251, pp. 183–214). Springer, Berlin, Heidelberg. https://doi.org/10.1007/164_2018_150
- Dieckmann, S., Maurer, S., Fromme, T., Colson, C., Virtanen, K. A., Amri, E. Z., & Klingenspor, M. (2020). Fatty Acid Metabolite Profiling Reveals Oxylipins as Markers of Brown but Not Brite Adipose Tissue. *Frontiers in Endocrinology*, *11*(February). <https://doi.org/10.3389/fendo.2020.00073>
- Maurer, S. F., Dieckmann, S., Lund, J., Fromme, T., Hess, A. L., Colson, C., Kjølback, L., Astrup, A., Gillum, M. P., Larsen, L. H., Liebisch, G., Amri, E. Z., & Klingenspor, M. (2021). No Effect of Dietary Fish Oil Supplementation on the Recruitment of Brown and Brite Adipocytes in Mice or Humans under Thermoneutral Conditions. *Molecular Nutrition and Food Research*, *65*(2), 2000681. <https://doi.org/10.1002/mnfr.202000681>

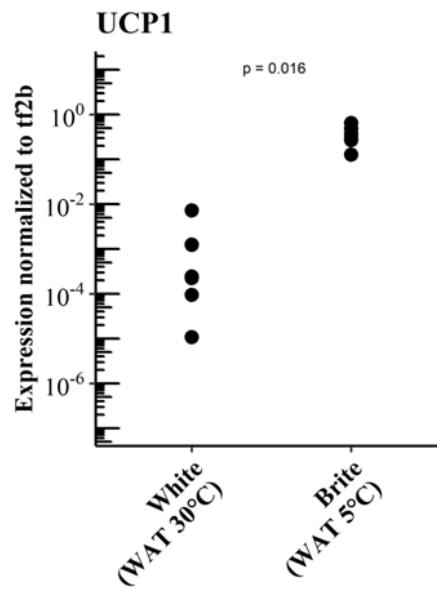
SUPPLEMENTS

Chapter 3: Fatty Acid Metabolite Profiling Reveals Oxylipins As Markers Of Brown But not Brite Adipose Tissue



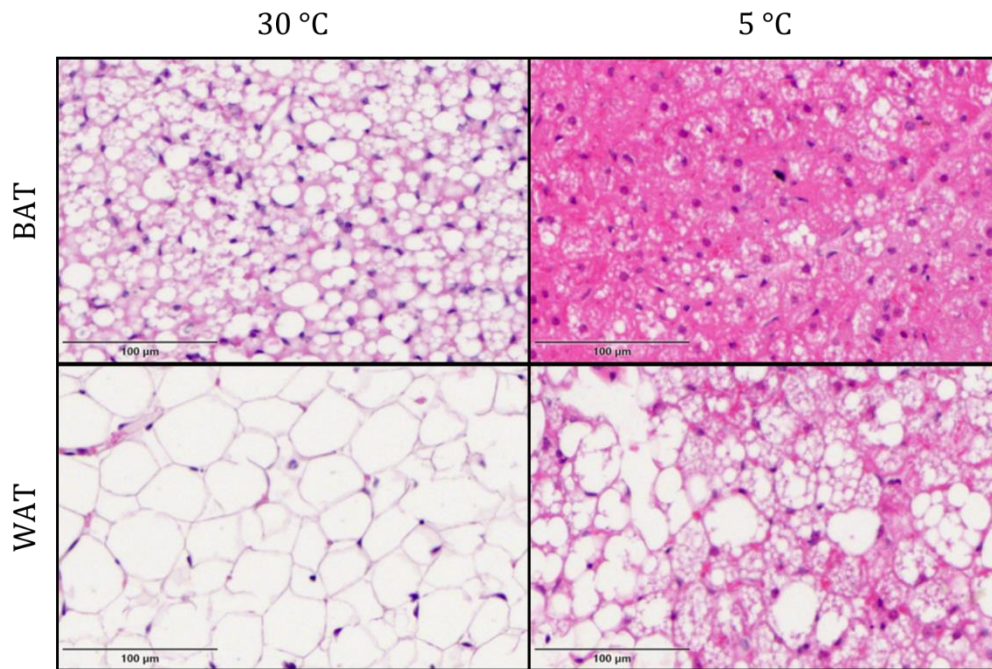
Supplementary Figure 1: Murine BAT but not brite or human BAT can be separated by oxylipin profiles.

(A) Principal component analysis of the oxylipins in human ($n = 8$) and murine ($n = 7$) BAT and WAT. (B) Predicted projection of human BAT and WAT based on principal components of oxylipins in murine BAT and WAT. (C) Predicted projection of murine BAT and WAT based on principal components of oxylipins in human BAT and WAT. (D) PCA of oxylipins in murine BAT and WAT acclimatized to 5 °C or 30 °C for one week ($n = 7$ for each temperature).



Supplementary Figure 2: Increased UCP1 expression in brite adipose tissue.

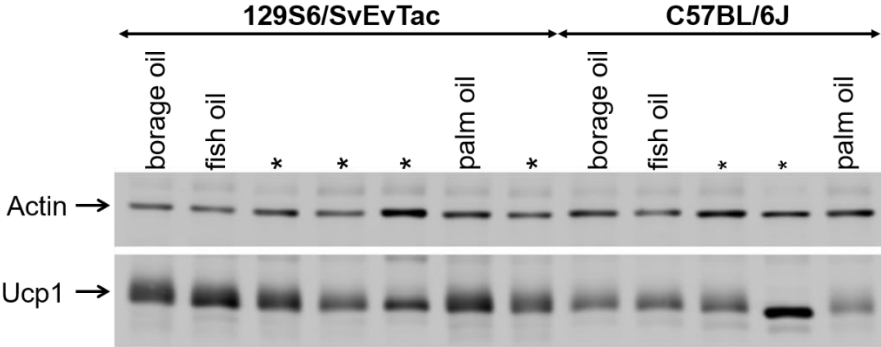
UCP1 mRNA expression in white adipose tissue of mice acclimatized to 30 °C (white) and 5 °C (brite) ($n = 7$). *P*-value determined by unpaired Wilcoxon test.



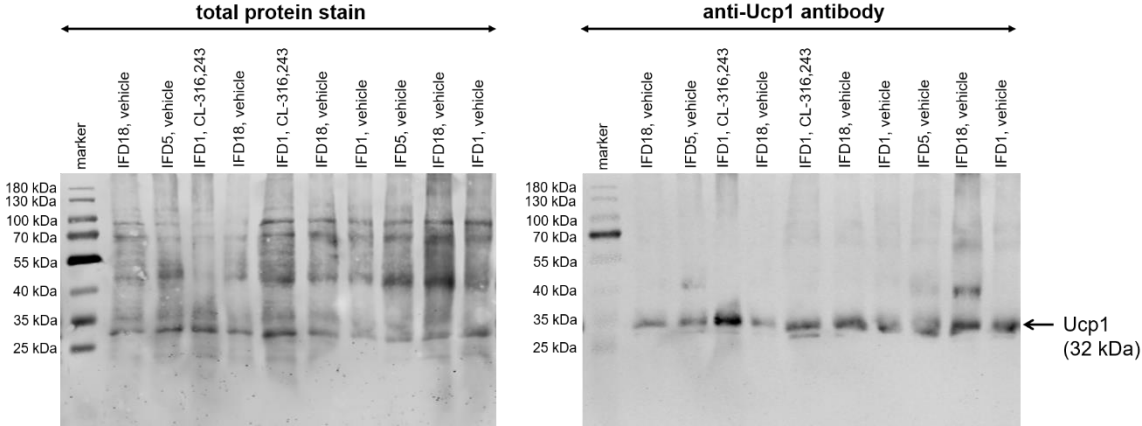
Supplementary Figure 3: Cold stimulation increases the abundance of multilocular brite adipocytes in WAT.

Representative images of H&E stained sections of BAT (upper panel) and WAT (lower panel) of mice acclimatized to 30 °C (left) or 5 °C (middle). For H&E staining, tissues were immediately fixed in 4 % paraformaldehyde, dehydrated and subsequently embedded in paraffin. Tissue sections of 5 µm thickness were deparaffinized and stained with hematoxylin and eosin.

Chapter 4: No Effect of Dietary Fish Oil Supplementation on the Recruitment of Brown and Brite Adipocytes in Mice or Humans under Thermoneutral conditions

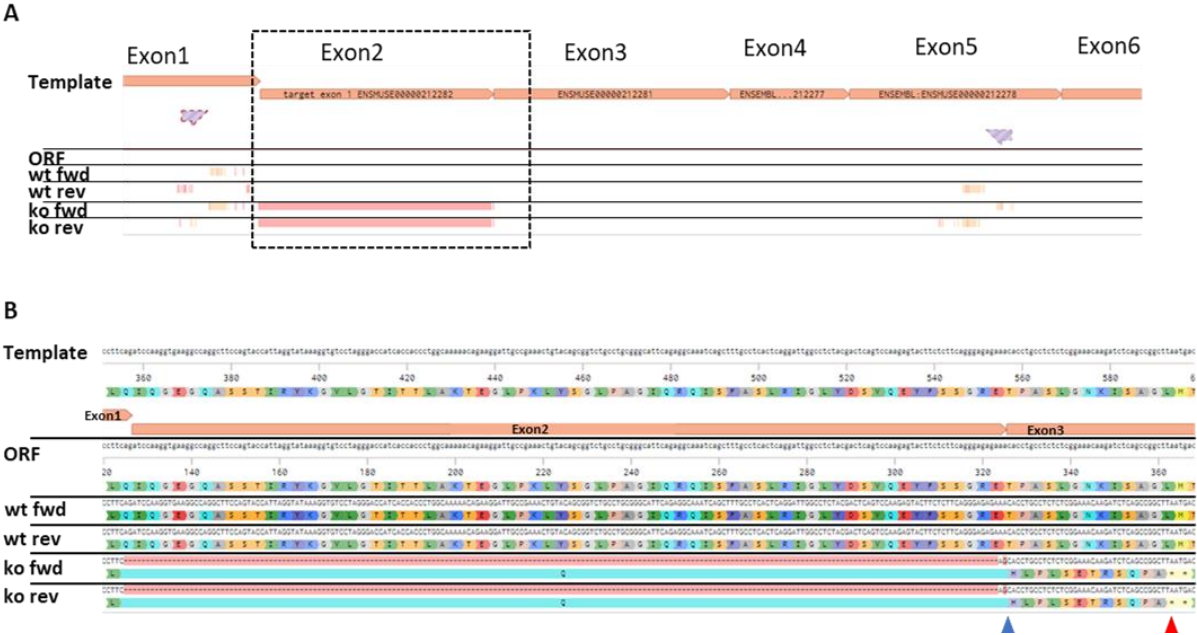


Supplementary Figure 4: Representative Western Blot image related to Figure 16 A.
Samples obtained from other mice () were analyzed on the same blot.*



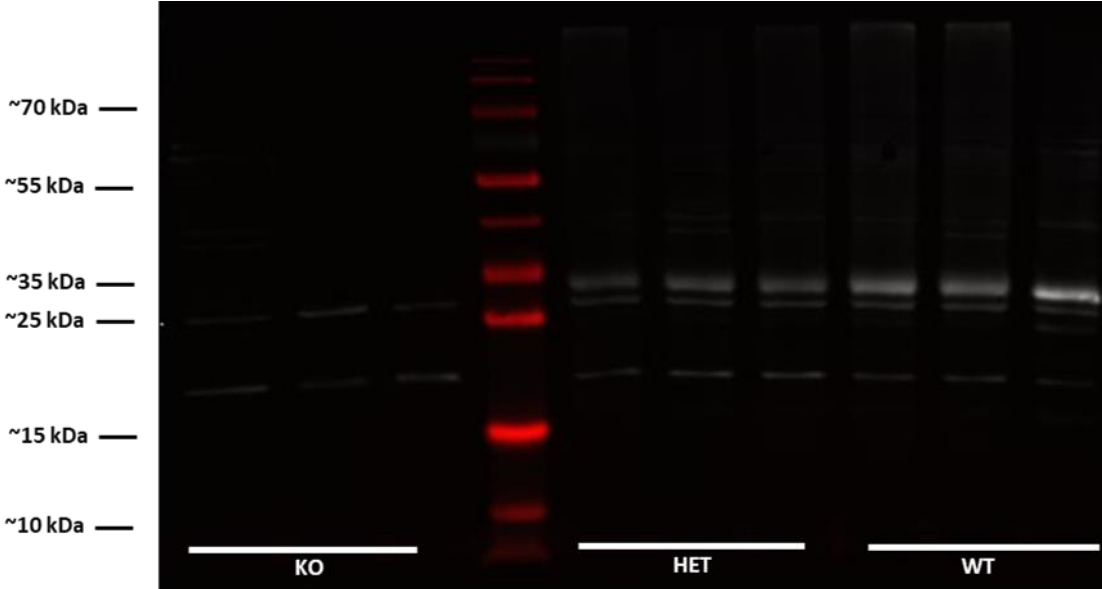
Supplementary Figure 5: Representative Western Blot images related to Figure 17 A.
Total protein and marker signals were detected at 700 nm and UCP1 signals at 800 nm.

Chapter 5: Susceptibility to Diet-induced Obesity at Thermoneutral Conditions is Independent of UCP1

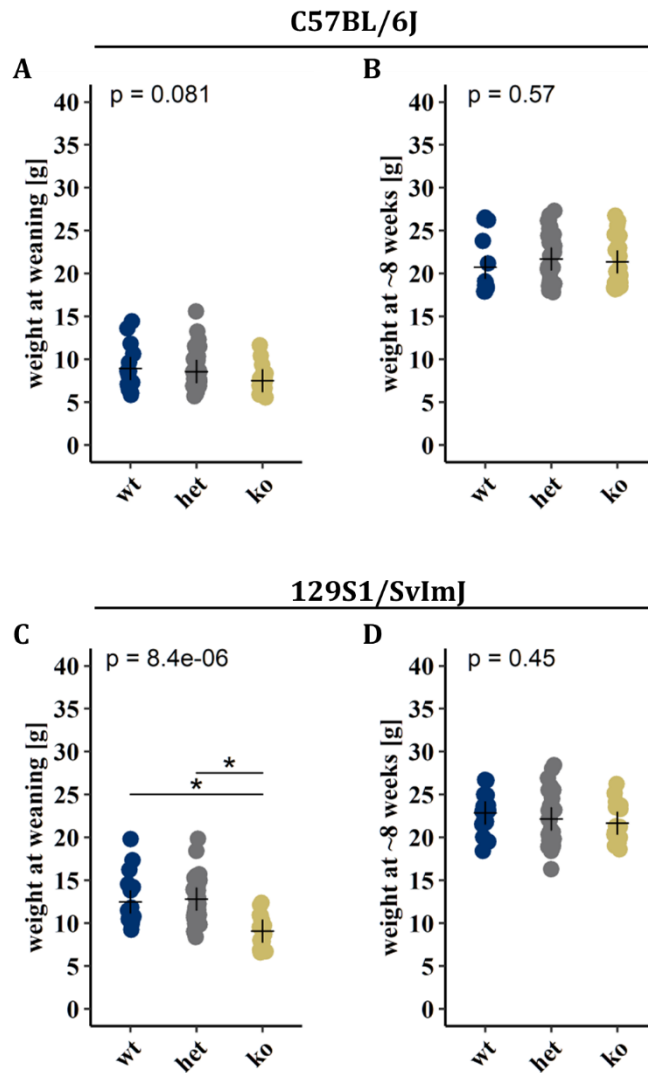


Supplementary Figure 6: Sequencing of RT-PCR products obtained from iBAT of Ucp1-KO and Ucp1-WT mice.

(A) Overview of the alignment of the Ucp1 coding sequence with open reading frame (ORF), as well as the sequencing results of Ucp1-WT (wt) and Ucp1-KO (ko) for forward (fwd) and reverse (rev) primer. (B) Magnification of the dashed box in (A), including amino acid translation matched to the ORF. Blue and red arrowhead indicate the position of the frame shift (blue) and the premature stop codon (red).

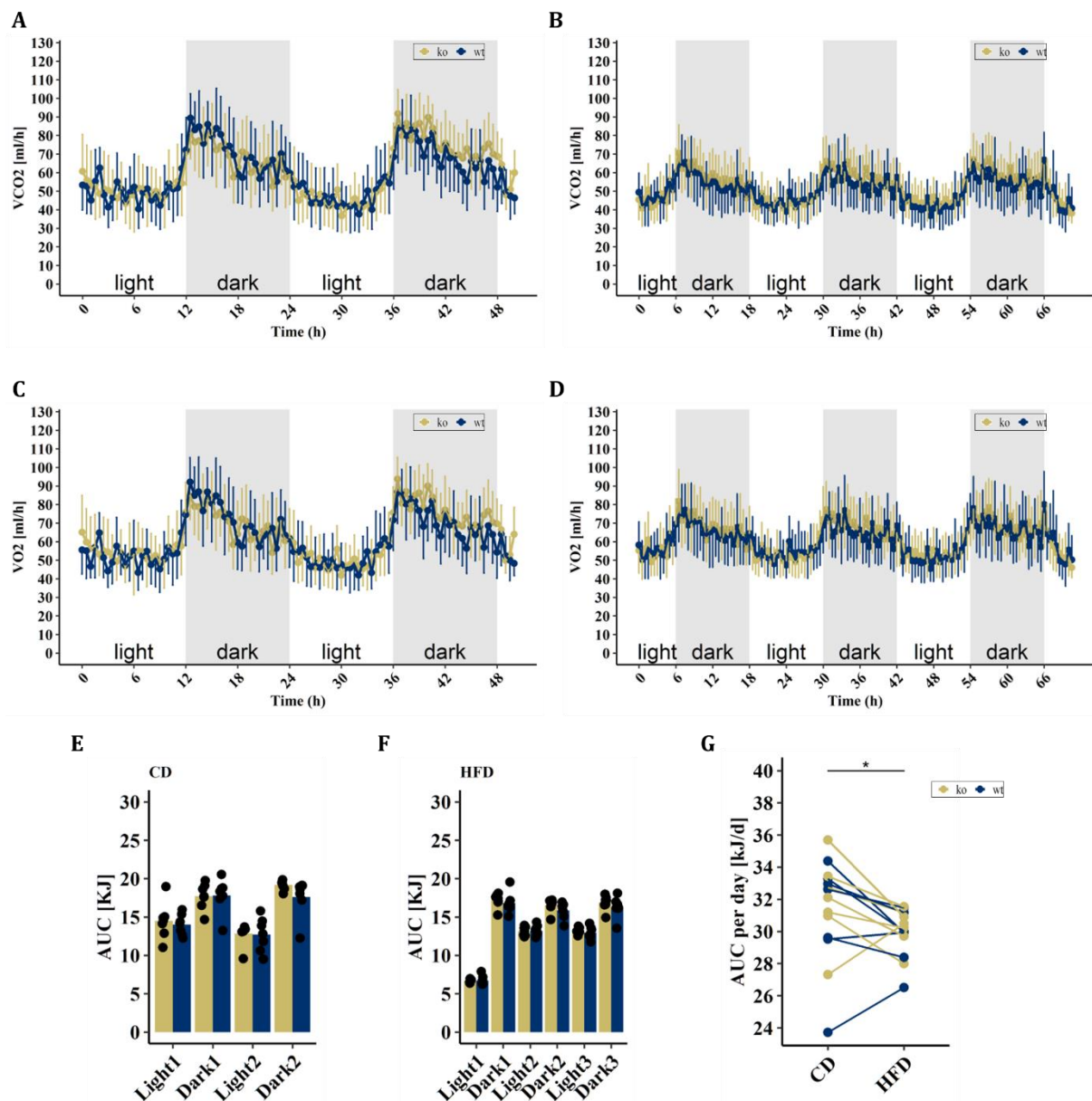


Supplementary Figure 7: Uncropped western blot image corresponding to Figure 1D. 800nm-Channel in white, 700nm-Channel in red.



Supplementary Figure 8: Body weights of offspring produced by HET/HET breeding of the conventional Ucp1-KO model on (A&B) C57BL/6J or (C&D) 129S1/SvImJ background.

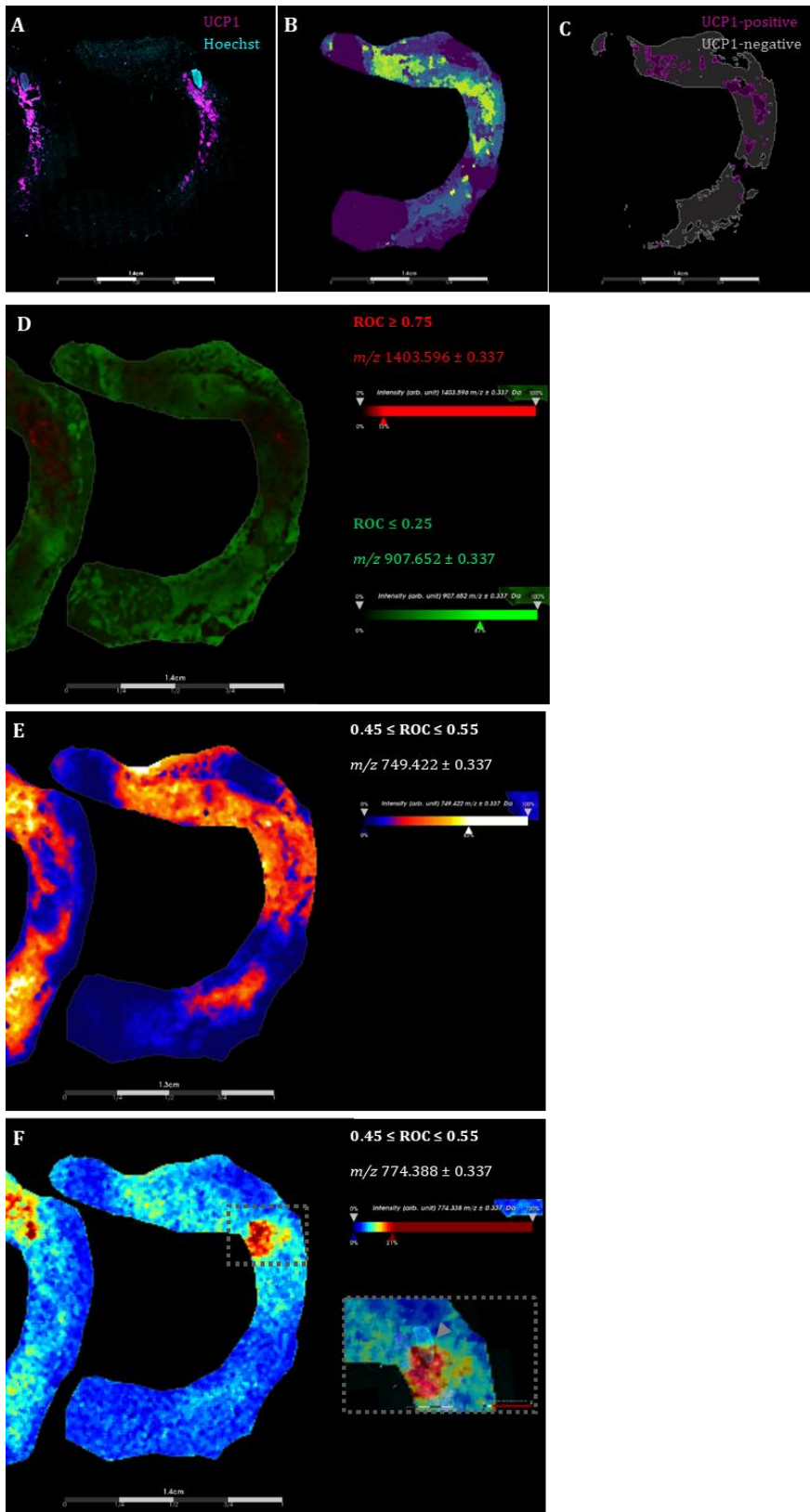
(A&C) at weaning ~3 weeks of age and (B&D) at the age of ~8-weeks. Crosses indicating group means. 1-Way ANOVA and t-test with bonferroni adjusted p-value, * = p-value < 0.05



Supplementary Figure 9: Energy expenditure at thermoneutrality is comparable between Ucp1-KO and UCP1-WT mice.

(A&B) CO₂ production and (C&D) VO₂ consumption during (A,C) CD and (B,D) HFD feeding. Area under the curve (AUC) of heat production during the different light phases corresponding to (E) Figure 31 E and (F) Figure 31 G. (G) Area under the curve (AUC) of heat production corresponding to Figure 31 E (CD) and Figure 31 G (HFD) per day. (A-D) Data represented as means and standard deviation, averaged over a period of 30 min. (E,F) Bars indicate group means. (G) Paired students *t*-test, * = *p*-value < 0.05

Chapter 6: Spatial Recruitment of Cardiolipins in White Adipose Tissue After Cold Stimulation is Independent of UCP1

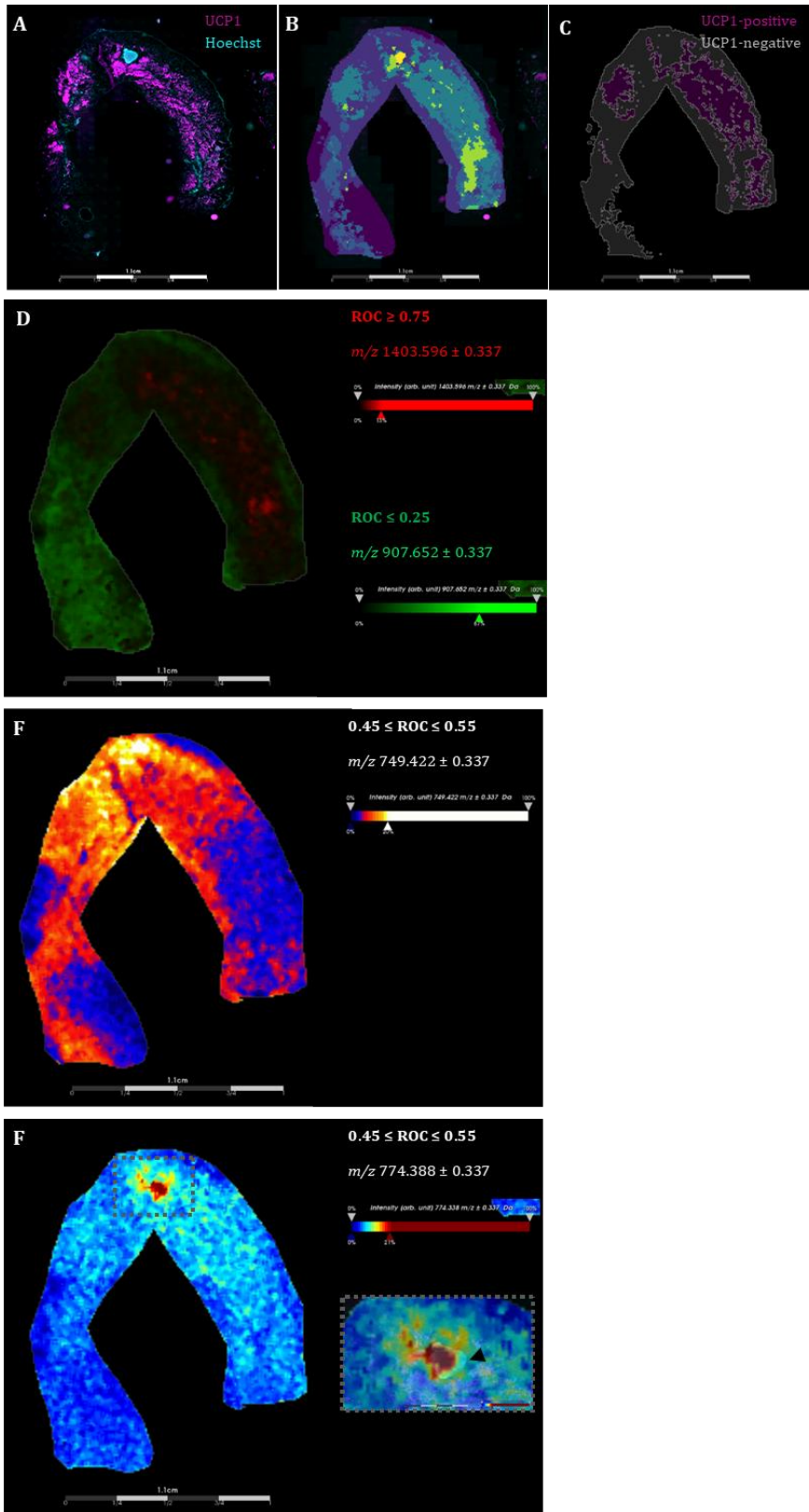


Supplementary Figure 10: Identification and validation of region-specific lipid species.

129S6/SvEvTac mice were housed at 5°C for 1 week. Inguinal white adipose tissue was dissected and four consecutive sections were prepared. The first used for MALDI-MSI, the second for immunohistochemistry staining of UCP1 and the last two for LC-MS/MS analysis.

(A) Immunohistochemistry of inguinal white adipose tissue stained for UCP1 (magenta) and Hoechst (cyan). **(B)** Segmentation map of the MALDI-data expanded to several levels to match the UCP1 pattern in B. **(C)** UCP1-positive (magenta) and UCP1-negative (grey) adipose tissue regions assigned based on the segmentation used for ROC-analysis. **(D)** MALDI images of two examples m/z intervals identified to be specific for the UCP1-negative (green, $ROC \leq 0.25$) and UCP1-positive (red, $ROC \geq 0.75$) regions depicted in D. **(E-F)** MALDI image of example m/z intervals not specific for any of the two regions assigned in D ($0.45 \leq ROC \leq 0.55$), being **(E)** ubiquitously present in the tissue or **(F)** associated to the lymph node. Inlet shows a magnification of the grey image.

dashed box overlaying the m/z image with the immunohistochemistry image. Black arrowhead indicates the lymph node.

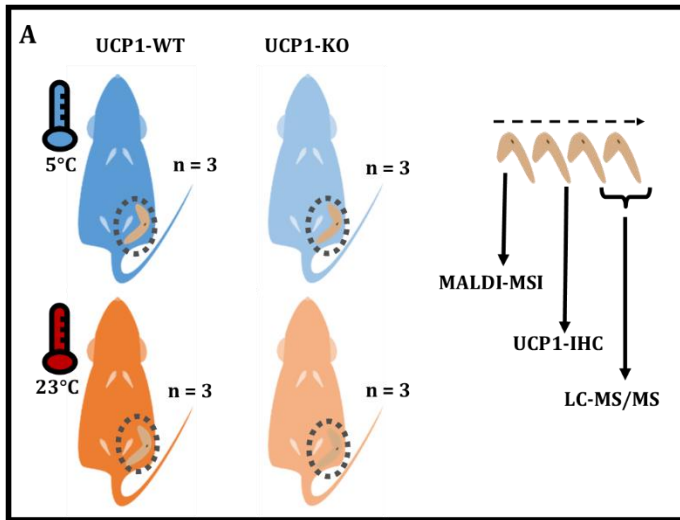


Supplementary Figure 11: Identification and validation of region-specific lipid species.

129S6/SvEvTac mice were housed at 5°C for 1 week. Inguinal white adipose tissue was dissected and four consecutive sections were prepared. The first used for MALDI-MSI, the second for immunohistochemistry staining of UCP1 and the last two for LC-MS/MS analysis.

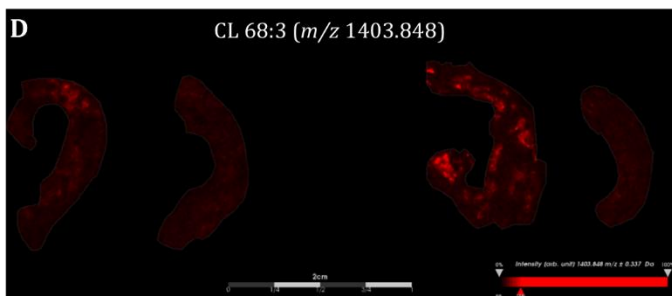
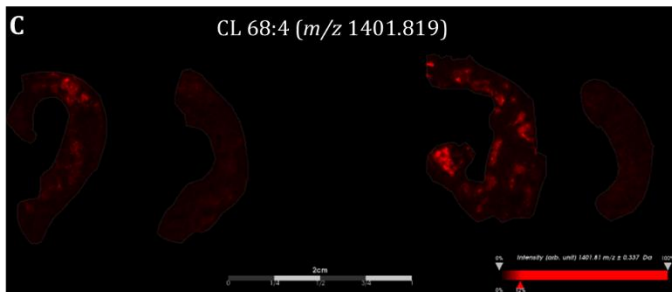
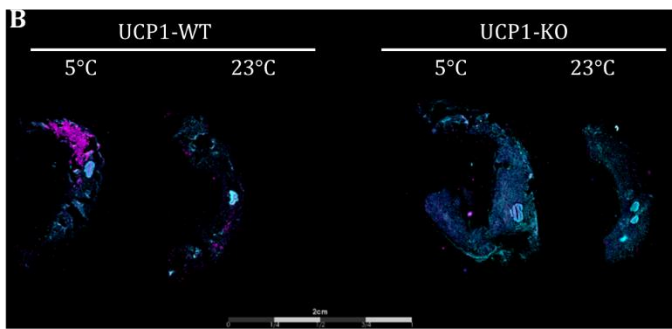
(A) Immunohistochemistry of inguinal white adipose tissue stained for UCP1 (magenta) and Hoechst (cyan). (B) Segmentation map of the MALDI-data expanded to several levels to match the UCP1 pattern in B. (C) UCP1-positive (magenta) and UCP1-negative (grey) adipose tissue regions assigned based on the segmentation used for ROC-analysis. (D) MALDI images of two examples m/z intervals identified to be specific for the UCP1-negative (green, $ROC \leq 0.25$) and UCP1-positive (red, $ROC \geq 0.75$) regions depicted in D. (E-F) MALDI image of example m/z intervals not specific for any of the two regions assigned in D ($0.45 \leq ROC \leq 0.55$), being (E) ubiquitously present in the tissue or (F) associated to the lymph node. Inlet shows a magnification of the grey

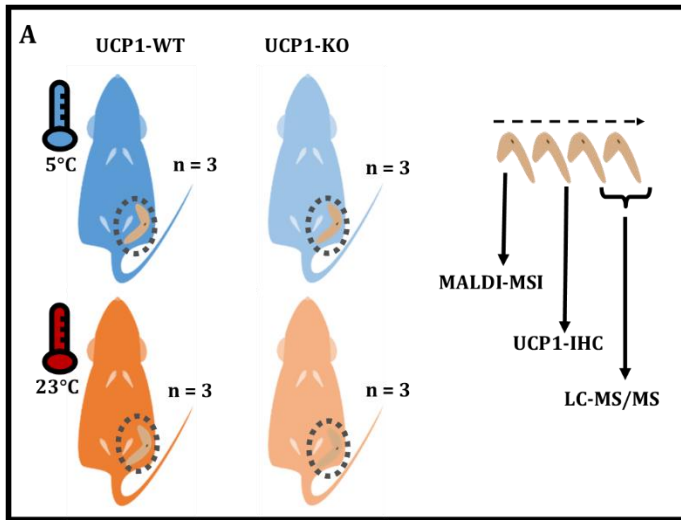
dashed box overlaying the m/z image with the immunohistochemistry image. Black arrowhead indicates the lymph node.



Supplementary Figure 12: CL 68:4 and CL 68:3 abundance is associated to cold, independent of UCP1.

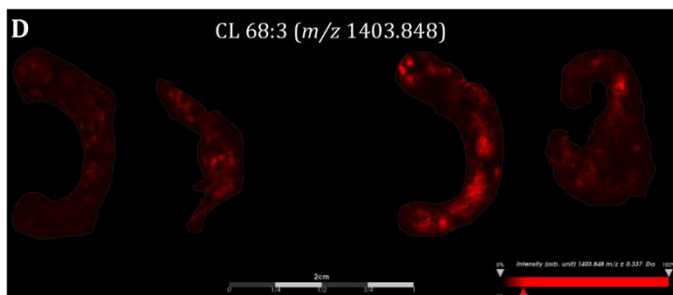
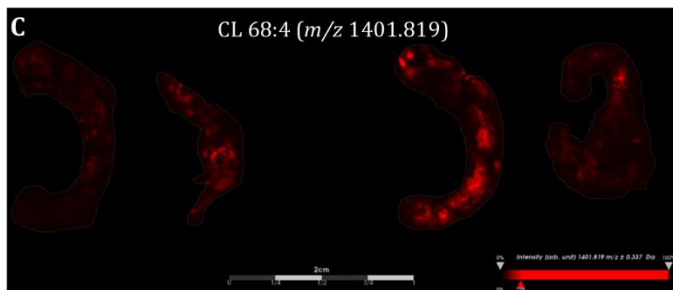
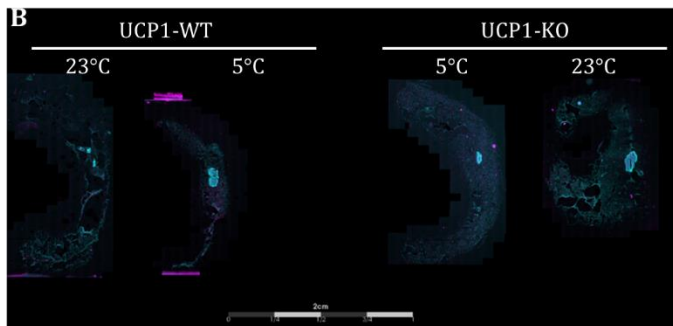
(A) Overview of the experimental setup. UCP1 knockout (UCP1-KO) and UCP1 wildtype (UCP1-WT) mice were either housed at 23°C or acclimatized to 5°C. Inguinal white adipose tissue was dissected (grey dashed circle). Four consecutive sections were prepared, the first used for MALDI-MSI, the second for immunohistochemistry staining of UCP1 and the last two for LC-MS/MS analysis. **(B)** Immunohistochemistry staining against UCP1 (magenta) and a Hoechst nuclear stain (cyan) of UCP1-WT and UCP1-KO mice. **(C-D)** MALDI images of **(C)** m/z 1401.819 \pm 0.338 Da representing CL 68:4 and **(D)** m/z 1403.848 \pm 0.338 Da representing CL 68:3.





Supplementary Figure 13: CL 68:4 and CL 68:3 abundance is associated to cold, independent of UCP1.

(A) Overview of the experimental setup. UCP1 knockout (UCP1-KO) and UCP1 wildtype (UCP1-WT) mice were either housed at 23°C or acclimatized to 5°C. Inguinal white adipose tissue was dissected (grey dashed circle). Four consecutive sections were prepared, the first used for MALDI-MSI, the second for immunohistochemistry staining of UCP1 and the last two for LC-MS/MS analysis. (B) Immunohistochemistry staining against UCP1 (magenta) and a Hoechst nuclear stain (cyan) of UCP1-WT and UCP1-KO mice. (C-D) MALDI images of (C) m/z 1401.819 \pm 0.338 Da representing CL 68:4 and (D) m/z 1403.848 \pm 0.338 Da representing CL 68:3.



ACKNOWLEDGMENTS

I would like to thank all the people who have supported me both scientifically and personally in the preparation of this work.

First, a great thanks to Martin for the possibility to work on this project. Thank you for your trust, support, and numerous ideas.

Second, thank you Stefanie for the excellent supervision during the first half of my project and the continuous support even after leaving the group. Without you this project would not have been successful.

Furthermore, I want to thank all my colleagues that helped me through my dissertation and made work a pleasant time. Thank you, Tobi, for always patiently answering every single question. Thank you, Eva and Josef, for always volunteering to help me to solve problems and the enjoyable times in the office that cheered me up. Special thanks to Kathi for always having an open ear for my problems, cheering me up and supporting the editing of my dissertation.

Thanks to all our collaboration partners that contributed enormously to the success of this work. Special thanks to Zoubir and Cécilia for your (hands-on) support during the project.

Furthermore, I would also like to acknowledge the German Research Foundation (DFG) and the Else-Kröner-Fresenius Foundation for the financing of this work.

I would also like to thank my examination committee, Prof. Dirk Haller as chairman, and Prof. Martin Klingenspor as well as Prof. Henriette Uhlenhaut as examiners.

Finally, I would like to thank my family for their support and trust, never doubting that I would succeed. Especially Madeline for your unlimited support!